Lars Kielhorn

A Time-Domain Symmetric Galerkin BEM for Viscoelastodynamics

Monographic Series TU Graz

Computation in Engineering and Science

Series Editors

Monographic Series TU Graz

Computation in Engineering and Science Volume 5

Lars Kielhorn

A Time-Domain Symmetric Galerkin BEM for Viscoelastodynamics

This work is based on the dissertation *A Time-Domain Symmetric Galerkin Boundary Element Method for Viscoelastodynamics*, presented by L. Kielhorn at Graz University of Technology, Institute of Applied Mechanics in February 2009.
Supervisor: M. Schanz (Graz University of Technology)
Reviewer: M. Schanz (Graz University of Technology), S. Sauter (University of Zurich)

Bibliographic information published by Die Deutsche Bibliothek.
Die Deutsche Bibliothek lists this publication in the Deutsche Nationalbibliografie; detailed bibliographic data are available at http://dnb.ddb.de.

Cover photo	Vier-Spezies-Rechenmaschine by courtesy of the Gottfried Wilhelm Leibniz Bibliothek – Niedersächsische Landesbibliothek Hannover
Layout	Wolfgang Karl, TU Graz / Universitätsbibliothek
Printed	by TU Graz / Büroservice

Verlag der Technischen Universität Graz

www.ub.tugraz.at/Verlag

978-3-85125-042-8

Abstract

The numerical solution of elliptic or hyperbolic boundary value problems via the Boundary Element Method has a long tradition and is well developed nowadays. The two most popular discretization schemes of the underlying boundary integral equations are the Collocation method and the Galerkin method. While the first one has been adopted to both types of boundary value problems the latter one has been mainly applied to elliptic boundary value problems. To close this gap, the present work is concerned with the derivation of a Symmetric Galerkin Boundary Element Method (SGBEM) for 3-dimensional mixed initial boundary value problems. Thereby, the deduction of the method is presented in an unified manner such that, finally, the scalar wave equation, the system of elastodynamics as well as viscoelastodynamic problems are covered. Contrary to unsymmetric Boundary Element formulations, the SGBEM demands the use of the second boundary integral equation featuring hyper-singularities. With the help of the Stokes theorem those hypersingularities as well as the strong singular integral kernels are transformed into weakly singular integral kernels. Afterwards, the Boundary Element Method is formulated by using standard techniques for the spatial discretization and by applying the Convolution Quadrature Method to the time-convolution integrals. The final numerical tests verify this method and approve its robustness and its reliability. These two properties are an essential prerequisite for a successful use of the proposed Boundary Element Method within a wide range of industrial applications.

Zusammenfassung

Randelementmethoden stellen ein bekanntes Werkzeug zur numerischen Lösung elliptischer sowie hyperbolischer Randwertprobleme dar. Dabei sind die Kollokationsmethode sowie das Galerkinverfahren als die am häufigsten zum Einsatz kommenden Diskretisierungsverfahren der zugrunde liegenden Randintegralgleichungen zu nennen. In Ingenieuranwendungen findet die Kollokationsmethode aufgrund ihres relativ einfachen Aufbaus heutzutage den meisten Zuspruch. Die Galerkin Formulierung hingegen wird hauptsächlich im Rahmen elliptischer Randwertprobleme genutzt und Anwendungen im Zeitbereich finden sich bisher selten. Um diese Lücke zu schließen, ist das Ziel der vorliegenden Arbeit die Entwicklung einer symmetrischen Galerkin-Randelementmethode zur Lösung dreidimensionaler Probleme im Zeitbereich. Die Herleitung der Methode wird dabei sehr allgemein präsentiert, so dass sich mit ihr letztlich Probleme der Akustik, der linearen Elastodynamik sowie der linearen Viskoelastodynamik behandeln lassen. Die symmetrische Formulierung verlangt jedoch die Verwendung einer hypersingulären Randintegralgleichung, deren zuverlässige numerische Auswertung ein erhebliches Problem darstellt. Daher werden sowohl die hypersingulären als auch die stark singulären Integrale mit Hilfe des Satzes von Stokes in für die Numerik günstigere, schwach singuläre Integrale transformiert. Anschließend wird die eigentliche Randelementmethode formuliert. Die örtliche Diskretisierung erfolgt dabei mit Standardtechniken während die Zeitintegrale mit Hilfe der Faltungsquadraturmethode gelöst werden. In den Beispielen zeigt sich, dass die vorgestellte Methode sehr gute Resultate liefert und ein äußerst stabiles Verhalten aufweist.

CONTENTS

Notation

As long as no other meaning is explicitly given to a certain quantity within the text, its meaning corresponds to the following notation list.

General symbols

$\simeq$	Linearization
$[a,b]$	Closed interval a,b
(a,b)	Open interval a,b
$(a,b]$, $[a,b)$	Half open intervals a,b
$a,b,\ldots,\alpha,\beta,\ldots$	Scalar values
$\mathbf{a},\mathbf{b},\ldots$	Vectors
$\mathbf{A}$	Second order tensor $[A_{ij}]_{1\leq i,j\leq 3}$
$\overset{(4)}{\mathbf{C}}$	Fourth order tensor $[C_{ijk\ell}]_{1\leq i,j,k,\ell\leq 3}$
$\mathrm{tr}(\mathbf{A})$	Trace of $\mathbf{A}$, $\mathrm{tr}(A) \coloneqq \sum_{i=1}^{3} A_{ii}$
ϵ_{ijk}	Permutation symbol
$\mathbf{a}\cdot\mathbf{b}, \langle\mathbf{a},\mathbf{b}\rangle$	Scalar product $\mathbf{a}\cdot\mathbf{b} = \langle\mathbf{a},\mathbf{b}\rangle \coloneqq \sum_{i=1}^{3} a_i b_i$
$\mathbf{a}\otimes\mathbf{b}$	Outer product $[a_i b_j]_{1\leq i,j\leq 3}$
$\mathbf{a}\times\mathbf{b}$	Vector product $\mathbf{a}\times\mathbf{b} \coloneqq \sum_{i=1}^{3} \epsilon_{ijk} a_j b_k$
$\mathbf{A}:\mathbf{B}$	Double contraction, double dot product
$\lVert\mathbf{a}\rVert_p$	The p-norm of the vector $\mathbf{a}$
$\lVert\mathbf{A}\rVert_p$	The p-norm of the matrix $\mathbf{A}$
$\mathrm{cond}_p(\mathbf{A})$	The condition number of $\mathbf{A}$, $\mathrm{cond}_p(\mathbf{A}) \coloneqq \lVert\mathbf{A}\rVert_p \lVert\mathbf{A}\rVert_p^{-1}$
∇	Nabla operator $\nabla \coloneqq [\partial/\partial x_i]_{i=1}^{3}$
Δ	Laplace operator $\Delta \coloneqq \sum_{i=1}^{3} \frac{\partial^2}{\partial x_i^2}$
$\nabla\cdot\mathbf{f}$	Divergence of $\mathbf{f}$
∇f	Gradient of f, $\nabla f = [\partial f/\partial x_i]_{i=1}^{3}$
$\nabla\mathbf{f}$	Component wise gradient $[\nabla f_i]_{i=1}^{3}$
$\widetilde{\nabla}\mathbf{f}$	Symmetric Gradient $\widetilde{\nabla}\mathbf{f} \coloneqq \frac{1}{2}(\nabla\mathbf{f} + (\nabla\mathbf{f})^{\top})$
$\nabla\times\mathbf{f}$	Rotation of the vector field $\mathbf{f}$
$\langle f,g\rangle_D$	Inner product of two functions f and g, $\langle f,g\rangle_D \coloneqq \int_D f(\mathbf{x})g(\mathbf{x})\,\mathrm{d}\mathbf{x}$
s	Complex Laplace parameter, $s\in\mathbb{C}$
ω	Frequency, $\omega\in\mathbb{R}$
$(\mathscr{L}f)(s)$	Laplace transform of $f(t)$
$(\mathscr{F}f)(\omega)$	Fourier transform of $f(t)$
$\hat{f}$	Laplace or Fourier transform, $\hat{f}(s) = (\mathscr{L}f)(s)$, or $\hat{f}(\omega) = (\mathscr{F}f)(\omega)$

$H(t)$	Heaviside step function, $H(t) \coloneqq 0, t < 0$; $H(t) \coloneqq 1, t > 0$
$(g \circ f)(x)$	composition, $(g \circ f)(x) \coloneqq g(f(x))$

Special symbols

$\mathbf{x}$	Location $\mathbf{x} = [x_i]_{i=1}^3$
t	Time
$\mathsf{I}, \mathbf{I}$	Second order identity matrix
$\overset{(4)}{\mathbf{I}}$	Fourth order identity matrix
$\bar{\varrho}, \varrho_0, \varrho$	Total density, equilibrium density, density fluctuation
$\bar{p}, p_0, p$	Total pressure, equilibrium pressure, pressure fluctuation
$\boldsymbol{\sigma}, \boldsymbol{\sigma}_H, \boldsymbol{\sigma}_D$	Cauchy stress tensor, hydrostatic part, deviatoric part
$\boldsymbol{\varepsilon}, \boldsymbol{\varepsilon}_H, \boldsymbol{\varepsilon}_D$	Linear strain tensor, hydrostatic part, deviatoric part
$\boldsymbol{\omega}$	Linear rotation tensor
$\boldsymbol{\varphi}$	Rotation vector
$\sigma^{(i)}$	Principal stress in the i-th direction
$\varepsilon^{(i)}$	Principal strain in the i-th direction
$\overset{(4)}{\mathbf{C}}, \overset{(4)}{\mathbf{G}}, \overset{(4)}{\mathbf{J}}$	Fourth order material tensors
$K, \hat{K}(s)$	Bulk modulus, complex bulk modulus
$E, \hat{E}(s)$	Young's modulus, complex Young's modulus
$\nu, \hat{\nu}(s)$	Poisson's ratio, complex Poisson's ratio
$\lambda, \mu; \hat{\lambda}(s), \hat{\mu}(s)$	Lamé's constants, complex Lamé's constants
c, c_1, c_2	Wave velocity, compressional wave velocity, shear wave velocity
$\hat{c}(s)$	Complex wave velocity
$\mathbf{u}(\mathbf{x}, t)$	Displacement vector
ε	Volume dilatation $\varepsilon \coloneqq \nabla \cdot \mathbf{u}$
$\mathcal{L}$	Elliptic partial differential operator of second order
$\mathcal{T}$	Generalized normal derivative operator
Tr	Boundary trace operator
$\mathcal{R}$	Space of rigid body motions
u_Γ	Trace of the Dirichlet data to the boundary
q_Γ	Trace of the Neumann data to the boundary
U	Fundamental solution for scalar problems
$\mathbf{U}$	Fundamental solution for vector problems
$\widehat{\mathcal{N}}_0, \widehat{\mathcal{N}}_1$	Elliptic Newton potentials
$\mathcal{N}_0, \mathcal{N}_1$	Hyperbolic Newton Potentials
$\widehat{\mathcal{V}}, \widehat{\mathcal{K}}, \widehat{\mathcal{K}}', \widehat{\mathcal{D}}$	Elliptic layer operators
$\mathcal{V}, \mathcal{K}, \mathcal{K}', \mathcal{D}$	Hyperbolic layer operators
$\widehat{\mathcal{I}}$	Elliptic identity operator
$\mathcal{I}$	Hyperbolic identity operator
$\mathsf{V}, \mathsf{K}, \mathsf{D}$	Discrete layer operators

$\partial/\partial\mathbf{S}(\partial_{\mathbf{y}},\mathbf{n}(\mathbf{y}))$	Surface curl $\frac{\partial}{\partial\mathbf{S}(\partial_{\mathbf{y}},\mathbf{n}(\mathbf{y}))} \coloneqq \mathbf{n}(\mathbf{y})\times\nabla_{\mathbf{y}}$
$\mathcal{M}(\partial_{\mathbf{y}},\mathbf{n}(\mathbf{y}))$	Günter derivatives
G	Triangulation
τ,τ_∞	Boundary element, infinite boundary element
$\hat{\tau},\hat{\tau}_\infty$	Reference element, infinite reference element
$\mathbf{J}_\tau$	Jacobi matrix of τ
g_τ	Gram determinant of τ
h_τ	Mesh size of τ
h_G	Global mesh size of the triangulation G
q_G	Quasi-uniformity of the triangulation G
S_h^γ	Test- and trial-space
$\operatorname{dist}(\tau_{\mathbf{x}},\tau_{\mathbf{y}})$	Distance between two elements $\tau_{\mathbf{x}}$ and $\tau_{\mathbf{y}}$
$\widetilde{\operatorname{dist}}(\tau_{\mathbf{x}},\tau_{\mathbf{y}})$	Approximate distance between two elements $\tau_{\mathbf{x}}$ and $\tau_{\mathbf{y}}$
$\widetilde{\delta}(\tau_{\mathbf{x}},\tau_{\mathbf{y}})$	normalized approximate distance $\widetilde{\delta}(\tau_{\mathbf{x}},\tau_{\mathbf{y}}) \coloneqq \frac{\widetilde{\operatorname{dist}}(\tau_{\mathbf{x}},\tau_{\mathbf{y}})}{\max(h_{\tau_{\mathbf{x}}},h_{\tau_{\mathbf{y}}})}$
θ	Characteristic polynomial
ω_n	The n-th quadrature weight within the CQM

1 INTRODUCTION

In engineering sciences a broad range of mechanical problems can be attributed to the solution of partial differential equations, or systems of it. But there exist only a few very special cases where those equations feature exact solutions. Hence, in almost any engineering field the approximate solution of the aforementioned differential equations gain more and more interest. At least, this fact is heavily owed to the enormous progress in computer technology within the recent decades.

For sure, the most established and probably the most versatile numerical approximation scheme is the Finite Element Method (FEM) which covers a wide range of applications. It has been successfully utilized for the solution of static and dynamic problems as well as for the solution of linear and non-linear problems. Nevertheless, also the FEM has its limitations such that there exist not (and there likely will not exist) one numerical scheme which covers every physical problem. In other words, different physical problems can be subsumed into certain problem classes for which special numerical discretization methods have to be developed.

This work is concerned with the deduction of a Boundary Element Method (BEM). In contrast to Finite Element Methods which, basically, utilize the partial differential equations for the discretization, Boundary Element Methods represent the discretization technique of boundary integral equations. These integral equations are boundary only representations of the considered physical problems, and they are obtained by an analytical transformation of the partial differential equations onto the boundary of the considered domain. For this transformation the knowledge of the so-called fundamental solution is essential. These solutions form the main ingredient of any Boundary Element Method and they are both a blessing and a curse at the same time. Fundamental solutions solve the underlying partial differential equations exactly everywhere except at the origin where they are singular. From this point of view they are helpful since the Boundary Element Method gains its accuracy from their involvement. On the other hand, the occurring singularities make the numerical scheme considerably more complex. In addition, the fundamental solutions restrict the application of the Boundary Element Method mostly to linear partial differential equations since respective fundamental solutions for non-linear problems are unknown in most instances.

Boundary Element Methods are definitely not as versatile as FEM but for certain problem classes they feature superior properties compared to the Finite Element Methods. Since the discretization is done for the boundary only and since the boundary integral equations satisfy certain decay or, respective, radiation conditions Boundary Element Methods are perfectly suitable to deal with the so-called outer or radiation problems. Those problems arise, e.g., if the sound emissions of some bounded body should be investigated and they

are hardly solvable with Finite Element Methods. In addition to that problems there exist mainly two more cases in which the use of Boundary Element Methods might be required. The one case is, again, related to the geometry on which the analysis takes place. If the geometry is very complex it is occasionally difficult to generate a volume discretization but it is often possible to discretize the geometry's surface. In such cases Finite Element Methods even do not come into play. The other case is, that standard Finite Element Methods perform weakly in situations where a good resolution of high stress concentrations is required. This good performance of Boundary Element Methods in stress calculations emerges from the mixed formulation approach the method consists of. In contrast to displacement based Finite Element Methods, the discretization and direct evaluation of boundary tractions is an elementary part of any Boundary Element Method. With these advantages, Boundary Element Methods serve as an expedient enhancement to the set of available numerical methods.

In general, the discretization of boundary integral equations results in fully populated system matrices. Of course, these dense matrices form a major problem concerning storage requirements as well as the computational complexity. But, in recent years several methods have been developed mostly by mathematicians to overcome this drawback. Those methods are usually subsumed under the title Fast Boundary Element Methods and they reduce the method's complexity considerably. It is known that those methods perform best if the underlying discretization scheme is based on variational principles. A well-known scheme is the Galerkin discretization which is usually applied to Finite Element Methods. As a result of this discretization the properties of the partial differential operators are mostly preserved on a discrete level. This means that, e.g., the discretization of elliptic boundary value problems results in positive definite system matrices. This work deals not with fast techniques but it marks a preliminary work since it utilizes the Galerkin discretization for the numerical approximation of time-dependent boundary integral equations. Contrary to the more common collocation based Boundary Element Methods this approach results in positive definite system matrices which clearly represent the underlying boundary integral operators' properties. As will be shown later on the application of the so-called Symmetric Galerkin Boundary Element Method (SGBEM) to mixed initial boundary value problems is not only more elegant from a mathematical point of view, it results also in a more robust and reliable numerical scheme — a fact which is important for the numerical solution of engineering applications.

1.1 State of the art

This thesis aims at a robust and reliable Boundary Element Method for elliptic and hyperbolic boundary value problems. Boundary Element Methods represent the discretization technique of the underlying boundary integral equations. Those equations are known since the days of Gauss, Green, and Dirichlet, just to note a few of them. A historical survey on this topic as well as a comprehensive overview on elliptic boundary integral equations is given in the recent book of Hsiao & Wendland [63]. The work of Chudinovich [26–28]

presents a mathematical treatment of initial boundary value problems by using hyperbolic boundary integral equations. Additionally, the excellent paper of Costabel [29] serves as comprehensive source to gain more information concerning the theory of time-dependent boundary integral equations.

An overview on elliptic boundary integral equations is also given in the books of Sauter & Schwab [107] and Steinbach [120]. But in addition, these books introduce the Boundary Element Method by means of the Galerkin discretization. From a more engineering point of view, further information about Galerkin Boundary Element Methods is given in the review article of Bonnet *et al.* [20] and in the references cited there. For an overview concerning the collocation methods the books of Gaul *et al.* [41], Bonnet [18], Hartmann [59], and Brebbia *et al.* [22] should be advised.

In this thesis, the Symmetric Galerkin Boundary Element Method (SGBEM) will be utilized to treat mixed initial boundary value problems. Amongst others this is mainly motivated by the positive results of the Galerkin approaches in elastostatics [115] as well as for parabolic problems [79] and the Helmholtz equation [78].

The drawback when considering mixed problems by symmetric methods is the evaluation of the second boundary integral equation which contains a non integrable hypersingularity. This integral has to be interpreted as a finite part integral in the sense of Hadamard [57]. Those singularities can be either treated numerically [108] or in an analytical way [50]. Here, an analytical transformation of the hypersingular integral operator based on integration by parts in 3-d elastodynamics will be presented which, finally, will lead to a bilinear form containing only weak singularities. The used approach is very similar to a regularization in elastostatics given by Han [58] since it takes advantage of the similar structure between the elastostatic and the elastodynamic fundamental solutions.

When dealing with singularities in dynamics it is a common practice to subtract and to add the corresponding static fundamental solution from its elastodynamic counterpart. This is due to the fact that the singular behavior of the static part coincides with the dynamic one (see, e.g., [19, 67]). Hence, an existing regularization for the static case can be used also to regularize the equivalent dynamic integral kernel. Unfortunately, the occurring residual kernel might cause numerical instabilities due to the fact that it involves the difference between the singular dynamic and the singular static kernel. The method presented here does not cause those instabilities since the elastodynamic hypersingular integral operator is treated as a whole.

Regularization approaches of non integrable kernel functions based on integration by parts have a long tradition and are well known nowadays. This technique was firstly used in 1949 by Maue [82] who applied it to the wave equation in frequency domain. A major enhancement was then given by Nedelec [87] who introduced regularized hypersingular bilinear forms for the Laplace equation, the Helmholtz equation as well as for the system of linear elastostatics. Further, regularizations in the field of 3-d time-harmonic elastodynamics were presented by Nishimura & Kobayashi [88] and Becache *et al.* [11]. While these both

approaches rely mainly on the previous work by Nedelec [87], the particular regularizations are nevertheless slightly different. In the first case, the hypersingular operator is used within a collocation scheme while in the other case a Galerkin scheme is formulated. Using the latter discretization scheme is advantageous since it features less restrictions concerning the choice of shape functions for the displacement field. Contrary to the collocation approach, the only requirement in Galerkin based regularizations is the continuity of the displacement field. Another regularization of the hypersingular bilinear form in case of 3-d elastostatics was presented by Han [58] who used some basic results from Kupradze [70]. Unlike Nedelec whose regularization is based on a very general approach and, therefore, results in rather complicated formulae, Han restricts his regularization a priori to the isotropic case and discards the possibility of describing also the anisotropic system. Hence, the resulting regularized bilinear form is simpler to deal with and motivates the use of Han's proof within the present work. As will be shown, the extension of his proof to the system of 3-d elastodynamics leads to a more convenient formulation with respect to the numerical implementation than the already established regularizations [11, 88].

The treatment of time-dependent problems by using the Boundary Element Method is mostly done within the engineering community. See the review articles of Beskos [15, 16] for an overview on this topic. In principle, for the time discretization of the underlying boundary integral equations there exist two approaches. Firstly, if time dependent fundamental solutions are available, the usage of ansatz functions with respect to time yields a time stepping procedure after an analytical time integration within each time step. This technique has been proposed by Mansur [80] and is sometimes denoted as the *classical* time domain boundary element formulation. Secondly, the Convolution Quadrature Method (CQM) developed by Lubich [76, 77] can be used to establish the same time stepping procedure as obtained by a direct time integration [111]. Contrary to the approach from Mansur for this methodology only the Laplace domain fundamental solutions have to be known and the time integration is performed numerically. Hence, this approach can easily be extended to the viscoelastic case [112] where the fundamental solutions in closed form are only available in Laplace or Fourier domain. Moreover, the regularization process is more advantageous since the fundamental solutions in Laplace domain are simpler to deal with which is due to the fact that no retarded potentials occur like in time-dependent fundamental solutions [53].

A quite popular benchmark for almost any Boundary Element Method is the treatment of outer problems and half-space problems. Within this work the half-space problem is difficult to deal with since it exhibits a boundary of infinite extent. Naturally, it is quite impossible to discretize such a surface, but it has become common practice to model just a truncated surface patch of the originally infinite boundary. While this works rather unexplainable in collocation methods [111] it fails completely in the present case. This failure is connected to the regularization of the hypersingular operator which demands either a closed surface or vanishing integral kernels on the surface's boundary. To overcome this drawback, infinite elements are introduced which have been mainly developed by Bettes [17] and are mostly used within Finite Element Methods where they are mostly applied to sound emission problems (see, e.g., [42, 43]). But, infinite elements have been also applied

to Boundary Element Methods. In the work of Beer & Meek [12], Beer & Watson [13], and Moser *et al.* [85], the infinite elements have been successfully used for the elastostatic half-space problem.

Although it is not the primary aim of this work, some comments about the so-called Fast Boundary Element Methods should be given. In the last two decades those methods gain a tremendous success since they reduce the Boundary Element Method's complexity considerably. The most popular fast methods are the $\mathcal{H}$-matrices mainly developed by Hackbush [56], the Adaptive Cross Approximation [9, 10, 100] as well as the Fast Multipole Method which has been originally proposed by Greengard [49]. For instance, the Fast Multipole Method has been successfully applied by Of [89] in conjunction with an Symmetric Galerkin Boundary Element Method for 3-dimensional elastostatics. Hence, this work is not only intended to present a reliable numerical method it also serves as a prerequisite for future research aiming at a Fast Symmetric Galerkin Boundary Element Method in time-domain.

1.2 Outline

In *chapter 2*, the governing equations are shortly derived. The problems which are covered in this work are the acoustic fluid, the system of elastodynamics as well as the system of linear viscoelastodynamics. If the inertia terms are neglected in the balance laws these material models pass over to their static counterparts which are also stated. In addition, the respective boundary value problems are given.

In *chapter 3*, the underlying boundary integral equations as well as the variational forms corresponding to the Galerkin scheme are deduced. The Galerkin formulation marks the basis of the later proposed Boundary Element Method.

Beside weak singularities the Symmetric Galerkin Boundary Element Method features integral operators which are originally defined in the sense of Cauchy principal values and Hadamard finite part integrals, respectively. In a numerical scheme those operators are difficult to treat. Therefore, to overcome these difficulties, in *chapter 4* a regularization is presented which transforms the higher order singularities into weak singularities.

The *chapter 5* is devoted to the formulation of the Boundary Element Method itself. There, classical techniques known form the Finite Element Method are introduced on which the discretization of the boundary integral equations is based. Further, some comments concerning the numerical evaluation of the regular and singular integral kernels are given. Additionally, special boundary elements are introduced which are constructed for the use with physical problems exhibiting not only an infinite domain but also an infinite boundary.

Finally, in *chapter 6*, the validation of the proposed Symmetric Galerkin Boundary Element Method is done by means of some standard numerical experiments featuring mostly analytical or semi-analytical solutions.

The main part of this thesis ends with a summary given in *chapter 7*. Additionally, some weaknesses of the present work are pointed out and are discussed briefly.

In the end, the *appendix* gives more detailed information concerning some minor aspects of this work.

2 WAVE EQUATIONS FOR ACOUSTICS, ELASTODYNAMICS, AND VISCOELASTODYNAMICS

In this chapter, the governing equations are introduced that build the basis for the later formulated Boundary Element Method. These are mainly the acoustic wave equation and the system of elastodynamics. Additionally, as a generalization of the elastodynamic system the concept of viscoelastodynamics is presented. If the influence of inertia effects is neglected in the balance of momentum all three models pass over to their static counterparts which can be referred to as the Poisson equation, the system of elastostatics, and the quasistatic model of viscoelasticity. With numerical solutions for these problems in mind, boundary and initial boundary value problems are formulated which embed the equations into a complete mathematical setting.

Under the assumption that the changes of the state variables (the pressure of the fluid or the displacements of the solid) are relatively small the considered physical models can be formulated in a linear setting. Therefore, higher order terms in the kinematic and the constitutive laws are neglected such that the description of every physical model finally results in linear partial differential equations. Moreover, the linear setting suffices to formulate all phenomena in the reference configuration only [90]. Thereby, a Cartesian coordinate system is used to describe the position of a vector $\mathbf{x} \in \mathbb{R}^3$. The vector $\mathbf{x}$ itself contains the coordinates x_i with $i = 1,2,3$.

2.1 The acoustic fluid

The derivation of the acoustic wave equation may be done in several ways. For instance a comprehensive derivation is given in [38] for the one dimensional case or may be found in [84] for higher dimensions. The procedure presented here summarizes briefly this approach.

At first, some restrictions have to be made concerning the acoustic media. It is assumed to be homogeneous, isotropic, perfectly elastic, and at rest in the initial state. Moreover, the fluid is either a gas or a liquid and gravity effects are negligible. A fluid with these properties is called an *acoustic fluid*. A further distinction can be made by the definition of an *inviscid acoustic fluid* and a *dissipative acoustic fluid* [91]. While in the inviscid case there is no dissipation inside the fluid, the dissipative model comprises such effects. Here, only the inviscid acoustic fluid is considered.

Now, taking the above mentioned restrictions into account the acoustic fluid is assumed to have an uniformly distributed total density $\bar{\varrho}(\mathbf{x},t)$ and a uniformly distributed total pressure

$\bar{p}(\mathbf{x},t)$. By introducing small fluctuations $\varrho(\mathbf{x},t)$ and $p(\mathbf{x},t)$ around the equilibrium states ϱ_0 and p_0 the density and pressure fields can be written as

$$\begin{aligned} \bar{\varrho}(\mathbf{x},t) &= \varrho_0 + \varrho(\mathbf{x},t), & \varrho \ll \varrho_0 \\ \bar{p}(\mathbf{x},t) &= p_0 + p(\mathbf{x},t), & p \ll p_0 \,. \end{aligned}$$

Let $\mathrm{d}V$ denote a differential volume at the position $\mathbf{x}$ and time t. In the reference configuration the differential volume is denoted by $\mathrm{d}V_0$. While the volume $\mathrm{d}V$ exhibits the total density $\bar{\varrho}$ the volume $\mathrm{d}V_0$ posses the density ϱ_0 at equilibrium state. Since it is assumed that no additional mass can be generated the *conservation of mass* reads as

$$(\varrho_0 + \varrho(\mathbf{x},t))\,\mathrm{d}V(\mathbf{x},t) = \varrho_0\,\mathrm{d}V_0(\mathbf{x}) \,. \tag{2.1}$$

In a linear setting the relative volume change or *dilatation* ε is small and, therefore, can be described by the divergence of the displacement field [118]. This yields

$$\varepsilon(\mathbf{x},t) := \frac{\mathrm{d}V(\mathbf{x},t) - \mathrm{d}V_0(\mathbf{x})}{\mathrm{d}V_0(\mathbf{x})} = \nabla\cdot\mathbf{u}(\mathbf{x},t) \,. \tag{2.2}$$

Using the above statement, the dilatation can be connected to the density by inserting (2.2) into (2.1)

$$\varrho(\mathbf{x},t) = -\bar{\varrho}(x,t)\varepsilon(\mathbf{x},t) \,.$$

Then, approximating $\bar{\varrho}(\mathbf{x},t)$ by ϱ_0 gives the linearized form

$$\varrho(\mathbf{x},t) \simeq -\varrho_0\varepsilon(\mathbf{x},t) \tag{2.3}$$

which can be regarded as the *kinematics* of the acoustic fluid.

Since the fluid is inviscid the stress state in the fluid must be of hydrostatic nature. Then, the Cauchy stress tensor is given by

$$\boldsymbol{\sigma}(\mathbf{x},t) = -p(\mathbf{x},t)\,\mathbf{I} \,. \tag{2.4}$$

Next, the *dynamic equilibrium* is needed. Starting from the *balance of momentum*

$$\int_{\partial V_0} \mathbf{t}(\mathbf{x},t)\,\mathrm{d}s_{\mathbf{x}} + \int_{V_0} \varrho_0\mathbf{b}(\mathbf{x},t)\,\mathrm{d}\mathbf{x} = \int_{V_0} \varrho_0\ddot{\mathbf{u}}(\mathbf{x},t)\,\mathrm{d}\mathbf{x}$$

with the body force $\mathbf{b}$ and the surface tractions $\mathbf{t}$, one obtains in conjunction with the Cauchy lemma $\mathbf{t} = \boldsymbol{\sigma}\cdot\mathbf{n}$

$$\int_{\partial V_0} \boldsymbol{\sigma}(\mathbf{x},t)\cdot\mathbf{n}(\mathbf{x})\,\mathrm{d}s_{\mathbf{x}} + \int_{V_0} \varrho_0\mathbf{b}(\mathbf{x},t)\,\mathrm{d}\mathbf{x} = \int_{V_0} \varrho_0\ddot{\mathbf{u}}(\mathbf{x},t)\,\mathrm{d}\mathbf{x} \,. \tag{2.5}$$

Finally, by means of the divergence theorem $\int_{\partial\Omega}\mathbf{f}\cdot\mathbf{n}\,\mathrm{d}s_{\mathbf{x}} = \int_{\Omega}\nabla\cdot\mathbf{f}\,\mathrm{d}\mathbf{x}$ (2.5) results in

$$\int_{V_0} (\nabla\cdot\boldsymbol{\sigma}(\mathbf{x},t) + \varrho_0\mathbf{b}(\mathbf{x},t))\,\mathrm{d}\mathbf{x} = \int_{V_0} \varrho_0\ddot{\mathbf{u}}(\mathbf{x},t)\,\mathrm{d}\mathbf{x} \,. \tag{2.6}$$

Since (2.6) holds for every sub-volume of V_0 and arbitrary dV the integral formulation holds also point-wise for the integrands. In conjunction with (2.4), the dynamic equilibrium for the inviscid fluid reads as

$$-\nabla p(\mathbf{x},t) + \varrho_0 \mathbf{b}(\mathbf{x},t) = \varrho_0 \ddot{\mathbf{u}}(\mathbf{x},t) \; . \tag{2.7}$$

Taking the divergence of (2.7) and combining the result with the second time derivative of (2.3) yields

$$-\Delta p(\mathbf{x},t) + \ddot{\varrho}(\mathbf{x},t) = \varrho_0 b(\mathbf{x},t) \tag{2.8}$$

with the abbreviation $b(\mathbf{x},t) := -\nabla \cdot \mathbf{b}(\mathbf{x},t)$. The left hand-side of (2.8) connects two state variables, the pressure's fluctuation p and the fluctuation of density ϱ. In order to relate these two variables with each other a *constitutive equation* is needed. Because the fluid is assumed to be perfectly elastic the pressure $\bar{p}$ must be a function of the density $\bar{\varrho}$ such that $\bar{p} = f(\bar{\varrho})$. A Taylor expansion of f about the equilibrium state yields

$$\bar{p} = p_0 + p = f(\varrho_0 + \varrho) = f(\varrho_0) + \left.\frac{\mathrm{d}f}{\mathrm{d}\bar{\varrho}}\right|_{\bar{\varrho}=\varrho_0} \varrho + \frac{1}{2} \left.\frac{\mathrm{d}^2 f}{\mathrm{d}\bar{\varrho}^2}\right|_{\bar{\varrho}=\varrho_0} \varrho^2 + \mathcal{O}(\varrho^3) \; .$$

Truncation after the linear term and the necessary condition $f(\varrho_0) = p_0$ result in the constitutive relation

$$p(\mathbf{x},t) \simeq f'(\varrho_0)\varrho(\mathbf{x},t), \qquad f'(\varrho_0) := \left.\frac{\mathrm{d}f}{\mathrm{d}\bar{\varrho}}\right|_{\bar{\varrho}=\varrho_0} \; .$$

In case of a linear constitutive behavior, as assumed here, the proportionality factor of the above relation is constant and can be identified with the square of the wave velocity, $c^2 = f'(\varrho_0)$. It should be noted that this linearization hypothesis is justified if for the fluid particles the condition $\|\dot{\mathbf{u}}\| \ll c$ holds. Alternatively, the pressure fluctuation is directly proportional to the relative density changes

$$p(\mathbf{x},t) = K \frac{\varrho(\mathbf{x},t)}{\varrho_0} = -K\,\varepsilon(\mathbf{x},t) \tag{2.9}$$

with the bulk modulus K ($K > 0$) as proportionality factor. Thus, the wave velocity can be expressed as

$$c = \sqrt{\frac{K}{\varrho_0}} \; . \tag{2.10}$$

Expressing (2.8) in terms of the volume dilatation ε, assuming $b \equiv 0$, and considering (2.3) and (2.9) gives

$$\ddot{\varepsilon} = \frac{K}{\varrho_0} \Delta \varepsilon \; . \tag{2.11}$$

The expression above is useful when in section 2.2 the characteristics of waves in elastic solids are considered.

Finally, inserting the linearized constitutive law into (2.8) yields the *acoustic wave equation* for an inviscid fluid

$$-\Delta p(\mathbf{x},t) + \frac{1}{c^2} \ddot{p}(\mathbf{x},t) = \varrho_0 b(\mathbf{x},t) \; . \tag{2.12}$$

Using operator notation (2.12) can be written as

$$\left(\mathcal{L} + \varrho_0 \frac{\partial^2}{\partial t^2}\right) p(\mathbf{x},t) = g(\mathbf{x},t) \tag{2.13}$$

where $\mathcal{L} = -K\Delta$ is an elliptic partial differential operator of second order and $g = K\varrho_0 b$ is some prescribed source. Moreover, the second order time derivative identifies the acoustic wave equation as a hyperbolic partial differential equation.

Note that the wave equation above has been derived under the assumptions that the fluid is compressible, inviscid, homogeneous, and perfectly elastic. In reality not a single of these assumptions will hold nor will all of these assumptions be fulfilled. Nevertheless, it has turned out that any occurring non-linear effects are often small enough such that the application of the linear wave equation is absolutely justified.

In order to dispose the time derivative in (2.13), the application of an appropriate integral transformation is useful. For instance the Laplace transformation $\hat{f}(s) = (\mathscr{L}f)(s) := \int_0^\infty f(t)\exp(-st)\,\mathrm{d}t$ with the complex Laplace parameter $s \in \mathbb{C}$ converts the time derivatives into multiplications. This yields

$$\left(\mathcal{L} + \varrho_0 s^2\right) \hat{p}(\mathbf{x},s) = \hat{g}(\mathbf{x},s) \qquad \forall\, s \in \mathbb{C}\,. \tag{2.14}$$

Note that (2.14) holds only for vanishing initial conditions, which means that $p(\mathbf{x},0) = 0$ as well as $\dot{p}(\mathbf{x},0) = 0$ hold. Restricting the complex parameter s to the imaginary axis and substituting $s = \mathrm{i}\omega$ one obtains the Helmholtz equation

$$\left(\mathcal{L} - \varrho_0 \omega^2\right) \hat{p}(\mathbf{x},\omega) = \hat{g}(\mathbf{x},\omega) \qquad \forall \omega \in \mathbb{R}\,,$$

which is equal to the Fourier transform $\hat{p} = (\mathscr{F}p)(\omega)$ of (2.13). Now, the equations above are of elliptic type with their corresponding differential operators $\mathcal{L} + \varrho_0 s^2$ and $\mathcal{L} - \varrho_0 \omega^2$ being named as Yukawa operator and Helmholtz operator, respectively.

Finally, neglecting the inertia effects (2.12) simplifies to the well-known Poisson equation

$$(\mathcal{L}p)(\mathbf{x}) = g(\mathbf{x}) \tag{2.15}$$

which itself is nothing else than an inhomogeneous formulation of the Laplace equation

$$(\mathcal{L}p)(\mathbf{x}) = 0\,.$$

The Laplace equation is the prototype of an elliptic partial differential equation. It is important in many fields of science since it describes the behavior of electric or gravitational potentials as well as heat conduction and the pressure field in a fluid.

2.2 Linear elastodynamics

In the following, the basic equations of linear elastodynamics are summarized. The derivation presented here is mainly based on lecture notes by Sommerfeld [118] and is structured in the way that, first, the kinematic equations are given, which are followed by the balance laws and the constitutive relationship, respectively. Of course the resulting governing equations can be found in any textbook dealing with the theory of elasticity. Nevertheless, as the focus is on dynamics the books of Achenbach [2], Kupradze [69], and Graff [47], among many others, should be mentioned.

As in the preceding section the considered medium is assumed to be of homogeneous, linear elastic, and isotropic behavior and is at rest in the initial state.

Sommerfeld enters his deduction of the kinematics with a quotation of the fundamental statement given by Helmholtz [60], namely, that every small change of location of a deformable body within a sufficiently small volume is formed by the addition of a *translation*, a *rotation*, and a *deformation* with respect to three orthogonal directions. Thereby, the small change of location is nothing else than the displacement $\mathbf{u}$ of a point $\mathbf{x}$ at the time t. To investigate this statement, a point $\mathbf{x}$ is considered which features a displacement $\mathbf{u}(\mathbf{x},t)$. Then let $\mathbf{o}$ be a neighboring point within the same volume exhibiting an initial displacement vector $\mathbf{u}_0(t)$. Without loss of generality this point $\mathbf{o}$ may define the origin of the considered volume, i.e., $\mathbf{o} = [0,0,0]^\top$. Expanding $\mathbf{u}$ in a Taylor series about the point $\mathbf{o}$ and truncate after the linear term yields

$$\mathbf{u}(\mathbf{x},t) \simeq \mathbf{u}_0(t) + (\nabla\mathbf{u})(\mathbf{o},t)\cdot\mathbf{x}\,. \tag{2.16}$$

Since the aim is the derivation of the kinematics the time t can be thought of being fixed for the moment. Therefore, it is justified to skip it in the following. Moreover, the argument $(\mathbf{o},t)$ of $\nabla\mathbf{u}$ will be skipped for sake of simplicity. It is advantageous to split $\nabla\mathbf{u}$ into an antisymmetric and a symmetric part such that (2.16) becomes

$$\begin{aligned}\mathbf{u}(\mathbf{x}) &= \mathbf{u}_0 + \frac{1}{2}\left(\nabla\mathbf{u} - (\nabla\mathbf{u})^\top\right)\cdot\mathbf{x} + \frac{1}{2}\left(\nabla\mathbf{u} + (\nabla\mathbf{u})^\top\right)\cdot\mathbf{x}\\ &=: \mathbf{u}_T + \boldsymbol{\omega}\cdot\mathbf{x} + \boldsymbol{\varepsilon}\cdot\mathbf{x}\\ &=: \mathbf{u}_T + \mathbf{u}_R(\mathbf{x}) + \mathbf{u}_D(\mathbf{x})\,.\end{aligned} \tag{2.17}$$

Obviously $\mathbf{u}_T$ is just a translation which is common to any point $\mathbf{x}$ in the considered volume. The second summand, $\mathbf{u}_R$, represents the rotational part. Since $\boldsymbol{\omega}$ is antisymmetric, i.e., $\omega_{ij} = -\omega_{ji}$, it consists of three distinct components only. Therefore, the multiplication $\boldsymbol{\omega}\cdot\mathbf{x}$ can be expressed via a series of cross products [45] such that

$$\mathbf{u}_R(\mathbf{x}) = \boldsymbol{\omega}\cdot\mathbf{x} = \frac{1}{2}(\nabla\times\mathbf{u})\times\mathbf{x} \tag{2.18}$$

where $\nabla\times$ denotes the *curl* operator. Thus, $\mathbf{u}_R$ is the cross product between the curl of the displacements $\mathbf{u}$ and the location vector $\mathbf{x}$. Contrary to the typical polar vectors $\mathbf{u}_R$ represents a so-called pseudo- or axial-vector. These kind of vectors feature not the complete

set of transformations polar vectors fulfill. Refer to Goldstein [45] for a more detailed discussion about axial vectors. Now, to verify that there is no contraction or prolongation associated with $\mathbf{u}_R$ the rotational displacement is added to the point $\mathbf{x}$. With the rotational vector

$$\boldsymbol{\varphi} = \tfrac{1}{2}\nabla \times \mathbf{u} \tag{2.19}$$

and under the assumption that $|\mathbf{u}_R| \ll |\mathbf{x}|$ holds, one gets

$$\begin{aligned} |\mathbf{x}+\mathbf{u}_R|^2 &= |\mathbf{x}|^2 + 2\langle \mathbf{x}, \boldsymbol{\varphi} \times \mathbf{x}\rangle + |\mathbf{u}_R|^2 \\ &= |\mathbf{x}|^2 + 2\langle \boldsymbol{\varphi}, \mathbf{x} \times \mathbf{x}\rangle + |\mathbf{u}_R|^2 \\ &= |\mathbf{x}|^2 + |\mathbf{u}_R|^2 \\ &\simeq |\mathbf{x}|^2 \,. \end{aligned}$$

With $\mathbf{u}_T$ and $\mathbf{u}_R$, the translational and rotational parts of the displacement field $\mathbf{u}$ are known. The remaining part $\mathbf{u}_D$ must denote the deformational behavior. It is represented via the symmetric strain tensor of second order

$$\boldsymbol{\varepsilon} := \frac{1}{2}\left(\nabla\mathbf{u} + (\nabla\mathbf{u})^\top\right) \,. \tag{2.20}$$

With the strain tensor (2.20) the derivation of the kinematic equations for a deformable solid body is completed. Finally, it is important to note that the stretched body must feature a continuous displacement field and that it has to be free of gaps. These constraints are subsumed in the so-called *compatibility condition*

$$\nabla \times \boldsymbol{\varepsilon}(\mathbf{x}) \times \nabla = \mathbf{0} \,. \tag{2.21}$$

Until now, only the deformations of a continuous body are described but not the causes being responsible for them. The description of those causes is the subject of *kinetics* resulting in appropriate balance laws. Since the dynamic equilibrium is already given in (2.6) it is sufficient to repeat its differential representation here

$$-\nabla \cdot \boldsymbol{\sigma}(\mathbf{x},t) + \varrho_0 \ddot{\mathbf{u}}(\mathbf{x},t) = \mathbf{b}(\mathbf{x},t) \tag{2.22}$$

where, now, $\mathbf{b}$ denotes a force per unit volume. Note that additionally to the *balance of momentum* resulting in the dynamic equilibrium above, the *balance of angular momentum* provides the symmetry of the Cauchy stress tensor (see, e.g. [70]).

At last, a material law is essential to connect the stress tensor $\boldsymbol{\sigma}$ with the strain tensor $\boldsymbol{\varepsilon}$. In its most general form the material law for a linear elastic body is

$$\boldsymbol{\sigma}(\mathbf{x},t) = \overset{(4)}{\mathbf{C}}(\mathbf{x},t) : \boldsymbol{\varepsilon}(\mathbf{x},t) \tag{2.23}$$

with the fourth-order material tensor $\overset{(4)}{\mathbf{C}}$. Under the assumption that the considered body is homogeneous and without any internal energy loss the material tensor is independent of the location $\mathbf{x}$ and of the time t, i.e., $C_{ijk\ell} = const$. Additionally, if the mechanical

responses are independent of the direction of stressing a material is called *isotropic*. This condition is the last assumption made here. Now, to obtain a material law for such a body it is advantageous to think of a volume element being orientated within its principal axes. Such a volume suffers only loads due to the principal stresses $\sigma^{(i)}$, $i = 1,2,3$. Then, per definition shear stresses do not occur and the volume undergoes only a dilatation. Therefore, the state of strain can be completely expressed using the principal strains $\varepsilon^{(i)}$, $i = 1,2,3$. Let a,b,c be a set of real valued constants. By the assumed material law's linearity the stress-strain relation for the first principal stress can be expressed as

$$\sigma^{(1)} = a\varepsilon^{(1)} + b\varepsilon^{(2)} + c\varepsilon^{(3)} \,. \tag{2.24}$$

With respect to the material's isotropy (2.24) can be generalized to

$$\sigma^{(i)} = a\varepsilon^{(i)} + b\varepsilon^{(i+1)} + c\varepsilon^{(i+2)} \tag{2.25}$$

for every direction $i = 1,2,3$[1]. Another consequence of the assumed isotropy is the equality of b and c since the material must feature the same characteristics for both directions $i+1$ and $i+2$. Hence, adding and subtracting the term $b\varepsilon^{(i)}$ to (2.25) and using $b \equiv c$ one gets

$$\sigma^{(i)} = (a-b)\,\varepsilon^{(i)} + b\left(\varepsilon^{(i)} + \varepsilon^{(i+1)} + \varepsilon^{(i+2)}\right) \,.$$

Replacing the constants a,b by introducing new constants $2\mu := a - b$ and $\lambda := b$ the principal stresses are given by

$$\sigma^{(i)} = 2\mu\varepsilon^{(i)} + \lambda\left(\varepsilon^{(1)} + \varepsilon^{(2)} + \varepsilon^{(3)}\right) \,. \tag{2.26}$$

The expression (2.26) quantifies the principal stresses. Then, with $\sigma_{ij} = 0$ for $i \neq j$ and by using the identity tensor $\mathbf{I}$ as well as the trace operator $\mathrm{tr}(\boldsymbol{\varepsilon}) = \sum_{i=1}^{3} \varepsilon^{(i)}$ the Cauchy stress tensor reads as

$$\boldsymbol{\sigma} = 2\mu\boldsymbol{\varepsilon} + \lambda\,\mathrm{tr}(\boldsymbol{\varepsilon})\mathbf{I} \tag{2.27}$$

which coincides with (2.26). The above statement is not only valid for stresses and strains represented in a principal axes system but also for arbitrary coordinate systems. This conclusion becomes immediately apparent if the properties of $\boldsymbol{\sigma}$ and $\boldsymbol{\epsilon}$ are taken into account. Both quantities are tensors and, therefore, they must be invariant against a change of the coordinate system. Moreover, the tensor's trace is an invariant so that $\mathrm{tr}(\boldsymbol{\varepsilon}) = \sum_{i=1}^{3} \varepsilon^{(i)} = \sum_{i=1}^{3} \varepsilon_{ii}$ holds for any choice of the coordinate system. Of course, the introduced constants λ and μ are the Lamé constants and (2.27) is known as *generalized Hooke's law*. Introducing the identity tensor of fourth order $\overset{(4)}{\mathbf{I}}$, the material tensor $\overset{(4)}{\mathbf{C}}$ from (2.23) reads as

$$\overset{(4)}{\mathbf{C}} = \lambda\mathbf{I}\otimes\mathbf{I} + 2\mu\overset{(4)}{\mathbf{I}} \,. \tag{2.28}$$

Instead of using the more formally than physically introduced Lamé constants it is also possible to work with the more common Young's modulus E and the Poisson's ratio ν.

[1] The indices in (2.25) have to be understood as modulo 3

The relation between these material constants and the Lamé constants is also worked out nicely in [118] and given below

$$\lambda = \frac{E\nu}{(1+\nu)(1-2\nu)} \qquad \mu = \frac{E}{2(1+\nu)}$$
$$E = \mu\frac{3\lambda+2\mu}{\lambda+\mu} \qquad \nu = \frac{\lambda}{2(\lambda+\mu)} .$$

Finally, the elastodynamic wave equation is obtained by inserting the divergence of the material law (2.27) into the dynamic equilibrium (2.22). Further, bearing in mind the kinematic relation (2.20) gives

$$-(\lambda+\mu)\nabla(\nabla\cdot\mathbf{u}(\mathbf{x},t)) - \mu\Delta\mathbf{u}(\mathbf{x},t) + \varrho_0\ddot{\mathbf{u}}(\mathbf{x},t) = \mathbf{b}(\mathbf{x},t) . \tag{2.29}$$

To identify the different types of waves in an elastodynamic solid the body force is skipped for a moment and the divergence of the displacement field is replaced by the volume dilatation $\varepsilon = \nabla\cdot\mathbf{u}$. Then, (2.29) can be written in the form

$$\varrho_0\ddot{\mathbf{u}}(\mathbf{x},t) = (\lambda+\mu)\nabla\varepsilon(\mathbf{x},t) + \mu\Delta\mathbf{u}(\mathbf{x},t) . \tag{2.30}$$

Taking the divergence of (2.30) and under consideration of the identity $\nabla\cdot\Delta\mathbf{u} = \Delta(\nabla\cdot\mathbf{u})$ one obtains the scalar equation

$$\ddot{\varepsilon}(\mathbf{x},t) = \frac{\lambda+2\mu}{\varrho_0}\Delta\varepsilon(\mathbf{x},t) . \tag{2.31}$$

Similarly, evaluating the curl of (2.30) one obtains by means of the identities $\nabla\times\nabla\mathbf{f} = 0$ and $\nabla\times\Delta\mathbf{f} = \Delta(\nabla\times\mathbf{f})$

$$\varrho_0\nabla\times\ddot{\mathbf{u}}(\mathbf{x},t) = \mu\Delta(\nabla\times\mathbf{u}(\mathbf{x},t)) .$$

Finally, using the rotation vector from (2.19) the above statement becomes

$$\ddot{\boldsymbol{\varphi}}(\mathbf{x},t) = \frac{\mu}{\varrho_0}\Delta\boldsymbol{\varphi}(\mathbf{x},t) . \tag{2.32}$$

Thus, (2.31) and (2.32) express clearly the dilatation and rotation waves within the solid body. Moreover, comparing these expressions with (2.11) one can identify the two corresponding wave velocities

$$c_1 = \sqrt{\frac{\lambda+2\mu}{\varrho_0}} \qquad \text{and} \qquad c_2 = \sqrt{\frac{\mu}{\varrho_0}} \tag{2.33}$$

which describe the speeds of the compression and shear wave, respectively. Note that the compression wave is always faster than the rotation wave since

$$\frac{c_1^2}{c_2^2} = \frac{\lambda}{\mu} + 2 = \frac{2-2\nu}{1-2\nu} > 1 \qquad \forall\,\nu\in[-1,\frac{1}{2})$$

holds. One comment must be given concerning the interval $[-1, \frac{1}{2})$ of the Poisson's ratio. Until now, no negative Poisson's ratios have been observed in natural materials but from a mechanical point of view there is no reason to restrict the Poisson's ratio only to positive values. In fact, man-made materials featuring negative Poisson's ratios are an actual field of research [3].

Analogous to (2.13) an operator notation can be introduced for the elastodynamic wave equation. With the Lamé-Navier operator

$$\mathcal{L} = -(\lambda + \mu)\nabla\nabla\cdot - \Delta \tag{2.34}$$

the equation (2.29) reads as

$$\left[\left(\mathcal{L} + \varrho_0 \frac{\partial^2}{\partial t^2}\right)\mathbf{u}\right](\mathbf{x},t) = \mathbf{b}(\mathbf{x},t)\ . \tag{2.35}$$

Under the assumption of vanishing initial conditions $\mathbf{u}(\mathbf{x},0^+) = \mathbf{0}$ and $\dot{\mathbf{u}}(\mathbf{x},0^+) = \mathbf{0}$ the wave equation (2.35) can be also represented in Laplace domain by

$$\left[\left(\mathcal{L} + \varrho_0 s^2\right)\hat{\mathbf{u}}\right](\mathbf{x},s) = \hat{\mathbf{b}}(\mathbf{x},s) \qquad \forall s \in \mathbb{C}\ . \tag{2.36}$$

Finally, the system of elastostatics is obtained by neglecting the inertia terms in (2.35) such that

$$(\mathcal{L}\mathbf{u})(\mathbf{x}) = \mathbf{b}(\mathbf{x}) \tag{2.37}$$

holds.

2.3 Linear viscoelasticity

In the preceding sections, linear constitutive laws were used under the assumption that the material behaves homogeneous in space as well as constant in time. Thus, a perfect elastic body stores all of the energy it gains due to a loading and dispense it completely when being unloaded, i.e., any deformations vanish and the body turns over to its initial state. For instance steel which is loaded within its stress limit can be modeled sufficiently by such a material law.

Contrary, there exist a wide range of materials which dispense their gained energy only partially. Examples for materials featuring those properties are, e.g., elastomers and ceramics at high temperature. They are denoted as viscoelastic materials and the elaboration of an appropriate constitutive law is the aim of this section. Thereby, the viscoelastic solid is assumed to be properly described within the isothermal linear theory of homogeneous and isotropic media.

As will be shown in the forthcoming chapters the benefit of the Boundary Element formulation presented within this work is the fact that the described viscoelastic material

behavior can be simply embedded in the numerical scheme by making use of the so-called *elastic-viscoelastic correspondence principle*. Thus, the derivation of this principle comprises a major part within this section. For a deeper insight in the theory of viscoelasticity the books of Christensen [25] and Flügge [39] provide more detailed information. Moreover, the book of Lakes [72] covers the more experimental methods according to this topic. Finally, a well-founded mathematical theory of linear viscoelasticity is given by Gurtin & Sternberg [52].

The energy dissipation of a material can be interpreted as a damping mechanism which is caused by inner friction. This inner friction may be explained on a molecular level which is not investigated here any further since such effects are beyond the scope of this thesis. On a macroscopic level this inner friction results mainly in two observable phenomena being characteristic for a viscoelastic material, namely *creeping* and *relaxation* [72]. To understand these phenomena more clearly a tension bar under load is considered being subjected to a two-stage standard test. In the first stage, a constant stress $\sigma(t) = \sigma_0 H(t)$ is applied and the strain $\varepsilon(t)$ is asked for. In the second stage, beginning at $t = t'$, the strain is fixed and the stress is unknown. In the first stage, the strain increases under constant stress. This phenomenon is denoted as creeping. Afterwards, under constant strain, the stress decreases and the material is in its relaxation phase. Figure 2.1 depicts the relaxation and creeping processes. Both observations give raise to the conclusion that the current stress state depends not only on the current strain but on the complete history of deformation. The same holds, of course, for the strain being a function of the whole loading history. Thus, the stresses and strains can be described via convolution integrals resulting in integral representations of the constitutive laws [52].

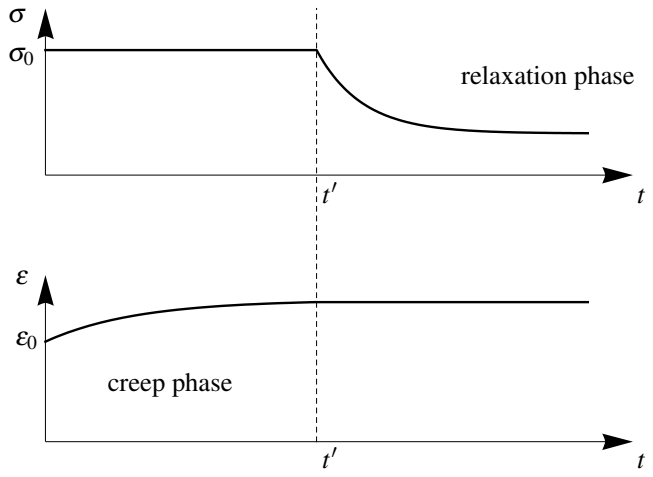

Figure 2.1: The two-stage standard test: Relaxation and creep phase

Rheological models. To keep things as simple as possible, it is advantageous to start with some one dimensional introductory examples. This rather heuristic approach allows the use of simple rheological elements like *springs* and *dashpots* whose combination enables

the creation of viscoelastic models for solids. The spring element represent a perfectly elastic body with the stress-strain relation based on Hooke's law

$$\sigma = E\varepsilon \, .$$

In contrast a dashpot acts as a Newtonian fluid where the stress is proportional to the strain's (time) rate of change. With the viscosity B one obtains

$$\sigma = B\dot{\varepsilon} \, .$$

By combining these basic elements several models can be derived in order to model viscoelastic material behavior. Figure 2.2 depicts three such systems denoted as Maxwell model (Fig. 2.2a), Kelvin model (Fig. 2.2b), and Poynting model[2] (Fig. 2.2c), respectively [66]. The first two models consist of one spring and one damping element and differ in the connection only. The Maxwell model is of serial type and the Kelvin model is a parallel connection. The third model, the Poynting model, contains two spring elements and one damping element and reflects a serial connection of a spring and a Kelvin model[3].

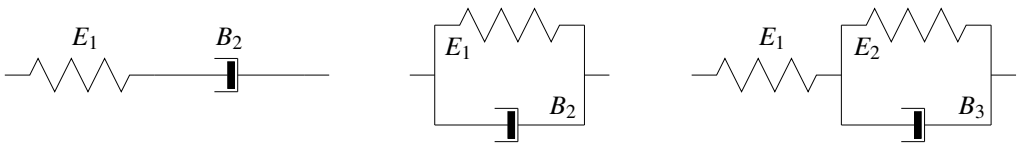

(a) Maxwell model (b) Kelvin model (c) Poynting model

Figure 2.2: One dimensional viscoelasticity: Rheological models

Now, formulating equilibrium and taking the kinematics of the rheological models into account yields the ordinary differential equations

$$\begin{aligned}
&\sigma + p_1\dot{\sigma} = q_2\dot{\varepsilon}, && p_1 = \tfrac{B_2}{E_1}, && && q_2 = B_2 && \text{(Maxwell)} \\
&\sigma = q_1\left(\varepsilon + q_2\dot{\varepsilon}\right), && && q_1 = E_1, && q_2 = \tfrac{B_2}{E_1} && \text{(Kelvin)} \\
&\sigma + p_1\dot{\sigma} = q_1\left(\varepsilon + q_2\dot{\varepsilon}\right), && p_1 = \tfrac{B_3}{E_1+E_2}, && q_1 = \tfrac{E_1E_2}{E_1+E_2}, && q_2 = \tfrac{B_3}{E_2} && \text{(Poynting)}
\end{aligned} \tag{2.38}$$

for each of the considered models. Regarding to the standard test, first, the stress is thought to be fixed. Thus, the solution of (2.38) in terms of the creep compliance takes the general form

$$\varepsilon_\ell(t) = J_\ell(t)\sigma_0 \tag{2.39}$$

where the subscripts $\ell = M, K, P$ are chosen in accordance to the three different rheological models. The function $J(t)$ is called creep function and is determined by the material. The

[2] Synonymous, this model is referred to as 3-parameter-model.

[3] The Poynting model can be constructed also by a parallel connection of a spring and a Maxwell body.

creep functions J_ℓ are given as [39]

$$\begin{aligned} J_M(t) &= \frac{1}{q_2}(p_1+t)H(t) \\ J_K(t) &= \frac{1}{q_1}\left(1-\exp(-t/q_2)\right)H(t) \\ J_P(t) &= \frac{1}{q_1}\left(1+\left(\frac{p_1}{q_2}-1\right)\exp(-t/q_2)\right)H(t)\,. \end{aligned} \tag{2.40}$$

Note that (2.39) emphasizes the linearity of the constitutive model since ε is proportional to the initial stress state σ_0.

Now, bearing in mind the second stage of the standard test the stress is given in terms of the strains

$$\sigma_\ell(t) = G_\ell(t)\varepsilon_0$$

using the relaxation function G_ℓ. Again, the explicit form of G_ℓ is material dependent and reads as [39]

$$\begin{aligned} G_M(t) &= \frac{q_2}{p_1}\exp(-(t-t')/p_1)H(t-t') \\ G_K(t) &= q_1\left(H(t-t')+q_2\delta(t-t')\right) \\ G_P(t) &= q_1\left(1+\left(\frac{q_2}{p_1}-1\right)\exp(-(t-t')/p_1)\right)H(t-t')\,. \end{aligned}$$

Note that without loss of generality $J_\ell(t) \equiv 0$ for all $t \in (-\infty, 0)$ as well as $G_\ell(t) \equiv 0$ for all $t \in (-\infty, t')$ is assumed. Moreover, throughout this section any initial values like, e.g., $\varepsilon(0) = \varepsilon_0$ have to be understood in the limiting sense, i.e., $\varepsilon_0 := \varepsilon(0^+) = \lim_{\tau\to 0}\varepsilon(\tau)$ with $\tau > 0$.

At next, the three models need to be examined more closely. Starting with the Maxwell model one observes that the creep function increases linear. Thus, the strain is growing beyond all bounds which is totally unphysical. Moreover, the relaxation function indicates that the stress tends rapidly to zero for larger times which obviously holds not for solids. The Kelvin model exhibit also a weakness, since the creep function is zero in the initial state and, therefore, this model is not capable to represent any initial strain according to a stress jump. The only model of the three which does not feature such defects is the Poynting model. Hence, it is the simplest one which suffices to model viscoelastic material behavior properly.

Hereditary integrals. Until now, all viscoelastic effects are described by using rheological models which itself are mathematically described via ordinary differential equations. As mentioned previously, viscoelasticity is a property of materials with memory. Thus the strain or stress state depends on the complete history of loading. Mathematically such effects are formulated using hereditary integrals which will be worked out briefly below.

Thereby, all relations are formulated in terms of the creep compliance but, in fact, they can be expressed by relaxation functions analogously. Recalling (2.39)

$$\varepsilon(t) = J(t)\sigma_0$$

one can state that if a stress $\sigma(t) = \sigma_0 H(t)$ is applied suddenly and is kept constant afterwards the above relation describes the strain for the entire future. But what happens if arbitrary stresses $\sigma(t)$ are applied?

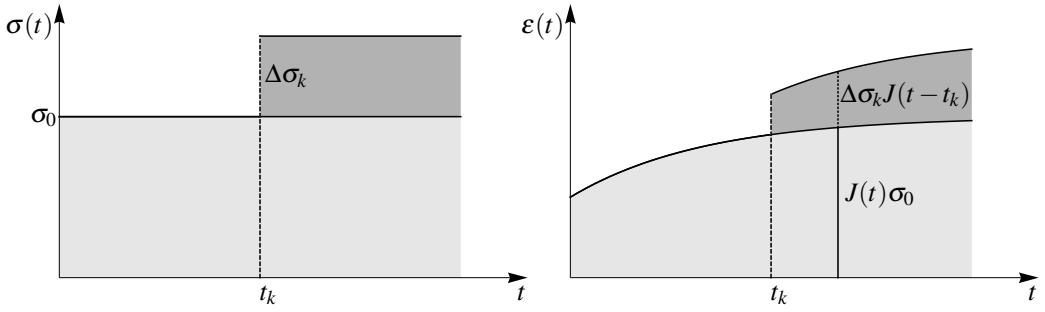

(a) Stress increment (b) Strain increment

Figure 2.3: Linear superposition of step inputs

Since the material is assumed to be linear, the rule of linear superposition can be used to determine the strain caused by several loads. Therefore, it is assumed that there is some more stress $\sigma(t) = \sigma_0 H(t) + \Delta\sigma_k H(t - t_k)$ added at the time $t = t_k$ (Fig. 2.3). Then, for $t > t_k$ additional strain will be produced which must be proportional to the stress jump $\Delta\sigma_k = \Delta\sigma(t_k)$. Moreover, the strain must depend on the same creep compliance J. Thus, for several additional stresses, the overall strain is

$$\varepsilon(t) = \sigma_0 J(t) + \sum_k \Delta\sigma(t_k) J(t - t_k) \, .$$

Finally, taking the limit of infinitesimal step functions $\mathrm{d}\sigma(\tau)$ one ends up with the hereditary integral representation for arbitrary loads $\sigma(t)$

$$\varepsilon(t) = \sigma_0 J(t) + \int_{0^+}^{t} J(t - \tau) \, \mathrm{d}\sigma(\tau) \, . \tag{2.41}$$

The integral above can be subjected to some formal changes. First, since there is no $\mathrm{d}\sigma(\tau)$ for $\tau < 0$ the lower bound of the integral can be set to $-\infty$, and the initial state is also absorbed into the integral. Further, even the upper bound can be changed into $+\infty$ due to the fact that for negative arguments the creep function $J(t - \tau)$ is defined as zero. Hence, (2.41) becomes

$$\varepsilon(t) = \int_{-\infty}^{\infty} J(t - \tau) \, \mathrm{d}\sigma(\tau)$$

which is known as Stieltjes integral [52] and reads in abbreviated form as

$$\varepsilon(t) = J(t) * \mathrm{d}\sigma(t) \tag{2.42}$$

where the asterisk $*$ denotes the convolution in time. Following the calculus for Stieltjes integrals [52, 55] one obtains for continuous differentiable functions $\sigma(t)$

$$\varepsilon(t) = \int_{-\infty}^{\infty} J(t-\tau)\frac{\mathrm{d}\sigma}{\mathrm{d}\tau}\,\mathrm{d}\tau = \sigma_0 J(t) + \int_{0^+}^{t} J(t-\tau)\frac{\mathrm{d}\sigma}{\mathrm{d}\tau}\,\mathrm{d}\tau\,.$$

Now, it is left to illustrate that both representations, the hereditary integral formulation as well as the differential formulation, are two sides of the same medal. A rigorous mathematical proof for this is, again, given by Gurtin & Sternberg [52]. Here, the equivalence is presented only for the special case of the Poynting model. First, applying a Laplace transform to the integral (2.41) yields

$$\hat{\varepsilon}(s) = \sigma_0 \hat{J}(s) + \hat{J}(s)\left(s\hat{\sigma}(s) - \sigma_0\right)\,.$$

Thus, for the Poynting model one gets

$$\hat{\varepsilon}_P(s) = \hat{J}_P(s) s \hat{\sigma}(s) \tag{2.43}$$

with the the Laplace transform of the creep function J_P from (2.40)

$$\hat{J}_P(s) = \frac{1}{q_1}\frac{1+p_1 s}{(1+q_2 s)s}\,.$$

Transforming the associated differential equation (2.38) to the Laplace domain also yields

$$\hat{\varepsilon}_P(s) = \frac{1}{q_1}\frac{1+p_1 s}{(1+q_2 s)s} s\hat{\sigma}(s) + \frac{q_2}{1+q_2 s}\left(\varepsilon_0 - \frac{p_1}{q_1 q_2}\sigma_0\right)\,. \tag{2.44}$$

Under consideration of (2.39) which, in the limit $t \to 0$, must also hold for arbitrary stress functions $\sigma(t)$ the initial strain ε_0 is

$$\varepsilon_0 = J(0)\sigma_0 = \frac{p_1}{q_1 q_2}\sigma_0\,. \tag{2.45}$$

Therefore, the bracket term in (2.44) vanishes and one ends up with the same expression as already stated in (2.43).

Three dimensional constitutive law. Bearing in mind the one dimensional case it would be preferable to carry the rheological model forward to an elementary constitutive law in higher dimensions. Since the material is assumed to be isotropic and isothermal this

transfer is possible [66] and rather straightforward. According to (2.42) the constitutive law reads as

$$\boldsymbol{\varepsilon}(t) = \overset{(4)}{\mathbf{J}}(t) * \mathrm{d}\boldsymbol{\sigma}(t)$$

or, equivalent,

$$\boldsymbol{\sigma}(t) = \overset{(4)}{\mathbf{G}}(t) * \mathrm{d}\boldsymbol{\varepsilon}(t) \tag{2.46}$$

where $\overset{(4)}{\mathbf{J}}$ and $\overset{(4)}{\mathbf{G}}$ are fourth order material tensors. Further, the time convolution between two tensors $\mathbf{A}$ and $\mathbf{B}$ of order $n \geq 2$ is defined as

$$\mathbf{A}(t) * \mathbf{B}(t) := \int_{-\infty}^{\infty} \mathbf{A}(\tau) : \mathbf{B}(t-\tau)\, \mathrm{d}\tau \,.$$

Now, to obtain a constitutive law it is preferable to use the bulk modulus $K = \lambda + 2\mu/3$ instead of the Lamé parameter λ as an elastic material parameter. Then, according to (2.28) the most general representation of a fourth order isotropic viscoelastic material tensor is given by

$$\overset{(4)}{\mathbf{G}}(t) = \left(K - \frac{2}{3}\mu\right) F_1(t)\mathbf{I}\otimes\mathbf{I} + 2\mu F_2(t)\overset{(4)}{\mathbf{I}} \,. \tag{2.47}$$

Thereby, F_1 and F_2 are two independent dimensionless relaxation functions. Splitting both the stress tensor and the strain tensor into their hydrostatic and deviatoric parts

$$\begin{aligned} \boldsymbol{\sigma}_H &= \frac{1}{3}\mathrm{tr}(\boldsymbol{\sigma})\mathbf{I}, \qquad & \boldsymbol{\sigma}_D &= \boldsymbol{\sigma} - \boldsymbol{\sigma}_H \\ \boldsymbol{\varepsilon}_H &= \frac{1}{3}\mathrm{tr}(\boldsymbol{\varepsilon})\mathbf{I}, \qquad & \boldsymbol{\varepsilon}_D &= \boldsymbol{\varepsilon} - \boldsymbol{\varepsilon}_H \end{aligned} \tag{2.48}$$

and inserting (2.48) along with (2.47) into (2.46) yields

$$\begin{aligned} \boldsymbol{\sigma}_H(t) &= 3K(t) * \mathrm{d}\boldsymbol{\varepsilon}_H(t) \\ \boldsymbol{\sigma}_D(t) &= 2\mu(t) * \mathrm{d}\boldsymbol{\varepsilon}_D(t) \end{aligned} \tag{2.49}$$

with the time-dependent bulk modulus $K(t)$ and shear modulus $\mu(t)$

$$\begin{aligned} K(t) &:= K F_1(t) + \frac{2}{3}\mu\,(F_2(t) - F_1(t)) \\ \mu(t) &:= \mu\, F_2(t) \,. \end{aligned} \tag{2.50}$$

The relaxation functions' (2.50) labeling as time-dependent moduli already induces the existence of a correspondence between them and their elastic counterparts. Transforming (2.49) to the Laplace domain gives

$$\begin{aligned} \hat{\boldsymbol{\sigma}}_H(s) &= 3\hat{K}(s)\, s\hat{\boldsymbol{\varepsilon}}_H(s) \\ \hat{\boldsymbol{\sigma}}_D(s) &= 2\hat{\mu}(s)\, s\hat{\boldsymbol{\varepsilon}}_D(s) \,. \end{aligned}$$

Considering the time-independent material behavior (2.28), Hooke's law in Laplace domain reads as

$$\begin{aligned}\hat{\boldsymbol{\sigma}}_H(s) &= 3K\,\hat{\boldsymbol{\varepsilon}}_H(s)\\ \hat{\boldsymbol{\sigma}}_D(s) &= 2\mu\,\hat{\boldsymbol{\varepsilon}}_D(s)\end{aligned}$$

which yields the *elastic-viscoelastic correspondence principle*

$$\begin{aligned}K &\Longleftrightarrow \hat{K}(s)\,s\\ \mu &\Longleftrightarrow \hat{\mu}(s)\,s\,.\end{aligned} \tag{2.51}$$

The correspondence principle states that if a Laplace transformed elastodynamic solution is known, the Laplace transformed solution of the corresponding viscoelastic problem can be found by replacing the elastic constants according to (2.51). As it will be shown in chapter 5 the correspondence principle is of great benefit within a boundary element formulation.

There exist materials which exhibit different characteristics with respect to a hydrostatic strain state, and a deviatoric strain state. For instance, polymers react almost elastic for compression strain while they behave viscoelastic for shear strain. In contrast, no distinction between hydrostatic and deviatoric behavior can be made for some other materials like, e.g., concrete. Thus, the two relaxation functions $K(t)$ and $\mu(t)$ are not just essential from a theoretical point of view but are required also for practical needs.

As mentioned previously the integral representation has a differential representation equivalence which is more favorable in this context. To obtain a differential representation in accordance to (2.49), first, two time differential operators are defined

$$\mathcal{P}_i^K := \sum_{k=0}^{K} p_k^{(i)} \frac{\mathrm{d}^k}{\mathrm{d}t^k}\,, \qquad \mathcal{Q}_i^K := \sum_{k=0}^{K} q_k^{(i)} \frac{\mathrm{d}^k}{\mathrm{d}t^k}\,. \tag{2.52}$$

In (2.52), $p_k^{(i)}$ and $q_k^{(i)}$ denote some real valued material parameters whereby the superscript i indicates whether the hydrostatic or deviatoric part is under consideration. Thus, the differential stress-strain relation reads as

$$\begin{aligned}(\mathcal{P}_H^N \boldsymbol{\sigma}_H)(t) &= (\mathcal{Q}_H^M \boldsymbol{\varepsilon}_H)(t)\\ (\mathcal{P}_D^N \boldsymbol{\sigma}_D)(t) &= (\mathcal{Q}_D^M \boldsymbol{\varepsilon}_D)(t)\end{aligned} \tag{2.53}$$

with the numbers of material parameters $N, M \in \mathbb{N}$. This differential form of the material model may be imagined as a generalization of the Poynting model given in (2.38) but, of course, has probably no rheological representation. Applying a Laplace transform to (2.53) leads to

$$\begin{aligned}\hat{P}_H^N(s)\,\hat{\boldsymbol{\sigma}}_H(s) &= \hat{Q}_H^M(s)\,\hat{\boldsymbol{\varepsilon}}_H(s)\\ \hat{P}_D^N(s)\,\hat{\boldsymbol{\sigma}}_D(s) &= \hat{Q}_D^M(s)\,\hat{\boldsymbol{\varepsilon}}_D(s)\end{aligned} \tag{2.54}$$

with the polynomials

$$\hat{P}_i^K(s) = \sum_{k=0}^{K} p_k^{(i)} s^k\,, \qquad \hat{Q}_i^K(s) = \sum_{k=0}^{K} q_k^{(i)} s^k \tag{2.55}$$

representing the Laplace transformed operators $\mathcal{P}$ and $\mathcal{Q}$. Note that in (2.54), it is assumed that the initial conditions of stresses and strains fulfill the relations

$$\sum_{k=1}^{M}\sum_{i=1}^{k} p_k^{(H)} s^{i-1} \frac{\mathrm{d}^{k-i}}{\mathrm{d}t^{k-i}} \boldsymbol{\sigma}_H(0) = \sum_{k=1}^{M}\sum_{i=1}^{k} q_k^{(H)} s^{i-1} \frac{\mathrm{d}^{k-i}}{\mathrm{d}t^{k-i}} \boldsymbol{\varepsilon}_H(0)$$
$$\sum_{k=1}^{N}\sum_{i=1}^{k} p_k^{(D)} s^{i-1} \frac{\mathrm{d}^{k-i}}{\mathrm{d}t^{k-i}} \boldsymbol{\sigma}_D(0) = \sum_{k=1}^{N}\sum_{i=1}^{k} q_k^{(D)} s^{i-1} \frac{\mathrm{d}^{k-i}}{\mathrm{d}t^{k-i}} \boldsymbol{\varepsilon}_D(0)$$

which, again, are just a more general form of (2.45). With the assumption above the two representations of the viscoelastic constitutive equations (2.49) and (2.53) are equivalent and consequently

$$3s\hat{K}(s) = \frac{\hat{Q}_H^M(s)}{\hat{P}_H^M(s)}, \qquad 2s\hat{\mu}(s) = \frac{\hat{Q}_D^N(s)}{\hat{P}_D^N(s)}. \tag{2.56}$$

Generalization of the constitutive equations. To achieve a good agreement of the constitutive law (2.49) with the behavior of existing materials, usually, a large number of material parameters for the relaxation functions (2.56) is needed. Those parameters must be determined by curve fitting of measured data which, obviously, limits the practical application of the stated constitutive law considerably. By introducing fractional time derivatives the number of required material parameters can be reduced significantly. The idea of differentiation and integration of non-integer order has a quite long tradition and goes back to the days of Leibnitz and L'Hospital. A survey of the history of the so-called *Fractional Calculus* is, e.g., given by Ross [102, 103]. A profound application of fractional derivatives to viscoelasticity was given by Bagley & Torvik [6]. Further, the same authors developed constraints on the parameters that preserve the consistency with thermodynamic principles [7]. More recently, the work of Rossikhin & Shitikova [104] serves as a comprehensive review on this topic. For a general overview of the applications of Fractional Calculus to various scientific areas the book of Oldham & Spanier [92] is recommended. Finally, a rigorous mathematical treatise is given by Podlubny [96].

For later purpose it is sufficient to formulate the constitutive equations in Laplace domain which, fortunately, simplifies the use of fractional derivatives considerably. Opposite to the complicated time domain definitions of fractional derivatives [96], the Laplace transform reveals the useful result

$$\left(\mathscr{L}\frac{\mathrm{d}^{\gamma} f}{\mathrm{d}t^{\gamma}}\right)(s) = s^{\gamma}\left(\mathscr{L} f\right)(s) = s^{\gamma}\hat{f}(s), \qquad \gamma \in \mathbb{C}. \tag{2.57}$$

For sake of simplicity, any initial conditions are assumed to vanish in the expression above. Using (2.57) yields a more general expression of the polynomials (2.55)

$$\hat{P}_{i,\gamma}^K(s) = \sum_{k=0}^{K} p_k^{(i)} s^{\gamma_i(k)}, \qquad \hat{Q}_{i,\gamma}^K(s) = \sum_{k=0}^{K} q_k^{(i)} s^{\gamma_i(k)}.$$

Hence, the relaxation functions (2.56) become in their most general form

$$3s\hat{K}(s) = \frac{\hat{Q}^M_{H,\beta}(s)}{\hat{P}^M_{H,\alpha}(s)}, \qquad 2s\hat{\mu}(s) = \frac{\hat{Q}^N_{D,\beta}(s)}{\hat{P}^N_{D,\alpha}(s)} \tag{2.58}$$

whereas the non-integer differentiation orders $\alpha_i(k)$, and $\beta_i(k)$ are restricted to the interval $[0,2)$. Basically, expression (2.58) marks the end of the elaboration of general linear viscoelastic constitutive laws. But, since (2.58) is derived only formally, it is left to investigate the constraints of the material parameters in general and the constraints of the differential orders $\alpha_i(k)$ and $\beta_i(k)$ in particular. For special cases those constraints are given in [7] while for the general case it is suggested that $\alpha_i(k) = \beta_i(k)$ yields the best results [96].

The model which is used within this thesis forms a generalization of the already mentioned Poynting model and reads as

$$\hat{\boldsymbol{\sigma}}_H(s) = 3K\frac{1+q^{(H)}s^{\beta_H}}{\left(1+p^{(H)}s^{\alpha_H}\right)s}\, s\hat{\boldsymbol{\varepsilon}}_H$$
$$\hat{\boldsymbol{\sigma}}_D(s) = 2\mu\frac{1+q^{(D)}s^{\beta_D}}{\left(1+p^{(D)}s^{\alpha_D}\right)s}\, s\hat{\boldsymbol{\varepsilon}}_D\,.$$

Aiming at a viscoelastic constitutive law for a solid it follows that the initial moduli $K(0)$ and $\mu(0)$ have to be positive and finite, i.e., $K(0), \mu(0) \in (0,\infty)$. Therefore, $\alpha_H = \beta_H$ and $\alpha_D = \beta_D$ must hold. This could be easily proven by using the *initial value theorem* [33]. For instance, the initial bulk modulus is

$$K(0) = \lim_{s\to\infty} s\hat{K}(s) = K\lim_{s\to\infty}\frac{s^{-\alpha_H}+q^{(H)}s^{\beta_H-\alpha_H}}{s^{-\alpha_H}+p^{(H)}} = \begin{cases} 0 & \alpha_H > \beta_H \\ K\frac{q^{(H)}}{p^{(H)}} & \alpha_H = \beta_H \\ \infty & \alpha_H < \beta_H \end{cases}.$$

Doing so analogously for the initial shear modulus $\mu(0)$ the relation $\alpha_D = \beta_D$ is obtained. Thus, the correspondence principle for the generalized Poynting model reads as

$$3K \Longleftrightarrow 3K\frac{1+q^{(H)}s^{\alpha_H}}{1+p^{(H)}s^{\alpha_H}}, \qquad 2\mu \Longleftrightarrow 2\mu\frac{1+q^{(D)}s^{\alpha_D}}{1+p^{(D)}s^{\alpha_D}}\,. \tag{2.59}$$

According to (2.33) and using (2.59), the initial compressional and shear wave velocities for a viscoelastic material are

$$c_{1v} = \sqrt{\frac{K\frac{q^{(H)}}{p^{(H)}} + \frac{4}{3}\mu\frac{q^{(D)}}{p^{(D)}}}{\varrho_0}} \qquad \text{and} \qquad c_{2v} = \sqrt{\frac{\mu\frac{q^{(D)}}{p^{(D)}}}{\varrho_0}}\,. \tag{2.60}$$

Governing equations. Closing this section, finally, an abstract operator notation[4] for the system of viscoelastodynamics is introduced. Since the time-dependent relaxation functions can be interpreted as time-dependent moduli a generalized Lamé-Navier operator (2.34) is formulated

$$\mathcal{L} = -\left(\lambda(t) + \mu(t)\right) \nabla\nabla\cdot - \mu(t)\Delta \tag{2.61}$$

exhibiting the relaxation functions $\lambda(t)$ and $\mu(t)$, respectively. Therefore, the governing equation reads as

$$\left(\mathcal{L} * \mathrm{d}\mathbf{u}\right)(\mathbf{x},t) + \varrho_0 \frac{\partial^2}{\partial t^2}\mathbf{u}(\mathbf{x},t) = \mathbf{b}(\mathbf{x},t) \tag{2.62}$$

with the asterisk $*$, again, denoting the convolution integral in time. The expression above is obviously not a pure differential equation. In fact, it is an integro-differential equation due to the convolution integral in time. Thus, the time-dependent representation (2.62) is not suitable to be treated via a Boundary Element formulation. The situation changes if the Laplace transform of (2.62) is considered. Since the convolution becomes a multiplication one ends up with the simple expression

$$\left(\left(s\hat{\mathcal{L}} + \varrho_0 s^2\right)\hat{\mathbf{u}}\right)(\mathbf{x},s) = \hat{\mathbf{b}}(\mathbf{x},s) \tag{2.63}$$

where the Laplace transformed Lamé-Navier operator is given by

$$\hat{\mathcal{L}} = -\left(\hat{\lambda}(s) + \hat{\mu}(s)\right) \nabla\nabla\cdot - \hat{\mu}(s)\Delta\,.$$

Again, (2.63) depicts clearly the existence of the correspondence principle since it exhibits the same form as the Laplace transformed system of elastodynamics (2.36). Therefore, (2.63) is fitting perfectly into a Boundary Element formulation being proposed in the forthcoming chapters. Finally, it is left to note that the Lamé parameter $\hat{\lambda}(s)$ is consistently given by

$$\hat{\lambda}(s) = \hat{K}(s) - \frac{2}{3}\hat{\mu}(s)\,.$$

Quasi-static viscoelasticity. Beside the modeling of wave propagation phenomena the description of creep processes is of great importance within many engineering applications. Those processes are modeled using a time-dependent material law but a static balance law. Using the static equilibrium, i.e., neglecting the inertia terms in (2.22), yields a quasi-static viscoelastic model. In accordance to (2.62) the governing equation then reads as

$$\left(\mathcal{L} * \mathrm{d}\mathbf{u}\right)(\mathbf{x},t) = \mathbf{b}(\mathbf{x},t)\,.$$

[4] The time-domain formulation is not given in a pure operator form since there is not one operator applied to the displacement field but two operators, the integro-differential operator and the time-derivative operator, respectively. An appropriate and complete time-domain operator definition is a difficult task and omitted herein since the formulation (2.62) is not considered any further.

Again, it is advantageous to use the Laplace transform of the above expression

$$\left(s\hat{\mathcal{L}}\hat{\mathbf{u}}\right)(\mathbf{x},s) = \hat{\mathbf{b}}(\mathbf{x},s)$$

which reveals clearly the similarity to the system of elastostatics (2.37).

2.4 Boundary value problems

The mathematical models for the considered physical problems described by the equations given in sections 2.1, 2.2, and 2.3 are stated as boundary value problems. Since the underlying partial differential equations are usually termed as being of *elliptic*, *parabolic*, or *hyperbolic* type the according boundary value problem is either an elliptic, a parabolic, or a hyperbolic boundary value problem. Elliptic boundary value problems occur mainly for stationary problems. Within this context the Poisson equation, the system of elastostatics as well as any Laplace- or Fourier-transformed system are formulated as an elliptic boundary value problem. Contrary to that, all time-dependent problems described within this work refer to hyperbolic boundary value problems. The last type, the parabolic boundary value problem, is not considered within this thesis and, therefore, omitted in the following. For a distinction of different types of partial differential equations the book of Sommerfeld [117] should be mentioned. A detailed treatment of boundary value problems can be found in the book of Reddy [98].

2.4.1 Elliptic boundary value problems

As already stated, all physical problems considered in this thesis are described within the three dimensional Euclidean space $\mathbb{R}^3$. The domain for which an underlying partial differential is defined is denoted by Ω being a subset of the three dimensional space, i.e., $\Omega \subset \mathbb{R}^3$. Unless mentioned otherwise, the domain Ω is assumed to be bounded. This means that it can be embedded into a full sphere $B_R(\mathbf{y}) \coloneqq \{\mathbf{x} \in \mathbb{R}^3 : |\mathbf{y}-\mathbf{x}| < R\}$ of radius $R > 0$ such that $\Omega \subset B_R(\mathbf{0})$ holds. The domain's boundary is denoted as Γ. It forms a two dimensional closed surface and contains the outward unit normal vector $\mathbf{n}$. In addition, the union of the domain Ω with its boundary Γ is called closure and is symbolized by $\overline{\Omega}$.

For the unique solvability of static or frequency dependent problems the underlying partial differential equations have to meet certain prescribed boundary values. The governing equations given in the previous sections describe the physical problem either in terms of the acoustic pressure p or in terms of the displacement field $\mathbf{u}$. In order to use an unified notation both quantities are abstracted by the variable u in the following. Moreover, u shall also represent any Laplace (or Fourier) transform whereas the parameter s (or ω) is skipped throughout this section as long as it is not mandatory for the formulation of the following

boundary value problems. In this abstract setting, the partial differential equation reads as

$$(\mathcal{L}u)(\tilde{\mathbf{x}}) = f(\tilde{\mathbf{x}}), \qquad \forall \tilde{\mathbf{x}} \in \Omega \tag{2.64}$$

where $\mathcal{L}$ represents an elliptic partial differential operator with constant coefficients of second order and f is a given inhomogeneity. Again, the operator $\mathcal{L}$ may contain also some frequency ω. Note that if u_0 is a solution of the homogeneous problem $\mathcal{L}u_0 = 0$ then the superposition $u_C = u + Cu_0$ with $C \in \mathbb{R}$ is also a solution of the partial differential equation (2.64).

Now, to ensure the uniqueness of a solution it is necessary to demand that the partial differential equation meet certain data on the boundary Γ. In case of an acoustic fluid these boundary data can be either the acoustic pressure, the flux or some sound impedances, respectively. For an elastic/viscoelastic solid, usually, the displacements or surface tractions are prescribed. In the following, the first kind of boundary data (sound pressure and displacement field) are subsumed under the more general term *Dirichlet data* while the remaining data are labeled as *Neumann data* [120]. Hence, if the prescribed boundary values depend only on the values the function u takes on the boundary a Dirichlet boundary value problem can be formulated

$$\begin{aligned} (\mathcal{L}u)(\tilde{\mathbf{x}}) &= f(\tilde{\mathbf{x}}) && \forall \tilde{\mathbf{x}} \in \Omega \\ u_\Gamma(\mathbf{y}) &= g_D(\mathbf{y}) && \forall \mathbf{y} \in \Gamma \end{aligned} \tag{2.65}$$

with a given function g_D. In (2.65) and in the following, u_Γ explicitly denotes only the boundary values of u and represents the trace of u. This trace is defined as the limit

$$u_\Gamma(\mathbf{x}) = \operatorname{Tr} u(\tilde{\mathbf{x}}) \coloneqq \lim_{\Omega \ni \tilde{\mathbf{x}} \to \mathbf{x} \in \Gamma} u(\tilde{\mathbf{x}}) \,. \tag{2.66}$$

Here, the distinction between u inside the domain and u_Γ on the boundary is mainly made for clarity. Moreover, u_Γ and u differ from a mathematical point of view since they feature not the same regularity requirements [120].

Contrary to the Dirichlet boundary value problem, a Neumann boundary value problem arises if the boundary data are prescribed only in terms of the Neumann data. These Neumann data have to be defined first. In case of the acoustic fluid the flux is given by the normal derivative of the pressure on the boundary

$$q(\mathbf{y}) = \lim_{\Omega \ni \tilde{\mathbf{x}} \to \mathbf{y} \in \Gamma} [\nabla p(\tilde{\mathbf{x}}) \cdot \mathbf{n}(\mathbf{y})] \,. \tag{2.67}$$

Equivalent, the surface tractions of an elastic solid are

$$\mathbf{t}(\mathbf{y}) = \lim_{\Omega \ni \tilde{\mathbf{x}} \to \mathbf{y} \in \Gamma} [\boldsymbol{\sigma}(\tilde{\mathbf{x}}) \cdot \mathbf{n}(\mathbf{y})] \,. \tag{2.68}$$

Since the Cauchy stress tensor depends on the displacement field the two expressions (2.67) and (2.68) can be considered as mappings from the pressure onto the surface fluxes

and, from the displacements onto the surface tractions. Thus, the Neumann data q_Γ read in its abstract form as

$$q_\Gamma(\mathbf{y}) = (\mathcal{T}u)(\mathbf{y}) \qquad \forall \mathbf{y} \in \Gamma \tag{2.69}$$

where the operator $\mathcal{T}$ represents either the normal derivative in case of an acoustic fluid or the stress-strain relation based on Hooke's law in elasticity. Again, the boundary data q_Γ differ in its regularity requirements from the data q within the domain and, therefore, are clearly distinguished by that. It is worth to mention that the mapping (2.69) is not necessarily unique. For instance, on edges and/or corners of the boundary surface no normal vector can be defined and, therefore, the Neumann data q_Γ cannot be measured. Within this thesis it is assumed that the boundary is at least piecewise smooth such that the operation (2.69) is well-defined *almost everywhere*.

Using the definition of the Neumann data q_Γ the pure Neumann boundary value problem reads as

$$\begin{aligned} (\mathcal{L}u)(\tilde{\mathbf{x}}) &= f(\tilde{\mathbf{x}}) \qquad && \forall \tilde{\mathbf{x}} \in \Omega \\ q_\Gamma(\mathbf{y}) &= g_N(\mathbf{y}) \qquad && \forall \mathbf{y} \in \Gamma \end{aligned} \tag{2.70}$$

for some given function g_N.

Additionally, if $\mathcal{L}$ corresponds to a static problem the *solvability condition* [120]

$$\int_\Omega f(\tilde{\mathbf{x}}) u_\mathcal{R} \, \mathrm{d}\tilde{\mathbf{x}} + \int_\Gamma g_N(\mathbf{y}) u_{\mathcal{R}_\Gamma} \, \mathrm{d}s_\mathbf{y} = 0$$

has to be fulfilled by the functions f and g_N. In the expression above, $u_\mathcal{R}$ is from the space of rigid body motions $\mathcal{R}$ and represents a non-trivial solution of the homogeneous Neumann boundary value problem

$$\mathcal{L}u_\mathcal{R} = 0 \quad \wedge \quad \mathcal{T}u_\mathcal{R} = 0 \,. \tag{2.71}$$

Hence, also $u_C = u + Cu_\mathcal{R}$ is a solution of (2.70) indicating that the Neumann boundary value problem is unique up to the rigid body motions only.

The spaces of rigid body motions are given by

$$\mathcal{R} = \mathrm{span}\{1\} \tag{2.72}$$

for the Poisson equation, and by

$$\mathcal{R} = \mathrm{span}\left\{ \begin{bmatrix} 1 \\ 0 \\ 0 \end{bmatrix}, \begin{bmatrix} 0 \\ 1 \\ 0 \end{bmatrix}, \begin{bmatrix} 0 \\ 0 \\ 1 \end{bmatrix}, \begin{bmatrix} -x_2 \\ x_1 \\ 0 \end{bmatrix}, \begin{bmatrix} 0 \\ -x_3 \\ x_2 \end{bmatrix}, \begin{bmatrix} x_3 \\ 0 \\ -x_1 \end{bmatrix} \right\} \tag{2.73}$$

for elasticity problems. Functions from the space of constant functions (2.72) obviously fulfill (2.71) and induces zero pressure and zero fluxes. In elasticity functions from the space (2.73) induces zero strains $\boldsymbol{\varepsilon}(\mathbf{u}_\mathcal{R}) = \mathbf{0}$ and, therefore, zero tractions. The space of

rigid body motions (2.73) contains three rigid body translations as well as as three infinitesimal rigid body rotations. Note that one has to restrict the rotations to be infinitesimal small since finite rotations induce no zero strains in a linear setting.

The last considered boundary value problem is a mixture of the previous ones and, thus, denoted as mixed boundary value problem

$$\begin{aligned} (\mathcal{L}u)(\tilde{\mathbf{x}}) &= f(\tilde{\mathbf{x}}) && \forall \tilde{\mathbf{x}} \in \Omega \\ u_\Gamma(\mathbf{y}) &= g_D(\mathbf{y}) && \forall \mathbf{y} \in \Gamma_D \\ q_\Gamma(\mathbf{y}) &= g_N(\mathbf{y}) && \forall \mathbf{y} \in \Gamma_N \, . \end{aligned} \tag{2.74}$$

Thereby, the boundary $\Gamma = \Gamma_D \cup \Gamma_N$ is decomposed into two non-overlapping subsets Γ_D and Γ_N on which the Dirichlet data g_D and the Neumann data g_N are prescribed, respectively. Since $\Gamma_D \cap \Gamma_N = \emptyset$ no data of Dirichlet and Neumann type can be prescribed at the same location, at least for scalar problems. In elasticity, the situation slightly changes. There, it might happen that at certain locations a Dirichlet datum for the i-th direction is prescribed while a Neumann datum is given in the j-th direction. Thus, in elasticity the subsets $\Gamma_{D,i}$ and $\Gamma_{N,j}$ contain an additional index denoting the direction of the respective given data. Nevertheless, it is obvious that for every direction $\Gamma = \Gamma_{D,i} \cup \Gamma_{N,i}$ and $\Gamma_{D,i} \cap \Gamma_{N,i} = \emptyset$ must hold. As well as the Neumann boundary value problem (2.70) the mixed boundary value problem (2.74) is not necessarily uniquely solvable. If no Dirichlet data are prescribed in a certain direction the system exhibit the according rigid body motions since $\Gamma_{D,i} = \emptyset$ and $\Gamma = \Gamma_{N,i}$ holds.

2.4.2 Hyperbolic boundary value problems

Contrary to the elliptic boundary value problem as discussed previously the hyperbolic systems exhibit a time-dependency in addition to the spatial dimensions. As before the unknown state variable will be abstracted by u and becomes now a function of space and time

$$u = u(\tilde{\mathbf{x}}, t), \qquad \forall \tilde{\mathbf{x}} \in \overline{\Omega}, t \in [0, \infty) \, .$$

Again, $\overline{\Omega}$ denotes the bounded domain $\Omega \subset \mathbb{R}^3$ together with its closed boundary surface Γ. As already mentioned, all presented physical models are formulated within a linearized setting. Hence, a distinction between a reference configuration and the current configuration is dispensable because in the linear case both configurations coincide. It is common to combine the spatial and time variable into the pair $(\tilde{\mathbf{x}}, t)$ which determines an event in the half-infinite space-time cylinder $\overline{\Omega} \times [0, \infty)$ uniquely.

In contrast to the elliptic boundary value problem, the hyperbolic boundary value problem is well-posed since in addition to spatial boundary conditions the solution has also to meet the initial boundary conditions. Now, to continue with the abstract formulation of the

hyperbolic boundary value problem the hyperbolic differential equation shall be written as

$$\left[\left(\mathcal{L}+\varrho_0\frac{\partial^2}{\partial t^2}\right)u\right](\tilde{\mathbf{x}},t)=f(\tilde{\mathbf{x}},t)\qquad\forall(\tilde{\mathbf{x}},t)\in\Omega\times[0,\infty) \tag{2.75}$$

where, again, $\mathcal{L}$ denotes an elliptic partial differential operator of second order and f represents either a source term or an internal body force. Further, it is assumed that $\mathcal{L}$ exhibit no time-dependency. At this point, a notational inconsistency must be mentioned: Unfortunately, the viscoelastodynamic system (2.62) does not fit into the set of appropriate partial differential equations since it is in fact no partial differential equation but an integro-differential equation. This is due to the properties of the material tensor (2.47) which, finally, result in an integro-differential operator. An integro-differential equation marks somehow a generalization of a partial differential equation so that an introduction of an abstract integro-differential operator $\mathcal{H}$ would be more accurate. Then, the governing equations would take the more general form $(\mathcal{H}*\mathrm{d}u)(\tilde{\mathbf{x}},t)=f(t)$. This equation reveals the same hyperbolic characteristics as the partial differential equation (2.75). Therefore, an equivalent hyperbolic boundary value problem could be established for this equation. Nevertheless, as an operator $\mathcal{H}$ is not explicit defined within this work and as this operator does not affect the proper formulation of the boundary value problem the more special case of an hyperbolic partial differential equation is treated herein.

Equivalent to the elliptic boundary value problem the prescribed data can be either of pure Dirichlet or pure Neumann type. For brevity, here only the mixed boundary value problem is considered

$$\begin{aligned}\left[\left(\mathcal{L}+\varrho_0\frac{\partial^2}{\partial t^2}\right)u\right](\tilde{\mathbf{x}},t)&=f(\tilde{\mathbf{x}},t) && \forall(\tilde{\mathbf{x}},t)\in\Omega\times(0,\infty)\\ u_\Gamma(\mathbf{y},t)&=g_D(\mathbf{y},t) && \forall(\mathbf{y},t)\in\Gamma_D\times(0,\infty)\\ q_\Gamma(\mathbf{y},t)&=g_N(\mathbf{y},t) && \forall(\mathbf{y},t)\in\Gamma_N\times(0,\infty)\end{aligned} \tag{2.76}$$

where, again, u_Γ and q_Γ denote the inner fields' traces to the boundary Γ, and g_D and g_N are the prescribed boundary data, respectively. While the prescribed data exhibit a time-dependency their respective boundaries do not, i.e., Γ_D and Γ_N are considered to be constant in time and do not change their types with evolving time.

The above set of constraints is not sufficient since it lacks the initial conditions which are usually formulated in terms of the state variable u and its velocity $\dot{u}$ at the initial time $t=0$. The boundary value problem (2.76) is not defined for times $t<0$. Hence, the first time derivative of u is not properly defined for $t=0$ which motivates the use of traces

$$u(\tilde{\mathbf{x}},0^+):=\lim_{\substack{\tau\to0\\\tau>0}}u(\tilde{\mathbf{x}},\tau)\,,\qquad\dot{u}(\tilde{\mathbf{x}},0^+):=\lim_{\substack{\tau\to0\\\tau>0}}\dot{u}(\tilde{\mathbf{x}},\tau)\,.$$

The necessary initial conditions are then formulated as

$$\begin{aligned}u(\tilde{\mathbf{x}},0^+)&=u_0(\tilde{\mathbf{x}}) && \forall\tilde{\mathbf{x}}\in\Omega\\ \dot{u}(\tilde{\mathbf{x}},0^+)&=u_1(\tilde{\mathbf{x}}) && \forall\tilde{\mathbf{x}}\in\Omega\,.\end{aligned} \tag{2.77}$$

Eqns. (2.76) and (2.77) together form the complete set of equations any solution has to meet.

3 BOUNDARY INTEGRAL EQUATIONS

The previous chapter was devoted to the development of partial differential equations (and one integro-differential equation) as well as to the formulation of adequate boundary value problems. In this chapter, those problem statements are transformed to equivalent boundary integral equations. Again, the derivation of boundary integral equations is done mostly in an abstract setting and it is split into several parts. At first, appropriate representation formulae are deduced which build the basis for the integral operators introduced afterwards. Finally, the obtained boundary integral equations are formulated via weighted residuals resulting in the so-called symmetric Galerkin formulation.

Nevertheless, the derivation of the boundary integral formulation given herein is not based on rigorous mathematical proofs but depicts rather a simplified engineering approach. A well-founded mathematical treatment in case of elliptic problems is given in the textbooks of Steinbach [120], Sauter & Schwab [107], and, probably most recent, of Hsiao & Wendland [63], respectively. A treatment of time-dependent problems may be found in the works of Ha-Duong [53] for scalar problems and of Chudinovich [26–28] for elastodynamic problems. For an introduction from an engineering point of view the books of Hartmann [59], Gaul *et al.* [41], and Bonnet [18] are recommended. Finally, integral formulations for hyperbolic problems may be found, e.g., in the books of Achenbach [2] and Domínguez [34].

3.1 Representation formulae

A representation formula is an integral statement of the underlying partial differential equation. Thereby, the sought-after solution is represented by its boundary data, source terms and, in case of hyperbolic problems, by some initial values only. An almost indispensable tool for the derivation of representation formulae are identities being commonly denoted as *Green's identities* or *reciprocity theorems*. While the first labeling is more common for mathematicians the second one is the term engineers mostly prefer, especially within the treatment of elasticity problems. Here, both termini are used equally. Further, closely connected to the concept of representation formulae is the term *fundamental solution* which is introduced and defined in this section as well.

Elliptic representation formulae. Probably the simplest case to deal with is the Poisson equation

$$\mathcal{L}u(\mathbf{x}) = f(\mathbf{x}) \qquad \forall \mathbf{x} \in \Omega \subset \mathbb{R}^3 \tag{3.1}$$

with $\mathcal{L} = -\Delta$ by what Green's second identity will be deduced exemplary. This equation exhibits with the Laplacian the most simple second order differential operator such that it serves as an adequate introductory example. Afterwards this approach is augmented to the more general case of self-adjoint linear partial differential operators of second order.

As a starting point serves the divergence theorem

$$\int_\Omega \nabla \cdot \mathbf{g}(\mathbf{x}) \, \mathrm{d}\mathbf{x} = \int_\Gamma \mathbf{g}(\mathbf{y}) \cdot \mathbf{n}(\mathbf{y}) \, \mathrm{d}s_\mathbf{y}, \qquad \forall \mathbf{x} \in \Omega,\ \mathbf{y} \in \Gamma \tag{3.2}$$

for an arbitrary but sufficiently differentiable vector function $\mathbf{g}$ and a sufficiently regular boundary Γ. The subscript $\mathbf{y}$ in the surface integral on the right hand side denotes that all integrations over the surface s have to be performed with respect to the variable $\mathbf{y}$. Now, the vector function $\mathbf{g}$ may be thought as a composition of a scalar function's gradient with another scalar function such that $\mathbf{g} := \nabla u\, v$. Then, following the product rule the divergence of $\mathbf{g}$ becomes

$$\nabla \cdot \mathbf{g}(\mathbf{x}) = \Delta u(\mathbf{x})\, v(\mathbf{x}) + \nabla u(\mathbf{x}) \cdot \nabla v(\mathbf{x}) \tag{3.3}$$

for sufficiently differentiable functions u and v. Inserting (3.3) into (3.2) yields *Green's first identity*

$$\int_\Omega \Delta u(\mathbf{x})\, v(\mathbf{x}) \, \mathrm{d}\mathbf{x} = \int_\Gamma \frac{\partial u}{\partial \mathbf{n}(\mathbf{y})}\, v(\mathbf{y}) \, \mathrm{d}s_\mathbf{y} - \int_\Omega \nabla u(\mathbf{x}) \cdot \nabla v(\mathbf{x}) \, \mathrm{d}\mathbf{x} \tag{3.4}$$

where $\partial u / \partial \mathbf{n}(\mathbf{y}) := \nabla u \cdot \mathbf{n}(\mathbf{y})$ denotes the normal derivative of u. For another vector function $\mathbf{h} := u \nabla v$ one obtains vice versa

$$\int_\Omega u(\mathbf{x})\, \Delta v(\mathbf{x}) \, \mathrm{d}\mathbf{x} = \int_\Gamma u(\mathbf{y}) \frac{\partial v}{\partial \mathbf{n}(\mathbf{y})} \, \mathrm{d}s_\mathbf{y} - \int_\Omega \nabla u(\mathbf{x}) \cdot \nabla v(\mathbf{x}) \, \mathrm{d}\mathbf{x}\,. \tag{3.5}$$

Finally, subtracting (3.5) from (3.4) results in *Green's second identity*

$$\int_\Omega \left[\Delta u(\mathbf{x})\, v(\mathbf{x}) - u(\mathbf{x})\, \Delta v(\mathbf{x})\right] \mathrm{d}\mathbf{x} = \int_\Gamma \left[\frac{\partial u}{\partial \mathbf{n}(\mathbf{y})} v(\mathbf{y}) - u(\mathbf{y}) \frac{\partial v}{\partial \mathbf{n}(\mathbf{y})}\right] \mathrm{d}s_\mathbf{y}$$

which, at the moment, holds for the Laplacian only. Nevertheless, it can be enhanced to more general operators as well. For that purpose the Laplacian is substituted by a self-adjoint linear partial differential operator of second order $-\mathcal{L}$, and the normal derivatives are replaced by the generalized normal derivatives $\mathcal{T}$, respectively. Finally, using appropriate traces the generalized Green's second identity [69] reads as

$$\int_\Omega \left[(\mathcal{L}v)\, u - v\,(\mathcal{L}u)\right] \mathrm{d}\mathbf{x} = \int_\Gamma \left[(\mathcal{T}u)\, \mathrm{Tr}\, v - \mathrm{Tr}\, u\,(\mathcal{T}v)\right] \mathrm{d}s_\mathbf{y} \tag{3.6}$$

whereas the functions' arguments have been skipped for sake of simplicity. Note that if the operator $\mathcal{L}$ was not self-adjoint the term $\mathcal{L}v$ would have to be replaced by $\mathcal{L}^* v$ where $\mathcal{L}^*$

denotes the adjoint operator according to $\mathcal{L}$. Here, all occurring operators are self-adjoint and, therefore, this distinction is needless. For instance, the book of Stakgold [119] can be referred to for more details on adjoint operators.

If, according to (3.1), the expression $\mathcal{L}u$ is replaced by f and $\mathcal{L}v$ by f', i.e., the function v solves a similar problem with given body forces f', *Betti's reciprocity theorem* is obtained [75].

Now, a function $v(\mathbf{x}) \coloneqq U(\mathbf{x},\tilde{\mathbf{x}})$ featuring the property

$$\int_{\Omega} (\mathcal{L}_{\mathbf{x}} U)(\mathbf{x},\tilde{\mathbf{x}}) u(\mathbf{x}) \, \mathrm{d}\mathbf{x} = u(\tilde{\mathbf{x}}) \qquad \forall \tilde{\mathbf{x}} \in \Omega \tag{3.7}$$

is introduced [120] which will turned out as being the *fundamental solution* of the underlying partial differential equation. Inserting this into (3.6) and using the abbreviations $u_\Gamma = \mathrm{Tr}\, u$ and $q_\Gamma = \mathcal{T} u$ yields the representation formula

$$u(\tilde{\mathbf{x}}) = \int_{\Gamma} [q_\Gamma(\mathbf{y})(\mathrm{Tr}_{\mathbf{y}} U)(\mathbf{y},\tilde{\mathbf{x}}) - u_\Gamma(\mathbf{y})(\mathcal{T}_{\mathbf{y}} U)(\mathbf{y},\tilde{\mathbf{x}})] \, \mathrm{d}s_{\mathbf{y}} + \int_{\Omega} f(\mathbf{x}) U(\mathbf{x},\tilde{\mathbf{x}}) \, \mathrm{d}\mathbf{x} \, . \tag{3.8}$$

In (3.7) and (3.8), the operators' subscripts denote that the operators have to be applied with regard to their respective index onto the according quantities, e.g., in (3.7) all derivatives within the operator $\mathcal{L}$ are meant to be taken with respect to the variable $\mathbf{x}$.

With the screening property of the Dirac delta distribution δ [101]

$$\int_{\mathbb{R}^3} u(\mathbf{x}) \delta(\mathbf{x} - \tilde{\mathbf{x}}) \, \mathrm{d}\mathbf{x} = u(\tilde{\mathbf{x}}) \qquad \forall \tilde{\mathbf{x}} \in \mathbb{R}^3 \, , \tag{3.9}$$

the range of integration in (3.7) can be extended to the three dimensional space since Ω is a subset of $\mathbb{R}^3$, and – without loss of generality – it can be assumed that u vanishes outside the domain $\overline{\Omega}$, i.e., $u(\tilde{\mathbf{x}}) \equiv 0$ for any $\tilde{\mathbf{x}} \notin \overline{\Omega}$. Hence, equating (3.9) with (3.7) induces that the fundamental solution U solves the partial differential equation

$$(\mathcal{L}_{\mathbf{x}} U)(\mathbf{x},\tilde{\mathbf{x}}) = \delta(\mathbf{x} - \tilde{\mathbf{x}}) \qquad \forall \mathbf{x},\tilde{\mathbf{x}} \in \mathbb{R}^3$$

in a distributional sense. The fundamental solutions used within this work feature a high degree of symmetry. This is caused by the fact that, firstly, the fundamental solution is valid for the complete space $\mathbb{R}^3$ and, additionally, all considered problems are isotropic. Therefore, the fundamental solutions depend only on the distance between the two points $\mathbf{x}$ and $\tilde{\mathbf{x}}$. To emphasize this property the notation $U(\mathbf{x} - \tilde{\mathbf{x}}) = U(\mathbf{x},\tilde{\mathbf{x}})$ is preferred from now on, and it becomes immediately obvious that all integrations in (3.8) are nothing but spatial convolutions. Finally, the fundamental solution is of scalar type in case of the Poisson equation and exhibit tensorial properties in elasticity problems. There, the fundamental solutions $\mathbf{U}$ are (3×3)-tensors with components $\mathbf{U}_{ij}$, $i,j = 1,2,3$.

Hyperbolic representation formulae. Similar to the derivation of elliptic representation formulae where Green's second identity (or Betti's reciprocity theorem) serves as the starting point, for dynamic problems one uses the *dynamic reciprocity theorem*. This theorem is available for the scalar wave equation [5] as well as for elasticity problems. For elastodynamics it was given by Graffi [48] for closed domains. Later, his proof was generalized and extended to open domains by Wheeler & Sternberg [126]. For viscoelastic problems Gurtin & Sternberg [52] formulated the theorem in the case of quasi-statics and de Hoop [62] deduced it for viscoelastodynamics. Exemplary, a very brief derivation of this theorem is given for elastodynamics as well as for viscoelastodynamics. Therefore, one postulates that there exist two different states of stresses $[\boldsymbol{\sigma}(\mathbf{u}), \boldsymbol{\sigma}(\mathbf{v})]$ and of strains $[\boldsymbol{\varepsilon}(\mathbf{u}), \boldsymbol{\varepsilon}(\mathbf{v})]$ caused by two independent displacement fields $\mathbf{u}(\mathbf{x},t)$ and $\mathbf{v}(\mathbf{x},t)$ with $\mathbf{x} \in \Omega \subset \mathbb{R}^3$ and $t \in (0,\infty)$ for which

$$\int_{\Omega} \boldsymbol{\sigma}(\mathbf{u}) * \boldsymbol{\varepsilon}(\mathbf{v}) \, \mathrm{d}\mathbf{x} = \int_{\Omega} \boldsymbol{\sigma}(\mathbf{v}) * \boldsymbol{\varepsilon}(\mathbf{u}) \, \mathrm{d}\mathbf{x} \tag{3.10}$$

holds. Again, the operator $*$ denotes the convolution with respect to time

$$(\boldsymbol{\sigma} * \boldsymbol{\epsilon})(t) \coloneqq \int_0^t \boldsymbol{\sigma}(\tau) : \boldsymbol{\varepsilon}(t-\tau) \, \mathrm{d}\tau \, .$$

Using the associativity and the commutativity of the double contraction and the time convolution, respectively, the validity of (3.10) can be verified since

$$\boldsymbol{\sigma}(\mathbf{u}) * \boldsymbol{\varepsilon}(\mathbf{v}) = \overset{(4)}{\mathbf{C}} : \boldsymbol{\varepsilon}(\mathbf{u}) * \boldsymbol{\varepsilon}(\mathbf{v}) = \overset{(4)}{\mathbf{C}} : \boldsymbol{\varepsilon}(\mathbf{v}) * \boldsymbol{\varepsilon}(\mathbf{u}) = \boldsymbol{\sigma}(\mathbf{v}) * \boldsymbol{\varepsilon}(\mathbf{u})$$

holds in the elastodynamic case. Analogously, one obtains for the viscoelastic continuum by, additionally, exploiting the properties of the Stieltjes convolution

$$\boldsymbol{\sigma}(\mathbf{u}) * \boldsymbol{\varepsilon}(\mathbf{v}) = \overset{(4)}{\mathbf{C}} * \mathrm{d}\boldsymbol{\varepsilon}(\mathbf{u}) * \boldsymbol{\varepsilon}(\mathbf{v}) = \mathrm{d}\overset{(4)}{\mathbf{C}} * \boldsymbol{\varepsilon}(\mathbf{v}) * \boldsymbol{\varepsilon}(\mathbf{u}) = \boldsymbol{\sigma}(\mathbf{v}) * \boldsymbol{\varepsilon}(\mathbf{u}) \, .$$

Substituting $\boldsymbol{\varepsilon}(\mathbf{v})$ by its linear strain-displacement relation (2.20) one obtains the equality $\boldsymbol{\sigma}(\mathbf{u}) * \boldsymbol{\varepsilon}(\mathbf{v}) = \boldsymbol{\sigma}(\mathbf{u}) * \nabla\mathbf{v}$. Further, calculating the divergence of the product $\boldsymbol{\sigma} * \mathbf{v}$ yields

$$\nabla \cdot [\boldsymbol{\sigma}(\mathbf{u}) * \mathbf{v}] = \nabla \cdot \boldsymbol{\sigma}(\mathbf{u}) * \mathbf{v} + \boldsymbol{\sigma}(\mathbf{u}) * \nabla\mathbf{v} \, .$$

Inserting this into the left hand-side of (3.10) leads to

$$\int_{\Omega} \boldsymbol{\sigma}(\mathbf{u}) * \boldsymbol{\varepsilon}(\mathbf{v}) \, \mathrm{d}\mathbf{x} = \int_{\Gamma} \mathcal{T}\mathbf{u} * \operatorname{Tr}\mathbf{v} \, \mathrm{d}s_{\mathbf{x}} + \int_{\Omega} \mathbf{f}(\mathbf{u}) * \mathbf{v} \, \mathrm{d}\mathbf{x} - \int_{\Omega} \varrho_0 \ddot{\mathbf{u}} * \mathbf{v} \, \mathrm{d}\mathbf{x} \, . \tag{3.11}$$

Note that the first term on the right hand-side in (3.11) emerges from an application of the divergence theorem while the remaining terms appear due to a substitution of the stresses'

divergence by the equation of motion (2.22). Recalling the second time derivative of the convolution integral

$$\frac{\partial^2}{\partial t^2}\left\{(h*g)(t)\right\} = \ddot{h}*g + h(0)\dot{g}(t) + \dot{h}(0)g(t)\,,$$

the expression (3.11) is augmented by the initial terms $\mathbf{u}_0 = \mathbf{u}(\mathbf{x},0^+)$ and $\mathbf{u}_1 = \dot{\mathbf{u}}(\mathbf{x},0^+)$ and, finally, reads as

$$\begin{aligned}\int_\Omega \boldsymbol{\sigma}(\mathbf{u})*\boldsymbol{\varepsilon}(\mathbf{v})\,\mathrm{d}\mathbf{x} = \int_\Gamma \mathcal{T}\mathbf{u}*\operatorname{Tr}\mathbf{v}\,\mathrm{d}s_\mathbf{y} + \int_\Omega \mathbf{f}(\mathbf{u})*\mathbf{v}\,\mathrm{d}\mathbf{x} + \int_\Omega \varrho_0\left[\mathbf{u}_0\dot{\mathbf{v}} + \mathbf{u}_1\mathbf{v}\right]\mathrm{d}\mathbf{x} \\ - \int_\Omega \varrho_0 \frac{\partial^2}{\partial t^2}\left(\mathbf{u}*\mathbf{v}\right)\mathrm{d}\mathbf{x}\,.\end{aligned} \tag{3.12}$$

The expression above can be seen as the elastodynamic equivalence of the first Green's identity given in (3.4). Thus, applying the same steps to the right hand-side of (3.10) and equating the result with (3.12) yields the dynamic reciprocal theorem. Exchanging the source terms by the according hyperbolic differential operators and switching over to the more abstract operator notation the theorem

$$\begin{aligned}\int_\Gamma \mathcal{T}u*\operatorname{Tr}v\,\mathrm{d}s_\mathbf{y} + \int_\Omega \left[\left(\mathcal{L} + \varrho_0\frac{\partial^2}{\partial t^2}\right)u\right]*v\,\mathrm{d}\mathbf{x} + \int_\Omega \varrho_0\left[u_0\dot{v}(t) + u_1 v(t)\right]\mathrm{d}\mathbf{x} = \\ \int_\Gamma \operatorname{Tr}u*\mathcal{T}v\,\mathrm{d}s_\mathbf{y} + \int_\Omega \left[\left(\mathcal{L} + \varrho_0\frac{\partial^2}{\partial t^2}\right)v\right]*u\,\mathrm{d}\mathbf{x} + \int_\Omega \varrho_0\left[v_0\dot{u}(t) + v_1 u(t)\right]\mathrm{d}\mathbf{x}\end{aligned} \tag{3.13}$$

is obtained, whereas the function v has to meet the initial conditions $v_0 = v(\mathbf{x},0^+)$ and $v_1 = v(\mathbf{x},0^+)$. In accordance to the previous section the test function is chosen to be $v(\mathbf{x},t) = U(\mathbf{x}-\tilde{\mathbf{x}},t)$ such that

$$\int_0^t\int_\Omega \left[\left(\mathcal{L}_\mathbf{x} + \varrho_0\frac{\partial^2}{\partial t^2}\right)U\right](\mathbf{x}-\tilde{\mathbf{x}},t-\tau)\,u(\mathbf{x},\tau)\,\mathrm{d}\mathbf{x}\,\mathrm{d}\tau = u(\tilde{\mathbf{x}},t), \quad \forall\,(\tilde{\mathbf{x}},t)\in\Omega\times(0,\infty)$$

holds. Again the function U turns out to be a fundamental solution of the underlying partial differential equation and, again, this function behaves in its time variable analogous to its behavior for the spatial variables. Therefore, it is not depending on the absolute time t but only on the time difference $t-\tau$ which is notationally marked as $U(\mathbf{x}-\tilde{\mathbf{x}},t) = U(\mathbf{x}-\tilde{\mathbf{x}},t-\tau)$ from now on. Thus, since $u(\tilde{\mathbf{x}},t)$ can be written in terms of the Dirac distribution

$$u(\tilde{\mathbf{x}},t) = \int_0^\infty\int_{\mathbb{R}^3} u(\mathbf{x},\tau)\,\delta(\mathbf{x}-\tilde{\mathbf{x}},t-\tau)\,\mathrm{d}\mathbf{x}\,\mathrm{d}\tau$$

a hyperbolic fundamental solution is the distributional solution of

$$\left[\left(\mathcal{L}_{\mathbf{x}}+\frac{\partial^2}{\partial t^2}\right)U\right](\mathbf{x}-\tilde{\mathbf{x}},t-\tau)=\delta(\mathbf{x}-\tilde{\mathbf{x}},t-\tau)\,.$$

Physically, the fundamental solution can be interpreted as a single force acting on a certain point at a specific moment in the three dimensional space. Before that specific moment the continuum can be assumed to exhibit a quiescent past and, therefore, the fundamental solution satisfies the initial conditions $U(\mathbf{x}-\tilde{\mathbf{x}},0)=0$ and $\dot{U}(\mathbf{x}-\tilde{\mathbf{x}},0)=0$. Hence, inserting U into (3.13) yields the hyperbolic representation formula

$$\begin{aligned}u(\tilde{\mathbf{x}},t)=&\int_\Gamma\left[q_\Gamma(\mathbf{y},t)*U(\mathbf{y}-\tilde{\mathbf{x}},t)-u_\Gamma(\mathbf{y},t)*(\mathcal{T}_{\mathbf{y}}U)(\mathbf{y}-\tilde{\mathbf{x}},t)\right]\mathrm{d}s_{\mathbf{y}}\\&+\int_\Omega f(\mathbf{x},t)*U(\mathbf{x}-\tilde{\mathbf{x}},t)\,\mathrm{d}\mathbf{x}\\&+\int_\Omega\varrho_0\left[u_0\dot{U}(\mathbf{x}-\tilde{\mathbf{x}},t)+u_1U(\mathbf{x}-\tilde{\mathbf{x}},t)\right]\mathrm{d}\mathbf{x}\qquad\forall(\tilde{\mathbf{x}},t)\in\Omega\times(0,\infty)\,.\end{aligned}\tag{3.14}$$

Fundamental solutions are the main ingredients of any boundary integral formulation since they are essential for the derivation of the representation formula. Moreover, a fundamental solution is characteristic for the underlying partial differential equation and, hence, has to be deduced for every distinct partial differential operator anew. This gives raise to the assumption that a general fundamental solution for viscoelastic problems does not exist in a closed form. This is due to the material law's time-dependency. Since there exist basically infinitely many material laws (cf. Eqn. (2.46)), there exist also infinitely many integro-differential operators associated with these material models. Thus, fundamental solutions in closed form are known for some special material models only and are mostly derived for the quasi-static case. On the other hand the situation changes in Laplace- or Frequency domain. There, a fundamental solution can easily be adopted from the respective elastic fundamental solution just by making use of the correspondence principle (2.51).

3.2 Boundary integral operators

The introduced type of elliptic representation formulae state that u is determined uniquely for an internal point $\tilde{\mathbf{x}}$ just by its boundary data u_Γ, q_Γ, and the sources f. In dynamics, all quantities become time-dependent. Due to the time convolution integrals the state variable u depends on its Cauchy data time history up to the actual time t as well as on the time-dependent sources f, and the initial values u_0 and u_1. Since both the solution u in the domain and the complete Cauchy data are unknown the integral formulae presented so far are obviously unsuitable for a solution procedure. To overcome this drawback the interior point $\tilde{\mathbf{x}}$ is shifted to the boundary so that the resulting formulae contain unknown quantities on the boundary only. Referring to the stated boundary value problems given in section

2.4 there exist two possibilities to perform this shifting process. On one hand, the trace operator (2.66) can be applied to a representation formula or, otherwise, an application of the traction operator can be used to obtain a boundary integral representation. Since the aim is to establish a symmetric formulation both the trace operator and the traction operator have to be applied onto the representation formulae which, finally, results in two *boundary integral equations*. Again, the deduction of those integral equations is done for the elliptic system and the hyperbolic system separately.

Elliptic boundary integral equations. The following is mainly adopted from the textbooks of Steinbach [120] and Sauter & Schwab [107]. Applying the boundary trace to the the representation formula (3.8) yields the first integral equation

$$\begin{aligned} u_\Gamma(\mathbf{x}) = &\operatorname{Tr}_{\tilde{\mathbf{x}}} \int_\Gamma q_\Gamma(\mathbf{y}) U(\mathbf{y}-\tilde{\mathbf{x}}) \, \mathrm{d}s_\mathbf{y} - \operatorname{Tr}_{\tilde{\mathbf{x}}} \int_\Gamma u_\Gamma(\mathbf{y}) (\mathcal{T}_\mathbf{y} U)^\top (\mathbf{y}-\tilde{\mathbf{x}}) \, \mathrm{d}s_\mathbf{y} \\ &+ \operatorname{Tr}_{\tilde{\mathbf{x}}} \int_\Omega f(\bar{\mathbf{x}}) U(\bar{\mathbf{x}}-\tilde{\mathbf{x}}) \, \mathrm{d}\bar{\mathbf{x}} \qquad\qquad \forall \mathbf{x} \in \Gamma \, . \end{aligned} \tag{3.15}$$

Note that the transposed $(\mathcal{T}_\mathbf{y} U)^\top$ does not occur in (3.8). For sake of simplicity it has been omitted in the representation formula's deduction. In the following, the transposed is consequently denoted since it is evident for vector problems. More details on it can be found in the work of Kupradze [69, 70].

Next, an application of the stress operator to (3.8) gives the second integral equation

$$\begin{aligned} q_\Gamma(\mathbf{x}) = &\mathcal{T}_{\tilde{\mathbf{x}}} \int_\Gamma q_\Gamma(\mathbf{y}) U(\mathbf{y}-\tilde{\mathbf{x}}) \, \mathrm{d}s_\mathbf{y} - \mathcal{T}_{\tilde{\mathbf{x}}} \int_\Gamma u_\Gamma(\mathbf{y}) (\mathcal{T}_\mathbf{y} U)^\top (\mathbf{y}-\tilde{\mathbf{x}}) \, \mathrm{d}s_\mathbf{y} \\ &+ \mathcal{T}_{\tilde{\mathbf{x}}} \int_\Omega f(\bar{\mathbf{x}}) U(\bar{\mathbf{x}}-\tilde{\mathbf{x}}) \, \mathrm{d}\bar{\mathbf{x}} \qquad\qquad \forall \mathbf{x} \in \Gamma \, . \end{aligned} \tag{3.16}$$

Note that the integration variables within the domain integrals in (3.15) and (3.16) were exchanged by $\bar{\mathbf{x}}$ since the point $\mathbf{x}$ denotes a point on the boundary now. At this point one has to advert to the fundamental solution's behavior when the point $\mathbf{x}$ approaches the point $\mathbf{y}$. The fundamental solution gets singular. This singularity prohibits a naive commutation of the limiting processes and the integrations since the integral kernels may diverge. The term *integral kernel* is commonly used in conjunction with *integral transformations* [97]. In fact, the boundary integral equations above represent nothing else but integral transformations so that the fundamental solutions and their derivatives can be conveniently termed as integral kernels. The singularities considered here are common to all fundamental solutions used within this work and have to be taken into account carefully. Therefore, every integral in (3.15) and (3.16) will be investigated separately and will be associated with a distinctive boundary integral operator.

At first, the domain integrals are treated. There the integral kernel is made up of the fundamental solution itself and since the integral exists the trace operators and integrations

may be interchanged such that the *Newton operator of the first kind* is obtained

$$(\widehat{\mathcal{N}}_0 f)_\Omega(\mathbf{x}) := \mathrm{Tr}_{\tilde{\mathbf{x}}} \int_\Omega f(\bar{\mathbf{x}}) U(\bar{\mathbf{x}} - \tilde{\mathbf{x}}) \, \mathrm{d}\bar{\mathbf{x}} = \int_\Omega f(\bar{\mathbf{x}}) U(\bar{\mathbf{x}} - \mathbf{x}) \, \mathrm{d}\bar{\mathbf{x}} \, .$$

Consequently, the *Newton operator of the second kind* is

$$(\widehat{\mathcal{N}}_1 f)_\Omega(\mathbf{x}) := \mathcal{T}_{\tilde{\mathbf{x}}} \int_\Omega f(\bar{\mathbf{x}}) U(\bar{\mathbf{x}} - \tilde{\mathbf{x}}) \, \mathrm{d}\bar{\mathbf{x}} = \int_\Omega f(\bar{\mathbf{x}}) (\mathcal{T}_{\mathbf{x}} U)(\bar{\mathbf{x}} - \mathbf{x}) \, \mathrm{d}\bar{\mathbf{x}} \, .$$

The first boundary integral of the first boundary integral equation (3.15) exhibit the same singularity as the Newton potentials. Therefore the trace operation can be commuted with the integration. This yields the *single layer operator*

$$(\widehat{\mathcal{V}} q)_\Gamma(\mathbf{x}) := \mathrm{Tr}_{\tilde{\mathbf{x}}} \int_\Gamma q_\Gamma(\mathbf{y}) U(\mathbf{y} - \tilde{\mathbf{x}}) \, \mathrm{d}s_{\mathbf{y}} = \int_\Gamma q_\Gamma(\mathbf{y}) U(\mathbf{y} - \mathbf{x}) \, \mathrm{d}s_{\mathbf{y}} \, .$$

Up to this point the treatment of singularities is quite simple. But the remaining integrals involve differentiations with respect to their kernel functions which increase the order of singularity. This is where the problems start since one has to be much more attentive in treating those integral kernels properly. The following two integral operators will be denoted as *double layer operator* and *adjoint double layer operator*, respectively. Within the limiting process one obtains additional expressions, the so-called *integral-free terms*. Although those integral terms collapse to very simple expressions at the end, the derivation of them is rather demanding and not as obvious as it appears to be. A rigorous mathematical derivation of those terms is, again, given in the textbooks of Sauter & Schwab [107] and Steinbach [120]. While in the book of Sauter & Schwab the derivation of these terms is done quite abstract in the latter one those terms are deduced in detail for Poisson's equation. According to this deduction an appropriate definition of the double layer operators is given in the following.

The strategy of treating singularities follows often the same technique. At first, the singularity is excluded from the region of integration, and afterwards, a limiting process towards the singular point is applied. For a given $\varepsilon > 0$ the boundary Γ is split into two disjunct sets. For two points $(\mathbf{x}, \mathbf{y}) \in \Gamma$ the first set contains all points such that $|\mathbf{y} - \mathbf{x}| \geq \varepsilon$ holds while the remaining set contains the singularity, i.e., $|\mathbf{y} - \mathbf{x}| < \varepsilon$ holds. Note that in the limiting process $\varepsilon \to 0$ one tends uniformly towards the singular point. Here, this kind of limiting process is advantageous but it is not mandatory at all [125].

With the definition of the *double layer operator*

$$(\widehat{\mathcal{K}} u)_\Gamma(\mathbf{x}) := \lim_{\varepsilon \to 0} \int_{\mathbf{y} \in \Gamma : |\mathbf{y} - \mathbf{x}| \geq \varepsilon} u_\Gamma(\mathbf{y}) (\mathcal{T}_{\mathbf{y}} U)^\top (\mathbf{y} - \mathbf{x}) \, \mathrm{d}s_{\mathbf{y}} \tag{3.17}$$

one obtains for the remaining boundary integral in the first boundary integral equation

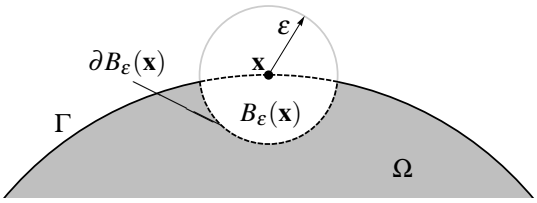

Figure 3.1: Augmented boundary Γ

(3.15)

$$\mathrm{Tr}_{\tilde{\mathbf{x}}} \int_\Gamma u_\Gamma(\mathbf{y})(\mathcal{T}_\mathbf{y} U)^\top(\mathbf{y}-\tilde{\mathbf{x}})\,\mathrm{d}s_\mathbf{y} - (\widehat{\mathcal{K}}u)_\Gamma(\mathbf{x}) = \lim_{\varepsilon\to 0} \int_{\mathbf{y}\in\Gamma:|\mathbf{y}-\mathbf{x}|<\varepsilon} u_\Gamma(\mathbf{y})(\mathcal{T}_\mathbf{y} U)^\top(\mathbf{y}-\tilde{\mathbf{x}})\,\mathrm{d}s_\mathbf{y}\,. \tag{3.18}$$

The integral on the right-hand side can be modified such that

$$\begin{aligned}\lim_{\varepsilon\to 0} \int_{\mathbf{y}\in\Gamma:|\mathbf{y}-\mathbf{x}|<\varepsilon} u_\Gamma(\mathbf{y})(\mathcal{T}_\mathbf{y} U)^\top(\mathbf{y}-\tilde{\mathbf{x}})\,\mathrm{d}s_\mathbf{y} &= u_\Gamma(\mathbf{x}) \lim_{\varepsilon\to 0} \int_{\mathbf{y}\in\Gamma:|\mathbf{y}-\mathbf{x}|<\varepsilon} (\mathcal{T}_\mathbf{y} U)^\top(\mathbf{y}-\tilde{\mathbf{x}})\,\mathrm{d}s_\mathbf{y} \\ &\quad + \lim_{\varepsilon\to 0} \int_{\mathbf{y}\in\Gamma:|\mathbf{y}-\mathbf{x}|<\varepsilon} [u_\Gamma(\mathbf{y}) - u_\Gamma(\mathbf{x})]\,(\mathcal{T}_\mathbf{y} U)^\top(\mathbf{y}-\tilde{\mathbf{x}})\,\mathrm{d}s_\mathbf{y}\,.\end{aligned}$$

The last term of the above expression contains the difference $u_\Gamma(\mathbf{y}) - u_\Gamma(\mathbf{x})$. This difference vanishes in the limit. Thus, it can be shown that the whole term tends to zero for $\varepsilon \to 0$ [120], [70]. The integration path of the remaining integral can be expressed as the difference of a contour integral and an integral over a part of a sphere (see Fig. 3.1). With the domain

$$B_\varepsilon(\mathbf{x}) := \{\mathbf{y}\in\Omega\colon\ |\mathbf{y}-\mathbf{x}| < \varepsilon\}$$

and its surface $\partial B_\varepsilon(\mathbf{x})$ this integral reads as

$$\begin{aligned}u_\Gamma(\mathbf{x}) \lim_{\varepsilon\to 0} \int_{\mathbf{y}\in\Gamma:|\mathbf{y}-\mathbf{x}|<\varepsilon} (\mathcal{T}_\mathbf{y} U)^\top(\mathbf{y}-\tilde{\mathbf{x}})\,\mathrm{d}s_\mathbf{y} &= \\ u_\Gamma(\mathbf{x}) \lim_{\varepsilon\to 0} \left(\int_{\partial B_\varepsilon(\mathbf{x})} (\mathcal{T}_\mathbf{y} U)^\top(\mathbf{y}-\tilde{\mathbf{x}})\,\mathrm{d}s_\mathbf{y} - \int_{\mathbf{y}\in\Omega:|\mathbf{y}-\mathbf{x}|=\varepsilon} (\mathcal{T}_\mathbf{y} U)^\top(\mathbf{y}-\tilde{\mathbf{x}})\,\mathrm{d}s_\mathbf{y} \right)\,.\end{aligned}$$

Using the representation formula (3.8) for $u_\Gamma(\mathbf{y}) \equiv 1$ and with $\tilde{\mathbf{x}} \in B_\varepsilon(\mathbf{x})$ due to $|\mathbf{x}-\tilde{\mathbf{x}}| < \varepsilon$ the contour integral becomes

$$\int_{\partial B_\varepsilon(\mathbf{x})} (\mathcal{T}_\mathbf{y} U)^\top(\mathbf{y}-\tilde{\mathbf{x}})\,\mathrm{d}s_\mathbf{y} = -I\,.$$

The remaining integral is defined as

$$C(\mathbf{x}) := -\lim_{\varepsilon\to 0} \int\limits_{\mathbf{y}\in\Omega:|\mathbf{y}-\mathbf{x}|=\varepsilon} (\mathcal{T}_{\mathbf{y}}U)^{\top}(\mathbf{y}-\tilde{\mathbf{x}})\,\mathrm{d}s_{\mathbf{y}} \tag{3.19}$$

such that, at the end, the trace in (3.18) becomes

$$\mathrm{Tr}_{\tilde{\mathbf{x}}} \int\limits_{\Gamma} u_{\Gamma}(\mathbf{y})(\mathcal{T}_{\mathbf{y}}U)^{\top}(\mathbf{y}-\tilde{\mathbf{x}})\,\mathrm{d}s_{\mathbf{y}} = -[I-C(\mathbf{x})]u_{\Gamma}(\mathbf{x}) + (\widehat{\mathcal{K}}u)(\mathbf{x})\,. \tag{3.20}$$

The terms I and $C(\mathbf{x})$ are scalars in case of the Poisson equation and (3×3)-matrices for elasticity models. Thereby, I represents the identity and the expression $C(\mathbf{x})$ is determined by the boundary shape at the point $\mathbf{x}$, i.e., the integral-free term depends on the solid angle at this point. Moreover, in elasticity problems it depends also on some material data. Explicit expressions for the integral-free term can be found in [41] and [81]. If the boundary Γ is at least differentiable at the point $\mathbf{x}$, $C(\mathbf{x})$ collapses to the simple expression

$$C(\mathbf{x}) = \frac{1}{2}I\,.$$

Applying the trace to the first boundary integral in the second boundary integral equation (3.16) yields

$$\mathcal{T}_{\tilde{\mathbf{x}}} \int\limits_{\Gamma} q_{\Gamma}(\mathbf{y})U(\mathbf{y}-\tilde{\mathbf{x}}) = C(\mathbf{x})q_{\Gamma}(\mathbf{x}) + (\widehat{\mathcal{K}}'q)_{\Gamma}(\mathbf{x}) \tag{3.21}$$

with the *adjoint double layer potential*

$$(\widehat{\mathcal{K}}'q)_{\Gamma}(\mathbf{x}) := \lim_{\varepsilon\to 0} \int\limits_{\mathbf{y}\in\Gamma:|\mathbf{y}-\mathbf{x}|\geq\varepsilon} q_{\Gamma}(\mathbf{y})(\mathcal{T}_{\mathbf{x}}U)(\mathbf{y}-\mathbf{x})\,\mathrm{d}s_{\mathbf{y}} \tag{3.22}$$

and the integral-free term as it is defined in (3.19). The proof of the identity (3.21) is similar to the deduction of (3.20). It is omitted herein for sake of brevity but its outline should be sketched briefly. In principle the derivation of (3.21) is more demanding than that of (3.20) since the regularity properties of q_{Γ} differ significantly from u_{Γ} which is embodied in the double layer potential (3.17). To overcome this limitation the proof is embedded into the application of Green's first identity. With its help a smoother integral kernel is obtained which can be treated rather similar to the double layer potential. Detailed derivations of (3.21) can be found in [120] and [107] for the Poisson equation and the more general case of an arbitrary scalar elliptic differential operator. In [70] the identity is deduced for elasticity problems.

The double layer potential (3.17) as well as the adjoint double layer potential (3.22) have to be considered in the sense of a *Cauchy principal value*. Nevertheless, the integral kernel in case of scalar problems depends distinctively on the normal derivative of the distance between $\mathbf{x}$ and $\mathbf{y}$. This normal derivative tends to zero when $\mathbf{x}$ approaches $\mathbf{y}$. Therefore,

the double layer potentials in scalar problems exhibit no singularities. Unfortunately, the situation changes in elasticity problems. There, the Cauchy principal value has to be used. In chapter 4, a regularization will be presented which transforms the strong singularity to a weak one.

Now, it is left to present a definition for the leftover integral in (3.16). This operator involves two differentiations of the kernel function and is denoted as *hypersingular integral operator*. Its definition is

$$(\widehat{\mathcal{D}}u)_\Gamma(\mathbf{x}) \coloneqq -\mathcal{T}_{\tilde{\mathbf{x}}} \int_\Gamma u_\Gamma(\mathbf{y})(\mathcal{T}_\mathbf{y} U)^\top(\mathbf{y}-\tilde{\mathbf{x}})\,\mathrm{d}s_\mathbf{y}\,. \tag{3.23}$$

As the name already induces, this integral operator features a hypersingularity when $\mathbf{x}$ tends to $\mathbf{y}$ and, therefore, the integral has to be understood as a *finite part* in the sense of Hadamard [54, 57]. Hence, it is obvious that the numerical treatment of this integral kernel is probably the most challenging part in the upcoming boundary element method. Fortunately, there exist regularizations of this type of singularity which will be a major topic in chapter 4.

Now, since every boundary integral in (3.15) and (3.16) is associated with an appropriate boundary integral operator the system of boundary integral equations can be written more compact

$$\begin{pmatrix} u_\Gamma \\ q_\Gamma \end{pmatrix} = \begin{pmatrix} (I-C)\widehat{\mathcal{I}} - \widehat{\mathcal{K}} & \widehat{\mathcal{V}} \\ \widehat{\mathcal{D}} & C\widehat{\mathcal{I}} + \widehat{\mathcal{K}}' \end{pmatrix} \begin{pmatrix} u_\Gamma \\ q_\Gamma \end{pmatrix} + \begin{pmatrix} \widehat{\mathcal{N}}_0 f \\ \widehat{\mathcal{N}}_1 f \end{pmatrix} \qquad \forall \mathbf{x},\mathbf{y} \in \Gamma\,. \tag{3.24}$$

The operator $\widehat{\mathcal{I}}$ above denotes the identity operator

$$(\widehat{\mathcal{I}}w)(\mathbf{x}) \coloneqq \int_\Gamma \delta(\mathbf{y}-\mathbf{x}) w(\mathbf{y})\,\mathrm{d}s_\mathbf{y}\,. \tag{3.25}$$

Moreover, the operator matrix in (3.24) is commonly denoted as *Calderón projector* $\mathcal{C}$. Since this matrix is a projector it features the identity $\mathcal{C} = \mathcal{C}^2$ by what very useful relationships between the particular integral operators are gained. More details about them and the Calderón projector are given in [120].

Hyperbolic boundary integral equations. In case of time-dependent problems the procedure to obtain a system of boundary integral equations is exactly the same as before. Again, the trace operators $\mathrm{Tr}_{\tilde{\mathbf{x}}}$ and $\mathcal{T}_{\tilde{\mathbf{x}}}$ have to be applied. But now with respect to the representation formula (3.14). Since the limiting processes are independent on the time the integral operators are defined in accordance to the elliptic case.

Thus, the single layer operator reads as

$$(\mathcal{V} * q)_\Gamma(\mathbf{x},t) \coloneqq \int_0^t \int_\Gamma q_\Gamma(\mathbf{y},\tau) U(\mathbf{y}-\mathbf{x}, t-\tau)\,\mathrm{d}s_\mathbf{y}\,\mathrm{d}\tau\,.$$

Moreover, the double layer operator is

$$(\mathcal{K} * u)_\Gamma(\mathbf{x},t) := \int_0^t \lim_{\varepsilon\to 0} \int_{\mathbf{y}\in\Gamma:|\mathbf{y}-\mathbf{x}|\geq\varepsilon} u_\Gamma(\mathbf{y},\tau)(\mathcal{T}_\mathbf{y} U)^\top(\mathbf{y}-\mathbf{x},t-\tau)\,\mathrm{d}s_\mathbf{y}\,\mathrm{d}\tau$$

and the adjoint double layer operator is

$$(\mathcal{K}' * q)_\Gamma(\mathbf{x},t) := \int_0^t \lim_{\varepsilon\to 0} \int_{\mathbf{y}\in\Gamma:|\mathbf{y}-\mathbf{x}|\geq\varepsilon} q_\Gamma(\mathbf{y},\tau)(\mathcal{T}_\mathbf{x} U)(\mathbf{y}-\mathbf{x},t-\tau)\,\mathrm{d}s_\mathbf{y}\,\mathrm{d}\tau\,.$$

Again, both the double and the adjoint double layer potential are defined as Cauchy principal value integrals. In the same manner the hypersingular operator is the finite part of

$$(\mathcal{D} * u)_\Gamma(\mathbf{x},t) := -\int_0^t \mathcal{T}_{\tilde{\mathbf{x}}} \int_\Gamma u_\Gamma(\mathbf{y},\tau)(\mathcal{T}_\mathbf{y} U)^\top(\mathbf{y}-\tilde{\mathbf{x}},t-\tau)\,\mathrm{d}s_\mathbf{y}\,\mathrm{d}\tau\,.$$

Finally, together with the Newton potentials

$$(\mathcal{N}_0 * f)_\Omega(\mathbf{x},t) := \int_0^t \int_\Omega f(\bar{\mathbf{x}},\tau)U(\bar{\mathbf{x}}-\mathbf{x},t-\tau)\,\mathrm{d}\bar{\mathbf{x}}\,\mathrm{d}\tau + \int_\Omega \varrho_0\left[u_0\dot{U}(\bar{\mathbf{x}}-\mathbf{x},t)+u_1 U(\bar{\mathbf{x}}-\mathbf{x},t)\right]\mathrm{d}\bar{\mathbf{x}}$$

and

$$(\mathcal{N}_1 * f)_\Omega(\mathbf{x},t) := \int_0^t \int_\Omega f(\bar{\mathbf{x}},\tau)(\mathcal{T}_{\bar{\mathbf{x}}} U)(\bar{\mathbf{x}}-\mathbf{x},t-\tau)\,\mathrm{d}\bar{\mathbf{x}}\,\mathrm{d}\tau + \int_\Omega \varrho_0\left[u_0(\mathcal{T}_{\bar{\mathbf{x}}}\dot{U})(\bar{\mathbf{x}}-\mathbf{x},t)+u_1(\mathcal{T}_{\bar{\mathbf{x}}} U)(\bar{\mathbf{x}}-\mathbf{x},t)\right]\mathrm{d}\bar{\mathbf{x}}$$

the system of boundary integral equations becomes

$$\begin{pmatrix} u_\Gamma \\ q_\Gamma \end{pmatrix} = \begin{pmatrix} (I-C)\mathcal{I}-\mathcal{K} & \mathcal{V} \\ \mathcal{D} & C\mathcal{I}+\mathcal{K}' \end{pmatrix} * \begin{pmatrix} u_\Gamma \\ q_\Gamma \end{pmatrix} + \begin{pmatrix} \mathcal{N}_0 * f \\ \mathcal{N}_1 * f \end{pmatrix} \quad \forall \mathbf{x},\mathbf{y}\in\Gamma \wedge t\in(0,\infty)\,. \tag{3.26}$$

Note that the integral free terms in (3.26) are computed in accordance to equation (3.19) just by inserting the time-dependent fundamental solutions

$$C(\mathbf{x},t) := -\int_0^t \lim_{\varepsilon\to 0} \int_{\mathbf{y}\in\Omega:|\mathbf{y}-\mathbf{x}|=\varepsilon} (\mathcal{T}_\mathbf{y} U)^\top(\mathbf{y}-\mathbf{x},t-\tau)\,\mathrm{d}s_\mathbf{y}\,\mathrm{d}\tau\,.$$

The identity operator in (3.26) is given by

$$(\mathcal{I} * w)(\mathbf{x},t) \coloneqq \int_0^t \int_\Gamma \delta(\mathbf{y}-\mathbf{x},t-\tau) w(\mathbf{y},\tau)\, \mathrm{d}s_{\mathbf{y}}\, \mathrm{d}\tau \tag{3.27}$$

which is an analogous definition to the elliptic case (3.25).

For all material models except the viscoelastic case it turns out that C exhibit no time-dependency. There, the integral free term consists of a time-dependency if it is evaluated for a point $\mathbf{x}$ lying at a corner or an edge. More information about the time-dependency of the integral-free term can be found in [110]. In all other cases C is constant in time and, additionally, equals

$$C(\mathbf{x},t) = \frac{1}{2} I$$

if the boundary is sufficiently smooth at the point $\mathbf{x}$.

3.3 Symmetric Galerkin formulation

Until now the derived systems of boundary integral equations are just another representation of the underlying partial differential equations being defined in some bounded region. But they still lack of any boundary conditions which, of course, are essential in view of a numerical solution procedure. Since the aim is a symmetric formulation, the boundary conditions are incorporated by making use of the whole system of boundary integral equations. Thereby, the embedding of boundary conditions is done exemplary for the mixed hyperbolic boundary value problem (2.76). Afterwards, the resulting system of integral equations serves as an initial system from which integral formulations for all other boundary value problems can be derived.

The main strategy to formulate a system which exhibits prescribed boundary data may probably be described as a technique which is somehow similar to the *separation of variables*. Therefore, both integral equations are evaluated not on the complete boundary Γ but partially on the two sets Γ_D and Γ_N only. This gives

$$\begin{aligned} C g_D(\mathbf{x},t) &= (\mathcal{V} * q)_\Gamma(\mathbf{x},t) - (\mathcal{K} * u)_\Gamma(\mathbf{x},t) + (\mathcal{N}_0 * f)_\Omega(\mathbf{x},t) \qquad \forall\, (\mathbf{x},t) \in \Gamma_D \times (0,\infty) \\ [I-C]\, g_N(\mathbf{x},t) &= (\mathcal{K}' * q)_\Gamma(\mathbf{x},t) + (\mathcal{D} * u)_\Gamma(\mathbf{x},t) + (\mathcal{N}_1 * f)_\Omega(\mathbf{x},t) \qquad \forall\, (\mathbf{x},t) \in \Gamma_N \times (0,\infty) \end{aligned} \tag{3.28}$$

whereas u_Γ and q_Γ on the left hand-side have been already substituted by the prescribed Cauchy data g_D and g_N. Since the boundary integral operators in (3.28) are still applied on the whole boundary Γ they operate on prescribed data as well as on unknown Cauchy data. To make the integral operators acting on known and unknown Cauchy data separately the decompositions

$$\begin{aligned} u_\Gamma(\mathbf{y},t) &= \tilde{u}_\Gamma(\mathbf{y},t) + \tilde{g}_D(\mathbf{y},t) \\ q_\Gamma(\mathbf{y},t) &= \tilde{q}_\Gamma(\mathbf{y},t) + \tilde{g}_N(\mathbf{y},t) \end{aligned} \tag{3.29}$$

are introduced in which the unknown Cauchy data are denoted as $\tilde{u}_\Gamma$ and $\tilde{q}_\Gamma$, respectively. The quantities $\tilde{g}_D$ and $\tilde{g}_N$ are arbitrary but fixed extensions of the given Dirichlet and Neumann data such that

$$\begin{aligned} \tilde{g}_D(\mathbf{y},t) &= g_D(\mathbf{y},t) \qquad \forall\,(\mathbf{y},t) \in \Gamma_D \times (0,\infty) \\ \tilde{g}_N(\mathbf{y},t) &= g_N(\mathbf{y},t) \qquad \forall\,(\mathbf{y},t) \in \Gamma_N \times (0,\infty) \end{aligned}$$

holds. Obviously, it is preferable to chose the extensions such that $\tilde{g}_D$ and $\tilde{g}_N$ vanish on the complementary boundary sets Γ_N and Γ_D, respectively. One has just to keep in mind that the extension $\tilde{g}_D$ of the Dirichlet data has to be continuous due to regularity requirements [120].

Now, inserting the decompositions (3.29) into (3.28) yields

$$\begin{aligned} (\mathcal{V} * \tilde{q})_{\Gamma_D}(\mathbf{x},t) - (\mathcal{K} * \tilde{u})_{\Gamma_N}(\mathbf{x},t) &= f_D(\mathbf{x},t) \qquad \forall\,(\mathbf{x},t) \in \Gamma_D \times (0,\infty) \\ (\mathcal{K}' * \tilde{q})_{\Gamma_D}(\mathbf{x},t) + (\mathcal{D} * \tilde{u})_{\Gamma_N}(\mathbf{x},t) &= f_N(\mathbf{x},t) \qquad \forall\,(\mathbf{x},t) \in \Gamma_N \times (0,\infty) \end{aligned} \tag{3.30}$$

with the load vectors

$$\begin{aligned} f_D(\mathbf{x},t) &= ((C\mathcal{I} + \mathcal{K}) * \tilde{g}_D)_{\Gamma_D}(\mathbf{x},t) - (\mathcal{V} * \tilde{g}_N)_{\Gamma_N}(\mathbf{x},t) - (\mathcal{N}_0 * f)_\Omega(\mathbf{x},t) \\ f_N(\mathbf{x},t) &= (([I - C]\mathcal{I} - \mathcal{K}') * \tilde{g}_N)_{\Gamma_N}(\mathbf{x},t) - (\mathcal{D} * \tilde{g}_D)_{\Gamma_D}(\mathbf{x},t) - (\mathcal{N}_1 * f)_\Omega(\mathbf{x},t)\,. \end{aligned} \tag{3.31}$$

Transfering the system (3.30) into a residual form and testing it with appropriate test-functions $w(\mathbf{x})$ and $v(\mathbf{x})$ gives, finally, the symmetric Galerkin formulation. This constitutes a weak formulation of the system of boundary integral equations (3.30) to find the unknown Cauchy data $\tilde{u}$ and $\tilde{q}$ such that

$$\begin{aligned} \langle \mathcal{V} * \tilde{q}, w\rangle_{\Gamma_D} - \langle \mathcal{K} * \tilde{u}, w\rangle_{\Gamma_D} &= \langle f_D, w\rangle_{\Gamma_D} \\ \langle \mathcal{K}' * \tilde{q}, v\rangle_{\Gamma_N} + \langle \mathcal{D} * \tilde{u}, v\rangle_{\Gamma_N} &= \langle f_N, v\rangle_{\Gamma_N}\,. \end{aligned} \tag{3.32}$$

holds for all test-functions $w(\mathbf{x}), v(\mathbf{x})$. In (3.32), terms of the form $\langle f, g\rangle_\Gamma := \int_\Gamma f(\mathbf{x}) g(\mathbf{x})\,\mathrm{d}\mathbf{x}$ denote the inner product of two functions f and g. Moreover, since the boundary integral equations are formulated in an integral sense, the integral-free terms in f_D and f_N can be set to $C = \frac{1}{2} I$ uniformly. Finally, as the Galerkin scheme is used only with respect to the spatial variables the test-functions $w(\mathbf{x})$ and $v(\mathbf{x})$ exhibit no time-dependency and the weak formulation used here is equivalent to the variational formulations commonly used in Finite Element analysis (cf. [21, 121]).

As already mentioned, weak formulations for the remaining boundary value problems are obtained just by simplifying (3.32). In case of a pure Dirichlet initial boundary problem the boundary Γ_D coincides with Γ and it is the Neumann data only which is sought-after. Thus, (3.32) simplifies to

$$\langle \mathcal{V} * \tilde{q}, w\rangle_\Gamma = \langle (\tfrac{1}{2}\mathcal{I} + \mathcal{K}) * g_D - \mathcal{N}_0 * f, w\rangle_\Gamma$$

and for a pure Neumann initial boundary value problem one obtains vice versa

$$\langle \mathcal{D} * \tilde{u}, v \rangle_\Gamma = \langle (\tfrac{1}{2}\mathcal{I} - \mathcal{K}') * g_N - \mathcal{N}_1 * f, v \rangle_\Gamma \, .$$

In case of elliptic boundary value problems the according weak formulations read as

$$\begin{aligned} \langle \widehat{\mathcal{V}}\tilde{q}, w \rangle_{\Gamma_D} - \langle \widehat{\mathcal{K}}\tilde{u}, w \rangle_{\Gamma_D} &= \langle (\tfrac{1}{2}\widehat{\mathcal{I}} + \widehat{\mathcal{K}})\tilde{g}_D - \widehat{\mathcal{V}}\tilde{g}_N - \widehat{\mathcal{N}}_0 f, w \rangle_{\Gamma_D} \\ \langle \widehat{\mathcal{K}}'\tilde{q}, v \rangle_{\Gamma_N} + \langle \widehat{\mathcal{D}}\tilde{u}, v \rangle_{\Gamma_N} &= \langle (\tfrac{1}{2}\widehat{\mathcal{I}} - \widehat{\mathcal{K}}')\tilde{g}_N - \widehat{\mathcal{D}}\tilde{g}_D - \widehat{\mathcal{N}}_1 f, v \rangle_{\Gamma_N} \end{aligned} \tag{3.33}$$

for the mixed boundary value problem (2.74) and

$$\langle \widehat{\mathcal{V}}\tilde{q}, w \rangle_\Gamma = \langle (\tfrac{1}{2}\widehat{\mathcal{I}} + \widehat{\mathcal{K}}) g_D - \widehat{\mathcal{N}}_0 f, w \rangle_\Gamma$$

for the Dirichlet boundary value problem (2.65). An exceptional position receives the weak formulation according to the Neumann boundary value problem (2.70). Formally this is

$$\langle \widehat{\mathcal{D}}\tilde{u}, v \rangle_\Gamma = \langle (\tfrac{1}{2}\widehat{\mathcal{I}} - \widehat{\mathcal{K}}') g_N - \widehat{\mathcal{N}}_1 f, v \rangle_\Gamma \, ,$$

but one has to be cautious using this formulation without modifications within a numerical scheme since it is not uniquely solvable. In a certain sense, this corresponds to the underlying boundary value problem which is in general also not uniquely determined. Techniques to overcome this drawback are presented in [120]. Moreover, a detailed analysis concerning uniqueness and solvability of the weak formulations and the respective bilinear forms may be found in the books [120] and [107] for the elliptic case. Unfortunately, the literature on the weak formulations in case of hyperbolic system is somewhat rare. Nevertheless, there exist some references. For instance, a very good survey on this topic is given in [29]. Further, the special cases of the scalar wave equation and the system of elastodynamics are treated extensively in [53] and [26–28], respectively.

3.4 Unbounded domains

Until now, only problems for bounded regions of interest have been considered. But additionally, there exist a lot of physical problems which are formulated on unbounded regions. In such cases either the domain Ω tends to infinity while the boundary Γ remains finite or both the domain Ω as well as its boundary Γ become infinitely large.

An example for the former situation is the sound emission of some bounded body which occupies the domain Ω_{int} and which exhibit the boundary $\Gamma_{int} = \partial\Omega_{int}$. Then, it is the complement region $\Omega_{ext} = \mathbb{R}^3 \setminus \overline{\Omega}_{int}$ with the boundary $\Gamma = \partial\Omega_{ext}$ in which the acoustic pressure is searched for. Note that Γ_{int} and Γ are equivalent since they occupy the same space. But it is important to mention that they differ in their particular orientation. As a consequence, the normal vector $\mathbf{n}$ always point out of the domain Ω (see Fig. 3.2a).

In Fig. 3.2b an infinitely large surface is sketched. It appears if, e.g., an elastic halfspace $\Omega := \{\tilde{\mathbf{x}} \in \mathbb{R}^3 : \tilde{x}_3 < 0\}$ is stressed on its surface $\Gamma = \{\mathbf{y} \in \mathbb{R}^3 : y_3 = 0\}$ by some given Neumann data g_N. This problem is of major interest in many engineering applications. While its formulation is rather simple its discretization is challenging within the forthcoming Boundary Element Method. Section 5.5 is dedicated to this particular problem.

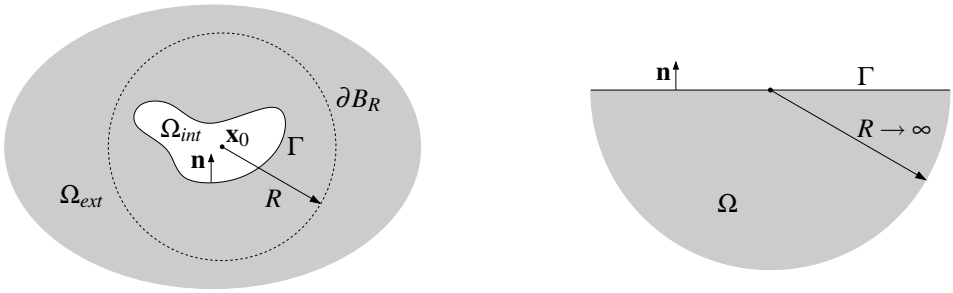

(a) Unbounded Ω_{ext}, bounded Γ (b) Unbounded Ω, unbounded Γ

Figure 3.2: Types of unbounded domains

To guarantee the unique solvability of a boundary value problem stated for an unbounded domain the solution $u(\tilde{\mathbf{x}})$ has to match certain additional *far field conditions* in the limit $|\tilde{\mathbf{x}}| \to \infty$. Those conditions differ whether a static, a time-harmonic, or a time-dependent problem is under consideration. In the following, the far field conditions are stated and their impact on the representation formulae is investigated briefly. At first, the unbounded domain with bounded surface is considered.

Static case. For the static case the far field condition may be found, e.g., in the book of Kupradze [70] where its derivation is done by making use of energy principles. At the end, the far field condition is given by

$$\lim_{|\tilde{\mathbf{x}}|\to\infty} |\tilde{\mathbf{x}}| u(\tilde{\mathbf{x}}) = C \qquad \wedge \qquad \lim_{|\tilde{\mathbf{x}}|\to\infty} |\tilde{\mathbf{x}}| \, |\nabla u(\tilde{\mathbf{x}})| = 0 \qquad \forall \tilde{\mathbf{x}} \in \Omega_{ext} \tag{3.34}$$

with some given real number $C \in \mathbb{R}$. Throughout this work, homogeneous far field conditions are assumed, i.e., $C \equiv 0$.

An important comment has to be given on the pure Neumann problem. If such a problem is formulated on an unbounded domain it yields a unique solution. Due to the far field conditions there exist no rigid body motions which could alter the solution.

Time-harmonic case. Probably the most established far field condition has been posed by Sommerfeld and is usually denoted as *Sommerfeld's radiation condition*. It has been published primarily in [116] and has been recalled in [117]. In the time-harmonic case, it is not sufficient that the solution matches just a certain decay as it is stated in (3.34). In fact,

it has to be assured that there are no incoming waves from infinity. Therefore, the solution $u(\tilde{\mathbf{x}})$ is subjected to more restrictions than in the static case. The radiation condition for the Helmholtz equation is

$$\lim_{|\tilde{\mathbf{x}}|\to\infty} |\tilde{\mathbf{x}}| \left(\langle \frac{\tilde{\mathbf{x}}}{|\tilde{\mathbf{x}}|}, \nabla u \rangle - \mathrm{i}ku \right) = 0 \qquad \forall \tilde{\mathbf{x}} \in \Omega_{ext} \,. \tag{3.35}$$

Above, the term $\langle \frac{\tilde{\mathbf{x}}}{|\tilde{\mathbf{x}}|}, \nabla u \rangle$ denotes the derivative of u in direction of the radius vector $\tilde{\mathbf{x}}$, and $k \in \mathbb{R}$ is the wave number defined as the quotient of the Frequency $\omega \in \mathbb{R}$ and the wave velocity $c \in \mathbb{R}$, i.e., $k \coloneqq \omega/c$. By substituting k with $-k$ one obtains the complement of the radiation condition. In that case the solution is subjected to incoming waves. Hence, it is obviously not sufficient to formulate a condition in form of (3.34) since both far field conditions describe the same decay behavior of the solution u while they differ essentially in their physical model. For a profound theoretical background on this topic the book of Sommerfeld [117] is recommended.

In elasticity the radiation condition is formulated equivalently. But since there exists two waves the displacement field $\mathbf{u} = \mathbf{u}_p + \mathbf{u}_s$ is split into its compressional and rotational parts. Then the radiation condition (3.35) is formulated for $\mathbf{u}_p$ and $\mathbf{u}_s$ and their respective wave numbers separately [70].

Time-dependent case. Contrary to the both previously considered problems in the time domain the situation somehow turns around. While an elliptic problem must include a far field condition in order to be well posed, no such conditions have to be prescribed for the hyperbolic problem [44]. Nevertheless, if the initial conditions vanish at infinity (this corresponds to the exclusion of incoming waves) the solution u fulfills a Sommerfeld radiation condition which is the analogue of (3.35). For the acoustic fluid it reads as

$$\lim_{\substack{|\tilde{\mathbf{x}}|\to\infty \\ |\tilde{\mathbf{x}}|+ct=\text{const}}} |\tilde{\mathbf{x}}| \left(\langle \frac{\tilde{\mathbf{x}}}{|\tilde{\mathbf{x}}|}, \nabla u \rangle - \frac{1}{c}\frac{\partial u}{\partial t} \right) = 0 \qquad \forall \tilde{\mathbf{x}} \in \Omega_{ext} \,. \tag{3.36}$$

Representation formulae on unbounded domains. Now, the question arises whether the representation formulae also hold for unbounded domains. This will be investigated by means of the elliptic case.

First, an auxiliary domain $\Omega_R = \Omega_{ext} \cap B_R(\mathbf{x}_0)$ is defined as the intersection of the exterior domain Ω_{ext} and a sphere $B_R(\mathbf{x}_0)$ of radius R centered at the point $\mathbf{x}_0$ which circumscribes the interior domain Ω_{int} (cf. Fig. 3.2a). Now, using the representation formula (3.8) for $\tilde{\mathbf{x}} \in \Omega_R$ this gives

$$\begin{aligned} u(\tilde{\mathbf{x}}) = &\int_\Gamma q_\Gamma(\mathbf{y})\, U(\mathbf{y}-\tilde{\mathbf{x}})\, \mathrm{d}s_\mathbf{y} - \int_\Gamma u_\Gamma(\mathbf{y})\, (\mathcal{T}_\mathbf{y} U)(\mathbf{y}-\tilde{\mathbf{x}})\, \mathrm{d}s_\mathbf{y} \\ &+ \int_{\partial B_R(\mathbf{x}_0)} (\mathcal{T}_\mathbf{y} u)(\mathbf{y})\, U(\mathbf{y}-\tilde{\mathbf{x}})\, \mathrm{d}s_\mathbf{y} - \int_{\partial B_R(\mathbf{x}_0)} (\mathrm{Tr}_\mathbf{y}\, u)(\mathbf{y})\, (\mathcal{T}_\mathbf{y} U)(\mathbf{y}-\tilde{\mathbf{x}})\, \mathrm{d}s_\mathbf{y} \,. \end{aligned}$$

If the integrals over the sphere's boundary $\partial B_R(\mathbf{x}_0)$ vanish in the limit $R \to \infty$ the representation formula passes over to its formulation for bounded domains. Indeed, this advantageous behavior occurs [30] if the radiation conditions are taken into account. Since the considered elliptic fundamental solutions fulfill either the far field condition (3.34) or the condition (3.35) and under the assumption that the solution u vanishes in the limit $R \to \infty$ the sphere's boundary integrals drop out and the representation formula becomes exactly the same as for bounded domains

$$u(\tilde{\mathbf{x}}) = \int_\Gamma q_\Gamma(\mathbf{y})\, U(\mathbf{y}-\tilde{\mathbf{x}})\, \mathrm{d}s_\mathbf{y} - \int_\Gamma u_\Gamma(\mathbf{y})\, (\mathcal{T}_\mathbf{y} U)(\mathbf{y}-\tilde{\mathbf{x}})\, \mathrm{d}s_\mathbf{y} \quad \forall\, \tilde{\mathbf{x}} \in \Omega_{ext}\,. \tag{3.37}$$

In the hyperbolic case, the deduction of the representation formula for unbounded domains follows the same rules as for the elliptic case and is sketched only briefly herein. Again, an outer boundary $\Omega_R = \Omega_{ext} \cap B_R(\mathbf{x}_0)$ is introduced on which, now, the time-dependent representation formula holds. Then, under the assumption that there are homogeneous initial conditions prescribed the solution fulfills the radiation condition (3.36), and so do the time-dependent fundamental solutions. Next, taking this radiation condition into account the limiting process $R \to \infty$ yields that the surface integrals on the sphere's boundary vanish and the representation formula

$$\begin{aligned} u(\tilde{\mathbf{x}},t) = &\int_\Gamma q_\Gamma(\mathbf{y},t) * U(\mathbf{y}-\tilde{\mathbf{x}},t)\, \mathrm{d}s_\mathbf{y} \\ &- \int_\Gamma u_\Gamma(\mathbf{y},t) * (\mathcal{T}_\mathbf{y} U)(\mathbf{y}-\tilde{\mathbf{x}},t)\, \mathrm{d}s_\mathbf{y} \qquad \forall\, (\tilde{\mathbf{x}},t) \in \Omega_{ext} \times (0,\infty) \end{aligned} \tag{3.38}$$

is obtained. Additional information concerning some minor specific requirements on stresses and velocities are given in [126].

Notes on the representation formulae for Half-space problems. Until now, only unbounded domains with bounded surfaces have been considered. But, as mentioned earlier, there are some circumstances in which both the domain as well as its boundary surface are unbounded. Probably most notable is the elastic half-space which has been already mentioned as an introductory example. For this type of geometry uniqueness theorems in the case of elastostatics have been proposed in [65] but there is still a lack of extending these theorems to hyperbolic problems. Here, it is assumed that the representation formulae (3.37) and (3.38) hold also for geometries with unbounded surfaces.

Variational formulations for unbounded domains. Finally, an important note must be given concerning the associated boundary integral operators and the resulting variational forms. Although the exterior boundary value problems are uniquely solvable and although the representation formulae are left unchanged for unbounded domains the respective variational forms are not necessarily uniquely solvable. For instance, in the static case the hypersingular integral operator corresponds to the inner Neumann boundary value problem

as well as to the exterior Neumann boundary value problem. And since it is not invertible for the inner problem it also is not invertible for the outer problem. Thus, without modifications of the according variational formulation the outer problem is not uniquely solvable. A similar problem occurs for the time-harmonic case. There, the variational form usually yields a result due to the absence of rigid body motions. However, for the inner problem the operator is not invertible if the wave number corresponds to an eigenfrequency [120]. The exterior domain is free of eigenfrequencies such that the variational form should be solvable for every wave number. But again, since the underlying operator is the same for both the interior domain as well as the exterior domain the solution will exhibit so-called *fictitious frequencies* which are related to the eigenfrequencies of the interior domain. To eliminate those frequencies several methods have been established. Probably the best known methods for acoustic problems are the CHIEF method [14, 113] and the Burton-Miller formulation [23]. The time-dependent case is free of rigid body motions and resonances. Thus, from this point of view there is neither a restriction concerning the interior domain nor for the unbounded domain.

3.5 Representation formula for internal stresses

If the complete Cauch ydata $[u_\Gamma, q_\Gamma]$ are known the Dirichlet data $u(\mathbf{x})$ (or $u(\mathbf{x},t)$) are determined completely by the representation formula (3.8) (or (3.14)) for every $\mathbf{x} \in \Omega$ (or $(\mathbf{x},t) \in \Omega \times (0,t)$). But in real world applications it is often more important to make a prediction of the internal stress distribution. To achieve this the representation formulae have to be inserted into the respective material law. Exemplary, this representation formula will be deduced by means of an elastic solid. The deduction for scalar problems is straightforward.

Under the assumption of homogeneous initial conditions and vanishing body forces the hyperbolic representation formula (3.14) is recalled

$$\mathbf{u}(\tilde{\mathbf{x}},t) = (\mathcal{V} * \mathbf{t}_\Gamma)(\tilde{\mathbf{x}},t) - (\mathcal{K} * \mathbf{u}_\Gamma)(\tilde{\mathbf{x}},t) \qquad \forall\, (\tilde{\mathbf{x}},t) \in \Omega \times (0,t)\,. \tag{3.39}$$

With the symmetric gradient's definition

$$\widetilde{\nabla}_{\mathbf{x}} := \frac{1}{2}\left(\nabla_{\mathbf{x}} + \nabla_{\mathbf{x}}^{\top}\right)$$

the strain tensor (2.20) becomes $\boldsymbol{\varepsilon}(\mathbf{x},t) = \widetilde{\nabla}_{\tilde{\mathbf{x}}}\mathbf{u}(\tilde{\mathbf{x}},t)$ and the stress tensor is

$$\boldsymbol{\sigma}(\tilde{\mathbf{x}},t) = \overset{(4)}{\mathbf{C}} \colon \boldsymbol{\varepsilon}(\tilde{\mathbf{x}},t) = \overset{(4)}{\mathbf{C}} \colon \widetilde{\nabla}_{\tilde{\mathbf{x}}}\mathbf{u}(\mathbf{x},t)\,. \tag{3.40}$$

Finally, inserting the representation formula (3.39) into (3.40) yields the representation formula for the internal stresses

$$\boldsymbol{\sigma}(\tilde{\mathbf{x}},t) = (\mathcal{S}_1 * \mathbf{t}_\Gamma)(\tilde{\mathbf{x}},t) - (\mathcal{S}_2 * \mathbf{u}_\Gamma)(\tilde{\mathbf{x}},t)\,. \tag{3.41}$$

Above, the newly introduced operators $\mathcal{S}_1$ and $\mathcal{S}_2$ are obtained by the application of the operations $\overset{(4)}{\mathbf{C}}\colon \widetilde{\nabla}_{\tilde{\mathbf{x}}}$ onto the single layer operator $\mathcal{V}$ and onto the double layer operator $\mathcal{K}$

$$\begin{aligned}(\mathcal{S}_1 * \mathbf{t}_\Gamma)(\tilde{\mathbf{x}},t) &:= \int_\Gamma \left(\overset{(4)}{\mathbf{C}}\colon \widetilde{\nabla}_{\tilde{\mathbf{x}}}\mathbf{U}\right)(\mathbf{y}-\tilde{\mathbf{x}},t) * \mathbf{t}_\Gamma(\mathbf{y},t)\,\mathrm{d}s_{\mathbf{y}} \\ (\mathcal{S}_2 * \mathbf{u}_\Gamma)(\tilde{\mathbf{x}},t) &:= \int_\Gamma \left[\mathcal{T}_{\mathbf{y}}\left(\overset{(4)}{\mathbf{C}}\colon \widetilde{\nabla}_{\tilde{\mathbf{x}}}\mathbf{U}\right)\right](\mathbf{y}-\tilde{\mathbf{x}},t) * \mathbf{u}_\Gamma(\mathbf{y},t)\,\mathrm{d}s_{\mathbf{y}} \qquad \forall \mathbf{y}\in\Gamma\,.\end{aligned} \tag{3.42}$$

Note that these expressions are obtained by interchanging the differentiations with the integrations. Since $\Gamma \ni \mathbf{y} \neq \tilde{\mathbf{x}} \in \Omega$ holds no singularities occur and the commutation of these processes is allowed. In case of a static analysis the above operators are defined analogously by skipping the time convolution integrals and by the use of the corresponding elastostatic fundamental solutions. The explicit forms of the integral kernels in (3.42) are given in the appendix A.1.

4 REGULARIZATION OF STRONG- AND HYPER-SINGULAR INTEGRAL KERNELS

Bearing a numerical solution procedure in mind it becomes immediately clear that the evaluation of almost any bilinear form presented in the previous section implies the evaluation of singular integrals. The proper computation of those integrals is for sure the most demanding task within any Boundary Element formulation. While the first integral equation comprises weakly singular kernels as well as Cauchy principal values, the second boundary integral equation demands in addition the evaluation of hypersingular kernel functions. Within a symmetric Galerkin scheme this means that, except for the Dirichlet boundary value problem, one has to deal with three different kind of singularities. Weak singularities are nothing but improper integrals and, therefore, relatively easy to handle. Cauchy principal values are defined by a special limiting process and hypersingularities are defined in the sense of finite part integrals which means that the divergent parts of the integral kernels have to be cut off. Hence, the two latter types of singularities are quite challenging within a numerical scheme.

In principle, there exist two possibilities to compute singular integrals: Either the singularities are treated analytically [50] or they are transformed such that they are suitable for the application of some kind of quadrature rule [108]. But this is just a rough classification since there exist also hybrid approaches which are a mixture of analytical and numerical techniques. Of course, the analytical treatment of singularities has the one big advantage of being exact. But this is just half of the truth since the analytical integrations might result in very complex formulae which are very sensitive concerning a correct, robust, and stable implementation. Those complex formulae arise mostly in 3-d problems where the integrations are performed over some surface patches. Beside this rather subjective disqualification there exist one substantial drawback of this approach: Analytical integrations cannot be performed in general, i.e., every analytical integration is done for a special physical problem and for certain assumptions concerning the geometry (mostly assumed linear) and the trial functions (either constant or linear).

The purely numerical treatment of singular integrals can itself be subclassified into two different approaches. One approach leaves the singularity untouched and uses special quadrature rules, and the other one removes the singularity by special coordinate transformations. The first approach is restricted to weak singularities which are known to exist in an improper sense so that quadrature rules can be developed taking the singular behavior of the kernel functions into account [68]. Besides the restriction to weak singularities the drawback of this approach is mainly that it demands not only a special singularity but also a special integral kernel. This means that, for instance, despite that in statics and dynamics

the kernel functions exhibit the same type of singularity the kernel functions itself are different and, consequently, the formulae do not apply. Thus, the quadrature rule works for one kernel function and is, without modifying the kernel, inapplicable for the other.

Finally, special coordinate transformations remove the singularities such that standard Gaussian quadrature rules can be applied. These techniques offer at least two advantages. At first, they allow the biggest freedom concerning the geometry modeling as well as choosing appropriate test- and trial-functions. Secondly, the implementation of this approach is relatively easy, since the kernels underwent some coordinate transformations only. Nevertheless, special coordinate transformations suffer also some weaknesses. At first, the numerical approach works sufficiently only up to Cauchy principal value integrals. Although there exist some approaches to extent these techniques to Hadamard finite part integrals applicable formulae are quite rare. Moreover, the few existing formulae use some obscure and unsatisfactory parameters to guarantee a stable numerical scheme. The second drawback of these methods concerns the efficiency. In certain cases it might happen that an accurate integration demands a high number of kernel evaluations which increase the overall computing time considerably.

To summarize the different approaches so far, one definitely could state that there is neither a general way nor an optimal method to treat the occurring singularities. Moreover, none of the numerical methods is able to handle hypersingularities as a truly black box quadrature. To sufficiently deal with those kind of singular integrals the analytical way is probably the method of choice. But bearing the different physical models in mind (at least 3-d viscoelasticity) this approach is doomed to failure. As mentioned previously an analytical integration in this case is simply too demanding and impossible for curved, i.e., non-linear, geometries. Thus, one ends up with numerical techniques. Thereby, the use of coordinate transformations is most promising since they make almost no demands on the kernel functions.

Now, by using the numerical approach it is left to answer the question concerning the finite part integrals. Since all numerical schemes fail in this case, and since the analytical approach is impractical it is the hybrid approach mentioned already at the beginning which is chosen. Thus, the hypersingular bilinear forms are transformed analytically into bilinear forms featuring a lower degree of singularity. Afterwards, an appropriate numerical scheme can be applied to evaluate the resulting singular integrals.

The hypersingular operators consist of twice the application of the stress operator with respect to the fundamental solutions. Within the bilinear form this operator acts on the Dirichlet data and its result is weighted by a test function afterwards. Both the Dirichlet data as well as the test function have to be continuous and, therefore, are at least differentiable functions. Thus, it would be preferable to shift the (generalized) normal derivatives from the fundamental solutions over to the Dirichlet data and the test-function. Of course, this shifting is done by integration by parts or, to be more precise in this context, by applications of Stokes theorem. Certainly, this technique has to be done for scalar and elasticity problems separately since the kernel functions as well as the generalized normal derivatives differ clearly from each other for these two cases.

Regularization approaches of non integrable kernel functions based on integration by parts have a long tradition and are well known nowadays. This technique was firstly used in 1949 by Maue [82] who applied it to the wave equation in the frequency domain. A major enhancement was then given by Nedelec [87] who introduced regularized hypersingular bilinear forms for the Laplace equation, the Helmholtz equation as well as for the system of linear elastostatics. Further, regularizations in the field of 3-d time-harmonic elastodynamics were presented by Nishimura & Kobayashi [88] and Becache *et al.* [11]. While these both approaches rely mainly on the previous work by Nedelec [87], the particular regularizations are nevertheless slightly different. In the first case the hypersingular operator is used within a collocation scheme while in the other case a Galerkin scheme is formulated. Another regularization of the hypersingular bilinear form in case of 3-d elastostatics was presented by Han [58] who used some basic results from Kupradze [70]. Unlike Nedelec whose regularization is based on a very general approach and, therefore, results in rather complicated formulae, Han restricts his regularization a priori to the isotropic case and discards the possibility of describing also the anisotropic system.

Within this work Han's proof is extended to the Laplace transformed system of elastodynamics. As will be shown later the regularized form of the elastodynamic hypersingular bilinear form in Laplace domain completes the set of regularizations which are needed to model all the considered physical problems herein. Finally, the deduction of the regularized bilinear form using Han's proof is advantageous since it leads to a more convenient formulation with respect to the numerical implementation than the already established regularizations [11, 88].

Nevertheless, the whole regularization process requires some special derivative operators which, probably, are unfamiliar to engineers. Thus, in the following those kind of operators and their properties are defined briefly. Afterwards, the regularization for scalar models is given as an introductory example, which is, at the end, followed by the regularization of the elastodynamic kernel.

4.1 Tangential surface derivatives

As previously mentioned, the whole regularization process presented herein is mainly based on applications of Stokes theorem and its generalizations. To begin with, the classical Stokes theorem should be recalled briefly. Let Γ be a surface with the outward unit vector $\mathbf{n}(\mathbf{y})$ and let $\partial\Gamma$ denote the surface's boundary with the unit tangent vector $\boldsymbol{\nu}(\mathbf{y})$. Then, the classical Stokes theorem for some differentiable vector field $\mathbf{g}(\mathbf{y})$ reads as

$$\int_{\Gamma} (\nabla_{\mathbf{y}} \times \mathbf{g}(\mathbf{y})) \cdot \mathbf{n}(\mathbf{y}) \, \mathrm{d}s_{\mathbf{y}} = \int_{\partial\Gamma} \mathbf{g}(\mathbf{y}) \cdot \boldsymbol{\nu}(\mathbf{y}) \, \mathrm{d}\sigma_{\mathbf{y}} \, . \tag{4.1}$$

Throughout this section the nabla operator's subscript denotes that the derivatives have to be taken with respect to $\mathbf{y}$. By introducing the *surface curl*

$$\frac{\partial}{\partial \mathbf{S}(\partial_{\mathbf{y}}, \mathbf{n}(\mathbf{y}))} \coloneqq \mathbf{n}(\mathbf{y}) \times \nabla_{\mathbf{y}} \tag{4.2}$$

and by assuming that the boundary Γ is closed, i.e., $\partial\Gamma = \emptyset$, Stokes theorem (4.1) reads as

$$\int_{\Gamma} \frac{\partial}{\partial \mathbf{S}(\partial_{\mathbf{y}}, \mathbf{n}(\mathbf{y}))} \cdot \mathbf{g}(\mathbf{y}) \, \mathrm{d}s_{\mathbf{y}} = 0 \, . \tag{4.3}$$

The introduced surface curl (4.2) is a so-called *tangential surface derivative* operator. If this derivative is applied to a vector field normal to the boundary this gives

$$\frac{\partial}{\partial \mathbf{S}(\partial_{\mathbf{y}}, \mathbf{n}(\mathbf{y}))} \cdot \alpha \mathbf{n}(\mathbf{y}) = \alpha \left[\mathbf{n}(\mathbf{y}) \times \mathbf{n}(\mathbf{y}) \right] \cdot \nabla_{\mathbf{y}} = 0 \qquad \forall \, \alpha \in \mathbb{C} \, .$$

Due to the orthogonality of $\frac{\partial}{\partial \mathbf{S}}$ and $\mathbf{n}(\mathbf{y})$ the operator lies in the same plane as the tangent vector $\boldsymbol{\nu}(\mathbf{y})$ by what the labeling as tangential surface derivative comes from. Next, considering a differentiable vector field $\mathbf{g}(\mathbf{y}) \coloneqq v(\mathbf{y})\mathbf{u}(\mathbf{y})$ one obtains its rotation by an application of the product rule

$$\nabla_{\mathbf{y}} \times \mathbf{g}(\mathbf{y}) = \nabla_{\mathbf{y}} v(\mathbf{y}) \times \mathbf{u}(\mathbf{y}) + v(\mathbf{y}) \left(\nabla_{\mathbf{y}} \times \mathbf{u}(\mathbf{y}) \right) \, .$$

In conjunction with Stokes theorem (4.1) this gives under the assumption of a closed boundary

$$\int_{\Gamma} \left[\nabla_{\mathbf{y}} v(\mathbf{y}) \times \mathbf{u}(\mathbf{y}) \right] \cdot \mathbf{n}(\mathbf{y}) \, \mathrm{d}s_{\mathbf{y}} = - \int_{\Gamma} v(\mathbf{y}) \left[\nabla_{\mathbf{y}} \times \mathbf{u}(\mathbf{y}) \right] \cdot \mathbf{n}(\mathbf{y}) \, \mathrm{d}s_{\mathbf{y}} \, .$$

Rearranging the terms above and using the operator notation, (4.3) yields the identity

$$\int_{\Gamma} \frac{\partial v(\mathbf{y})}{\partial \mathbf{S}(\partial_{\mathbf{y}}, \mathbf{n}(\mathbf{y}))} \cdot \mathbf{u}(\mathbf{y}) \, \mathrm{d}s_{\mathbf{y}} = - \int_{\Gamma} v(\mathbf{y}) \frac{\partial}{\partial \mathbf{S}(\partial_{\mathbf{y}}, \mathbf{n}(\mathbf{y}))} \cdot \mathbf{u}(\mathbf{y}) \, \mathrm{d}s_{\mathbf{y}} \, . \tag{4.4}$$

Note that from now on until the end of this section it is assumed that the boundary Γ is closed. A special case is obtained if the vector field $\mathbf{u}$ is replaced by the Cartesian basis vector $\mathbf{e}_i$. Then the right hand-side in (4.4) vanishes and the expression simplifies to

$$\int_{\Gamma} \frac{\partial v(\mathbf{y})}{\partial S_i(\partial_{\mathbf{y}}, \mathbf{n}(\mathbf{y}))} \, \mathrm{d}s_{\mathbf{y}} = 0 \tag{4.5}$$

where $\frac{\partial}{\partial S_i}$ denotes the i-th component of the surface curl (4.2).

The identities considered so far are very useful in conjunction with the upcoming regularization for scalar problems. For the later proposed regularization of elasticity problems the

identities above need some enhancements. The previous expression (4.5) is very important to establish the vector identity

$$\int_\Gamma \frac{\partial}{\partial \mathbf{S}(\partial_{\mathbf{y}}, \mathbf{n}(\mathbf{y}))} \times \mathbf{u}(\mathbf{y}) \, \mathrm{d}s_{\mathbf{y}} = \mathbf{0} \tag{4.6}$$

which can be easily proven by performing the vector product. By skipping the functions' and derivatives' arguments this gives

$$\int_\Gamma \frac{\partial}{\partial \mathbf{S}(\partial_{\mathbf{y}}, \mathbf{n}(\mathbf{y}))} \times \mathbf{u}(\mathbf{y}) \, \mathrm{d}s_{\mathbf{y}} = \int_\Gamma \begin{pmatrix} \frac{\partial u_3}{\partial S_2} - \frac{\partial u_2}{\partial S_3} \\ \frac{\partial u_1}{\partial S_3} - \frac{\partial u_3}{\partial S_1} \\ \frac{\partial u_2}{\partial S_1} - \frac{\partial u_1}{\partial S_2} \end{pmatrix} \mathrm{d}s_{\mathbf{y}} \, .$$

According to (4.5) the integral with respect to every component of the right hand-side above vanishes. From this the identity (4.6) follows. Since the cross product between two vectors can be expressed by a multiplication of an antisymmetric matrix with a vector the expression (4.6) is alternatively written as

$$\int_\Gamma \frac{\partial}{\partial \mathbf{S}(\partial_{\mathbf{y}}, \mathbf{n}(\mathbf{y}))} \times \mathbf{u}(\mathbf{y}) \, \mathrm{d}s_{\mathbf{y}} = \int_\Gamma \mathcal{M}(\partial_{\mathbf{y}}, \mathbf{n}(\mathbf{y})) \cdot \mathbf{u}(\mathbf{y}) \, \mathrm{d}s_{\mathbf{y}} = \mathbf{0} \, . \tag{4.7}$$

Above, the newly introduced operator matrix $\mathcal{M}$ is usually denoted as *Günter derivatives* [51]. Its definition is

$$\mathcal{M}(\partial_{\mathbf{y}}, \mathbf{n}(\mathbf{y})) := \begin{pmatrix} 0 & -\frac{\partial}{\partial S_3(\partial_{\mathbf{y}}, \mathbf{n}(\mathbf{y}))} & \frac{\partial}{\partial S_2(\partial_{\mathbf{y}}, \mathbf{n}(\mathbf{y}))} \\ \frac{\partial}{\partial S_3(\partial_{\mathbf{y}}, \mathbf{n}(\mathbf{y}))} & 0 & -\frac{\partial}{\partial S_1(\partial_{\mathbf{y}}, \mathbf{n}(\mathbf{y}))} \\ -\frac{\partial}{\partial S_2(\partial_{\mathbf{y}}, \mathbf{n}(\mathbf{y}))} & \frac{\partial}{\partial S_1(\partial_{\mathbf{y}}, \mathbf{n}(\mathbf{y}))} & 0 \end{pmatrix} \tag{4.8}$$

and a simple computation yields the useful representation

$$\mathcal{M}(\partial_{\mathbf{y}}, \mathbf{n}(\mathbf{y})) = \begin{pmatrix} 0 & n_2 \frac{\partial}{\partial y_1} - n_1 \frac{\partial}{\partial y_2} & n_3 \frac{\partial}{\partial y_1} - n_1 \frac{\partial}{\partial y_3} \\ n_1 \frac{\partial}{\partial y_2} - n_2 \frac{\partial}{\partial y_1} & 0 & n_3 \frac{\partial}{\partial y_2} - n_2 \frac{\partial}{\partial y_3} \\ n_1 \frac{\partial}{\partial y_3} - n_3 \frac{\partial}{\partial y_1} & n_2 \frac{\partial}{\partial y_3} - n_3 \frac{\partial}{\partial y_2} & 0 \end{pmatrix} \tag{4.9}$$

which itself can be written more compact by help of the tensor product $\otimes$ as

$$\mathcal{M}(\partial_{\mathbf{y}}, \mathbf{n}(\mathbf{y})) = \nabla_{\mathbf{y}} \otimes \mathbf{n}(\mathbf{y}) - \mathbf{n}(\mathbf{y}) \otimes \nabla_{\mathbf{y}} \, . \tag{4.10}$$

Finally, a last representation of the Günter derivatives is obtained if one introduces the operator

$$\mathcal{U}(\partial_{\mathbf{y}}, \mathbf{n}(\mathbf{y})) := \nabla_{\mathbf{y}} \otimes \mathbf{n}(\mathbf{y}) \tag{4.11}$$

such that the operator $\mathcal{M}$ becomes

$$\mathcal{M}(\partial_{\mathbf{y}}, \mathbf{n}(\mathbf{y})) = \mathcal{U}(\partial_{\mathbf{y}}, \mathbf{n}(\mathbf{y})) - \mathcal{U}^\top(\partial_{\mathbf{y}}, \mathbf{n}(\mathbf{y})) \, . \tag{4.12}$$

The Günter derivatives are exceptional useful during the regularization process of hyper-singular bilinear forms in elasticity. Due to their definition via the surface curl they exhibit similar properties which are derived in the following. According to (4.5) it becomes immediately clear that

$$\int_\Gamma \mathcal{M}(\partial_{\mathbf{y}}, \mathbf{n}(\mathbf{y}))v(\mathbf{y})\, \mathrm{d}s_{\mathbf{y}} = \mathbf{0} \tag{4.13}$$

holds for an arbitrary scalar function v. Moreover, assuming that the scalar function v is the product of two scalar functions u and w one obtains

$$\int_\Gamma [\mathcal{M}(\partial_{\mathbf{y}}, \mathbf{n}(\mathbf{y}))u(\mathbf{y})]\, w(\mathbf{y})\, \mathrm{d}s_{\mathbf{y}} = -\int_\Gamma u(\mathbf{y})\, [\mathcal{M}(\partial_{\mathbf{y}}, \mathbf{n}(\mathbf{y}))w(\mathbf{y})]\, \mathrm{d}s_{\mathbf{y}} \tag{4.14}$$

just by using the product rule. Further the product rule can be used if $\mathcal{M}$ is applied to a vector field $v(\mathbf{y})\mathbf{u}(\mathbf{y})$. This leads in conjunction with (4.7) to

$$\begin{aligned}\int_\Gamma \mathcal{M}(\partial_{\mathbf{y}}, \mathbf{n}(\mathbf{y})) \cdot [v(\mathbf{y})\mathbf{u}(\mathbf{y})]\, \mathrm{d}s_{\mathbf{y}} = \\ \int_\Gamma \mathcal{M}(\partial_{\mathbf{y}}, \mathbf{n}(\mathbf{y}))v(\mathbf{y}) \cdot \mathbf{u}(\mathbf{y})\, \mathrm{d}s_{\mathbf{y}} + \int_\Gamma v(\mathbf{y})\mathcal{M}(\partial_{\mathbf{y}}, \mathbf{n}(\mathbf{y})) \cdot \mathbf{u}(\mathbf{y})\, \mathrm{d}s_{\mathbf{y}} = \mathbf{0}\,.\end{aligned} \tag{4.15}$$

If the vector function $\mathbf{u}$ is replaced by a matrix $\mathbf{U}(\mathbf{y}) \coloneqq (\mathbf{u}_i(\mathbf{y}))_{1\le i\le N}$ being made of N vector functions $\mathbf{u}_i$ the identity (4.15) can be generalized to

$$\int_\Gamma \mathcal{M}(\partial_{\mathbf{y}}, \mathbf{n}(\mathbf{y}))v(\mathbf{y}) \cdot \mathbf{U}(\mathbf{y})\, \mathrm{d}s_{\mathbf{y}} + \int_\Gamma v(\mathbf{y})\mathcal{M}(\partial_{\mathbf{y}}, \mathbf{n}(\mathbf{y})) \cdot \mathbf{U}(\mathbf{y})\, \mathrm{d}s_{\mathbf{y}} = \mathbf{0}\,. \tag{4.16}$$

For two vector functions $\mathbf{u}(\mathbf{y})$ and $\mathbf{v}(\mathbf{y})$ one obtains by help of (4.13) the identity

$$\sum_{i,j=1}^{3} \int_\Gamma \mathcal{M}_{ij}(\partial_{\mathbf{y}}, \mathbf{n}(\mathbf{y}))\, \big[u_i(\mathbf{y})v_j(\mathbf{y})\big]\, \mathrm{d}s_{\mathbf{y}} = 0\,.$$

Hence, by using the product rule the expression above gives a formula for integration by parts

$$\int_\Gamma \mathbf{u}(\mathbf{y}) \cdot [\mathcal{M}(\partial_{\mathbf{y}}, \mathbf{n}(\mathbf{y})) \cdot \mathbf{v}(\mathbf{y})]\, \mathrm{d}s_{\mathbf{y}} = \int_\Gamma [\mathcal{M}(\partial_{\mathbf{y}}, \mathbf{n}(\mathbf{y})) \cdot \mathbf{u}(\mathbf{y})] \cdot \mathbf{v}(\mathbf{y})\, \mathrm{d}s_{\mathbf{y}}\,. \tag{4.17}$$

Again, considering a matrix $\mathbf{U}(\mathbf{y})$ as already defined in (4.16) the identity (4.17) can be extended such that

$$\int_\Gamma \mathbf{U}^\top(\mathbf{y}) \cdot [\mathcal{M}(\partial_{\mathbf{y}}, \mathbf{n}(\mathbf{y})) \cdot \mathbf{v}(\mathbf{y})]\, \mathrm{d}s_{\mathbf{y}} = \int_\Gamma [\mathcal{M}(\partial_{\mathbf{y}}, \mathbf{n}(\mathbf{y})) \cdot \mathbf{U}(\mathbf{y})]^\top \cdot \mathbf{v}(\mathbf{y})\, \mathrm{d}s_{\mathbf{y}} \tag{4.18}$$

holds.

Finally, a last identity can be obtained by using (4.7) as a starting point. Assuming that the vector field $\mathbf{u}$ is the result of a matrix-vector multiplication $\mathbf{u}(\mathbf{y}) \coloneqq \mathbf{A}(\mathbf{y}) \cdot \mathbf{v}(\mathbf{y})$ between a (3×3)-matrix $\mathbf{A}(\mathbf{y})$ and another vector field $\mathbf{v}(\mathbf{y})$ the identity

$$\int_\Gamma \mathcal{M}(\partial_\mathbf{y}, \mathbf{n}(\mathbf{y})) \cdot [\mathbf{A}(\mathbf{y}) \cdot \mathbf{v}(\mathbf{y})] \, \mathrm{d}s_\mathbf{y} = \mathbf{0}$$

holds. Using the product rule one obtains

$$\int_\Gamma \sum_{j,\ell=1}^{3} \mathcal{M}_{ij} \left(A_{j\ell} v_\ell\right) \mathrm{d}s_\mathbf{y} = \int_\Gamma \sum_{j,\ell=1}^{3} \left(\mathcal{M}_{ij} A_{j\ell}\right) v_\ell \, \mathrm{d}s_\mathbf{y} + \int_\Gamma \sum_{j,\ell=1}^{3} A_{j\ell} \left(\mathcal{M}_{ij} v_\ell\right) \mathrm{d}s_\mathbf{y} \, .$$

Thus, one ends up with the rather cumbersome identity

$$\int_\Gamma [\mathcal{M}(\partial_\mathbf{y}, \mathbf{n}(\mathbf{y})) \cdot \mathbf{A}(\mathbf{y})] \cdot \mathbf{v}(\mathbf{y}) \, \mathrm{d}s_\mathbf{y} = - \left[\sum_{j,\ell=1}^{3} \int_\Gamma A_{j\ell} \left(\mathcal{M}_{ij}(\partial_\mathbf{y}, \mathbf{n}(\mathbf{y})) v_\ell(\mathbf{y})\right) \mathrm{d}s_\mathbf{y} \right]_{1 \le i \le 3} . \tag{4.19}$$

4.2 Scalar problems

The very first regularizations of hypersingular bilinear forms for scalar physical models were given by Nedelec [87] who introduced regularizations in case of the Laplace (Poisson) equation as well as for the Helmholtz equation. Nevertheless, in this section the regularization of hypersingular bilinear forms corresponding to those scalar models will be derived briefly. Thereby, this deduction serves mostly as a preliminary example since the regularization process in elasticity, though more cumbersome, follows almost the same rules as presented here. Moreover, this regularization is done largely as it is presented in [120] for the hypersingular bilinear form according to the Laplace equation. An extremely general regularization which holds for arbitrary scalar elliptic partial differential operators is given in [107].

As mentioned in section 3.1, the fundamental solutions are the distributional solutions of the partial differential equations for an unbounded domain containing the Dirac distribution as inhomogeneity. Those fundamental solutions are the basis for the definition of the boundary integral operators presented in section 3.2. Further, in section 3.3 bilinear forms were introduced which serve as starting point for the later proposed numerical methods. Since the hypersingular bilinear forms are inadequate for an ad hoc use within a numerical scheme they must be treated analytically in advance. Here, integration by parts based upon the previously introduced mathematical tools is used to transform the hypersingular bilinear forms to weakly singular bilinear forms.

To begin with, the scalar fundamental solutions U associated to the partial differential equations stated in section 2.1 will be introduced. According to (2.15) and (2.14), the

fundamental solutions have to fulfill

$$\Delta_{\mathbf{y}} U^L(\mathbf{y}-\mathbf{x}) = -\delta(\mathbf{y}-\mathbf{x}) \qquad \forall \mathbf{y} \in \mathbb{R}^3 \tag{4.20}$$

for the Laplace (Poisson) equation and

$$\left((\Delta_{\mathbf{y}} - k^2) U_k^W\right)(\mathbf{y}-\mathbf{x}) = -\delta(\mathbf{y}-\mathbf{x}) \qquad \forall \mathbf{y} \in \mathbb{R}^3 \tag{4.21}$$

for the Laplace transformed wave equation, respectively. In (4.21), the parameter $k \in \mathbb{C}$ is the complex wave number. In the Laplace domain, it is defined as $k := s/c$ where $s \in \mathbb{C}$ is the Laplace parameter and $c \in \mathbb{R}$ is the wave velocity. The fundamental solutions U of (4.20) and (4.21) can be elaborated by switching from Cartesian to spherical coordinates. Then, by taking their symmetry into account one ends up with an ordinary differential equation. This procedure is well-known and detailed documented in a lot of references, e.g., in [41] and [93]. Here, it is sufficient to recall the final fundamental solutions. The results are taken from [94] and are

$$U^L(\mathbf{y}-\mathbf{x}) = \frac{1}{4\pi} \frac{1}{|\mathbf{y}-\mathbf{x}|} \tag{4.22}$$

for the Laplace equation and

$$U_k^W(\mathbf{y}-\mathbf{x}) = \frac{1}{4\pi} \frac{\exp(-k|\mathbf{y}-\mathbf{x}|)}{|\mathbf{y}-\mathbf{x}|}$$

for the Laplace transformed wave equation. Since the exponential function occurring in U_k^W is bounded everywhere the two fundamental solutions U^L and U_k^W exhibit the same singular behavior when the point $\mathbf{y}$ approaches the point $\mathbf{x}$. Moreover, to obtain the associated integral operators the trace operations (2.66) and (2.67) which have to be carried out are identical in case of scalar problems. Due to these properties both physical models are treated simultaneously, i.e., there is no distinction made between U^L and U_k^W in the following. Unless no special physical model is considered the fundamental solution will be denoted by U only. Moreover, during the regularization one has to be extremely cautious with quantities belonging to the domain Ω and those which are defined on the boundary Γ only. To make this distinction clearer the points $\mathbf{x}, \mathbf{y} \in \Gamma$ are assumed to be exclusively defined on the boundary while $\tilde{\mathbf{x}} \in \Omega$ lies in the considered domain. Analogously, the function U denotes strictly the function $U(\mathbf{y}-\mathbf{x})$ while $\tilde{U}$ represents the function $U(\mathbf{y}-\tilde{\mathbf{x}})$.

In this general setting, the double layer potential according to (3.17) reads as

$$(\widehat{\mathcal{K}} u)(\tilde{\mathbf{x}}) = \int_\Gamma u(\mathbf{y}) \frac{\partial \tilde{U}}{\partial \mathbf{n}(\mathbf{y})} \, \mathrm{d}s_{\mathbf{y}} \qquad \forall \mathbf{y} \in \Gamma, \tilde{\mathbf{x}} \in \Omega \, .$$

Note that for sake of brevity the trace $u_\Gamma(\mathbf{y})$ is just denoted as $u(\mathbf{y})$ throughout this section. Next, applying the conormal derivative to the expression above yields

$$\nabla_{\tilde{\mathbf{x}}} (\widehat{\mathcal{K}} u)(\tilde{\mathbf{x}}) \cdot \mathbf{n}(\mathbf{x}) = \int_\Gamma u(\mathbf{y}) \left[\nabla_{\tilde{\mathbf{x}}} \frac{\partial \tilde{U}}{\partial \mathbf{n}(\mathbf{y})} \cdot \mathbf{n}(\mathbf{x}) \right] \mathrm{d}s_{\mathbf{y}} \quad \forall \mathbf{x}, \mathbf{y} \in \Gamma, \tilde{\mathbf{x}} \in \Omega \, . \tag{4.23}$$

Applying a limiting process $\Omega \ni \tilde{\mathbf{x}} \to \mathbf{x} \in \Gamma$ to (4.23) would result into the hypersingular operator as it is defined in (3.23). To avoid this, the expression in square brackets containing the singularity needs to be transformed. This is done by using an additional identity which connects this term to the surface derivatives stated in 4.1.

The application of the surface curl (4.2) to a vector field $\mathbf{g}(\mathbf{y}) := \mathbf{u}(\mathbf{y}) \times \mathbf{v}(\mathbf{y})$ being defined as the rotation of two vector fields $\mathbf{u}(\mathbf{y})$ and $\mathbf{v}(\mathbf{y})$ gives

$$\frac{\partial}{\partial \mathbf{S}(\partial_{\mathbf{y}}, \mathbf{n}(\mathbf{y}))} \cdot \mathbf{g}(\mathbf{y}) = [\nabla_{\mathbf{y}} \times (\mathbf{u}(\mathbf{y}) \times \mathbf{v}(\mathbf{y}))] \cdot \mathbf{n}(\mathbf{y}) \, .$$

Using simple vector calculus the expression in square brackets is equivalent to

$$\nabla_{\mathbf{y}} \times (\mathbf{u} \times \mathbf{v}) = (\nabla_{\mathbf{y}} \mathbf{u}) \cdot \mathbf{v} - (\nabla_{\mathbf{y}} \mathbf{v}) \cdot \mathbf{u} - (\nabla_{\mathbf{y}} \cdot \mathbf{u}) \, \mathbf{v} + (\nabla_{\mathbf{y}} \cdot \mathbf{v}) \, \mathbf{u} \, . \tag{4.24}$$

Now, bearing the derivative of the double layer operator (4.23) in mind it is advantageous to exchange $\mathbf{u}$ by the normal vector $\mathbf{n}(\mathbf{x})$ and $\mathbf{v}$ by the gradient of the fundamental solution $\nabla_{\tilde{\mathbf{x}}} \tilde{U}$. The normal vector $\mathbf{n}(\mathbf{x})$ is constant with respect to the point $\mathbf{y}$ and, hence, by using (4.24) one obtains the identity

$$\frac{\partial}{\partial \mathbf{S}(\partial_{\mathbf{y}}, \mathbf{n}(\mathbf{y}))} \cdot \big(\mathbf{n}(\mathbf{x}) \times \nabla_{\tilde{\mathbf{x}}} \tilde{U} \big) = - \left[\nabla_{\tilde{\mathbf{x}}} \frac{\partial \tilde{U}}{\partial \mathbf{n}(\mathbf{y})} \cdot \mathbf{n}(\mathbf{x}) \right] - \Delta_{\mathbf{y}} \tilde{U} \, \mathbf{n}(\mathbf{x}) \cdot \mathbf{n}(\mathbf{y}) \, . \tag{4.25}$$

Obviously, the term in parenthesis on the left hand-side of (4.25) equals $\partial \tilde{U} / \partial \mathbf{S}(\partial_{\tilde{\mathbf{x}}}, \mathbf{n}(\mathbf{x}))$ such that inserting the identity (4.25) into (4.23) yields

$$\begin{aligned} &\nabla_{\tilde{\mathbf{x}}} (\widehat{\mathcal{K}} u)(\tilde{\mathbf{x}}) \cdot \mathbf{n}(\mathbf{x}) = \\ &\qquad - \int_{\Gamma} u(\mathbf{y}) \left(\frac{\partial}{\partial \mathbf{S}(\partial_{\mathbf{y}}, \mathbf{n}(\mathbf{y}))} \cdot \frac{\partial \tilde{U}}{\partial \mathbf{S}(\partial_{\tilde{\mathbf{x}}}, \mathbf{n}(\mathbf{x}))} \right) \mathrm{d}s_{\mathbf{y}} - \int_{\Gamma} u(\mathbf{y}) \Delta_{\mathbf{y}} \tilde{U} \, \mathbf{n}(\mathbf{x}) \cdot \mathbf{n}(\mathbf{y}) \, \mathrm{d}s_{\mathbf{y}} \, . \end{aligned}$$

Using identity (4.4) the hypersingular integral operator reads as

$$\begin{aligned} (\widehat{\mathcal{D}} u)(\mathbf{x}) &= - \lim_{\Omega \ni \tilde{\mathbf{x}} \to \mathbf{x} \in \Gamma} \nabla_{\tilde{\mathbf{x}}} (\widehat{\mathcal{K}} u)(\tilde{\mathbf{x}}) \cdot \mathbf{n}(\mathbf{x}) \\ &= - \lim_{\varepsilon \to 0} \int_{\mathbf{y} \in \Gamma : |\mathbf{y} - \mathbf{x}| \geq \varepsilon} \frac{\partial u(\mathbf{y})}{\partial \mathbf{S}(\partial_{\mathbf{y}}, \mathbf{n}(\mathbf{y}))} \cdot \frac{\partial U}{\partial \mathbf{S}(\partial_{\mathbf{x}}, \mathbf{n}(\mathbf{x}))} \, \mathrm{d}s_{\mathbf{y}} \\ &\quad + \lim_{\varepsilon \to 0} \int_{\mathbf{y} \in \Gamma : |\mathbf{y} - \mathbf{x}| \geq \varepsilon} u(\mathbf{y}) \Delta_{\mathbf{y}} U \, \mathbf{n}(\mathbf{x}) \cdot \mathbf{n}(\mathbf{y}) \, \mathrm{d}s_{\mathbf{y}} \, . \end{aligned}$$

For the bilinear form of the hypersingular operator one therefore obtains

$$\begin{aligned} \langle \widehat{\mathcal{D}} u, v \rangle_{\Gamma} = - \int_{\Gamma} \lim_{\varepsilon \to 0} \int_{\mathbf{y} \in \Gamma : |\mathbf{y} - \mathbf{x}| \geq \varepsilon} &\left[v(\mathbf{x}) \frac{\partial u(\mathbf{y})}{\partial \mathbf{S}(\partial_{\mathbf{y}}, \mathbf{n}(\mathbf{y}))} \right] \cdot \frac{\partial U}{\partial \mathbf{S}(\partial_{\mathbf{x}}, \mathbf{n}(\mathbf{x}))} \, \mathrm{d}s_{\mathbf{y}} \, \mathrm{d}s_{\mathbf{x}} \\ &+ \int_{\Gamma} v(\mathbf{x}) \lim_{\varepsilon \to 0} \int_{\mathbf{y} \in \Gamma : |\mathbf{y} - \mathbf{x}| \geq \varepsilon} u(\mathbf{y}) \Delta_{\mathbf{y}} U \, \mathbf{n}(\mathbf{x}) \cdot \mathbf{n}(\mathbf{y}) \, \mathrm{d}s_{\mathbf{y}} \, \mathrm{d}s_{\mathbf{x}} \, . \end{aligned}$$

Using the identity (4.4) a last time the hypersingular bilinear form reads as

$$\langle \widehat{\mathcal{D}}u, v\rangle_\Gamma = \int_\Gamma \lim_{\varepsilon\to 0} \int_{\mathbf{y}\in\Gamma:|\mathbf{y}-\mathbf{x}|\geq\varepsilon} \frac{\partial}{\partial \mathbf{S}(\partial_\mathbf{x}, \mathbf{n}(\mathbf{x}))} \cdot \left[v(\mathbf{x}) \frac{\partial u(\mathbf{y})}{\partial \mathbf{S}(\partial_\mathbf{y}, \mathbf{n}(\mathbf{y}))} \right] U \, \mathrm{d}s_\mathbf{y} \, \mathrm{d}s_\mathbf{x} + \int_\Gamma v(\mathbf{x}) \lim_{\varepsilon\to 0} \int_{\mathbf{y}\in\Gamma:|\mathbf{y}-\mathbf{x}|\geq\varepsilon} u(\mathbf{y}) \Delta_\mathbf{y} U \, \mathbf{n}(\mathbf{x}) \cdot \mathbf{n}(\mathbf{y}) \, \mathrm{d}s_\mathbf{y} \, \mathrm{d}s_\mathbf{x} \, .$$

The application of the surface curl to the term in square brackets can be simplified since it is easy to verify that

$$\frac{\partial}{\partial \mathbf{S}(\partial_\mathbf{x}, \mathbf{n}(\mathbf{x}))} \cdot [v(\mathbf{x})\mathbf{g}(\mathbf{y})] = \frac{\partial v(\mathbf{x})}{\partial \mathbf{S}(\partial_\mathbf{x}, \mathbf{n}(\mathbf{x}))} \cdot \mathbf{g}(\mathbf{y})$$

holds for any vector function $\mathbf{g}(\mathbf{y})$. With this, the final hypersingular bilinear form is obtained

$$\langle \widehat{\mathcal{D}}u, v\rangle_\Gamma = \int_\Gamma \lim_{\varepsilon\to 0} \int_{\mathbf{y}\in\Gamma:|\mathbf{y}-\mathbf{x}|\geq\varepsilon} \frac{\partial v(\mathbf{x})}{\partial \mathbf{S}(\partial_\mathbf{x}, \mathbf{n}(\mathbf{x}))} \cdot \frac{\partial u(\mathbf{y})}{\partial \mathbf{S}(\partial_\mathbf{y}, \mathbf{n}(\mathbf{y}))} U(\mathbf{y}-\mathbf{x}) \, \mathrm{d}s_\mathbf{y} \, \mathrm{d}s_\mathbf{x} + \int_\Gamma \lim_{\varepsilon\to 0} \int_{\mathbf{y}\in\Gamma:|\mathbf{y}-\mathbf{x}|\geq\varepsilon} v(\mathbf{x}) u(\mathbf{y}) \Delta_\mathbf{y} U(\mathbf{y}-\mathbf{x}) \, \mathbf{n}(\mathbf{x}) \cdot \mathbf{n}(\mathbf{y}) \, \mathrm{d}s_\mathbf{y} \, \mathrm{d}s_\mathbf{x} \, . \quad (4.26)$$

The first term on the right hand-side contains no more derivatives of the fundamental solution, i.e., the integral is of improper type and converges. The second term embodies the Laplacian of the fundamental solution which is somehow indetermined at the moment. To assign a reasonable meaning to this term one has to specialize the underlying partial differential equation, i.e., the fundamental solution U must be chosen either to U^L or to U_k^W. According to the differential equation (4.20) the fundamental solution U^L fulfills

$$\Delta_\mathbf{y} U^L = 0$$

since $\mathbf{y} \neq \mathbf{x}$ because $|\mathbf{y}-\mathbf{x}| \geq \varepsilon$ holds. Thus, the last term vanishes and the regularized bilinear form for the Laplace equation is simply

$$\langle \widehat{\mathcal{D}}^L u, v\rangle_\Gamma = \int_\Gamma \int_\Gamma \frac{\partial v(\mathbf{x})}{\partial \mathbf{S}(\partial_\mathbf{x}, \mathbf{n}(\mathbf{x}))} \cdot \frac{\partial u(\mathbf{y})}{\partial \mathbf{S}(\partial_\mathbf{y}, \mathbf{n}(\mathbf{y}))} U^L(\mathbf{y}-\mathbf{x}) \, \mathrm{d}s_\mathbf{y} \, \mathrm{d}s_\mathbf{x} \, . \quad (4.27)$$

In case of the Laplace transformed wave equation the fundamental solution U_k^W fulfills in accordance to (4.21)

$$\Delta_\mathbf{y} U_k^W = k^2 U_k^W \, . \quad (4.28)$$

This is again due to the condition $\mathbf{y} \neq \mathbf{x}$. The right hand-side of (4.28) is clearly a weak singularity and, therefore, inserting this relation into the second term in (4.26) yields a

weakly singular integral. Finally, the complete regularized bilinear form in case of the Laplace transformed wave equation reads as

$$\langle \widehat{\mathcal{D}}_k^W u, v\rangle_\Gamma = \int_\Gamma \int_\Gamma \frac{\partial v(\mathbf{x})}{\partial \mathbf{S}(\partial_\mathbf{x}, \mathbf{n}(\mathbf{x}))} \cdot \frac{\partial u(\mathbf{y})}{\partial \mathbf{S}(\partial_\mathbf{y}, \mathbf{n}(\mathbf{y}))} U_k^W(\mathbf{y}-\mathbf{x}) \, \mathrm{d}s_\mathbf{y} \, \mathrm{d}s_\mathbf{x} + k^2 \int_\Gamma \int_\Gamma v(\mathbf{x}) u(\mathbf{y}) U_k^W(\mathbf{y}-\mathbf{x}) \, \mathbf{n}(\mathbf{x}) \cdot \mathbf{n}(\mathbf{y}) \, \mathrm{d}s_\mathbf{y} \, \mathrm{d}s_\mathbf{x} \, .$$

4.3 Elasticity problems

The previous section dealt with the regularization of hypersingular bilinear forms as they occur in scalar physical models. Here, this concept is picked up to regularize also the hypersingular forms corresponding to elasticity problems. Of course, the growth of dimensionality in the state variables involves more complex transformations and leads to more extensive formulae. But nevertheless, the main principle of using integration by parts is left unchanged.

The first regularization for the hypersingular bilinear form was deduced by Nedelec [87] who uses a very general approach. Further enhancements to time-harmonic elasticity based on that work were given by Nishimura & Kobayashi [88] and by Becache *et al.* [11]. While those formulations are not restricted to isotropic elasticity a priori they result in rather complicated formulae which are quite complicated to handle. Another, somehow more simple, regularization for the case of elastostatics was given by Han [58] who used some basic results already stated in the book of Kupradze [70]. Here, a regularization for the Laplace transformed system of elastodynamics is given which is based on Han's proof. While this regularization may also be found in [64] the deduction presented here is more detailed.

As in the scalar case the regularization demands some knowledge of the fundamental solutions which are involved. And since the present work extents Han's proof to the elastodynamic case the according fundamental solution must be known. As a preliminary work both the elastostatic as well as the elastodynamic fundamental solutions will be deduced in the following and their similarities will be pointed out.

Hörmander's method. Analogously to section 4.2 were the fundamental solutions for the Laplace equation and the Laplace transformed wave equation were merged for a simultaneous treatment, here, the same is done for the fundamental solution of the elastostatic and the Laplace transformed elastodynamic system. Of course, the necessary fundamental solutions are known for a long time. The elastostatic fundamental solution was firstly derived by Lord Kelvin in 1848 and, thus, is often denoted as Kelvin's solution. In the transient case the fundamental solution's derivation goes back to the work of G. Stokes in 1849. For instance, Kelvin's solution may be found in [75] while the transient fundamental

solution is given in [32, 99]. Normally, the representation of those two fundamental solutions differ highly from each other which is inadequate for the regularization process since it demands the same structure of the involved kernel functions. To elaborate the similar structure of the elastostatic and Laplace transformed elastodynamic fundamental solution both will be deduced briefly.

The derivation of fundamental solutions is done by making use of what is commonly denoted as *Hörmander's method*. Applications of this method are widely known and may be found, e.g., in [111] and [70]. Hörmander's method provides a simple scheme to obtain the solution of coupled elliptic partial differential equations. Thereby, the central idea is the reduction of the original system of partial differential equations to just one partial differential equation a characteristic scalar function has to fulfill. Afterwards the complete solution can be constructed with respect to this scalar function. As will be shown, the fundamental solutions deduced here differ mainly in this characteristic scalar function.

Like in the previous section as a starting point serve the underlying partial differential equations the fundamental solutions have to meet. The according partial differential equations are stated in section 2.2 and reads as

$$(\lambda+\mu)\nabla_{\mathbf{y}}\left(\nabla_{\mathbf{y}}\cdot\mathbf{U}(\mathbf{y}-\mathbf{x})\right)+\mu\Delta_{\mathbf{y}}\mathbf{U}(\mathbf{y}-\mathbf{x})=-\delta(\mathbf{y}-\mathbf{x})\mathbf{I}\qquad\forall\,\mathbf{y}\in\mathbb{R}^3 \tag{4.29}$$

for the system of elastostatics, and

$$(\lambda+\mu)\nabla_{\mathbf{y}}\left(\nabla_{\mathbf{y}}\cdot\mathbf{U}(\mathbf{y}-\mathbf{x})\right)+\mu\Delta_{\mathbf{y}}\mathbf{U}(\mathbf{y}-\mathbf{x})-\varrho_0 s^2\mathbf{U}(\mathbf{y}-\mathbf{x})=-\delta(\mathbf{y}-\mathbf{x})\mathbf{I}\qquad\forall\,\mathbf{y}\in\mathbb{R}^3 \tag{4.30}$$

for the Laplace transformed system of elastodynamics, respectively. Contrary to the scalar problems the fundamental solution in elasticity is a (3×3)-matrix which can be thought as the composition of three solution vectors $\mathbf{U}_i$ such that $\mathbf{U}=(\,\mathbf{U}_1\;\mathbf{U}_2\;\mathbf{U}_3\,)$. Then, every solution vector fulfills the equation $\mathcal{L}\mathbf{U}_i=\delta\mathbf{e}_i$ or $\left(\mathcal{L}+\varrho s^2\right)\mathbf{U}_i=\delta\mathbf{e}_i$, respectively. As before, $\mathbf{e}_i$ denotes a Cartesian basis vector and $\mathcal{L}$ is the Lamé-Navier operator as stated in (2.34).

The equations (4.29) and (4.30) can be abstracted by an operator matrix $\mathcal{B}$ such that

$$\mathcal{B}(\partial_{\mathbf{y}})\cdot\mathbf{U}(\mathbf{y}-\mathbf{x})=-\delta(\mathbf{y}-\mathbf{x})\mathbf{I} \tag{4.31}$$

holds. Thereby, the matrix $\mathcal{B}$ features two parameters A and B with

$$\mathcal{B}=\begin{pmatrix}A+B\partial_{11} & B\partial_{12} & B\partial_{13}\\ B\partial_{12} & A+B\partial_{22} & B\partial_{23}\\ B\partial_{13} & B\partial_{23} & A+B\partial_{33}\end{pmatrix}. \tag{4.32}$$

In (4.32) and for the rest of this section, the notation ∂_{ij} abbreviates the derivative $\frac{\partial^2}{\partial y_i\partial y_j}$. Above, the coefficient B is defined as

$$B=\lambda+\mu \tag{4.33}$$

being independent of the equation which is under consideration. Contrary, the parameter A is problem dependent and it is easy to verify that

$$A = A^{ES} = \mu\Delta \tag{4.34}$$

for the static case while it becomes

$$A = A^{ED} = \mu\Delta - \varrho_0 s^2 \tag{4.35}$$

in elastodynamics. Note that all differential operators are applied with respect to the point $\mathbf{y}$.

Contrary to the more common expressions (4.29) and (4.30) the advantage of representing the system of partial differential equations via the operator matrix (4.31) is the implication of the upcoming solution procedure. Besides the coefficient B which is actually an algebraic constant the expression A involves with the Laplacian a differential operator and, therefore, is itself a differential operator. Nevertheless, by the assumption that A and every matrix entry $\mathcal{B}[i,j]$ can be treated as ordinary algebraic quantities the solution $\mathbf{U}$ can be thought as result of a multiplication of (4.31) with its inverse operator matrix $\mathcal{B}^{-1}$. This is the central idea of Hörmander's method.

Recalling known rules from vector calculus the inverse of a matrix $\mathsf{A} \in \mathbb{C}^{n\times n}$ can be represented by help of its *adjugate matrix* $\mathsf{A}^* \in \mathbb{C}^{n\times n}$. Sometimes the adjugate matrix is also denoted as *adjoint matrix* or *classical adjoint matrix*. But these terms are somehow misleading since they could be confused with the adjoint operator. Thus, the term adjugate matrix is the preferred one within this thesis. The adjugate matrix is usually computed by using the matrix of cofactors which are itself nothing but signed minors (see, e.g. [74]). The entries of the matrix $\mathsf{C} \in \mathbb{C}^{n\times n}$ of cofactors are given by

$$\mathsf{C}[i,j] = (-1)^{i+j} \det(\mathsf{M}_{ij}(\mathsf{A})) \,. \tag{4.36}$$

In (4.36), the matrix $\mathsf{M}_{ij}(\mathsf{A}) \in \mathbb{C}^{(n-1)\times(n-1)}$ represents the sub-matrix of A where the i-th row and the j-th column of A have been deleted. The determinant of this sub-matrix is usually denoted as minor of A. Finally, the adjugate matrix A^* reads as

$$\mathsf{A}^* = \mathsf{C}^\top$$

with the property

$$\mathsf{A}\mathsf{A}^* = \mathsf{A}\mathsf{C}^\top = \det(\mathsf{A})\mathsf{I} \,. \tag{4.37}$$

Note that if A is symmetric (but not Hermitian!) then the adjugate matrix and the matrix of cofactors are identical, i.e., $\mathsf{A}^* \equiv \mathsf{C}$.

Transferring those principles to the operator matrix $\mathcal{B}$ one notice that $\mathcal{B} = \mathcal{B}^\top$ holds such that the matrix of cofactors and the adjugate matrix are identical. Moreover, it is assumed that the fundamental solution $\mathbf{U}$ is the composition of the adjugate matrix $\mathcal{B}^*(\partial_{\mathbf{y}})$ and some scalar function φ

$$\mathbf{U}(\mathbf{y}-\mathbf{x}) = \mathcal{B}^*\varphi(\mathbf{y}-\mathbf{x}) \,. \tag{4.38}$$

Inserting this into (4.31) one obtains

$$\mathcal{B}\mathcal{B}^*\varphi(\mathbf{y}-\mathbf{x}) = -\delta(\mathbf{y}-\mathbf{x})\mathbf{I}\,.$$

Now, making use of identity (4.37) one ends up with

$$[\det(\mathcal{B})\varphi(\mathbf{y}-\mathbf{x}) + \delta(\mathbf{y}-\mathbf{x})]\,\mathbf{I} = \mathbf{0} \quad \Longrightarrow \quad \det(\mathcal{B})\varphi(\mathbf{y}-\mathbf{x}) = -\delta(\mathbf{y}-\mathbf{x})\,. \tag{4.39}$$

Thus, the solution scheme is complete: From the scalar equation (4.39) one obtains the function φ which is, afterwards, inserted into (4.38) to obtain the fundamental solution $\mathbf{U}$. Moreover, the solution of the scalar equation requires the determinant $\det(\mathcal{B})$, and the adjugate matrix $\mathcal{B}^*$ is needed to build up the fundamental solution $\mathbf{U}$. The determinant of $\mathcal{B}$ is given by

$$\det(\mathcal{B}) = A^2(A + B\Delta) \tag{4.40}$$

and the adjugate matrix follows to

$$\mathcal{B}^* = \begin{pmatrix} A(A+B\Delta) - AB\partial_{11} & -AB\partial_{12} & -AB\partial_{13} \\ -AB\partial_{12} & A(A+B\Delta) - AB\partial_{22} & -AB\partial_{23} \\ -AB\partial_{13} & -AB\partial_{23} & A(A+B\Delta) - AB\partial_{33} \end{pmatrix}\,.$$

Using the Kronecker delta

$$\delta_{ij} \coloneqq \begin{cases} 1 & i = j \\ 0 & i \neq j \end{cases} \tag{4.41}$$

the entries of $\mathcal{B}^*$ are written as

$$\mathcal{B}^*_{ij} = A(A + B\Delta)\delta_{ij} - AB\partial_{ij}\,.$$

Elastostatic fundamental solution. Inserting the parameters A^{ES} from (4.34) and B from (4.33) into (4.40) yields the scalar differential equation corresponding to the elastostatic system

$$\Delta_{\mathbf{y}}\Delta_{\mathbf{y}}\left[\mu^2(\lambda + 2\mu)\Delta_{\mathbf{y}}\varphi^{ES}(\mathbf{y}-\mathbf{x})\right] = -\delta(\mathbf{y}-\mathbf{x})\,. \tag{4.42}$$

It is advantageous to substitute the term in square brackets by another scalar function χ^{ES} such that

$$\chi^{ES}(\mathbf{y}-\mathbf{x}) \coloneqq \mu^2(\lambda + 2\mu)\Delta_{\mathbf{y}}\varphi^{ES}(\mathbf{y}-\mathbf{x})\,. \tag{4.43}$$

Hence, (4.42) becomes the *Bi-Laplace equation*

$$\Delta_{\mathbf{y}}\Delta_{\mathbf{y}}\chi^{ES}(\mathbf{y}-\mathbf{x}) = -\delta(\mathbf{y}-\mathbf{x})\,. \tag{4.44}$$

For instance, the solution of this equation

$$\chi^{ES}(\mathbf{y}-\mathbf{x}) = \frac{1}{8\pi}|\mathbf{y}-\mathbf{x}| \tag{4.45}$$

can be found in [94]. Finally, inserting these results into (4.38) and employing the definition (4.43) the components of the elastostatic fundamental solution are obtained

$$\mathbf{U}_{ij}^{ES} = \mathcal{B}_{ij}^{*}\varphi^{ES} = \frac{1}{\mu}\Delta_{\mathbf{y}}\chi^{ES}\delta_{ij} - \frac{1}{\mu}\frac{\lambda+\mu}{\lambda+2\mu}\partial_{ij}\chi^{ES} .$$

Thus, Kelvin's solution is in operator notation

$$\mathbf{U}^{ES}(\chi^{ES}) = \frac{1}{\mu}\left[\Delta_{\mathbf{y}}\chi^{ES}\mathbf{I} - \frac{\lambda+\mu}{\lambda+2\mu}\nabla_{\mathbf{y}}\nabla_{\mathbf{y}}\chi^{ES}\right] . \tag{4.46}$$

For later purpose it is advantageous to leave the fundamental solution in its differential form. But, taking out the derivatives within the function χ^{ES} would, of course, lead to the classical representation of the elastostatic fundamental solution as already stated in [75].

Elastodynamic fundamental solution. Though more extensive the derivation of the elastodynamic fundamental solution follows the same steps as before. Starting with the determinant of the operator matrix $\mathcal{B}$ one gets by using A^{ED} from (4.35)

$$\det(\mathcal{B}^{ED}) = \left(\mu\Delta_{\mathbf{y}} - \varrho_0 s^2\right)^2 \left[(\lambda+2\mu)\Delta_{\mathbf{y}} - \varrho_0 s^2\right] .$$

Thus, by exploiting the identities (2.33) and, analogous to the scalar case, by defining the wave numbers $k_i := s/c_i$ with $i = 1,2$ the characteristic scalar equation becomes

$$\mu^2(\lambda+2\mu)\left(\Delta_{\mathbf{y}} - k_2^2\right)^2\left(\Delta_{\mathbf{y}} - k_1^2\right)\varphi^{ED}(\mathbf{y}-\mathbf{x}) = -\delta(\mathbf{y}-\mathbf{x}) . \tag{4.47}$$

As for the elastostatic case it is advantageous to use the substitution

$$\chi^{ED}(\mathbf{y}-\mathbf{x}) := \mu^2(\lambda+2\mu)\left(\Delta_{\mathbf{y}} - k_2^2\right)\varphi^{ED}(\mathbf{y}-\mathbf{x})$$

whereby the characteristic equation (4.47) becomes a *Helmholtz equation of higher order*

$$\left(\Delta_{\mathbf{y}} - k_1^2\right)\left(\Delta_{\mathbf{y}} - k_2^2\right)\chi^{ED}(\mathbf{y}-\mathbf{x}) = -\delta(\mathbf{y}-\mathbf{x}) . \tag{4.48}$$

Again, the solution of the above equation is taken from [94] and is given by

$$\chi^{ED}(\mathbf{y}-\mathbf{x}) = \frac{1}{4\pi}\frac{1}{k_1^2-k_2^2}\frac{\exp(-k_1|\mathbf{y}-\mathbf{x}|) - \exp(-k_2|\mathbf{y}-\mathbf{x}|)}{|\mathbf{y}-\mathbf{x}|} . \tag{4.49}$$

Thus, the fundamental solution $\mathbf{U}^{ED}$ is obtained by inserting the above relations into (4.38)

$$\mathbf{U}_{ij}^{ED} = \mathcal{B}_{ij}^{*}\varphi^{ED} = \frac{1}{\mu}\left(\Delta_{\mathbf{y}} - k_1^2\right)\chi^{ED}\delta_{ij} - \frac{1}{\mu}\frac{\lambda+\mu}{\lambda+2\mu}\partial_{ij}\chi^{ED} .$$

By using operator notation the fundamental solution can, finally, be written as

$$\mathbf{U}^{ED}(\chi^{ED}) = \frac{1}{\mu}\left[\Delta_{\mathbf{y}}\chi^{ED}\mathbf{I} - \frac{\lambda+\mu}{\lambda+2\mu}\nabla_{\mathbf{y}}\nabla_{\mathbf{y}}\chi^{ED}\right] - \frac{1}{\mu}k_1^2\chi^{ED}\mathbf{I} . \tag{4.50}$$

Note that the term $k_1^2/\mu\chi^{ED}\mathbf{I}$ has been separated and the fundamental solution exhibits the same differential operators as before. Thus, the similar structure between the elastodynamic and elastostatic fundamental solution becomes obvious. At the end, it is this similarity which enables an equivalent treatment during the regularization process of the elastostatic and elastodynamic fundamental solution. A deeper insight to this is given in the following.

Regularization of the hypersingular bilinear form. To start with the regularization the similar properties of the two deduced elastic fundamental solutions have to be worked out more clearly. First of all, one could state that both scalar functions χ^{ES} and χ^{ED} given in (4.45) and (4.49), respectively, exhibit no singularities in the limit $\mathbf{y} \to \mathbf{x}$. Moreover, by introducing the distance function r

$$\mathbf{r}(\mathbf{y},\mathbf{x}) := \mathbf{y}-\mathbf{x}, \quad r(\mathbf{y},\mathbf{x}) := |\mathbf{r}(\mathbf{y},\mathbf{x})| \tag{4.51}$$

a series expansion of χ^{ED} yields the expression

$$\chi^{ED}(\mathbf{r}) = -\frac{1}{4\pi}\frac{1}{k_1+k_2} + \frac{r}{8\pi} + \mathcal{O}(r^2)\,.$$

Obviously, the two scalar functions χ^{ES} and χ^{ED} are at least both of the order $\mathcal{O}(r)$. Therefore, they exhibit the same properties within their respective fundamental solutions, i.e., both functions become weakly singular when differentiating them twice. Concerning the last term in the elastodynamic fundamental solution (4.50) and bearing the hypersingular operator (3.23) in mind this term will become weakly singular at the end since it is achieved by twice the application of the stress operator $\mathcal{T}$. Hence, no special attention has to be given to those terms during the regularization and one can concentrate on the terms in brackets within the fundamental solutions (4.46) and (4.50), respectively. Those terms can be interpreted as being the result of the same operator applied on two different scalar functions χ^{ES} and χ^{ED}. Hence, in the following a kernel function $\mathbf{U}(\chi)$ of the general form

$$\mathbf{U}(\chi) = \frac{1}{\mu}\left[\Delta_{\mathbf{y}}\chi\mathbf{I} - \frac{\lambda+\mu}{\lambda+2\mu}\nabla_{\mathbf{y}}\nabla_{\mathbf{y}}\chi\right] \tag{4.52}$$

is thought depending on some arbitrary but differentiable scalar function $\chi(\mathbf{y}-\mathbf{x})$. As in the scalar case it is important to distinct points on the boundary from points within the domain. Thus, the variables $\mathbf{y},\mathbf{x} \in \Gamma$ belong to the boundary while $\tilde{\mathbf{x}} \in \Omega$ is strictly defined in the domain. Moreover, to keep the notation clear the functions' arguments are skipped whenever possible. Therefore, the function $\tilde{\chi}$ abbreviates $\chi(\mathbf{y}-\tilde{\mathbf{x}})$ while the function χ denotes $\chi(\mathbf{y}-\mathbf{x})$. The same holds also for the fundamental solution itself, i.e., the abbreviations $\tilde{\mathbf{U}} = \mathbf{U}(\tilde{\chi})$ and $\mathbf{U} = \mathbf{U}(\chi)$ are used.

As the regularization's main idea is based on integration by parts it is the traction operator which, roughly spoken, has to be shifted from the fundamental solution to the test- and trial-functions. But until now, only a very general definition of this operator is given which is, naturally, inadequate for the regularization. Thus, a much more detailed definition of

this operator will be elaborated. Recalling its definition (2.68) the traction operator reads as

$$(\mathcal{T}\mathbf{u})^{\top}(\mathbf{x}) = \mathbf{t}(\mathbf{x}) = \boldsymbol{\sigma}(\mathbf{u}(\mathbf{x})) \cdot \mathbf{n}(\mathbf{x}) \,. \tag{4.53}$$

Note that the right-hand side of (4.53) demands in fact the limiting process $\tilde{\mathbf{x}} \to \mathbf{x}$ as stated in the original definition (2.68). Here, this limit is omitted for the sake of simplicity. Now, inserting the stress-strain relation (2.27) into (4.53) yields

$$(\mathcal{T}\mathbf{u})^{\top}(\mathbf{x}) = \lambda(\nabla \cdot \mathbf{u})\mathbf{n} + \mu \left(\nabla\mathbf{u} + (\nabla\mathbf{u})^{\top}\right) \cdot \mathbf{n} \,. \tag{4.54}$$

Although it seems somehow dispensable it is useful to consider the special case when $\mathcal{T}$ is applied to a vector field of the form $f(\mathbf{y}-\mathbf{x})\mathbf{e}_\ell$ where $f(\mathbf{y}-\mathbf{x})$ is some differentiable scalar function and $\mathbf{e}_\ell$ is the ℓ-th Cartesian basis vector. Evaluating (4.54) with this data gives

$$(\mathcal{T}(f\mathbf{e}_\ell))^{\top}(\mathbf{y}-\mathbf{x}) = \lambda \frac{\partial f}{\partial y_\ell}\mathbf{n}(\mathbf{y}) + \mu n_\ell(\mathbf{y})\nabla f + \mu \frac{\partial f}{\mathbf{n}(\mathbf{y})}\mathbf{e}_\ell \,. \tag{4.55}$$

Furthermore, by the application of the traction operator to every Cartesian basis vector the expression (4.55) can be enhanced to

$$(\mathcal{T}(f\mathbf{I}))^{\top}(\mathbf{y}-\mathbf{x}) = \lambda \nabla f \otimes \mathbf{n}(\mathbf{y}) + \mu \mathbf{n}(\mathbf{y}) \otimes \nabla f + \mu \frac{\partial f}{\partial \mathbf{n}(\mathbf{y})}\mathbf{I} \,. \tag{4.56}$$

Due to adding and subtracting the term $\mu\nabla f \otimes \mathbf{n}(\mathbf{y})$ and by taking the definition of the Günter derivatives (4.10) into account the above expression can be transformed into

$$(\mathcal{T}(f\mathbf{I}))^{\top}(\mathbf{y}-\mathbf{x}) = (\lambda+\mu)\nabla f \otimes \mathbf{n}(\mathbf{y}) - \mu\mathcal{M}f + \mu \frac{\partial f}{\partial \mathbf{n}(\mathbf{y})}\mathbf{I} \,. \tag{4.57}$$

Expression (4.57) is useful for later purpose within the regularization process but the underlying traction operator is unsuitable in some sense. Thus, for the treatment within the regularization the stress relation (4.54) has to underwent some transformations. Of course, the aim of these transformations is the incorporation of the tangential derivatives presented in 4.1. Obviously, the expression (4.54) is equal to

$$(\mathcal{T}\mathbf{u})^{\top}(\mathbf{x}) = \lambda(\nabla \cdot \mathbf{u})\mathbf{n} + \mu \left(\nabla\mathbf{u} - (\nabla\mathbf{u})^{\top}\right) \cdot \mathbf{n} + 2\mu \left(\nabla\mathbf{u}\right)^{\top} \cdot \mathbf{n} \,. \tag{4.58}$$

The central term of this equation is double the skew-symmetric part of the displacement field's gradient. In accordance to (2.17) and (2.18) the identity

$$\left(\nabla\mathbf{u} - (\nabla\mathbf{u})^{\top}\right) \cdot \mathbf{n} = -\mathbf{n} \times (\nabla \times \mathbf{u}) \tag{4.59}$$

holds. Furthermore, the last term in (4.58) can be replaced by making use of the definition of the Günter derivatives (4.7). Based on this definition a simple computation gives

$$\mathcal{M} \cdot \mathbf{u} = (\mathbf{n} \times \nabla) \times \mathbf{u} = (\nabla\mathbf{u})^{\top} \cdot \mathbf{n} - (\nabla \cdot \mathbf{u})\,\mathbf{n} \,. \tag{4.60}$$

Finally, inserting (4.59) and (4.60) into (4.58) results in a suitable representation of the stress operator

$$(\mathcal{T}\mathbf{u})^\top = 2\mu\mathcal{M}\cdot\mathbf{u} + (\lambda+2\mu)\,(\nabla\cdot\mathbf{u})\,\mathbf{n} - \mu\mathbf{n}\times(\nabla\times\mathbf{u})\ . \tag{4.61}$$

Analogous to the scalar problem treated in the previous section as a starting point serves the double layer potential (3.17)

$$(\widehat{\mathcal{K}}\mathbf{u})(\tilde{\mathbf{x}}) = \int_\Gamma \left(\mathcal{T}_\mathbf{y}\tilde{\mathbf{U}}\right)^\top\cdot\mathbf{u}(\mathbf{y})\,\mathrm{d}s_\mathbf{y}\ . \tag{4.62}$$

Note that the stress operator's application on the fundamental solution has to be done column-wise, i.e., $(\mathcal{T}\mathbf{U})^\top = (\,\mathcal{T}\mathbf{U}_1\ \mathcal{T}\mathbf{U}_2\ \mathcal{T}\mathbf{U}_3\,)^\top$. In its definition above the traction operator consists of three distinct differential operators, namely the Günter derivatives, a divergence and a rotational part. While the Günter derivatives left unchanged for the moment the two remaining operations have to be taken out. Corresponding to the fundamental solution (4.52) the divergence of its ℓ-th column is simply

$$\nabla\cdot\tilde{\mathbf{U}}_\ell = \frac{1}{\lambda+2\mu}\frac{\partial}{\partial y_\ell}\Delta\tilde{\chi}\ . \tag{4.63}$$

The rotational part of the fundamental solution is a bit more cumbersome and reads as

$$\mathbf{n}(\mathbf{y})\times(\nabla\times\tilde{\mathbf{U}}_\ell) = \frac{1}{\mu}\left[(\nabla\Delta\tilde{\chi})\,n_\ell(\mathbf{y}) - \frac{\partial}{\partial\mathbf{n}(\mathbf{y})}\Delta\tilde{\chi}\mathbf{e}_\ell\right]\ . \tag{4.64}$$

Note that, unless mentioned otherwise, all derivatives are taken with respect to the point $\mathbf{y}$. Thus, the differential operators exhibit no subscript within the expressions above and in the following. Again, this is done for sake of brevity. Now, inserting (4.63) together with (4.64) into the operators definition (4.61) yields

$$(\mathcal{T}\tilde{\mathbf{U}}_\ell)^\top = 2\mu\mathcal{M}\cdot\tilde{\mathbf{U}}_\ell + \left(\frac{\partial}{\partial y_\ell}\Delta\tilde{\chi}\mathbf{n}(\mathbf{y}) - n_\ell(\mathbf{y})\nabla\Delta\tilde{\chi}\right) + \frac{\partial}{\partial\mathbf{n}(\mathbf{y})}\Delta\tilde{\chi}\mathbf{e}_\ell\ . \tag{4.65}$$

Comparing the term in parenthesis with the Günter derivatives from (4.9) it becomes obvious that it is nothing but the ℓ-th column of the operator $\mathcal{M}$ applied to the function $\Delta\tilde{\chi}$. Hence, the double layer operator (4.62) can be formulated as

$$(\widehat{\mathcal{K}}\mathbf{u})(\tilde{\mathbf{x}}) = 2\mu\int_\Gamma \left(\mathcal{M}\tilde{\mathbf{U}}\right)^\top\cdot\mathbf{u}(\mathbf{y})\,\mathrm{d}s_\mathbf{y} + \int_\Gamma(\mathcal{M}\Delta\tilde{\chi})\cdot\mathbf{u}\,\mathrm{d}s_\mathbf{y} + \int_\Gamma\frac{\partial}{\partial\mathbf{n}(\mathbf{y})}\Delta\tilde{\chi}\,\mathbf{u}(\mathbf{y})\,\mathrm{d}s_\mathbf{y}\ .$$

According to section 4.1, this formulation of the double layer operator is suitable to be integrated by parts. With the fundamental solution's symmetry property $\tilde{\mathbf{U}}^\top = \tilde{\mathbf{U}}$ and by using the identities (4.18) and (4.15)

$$(\widehat{\mathcal{K}}\mathbf{u})(\tilde{\mathbf{x}}) = 2\mu\int_\Gamma\tilde{\mathbf{U}}\cdot(\mathcal{M}\cdot\mathbf{u}(\mathbf{y}))\,\mathrm{d}s_\mathbf{y} - \int_\Gamma\Delta\tilde{\chi}\,(\mathcal{M}\cdot\mathbf{u}(\mathbf{y}))\,\mathrm{d}s_\mathbf{y} + \int_\Gamma\frac{\partial}{\partial\mathbf{n}(\mathbf{y})}\Delta\tilde{\chi}\mathbf{u}(\mathbf{y})\,\mathrm{d}s_\mathbf{y} \tag{4.66}$$

is obtained, which can be used to establish a weakly singular representation of the double layer operator in elasticity. In the elastostatic case the regularized double layer operator is achieved by simply exchanging $\tilde{\chi}$ by $\tilde{\chi}^{ES}$. With $\mathbf{U}^{ES} = \mathbf{U}(\chi^{ES})$ this gives

$$(\widehat{\mathcal{K}}^{ES}\mathbf{u})(\mathbf{x}) = 2\mu \int_\Gamma \mathbf{U}^{ES} \cdot (\mathcal{M} \cdot \mathbf{u}(\mathbf{y}))\, \mathrm{d}s_\mathbf{y} - \int_\Gamma \Delta\chi^{ES}(\mathcal{M} \cdot \mathbf{u}(\mathbf{y}))\, \mathrm{d}s_\mathbf{y} + \int_\Gamma \frac{\partial}{\partial \mathbf{n}(\mathbf{y})} \Delta\chi^{ES}\mathbf{u}(\mathbf{y})\, \mathrm{d}s_\mathbf{y} \qquad \forall \mathbf{x}, \mathbf{y} \in \Gamma\,. \quad (4.67)$$

It is easy to verify that the Laplacian of the function χ^{ES} (4.45) equals the fundamental solution of the Laplace equation (4.22). Thus, the regularized double layer operator in elastostatics can be expressed via the elastostatic single layer operator as well as by the single and double layer operators according to the Laplace equation [9, 89]. Analogous, the regularized double layer operator in elastodynamics is achieved by substituting $\tilde{\chi}$ by $\tilde{\chi}^{ED}$ where the remaining difference term $k_1^2/\mu\,\tilde{\chi}^{ED}\mathbf{I}$ has to be taken into account (cf. (4.50)). This gives with help of (4.56)

$$\frac{k_1^2}{\mu}(\mathcal{T}\tilde{\chi}^{ED}\mathbf{I})^\top = k_1^2 \left(\frac{\lambda}{\mu} \nabla\chi^{ED} \otimes \mathbf{n}(\mathbf{y}) + \mathbf{n}(\mathbf{y}) \otimes \nabla\chi^{ED} + \frac{\partial \chi^{ED}}{\partial \mathbf{n}(\mathbf{y})} \mathbf{I} \right)\,. \quad (4.68)$$

Under consideration of (2.33) the term λ/μ equals $k_2^2/k_1^2 - 2$. Inserting this into (4.68) and adding and subtracting the term $k_1^2 \mathbf{n}(\mathbf{y}) \otimes \nabla\chi^{ED}$ yields

$$\frac{k_1^2}{\mu}(\mathcal{T}\chi^{ED}\mathbf{I})^\top = -2k_1^2\mathcal{M}\chi^{ED} + k_2^2\mathcal{U}\chi^{ED} - k_1^2\mathcal{U}^\top\chi^{ED} + k_1^2\frac{\partial \chi^{ED}}{\partial \mathbf{n}(\mathbf{y})}\mathbf{I}\,. \quad (4.69)$$

Thus, using integration by parts for the first term of (4.69) the complete elastodynamic double layer operator reads as

$$(\widehat{\mathcal{K}}^{ED}\mathbf{u})(\mathbf{x}) = 2\mu \int_\Gamma \mathbf{U}^{ED} \cdot (\mathcal{M} \cdot \mathbf{u}(\mathbf{y}))\, \mathrm{d}s_\mathbf{y} - \int_\Gamma \Delta\chi^{ED}\,(\mathcal{M} \cdot \mathbf{u}(\mathbf{y}))\, \mathrm{d}s_\mathbf{y} + \int_\Gamma \frac{\partial \Delta\chi^{ED}}{\partial \mathbf{n}(\mathbf{y})}\,\mathbf{u}(\mathbf{y})\, \mathrm{d}s_\mathbf{y} + \int_\Gamma \left[k_1^2\mathcal{U}^\top\chi^{ED} - k_2^2\mathcal{U}\chi^{ED} - k_1^2\frac{\partial \chi^{ED}}{\partial \mathbf{n}(\mathbf{y})}\mathbf{I} \right] \cdot \mathbf{u}(\mathbf{y})\, \mathrm{d}s_\mathbf{y}\,. \quad (4.70)$$

The formulation (4.70) is a weakly singular representation of the elastodynamic double layer operator. This kind of singularity is obvious, since the first three terms exhibit the same properties as their elastostatic counterparts in (4.67). Furthermore, the last term is regular due to the regularity of the gradient of χ^{ED}. Bearing the distance function r in mind this gradient can be expressed by help of the chain rule as

$$\nabla\chi^{ED}(\mathbf{r}) = \frac{\mathrm{d}\chi^{ED}}{\mathrm{d}r}\nabla r\,.$$

Finally, a series expansion of $\mathrm{d}\chi^{ED}/\mathrm{d}r$ about $r = 0$ yields

$$\frac{\mathrm{d}\chi^{ED}}{\mathrm{d}r} = \frac{1}{8\pi} - \frac{k_1^2 + k_1 k_2 + k_2^2}{12\,(k_1 + k_2)\,\pi} r + \mathcal{O}(r^2)$$

which proves the regularity.

Now, to go ahead with the treatment of the hypersingular kernel, the next step is the application of the operator $\mathcal{T}_{\tilde{\mathbf{x}}} := \mathcal{T}(\partial_{\tilde{\mathbf{x}}}, \mathbf{n}(\mathbf{x}))$ to the double layer operator from (4.66). This results in

$$\left(\mathcal{T}_{\tilde{\mathbf{x}}}(\widehat{\mathcal{K}}\mathbf{u})\right)(\tilde{\mathbf{x}}) = \int_\Gamma \left(\mathcal{T}_{\tilde{\mathbf{x}}} \frac{\partial \Delta_{\mathbf{y}} \tilde{\chi}}{\partial \mathbf{n}(\mathbf{y})} \mathbf{I}\right) \cdot \mathbf{u}(\mathbf{y})\, \mathrm{d}s_{\mathbf{y}} + \int_\Gamma \left(2\mu \mathcal{T}_{\tilde{\mathbf{x}}} \tilde{\mathbf{U}} - \mathcal{T}_{\tilde{\mathbf{x}}} \Delta_{\mathbf{y}} \tilde{\chi} \mathbf{I}\right) \cdot (\mathcal{M}_{\mathbf{y}} \cdot \mathbf{u}(\mathbf{y}))\, \mathrm{d}s_{\mathbf{y}} \,. \tag{4.71}$$

Due to the second application of the stress operator it is mandatory to clarify the variables the differential operators work on. As before, this is done by subscribing the differential operator either with $\mathbf{y}$ or with $\tilde{\mathbf{x}}$. To simplify the expression above the abbreviations $\boldsymbol{\psi}^{(i)}$ are introduced

$$\boldsymbol{\psi}^{(1)} := \int_\Gamma \left(\mathcal{T}_{\tilde{\mathbf{x}}} \frac{\partial \Delta_{\mathbf{y}} \tilde{\chi}}{\partial \mathbf{n}(\mathbf{y})} \mathbf{I}\right) \cdot \mathbf{u}(\mathbf{y})\, \mathrm{d}s_{\mathbf{y}} \tag{4.72a}$$

$$\boldsymbol{\psi}^{(2)} := \int_\Gamma \left(2\mu \mathcal{T}_{\tilde{\mathbf{x}}} \tilde{\mathbf{U}} - \mathcal{T}_{\tilde{\mathbf{x}}} \Delta_{\mathbf{y}} \tilde{\chi} \mathbf{I}\right) \cdot (\mathcal{M}_{\mathbf{y}} \cdot \mathbf{u}(\mathbf{y}))\, \mathrm{d}s_{\mathbf{y}} \tag{4.72b}$$

corresponding to the first and second term of (4.71). Now, using the transposed identity (4.57) the term $\boldsymbol{\psi}^{(1)}$ (4.72a) reads as

$$\begin{aligned}\boldsymbol{\psi}^{(1)} = (\lambda + \mu) \int_\Gamma \left[\mathbf{n}(\mathbf{x}) \otimes \nabla_{\tilde{\mathbf{x}}} \frac{\partial \Delta_{\mathbf{y}} \tilde{\chi}}{\partial \mathbf{n}(\mathbf{y})}\right] \cdot \mathbf{u}(\mathbf{y})\, \mathrm{d}s_{\mathbf{y}} \\ + \mu \int_\Gamma \left(\mathcal{M}_{\tilde{\mathbf{x}}} \frac{\partial \Delta_{\mathbf{y}} \tilde{\chi}}{\partial \mathbf{n}(\mathbf{y})}\right) \cdot \mathbf{u}(\mathbf{y})\, \mathrm{d}s_{\mathbf{y}} + \mu \int_\Gamma \frac{\partial^2 \Delta_{\mathbf{y}} \tilde{\chi}}{\partial \mathbf{N}(\tilde{\mathbf{x}}) \partial \mathbf{n}(\mathbf{y})} \mathbf{u}(\mathbf{y})\, \mathrm{d}s_{\mathbf{y}} \,.\end{aligned}$$

Above, the operator $\partial / \partial \mathbf{N}(\tilde{\mathbf{x}})$ is introduced for simplicity and will be used in the following. Its definition is

$$\frac{\partial \varphi(\tilde{\mathbf{x}})}{\partial \mathbf{N}(\tilde{\mathbf{x}})} := \nabla_{\tilde{\mathbf{x}}} \varphi(\tilde{\mathbf{x}}) \cdot \mathbf{n}(\mathbf{x})$$

for some differentiable scalar function $\varphi(\tilde{\mathbf{x}})$. Next, considering the second term $\boldsymbol{\psi}^{(2)}$ the traction operator $\mathcal{T}_{\mathbf{x}}$ has to be applied onto the function $\tilde{\mathbf{U}}$ as well as onto the function $\Delta_{\mathbf{y}} \tilde{\chi} \mathbf{I}$. By means of (4.65) the first term of $\boldsymbol{\psi}^{(2)}$ evaluates to

$$2\mu \mathcal{T}_{\tilde{\mathbf{x}}} \tilde{\mathbf{U}} = 4\mu^2 \mathcal{M}_{\tilde{\mathbf{x}}} \tilde{\mathbf{U}} - 2\mu \mathcal{M}_{\tilde{\mathbf{x}}} \Delta_{\mathbf{y}} \tilde{\chi} + 2\mu \frac{\partial \Delta_{\mathbf{y}} \tilde{\chi}}{\partial \mathbf{N}(\tilde{\mathbf{x}})} \tag{4.73}$$

while the second term yields in accordance to (4.57)

$$\mathcal{T}_{\tilde{\mathbf{x}}} \Delta_{\mathbf{y}} \tilde{\chi} \mathbf{I} = (\lambda + \mu) \mathbf{n}(\mathbf{x}) \otimes \nabla_{\tilde{\mathbf{x}}} \Delta_{\mathbf{y}} \tilde{\chi} + \mu \mathcal{M}_{\tilde{\mathbf{x}}} \Delta_{\mathbf{y}} \tilde{\chi} + \mu \frac{\partial \Delta_{\mathbf{y}} \tilde{\chi}}{\partial \mathbf{N}(\tilde{\mathbf{x}})} \,. \tag{4.74}$$

Inserting (4.73) together with (4.74) into (4.72b) results in

$$\boldsymbol{\psi}^{(2)} = \int_\Gamma \left[4\mu^2 \mathcal{M}_{\tilde{\mathbf{x}}} \tilde{\mathbf{U}} - 3\mu \mathcal{M}_{\tilde{\mathbf{x}}} \Delta_{\mathbf{y}} \tilde{\chi} \mathbf{I}\right] \cdot (\mathcal{M}_{\mathbf{y}} \cdot \mathbf{u}(\mathbf{y})) \, \mathrm{d}s_{\mathbf{y}} - (\lambda+\mu) \int_\Gamma [\mathbf{n}(\mathbf{x}) \otimes \nabla_{\tilde{\mathbf{x}}} \Delta_{\mathbf{y}} \tilde{\chi}] \cdot (\mathcal{M}_{\mathbf{y}} \cdot \mathbf{u}(\mathbf{y})) \, \mathrm{d}s_{\mathbf{y}} + \mu \int_\Gamma \frac{\partial \Delta_{\mathbf{y}} \tilde{\chi}}{\partial \mathbf{N}(\tilde{\mathbf{x}})} \mathcal{M}_{\mathbf{y}} \cdot \mathbf{u}(\mathbf{y}) \, \mathrm{d}s_{\mathbf{y}} \, .$$

Hence, by addition of $\boldsymbol{\psi}^{(1)}$ and $\boldsymbol{\psi}^{(2)}$ the operator $\mathcal{T}_{\tilde{\mathbf{x}}}(\widehat{\mathcal{K}}\mathbf{u})$ from (4.71) becomes

$$\left(\mathcal{T}_{\tilde{\mathbf{x}}}(\widehat{\mathcal{K}}\mathbf{u})\right)(\tilde{\mathbf{x}}) = \mu \int_\Gamma \frac{\partial^2 \Delta_{\mathbf{y}} \tilde{\chi}}{\partial \mathbf{N}(\tilde{\mathbf{x}}) \partial \mathbf{n}(\mathbf{y})} \mathbf{u}(\mathbf{y}) \, \mathrm{d}s_{\mathbf{y}} + \int_\Gamma \left[\mathcal{M}_{\tilde{\mathbf{x}}} \cdot \left(4\mu^2 \tilde{\mathbf{U}} - 3\mu \Delta_{\mathbf{y}} \tilde{\chi} \mathbf{I}\right)\right] \cdot (\mathcal{M}_{\mathbf{y}} \cdot \mathbf{u}(\mathbf{y})) \, \mathrm{d}s_{\mathbf{y}} + \boldsymbol{\psi}^{(3)} + \boldsymbol{\psi}^{(4)} \tag{4.75}$$

with the two additional abbreviations

$$\boldsymbol{\psi}^{(3)} := (\lambda+\mu)\mathbf{n}(\mathbf{x}) \int_\Gamma \left[\nabla_{\tilde{\mathbf{x}}} \frac{\partial \Delta_{\mathbf{y}} \tilde{\chi}}{\partial \mathbf{n}(\mathbf{y})} \cdot \mathbf{u}(\mathbf{y}) - \nabla_{\tilde{\mathbf{x}}} \Delta_{\mathbf{y}} \tilde{\chi} \cdot (\mathcal{M}_{\mathbf{y}} \cdot \mathbf{u}(\mathbf{y}))\right] \mathrm{d}s_{\mathbf{y}} \tag{4.76a}$$

$$\boldsymbol{\psi}^{(4)} := \mu \int_\Gamma \left[\left(\mathcal{M}_{\tilde{\mathbf{x}}} \frac{\partial \Delta_{\mathbf{y}} \tilde{\chi}}{\partial \mathbf{n}(\mathbf{y})}\right) \cdot \mathbf{u}(\mathbf{y}) + \frac{\partial \Delta_{\mathbf{y}} \tilde{\chi}}{\partial \mathbf{N}(\tilde{\mathbf{x}})} (\mathcal{M}_{\mathbf{y}} \cdot \mathbf{u}(\mathbf{y}))\right] \mathrm{d}s_{\mathbf{y}} \, . \tag{4.76b}$$

Note that the identity

$$(\mathbf{a} \otimes \mathbf{b}) \cdot \mathbf{c} = \mathbf{a} (\mathbf{b} \cdot \mathbf{c}) \tag{4.77}$$

was employed to obtain $\boldsymbol{\psi}^{(3)}$. The expressions $\boldsymbol{\psi}^{(3)}$ and $\boldsymbol{\psi}^{(4)}$ are somehow a strange mixture of terms since they consist of differential operators which are applied with respect to the variable $\tilde{\mathbf{x}}$ (or $\mathbf{y}$) and whose results are, afterwards, connected to quantities depending on the complementary variable $\mathbf{y}$ (or $\tilde{\mathbf{x}}$). To cut this knot and to simplify those expressions two additional identities are needed which should be deduced in the following. To begin with, a differentiable scalar function of the form $f = f(\mathbf{y} - \tilde{\mathbf{x}})$ is introduced. An application of the Günter derivatives to the gradient of this function gives

$$\mathcal{M}_{\mathbf{y}} \cdot \nabla_{\tilde{\mathbf{x}}} f = (\nabla_{\mathbf{y}} \otimes \mathbf{n}(\mathbf{y})) \cdot \nabla_{\tilde{\mathbf{x}}} f - (\mathbf{n}(\mathbf{y}) \otimes \nabla_{\mathbf{y}}) \cdot \nabla_{\tilde{\mathbf{x}}} f \, .$$

The use of the identity (4.77) results in

$$\mathcal{M}_{\mathbf{y}} \cdot \nabla_{\tilde{\mathbf{x}}} f = \nabla_{\mathbf{y}} (\mathbf{n}(\mathbf{y}) \cdot \nabla_{\tilde{\mathbf{x}}} f) - \mathbf{n}(\mathbf{y}) (\nabla_{\mathbf{y}} \cdot \nabla_{\tilde{\mathbf{x}}} f) \, .$$

Since the function f is assumed to depend only on the distance $\mathbf{y} - \tilde{\mathbf{x}}$ the gradient with respect to $\mathbf{y}$ can be transformed into a gradient with respect to $\tilde{\mathbf{x}}$ and vice versa

$$\nabla_{\mathbf{y}} = -\nabla_{\tilde{\mathbf{x}}} \, . \tag{4.78}$$

Hence, by using this relation one obtains the final form

$$\mathcal{M}_{\mathbf{y}} \cdot \nabla_{\tilde{\mathbf{x}}} f = \nabla_{\tilde{\mathbf{x}}} \frac{\partial f}{\partial \mathbf{n}(\mathbf{y})} + \mathbf{n}(\mathbf{y}) \Delta_{\mathbf{y}} f \, . \tag{4.79}$$

Now, incorporating (4.79) into (4.76a) yields

$$\boldsymbol{\psi}^{(3)} = (\lambda + \mu)\, \mathbf{n}(\mathbf{x}) \int_{\Gamma} \left\{ [\mathcal{M}_{\mathbf{y}} \cdot (\nabla_{\tilde{\mathbf{x}}} \Delta_{\mathbf{y}} \tilde{\chi})] \cdot \mathbf{u}(\mathbf{y}) - \Delta_{\mathbf{y}}^2 \tilde{\chi}\, \mathbf{n}(\mathbf{y}) \cdot \mathbf{u}(\mathbf{y}) \right\} \mathrm{d}s_{\mathbf{y}} \\ - (\lambda + \mu)\, \mathbf{n}(\mathbf{x}) \int_{\Gamma} \nabla_{\tilde{\mathbf{x}}} \Delta_{\mathbf{y}} \tilde{\chi} \cdot (\mathcal{M}_{\mathbf{y}} \cdot \mathbf{u}(\mathbf{y})) \, \mathrm{d}s_{\mathbf{y}}$$

which simplifies by an integration by parts (4.17) to

$$\boldsymbol{\psi}^{(3)} = -(\lambda + \mu)\, \mathbf{n}(\mathbf{x}) \int_{\Gamma} \Delta_{\mathbf{y}}^2 \tilde{\chi}\, \mathbf{n}(\mathbf{y}) \cdot \mathbf{u}(\mathbf{y}) \, \mathrm{d}s_{\mathbf{y}} \, .$$

The term $\boldsymbol{\psi}^{(4)}$ in (4.76b) exhibit some kind of antisymmetry concerning the application of the Günter derivatives. The first term consist of an application of $\mathcal{M}_{\tilde{\mathbf{x}}}$ to the normal derivative of $\Delta\tilde{\chi}$ with respect to the normal vector $\mathbf{n}(\mathbf{y})$ while the second term is the normal derivative of $\Delta\tilde{\chi}$ with respect to $\mathbf{n}(\mathbf{x})$ multiplied with the Günter derivatives $\mathcal{M}_{\mathbf{y}}$ applied to the displacement field $\mathbf{u}(\mathbf{y})$. To tidy up this mess an operator $\mathcal{W}$ is defined such that

$$\mathcal{W}(\partial_{\mathbf{y}}, \mathbf{n}(\mathbf{y}), \partial_{\tilde{\mathbf{x}}}, \mathbf{n}(\mathbf{x})) \coloneqq \mathcal{M}(\partial_{\mathbf{y}}, \mathbf{n}(\mathbf{y})) \cdot \mathcal{M}(\partial_{\tilde{\mathbf{x}}}, \mathbf{n}(\mathbf{x})) - \mathcal{M}(\partial_{\tilde{\mathbf{x}}}, \mathbf{n}(\mathbf{x})) \cdot \mathcal{M}(\partial_{\mathbf{y}}, \mathbf{n}(\mathbf{y})) \tag{4.80}$$

holds. Now, the multiplications in (4.80) are taken out by using the representation (4.12). With the abbreviations

$$\mathcal{U}_{\mathbf{y}} \coloneqq \mathcal{U}(\partial_{\mathbf{y}}, \mathbf{n}(\mathbf{y})) \\ \mathcal{U}_{\tilde{\mathbf{x}}} \coloneqq \mathcal{U}(\partial_{\tilde{\mathbf{x}}}, \mathbf{n}(\mathbf{x}))$$

one, finally, obtains

$$\mathcal{W} = \mathcal{W}_1 - \mathcal{W}_2 - \mathcal{W}_3 + \mathcal{W}_4$$

with

$$\mathcal{W}_1 \coloneqq \mathcal{U}_{\mathbf{y}} \cdot \mathcal{U}_{\tilde{\mathbf{x}}} - \left(\mathcal{U}_{\mathbf{y}} \cdot \mathcal{U}_{\tilde{\mathbf{x}}} \right)^{\top} \\ \mathcal{W}_2 \coloneqq \mathcal{U}_{\mathbf{y}} \cdot \mathcal{U}_{\tilde{\mathbf{x}}}^{\top} - \left(\mathcal{U}_{\mathbf{y}} \cdot \mathcal{U}_{\tilde{\mathbf{x}}}^{\top} \right)^{\top} \\ \mathcal{W}_3 \coloneqq \mathcal{U}_{\mathbf{y}}^{\top} \cdot \mathcal{U}_{\tilde{\mathbf{x}}} - \left(\mathcal{U}_{\mathbf{y}}^{\top} \cdot \mathcal{U}_{\tilde{\mathbf{x}}} \right)^{\top} \\ \mathcal{W}_4 \coloneqq \mathcal{U}_{\mathbf{y}}^{\top} \cdot \mathcal{U}_{\tilde{\mathbf{x}}}^{\top} - \left(\mathcal{U}_{\mathbf{y}}^{\top} \cdot \mathcal{U}_{\tilde{\mathbf{x}}}^{\top} \right)^{\top} \, .$$

The first term of $\mathcal{W}_1$ reads by the definition (4.11) of the operator $\mathcal{U}$ as

$$\mathcal{U}_{\mathbf{y}} \cdot \mathcal{U}_{\tilde{\mathbf{x}}} = [\nabla_{\mathbf{y}} \otimes \mathbf{n}(\mathbf{y})] \cdot [\nabla_{\tilde{\mathbf{x}}} \otimes \mathbf{n}(\mathbf{x})] \, . \tag{4.81}$$

With the knowledge of using the Günter derivatives just in conjunction with functions depending on the distance $\mathbf{r} = \mathbf{y} - \tilde{\mathbf{x}}$ the differential operators above may be exchanged using (4.78). Furthermore, considering the vector identity

$$(\mathbf{a} \otimes \mathbf{b}) \cdot (\mathbf{c} \otimes \mathbf{d}) = (\mathbf{a} \otimes \mathbf{d})\,(\mathbf{b} \cdot \mathbf{c})$$

the expression (4.81) becomes

$$\mathcal{U}_{\mathbf{y}} \cdot \mathcal{U}_{\tilde{\mathbf{x}}} = [\nabla_{\tilde{\mathbf{x}}} \otimes \mathbf{n}(\mathbf{y})] \cdot [\nabla_{\mathbf{y}} \otimes \mathbf{n}(\mathbf{x})] = [\nabla_{\tilde{\mathbf{x}}} \otimes \mathbf{n}(\mathbf{x})]\,(\mathbf{n}(\mathbf{y}) \cdot \nabla_{\mathbf{y}}) = \mathcal{U}_{\tilde{\mathbf{x}}} \frac{\partial}{\partial \mathbf{n}(\mathbf{y})}$$

and the operator $\mathcal{W}_1$ follows to

$$\mathcal{W}_1 = \mathcal{M}(\partial_{\tilde{\mathbf{x}}}, \mathbf{n}(\mathbf{x})) \frac{\partial}{\partial \mathbf{n}(\mathbf{y})} .$$

Analogously, one obtains for the remaining operators

$$\begin{aligned} \mathcal{W}_2 &= 0 \\ \mathcal{W}_3 &= -\left(\mathbf{n}(\mathbf{y}) \otimes \mathbf{n}(\mathbf{x}) - \mathbf{n}(\mathbf{x}) \otimes \mathbf{n}(\mathbf{y})\right) \Delta_{\mathbf{y}} \\ \mathcal{W}_4 &= -\mathcal{M}(\partial_{\mathbf{y}}, \mathbf{n}(\mathbf{y})) \frac{\partial}{\partial \mathbf{N}(\tilde{\mathbf{x}})} . \end{aligned}$$

Hence, the operator $\mathcal{W}$ is simply

$$\begin{aligned} \mathcal{W}(\partial_{\mathbf{y}}, \mathbf{n}(\mathbf{y}), \partial_{\tilde{\mathbf{x}}}, \mathbf{n}(\mathbf{x})) = \mathcal{M}(\partial_{\tilde{\mathbf{x}}}, \mathbf{n}(\mathbf{x})) \frac{\partial}{\partial \mathbf{n}(\mathbf{y})} - \mathcal{M}(\partial_{\mathbf{y}}, \mathbf{n}(\mathbf{y})) \frac{\partial}{\partial \mathbf{N}(\tilde{\mathbf{x}})} \\ + \left(\mathbf{n}(\mathbf{y}) \otimes \mathbf{n}(\mathbf{x}) - \mathbf{n}(\mathbf{x}) \otimes \mathbf{n}(\mathbf{y})\right) \Delta_{\mathbf{y}} . \end{aligned} \tag{4.82}$$

Returning to the expression $\boldsymbol{\psi}^{(4)}$ from (4.76b) one obtains by help of (4.15)

$$\boldsymbol{\psi}^{(4)} = \mu \int_{\Gamma} \left[\left(\mathcal{M}_{\tilde{\mathbf{x}}} \frac{\partial}{\partial \mathbf{n}(\mathbf{y})} - \mathcal{M}_{\mathbf{y}} \frac{\partial}{\partial \mathbf{N}(\tilde{\mathbf{x}})} \right) \Delta_{\mathbf{y}} \tilde{\chi} \right] \cdot \mathbf{u}(\mathbf{y})\, \mathrm{d}s_{\mathbf{y}} .$$

Next, using the identity (4.82) the expression above is transformed into

$$\boldsymbol{\psi}^{(4)} = \mu \int_{\Gamma} (\mathcal{W} \Delta_{\mathbf{y}} \tilde{\chi}) \cdot \mathbf{u}(\mathbf{y})\, \mathrm{d}s_{\mathbf{y}} - \mu \int_{\Gamma} \left[\left(\mathbf{n}(\mathbf{y}) \otimes \mathbf{n}(\mathbf{x}) - \mathbf{n}(\mathbf{x}) \otimes \mathbf{n}(\mathbf{y})\right) \Delta_{\mathbf{y}}^2 \tilde{\chi} \right] \cdot \mathbf{u}(\mathbf{y})\, \mathrm{d}s_{\mathbf{y}} . \tag{4.83}$$

For a further treatment the first integral from above has to be expanded by inserting the operators definition (4.80). Furthermore, for two symmetric or antisymmetric matrices $\mathbf{A}$ and $\mathbf{B}$ the identity

$$\mathbf{A} \cdot \mathbf{B} = (\mathbf{B} \cdot \mathbf{A})^{\top}$$

holds such that the first integral of (4.83) becomes

$$\int_{\Gamma} (\mathcal{W} \Delta_{\mathbf{y}} \tilde{\chi}) \cdot \mathbf{u}(\mathbf{y})\, \mathrm{d}s_{\mathbf{y}} = \int_{\Gamma} \left[\mathcal{M}_{\tilde{\mathbf{x}}} \cdot (\mathcal{M}_{\mathbf{y}} \Delta_{\mathbf{y}} \tilde{\chi}) \right]^{\top} \cdot \mathbf{u}(\mathbf{y})\, \mathrm{d}s_{\mathbf{y}} - \int_{\Gamma} \left[\mathcal{M}_{\mathbf{y}} \cdot (\mathcal{M}_{\tilde{\mathbf{x}}} \Delta_{\mathbf{y}} \tilde{\chi}) \right]^{\top} \cdot \mathbf{u}(\mathbf{y})\, \mathrm{d}s_{\mathbf{y}}$$

whereas the associativity $(\mathcal{M}_{\tilde{\mathbf{x}}} \cdot \mathcal{M}_{\mathbf{y}})\Delta_{\mathbf{y}}\tilde{\chi} = \mathcal{M}_{\tilde{\mathbf{x}}} \cdot (\mathcal{M}_{\mathbf{y}}\Delta_{\mathbf{y}}\tilde{\chi})$ has already been taken into account. Applying the identity (4.18) to the last integral and inserting the result into (4.83) the expression $\boldsymbol{\psi}^{(4)}$ is

$$\begin{aligned}\boldsymbol{\psi}^{(4)} = \mu \int_{\Gamma} (\mathcal{M}_{\tilde{\mathbf{x}}}\Delta_{\mathbf{y}}\tilde{\chi}) \cdot (\mathcal{M}_{\mathbf{y}} \cdot \mathbf{u}(\mathbf{y}))\, \mathrm{d}s_{\mathbf{y}} + \mu \int_{\Gamma} [\mathcal{M}_{\tilde{\mathbf{x}}} \cdot (\mathcal{M}_{\mathbf{y}}\Delta_{\mathbf{y}}\tilde{\chi})]^{\top} \cdot \mathbf{u}(\mathbf{y})\, \mathrm{d}s_{\mathbf{y}} \\ - \mu \int_{\Gamma} \Delta_{\mathbf{y}}^2\tilde{\chi}\mathbf{n}(\mathbf{y})\,\mathbf{n}(\mathbf{x}) \cdot \mathbf{u}(\mathbf{y}) + \mu\mathbf{n}(\mathbf{x}) \int_{\Gamma} \Delta_{\mathbf{y}}^2\tilde{\chi}\,\mathbf{n}(\mathbf{y}) \cdot \mathbf{u}(\mathbf{y})\, \mathrm{d}s_{\mathbf{y}}\,.\end{aligned}$$

Now it is time to reconstruct the operator (4.75). Inserting the terms $\boldsymbol{\psi}^{(3)}$ and $\boldsymbol{\psi}^{(4)}$ into that equation yields

$$\begin{aligned}\left(\mathcal{T}_{\tilde{\mathbf{x}}}(\widehat{\mathcal{K}}\mathbf{u})\right)(\tilde{\mathbf{x}}) =& \mu \int_{\Gamma} \frac{\partial^2\Delta_{\mathbf{y}}\tilde{\chi}}{\partial\mathbf{N}(\tilde{\mathbf{x}})\partial\mathbf{n}(\mathbf{y})}\mathbf{u}(\mathbf{y})\, \mathrm{d}s_{\mathbf{y}} \\ &+ \int_{\Gamma} \left[\mathcal{M}_{\tilde{\mathbf{x}}} \cdot \left(4\mu^2\tilde{\mathbf{U}} - 2\mu\Delta_{\mathbf{y}}\tilde{\chi}\mathbf{I}\right)\right] \cdot (\mathcal{M}_{\mathbf{y}} \cdot \mathbf{u}(\mathbf{y}))\, \mathrm{d}s_{\mathbf{y}} \\ &+ \mu \int_{\Gamma} [\mathcal{M}_{\tilde{\mathbf{x}}} \cdot (\mathcal{M}_{\mathbf{y}}\Delta_{\mathbf{y}}\tilde{\chi})]^{\top} \cdot \mathbf{u}(\mathbf{y})\, \mathrm{d}s_{\mathbf{y}} \\ &- \int_{\Gamma} [\lambda\mathbf{n}(\mathbf{x})\,\mathbf{n}(\mathbf{y}) \cdot \mathbf{u}(\mathbf{y}) + \mu\mathbf{n}(\mathbf{y})\,\mathbf{n}(\mathbf{x}) \cdot \mathbf{u}(\mathbf{y})]\,\Delta_{\mathbf{y}}^2\tilde{\chi}\, \mathrm{d}s_{\mathbf{y}}\,.\end{aligned} \tag{4.84}$$

According to the identity (4.25) the first term of the expression above can be exchanged to get

$$\begin{aligned}\mu \int_{\Gamma} \frac{\partial^2\Delta_{\mathbf{y}}\tilde{\chi}}{\partial\mathbf{N}(\tilde{\mathbf{x}})\partial\mathbf{n}(\mathbf{y})}\mathbf{u}(\mathbf{y})\, \mathrm{d}s_{\mathbf{y}} = \\ - \mu \int_{\Gamma} \frac{\partial}{\partial\mathbf{S}(\partial_{\mathbf{y}}, \mathbf{n}(\mathbf{y}))} \cdot \frac{\partial\Delta_{\mathbf{y}}\tilde{\chi}}{\partial\mathbf{S}(\partial_{\tilde{\mathbf{x}}}, \mathbf{n}(\mathbf{x}))}\mathbf{u}(\mathbf{y})\, \mathrm{d}s_{\mathbf{y}} - \mu \int_{\Gamma} \Delta_{\mathbf{y}}^2\tilde{\chi}\,\mathbf{n}(\mathbf{x}) \cdot \mathbf{n}(\mathbf{y})\,\mathbf{u}(\mathbf{y})\, \mathrm{d}s_{\mathbf{y}}\,.\end{aligned} \tag{4.85}$$

This expression suffices for an application of the identity (4.4). But, since (4.4) holds only for a combination of a vector field with a scalar function one has to apply it with respect to every component u_i of the first integral of (4.85). Thus,

$$\begin{aligned}\mu \int_{\Gamma} \frac{\partial^2\Delta_{\mathbf{y}}\tilde{\chi}}{\partial\mathbf{N}(\tilde{\mathbf{x}})\partial\mathbf{n}(\mathbf{y})}\mathbf{u}(\mathbf{y})\, \mathrm{d}s_{\mathbf{y}} = \\ \mu \int_{\Gamma} \left[\frac{\partial}{\partial\mathbf{S}(\partial_{\mathbf{y}}, \mathbf{n}(\mathbf{y}))} \otimes \mathbf{u}(\mathbf{y})\right]^{\top} \cdot \frac{\partial\Delta_{\mathbf{y}}\tilde{\chi}}{\partial\mathbf{S}(\partial_{\tilde{\mathbf{x}}}, \mathbf{n}(\mathbf{x}))}\, \mathrm{d}s_{\mathbf{y}} - \mu \int_{\Gamma} \Delta_{\mathbf{y}}^2\tilde{\chi}\,\mathbf{n}(\mathbf{x}) \cdot \mathbf{n}(\mathbf{y})\,\mathbf{u}(\mathbf{y})\, \mathrm{d}s_{\mathbf{y}}\end{aligned}$$

is achieved. Inserting this expression into (4.84) the hypersingular operator reads as

$$
\begin{aligned}
(\widehat{\mathcal{D}}\mathbf{u})(\mathbf{x}) =& -\lim_{\Omega\ni\tilde{\mathbf{x}}\to\mathbf{x}\in\Gamma}\left(\mathcal{T}_{\tilde{\mathbf{x}}}(\widehat{\mathcal{K}}\mathbf{u})\right)(\tilde{\mathbf{x}}) \\
=& -\mu\lim_{\varepsilon\to 0}\int\limits_{\mathbf{y}\in\Gamma:|\mathbf{y}-\mathbf{x}|>\varepsilon}\left[\frac{\partial}{\partial\mathbf{S}(\partial_{\mathbf{y}},\mathbf{n}(\mathbf{y}))}\otimes\mathbf{u}(\mathbf{y})\right]^{\top}\cdot\frac{\partial\Delta_{\mathbf{y}}\chi}{\partial\mathbf{S}(\partial_{\mathbf{x}},\mathbf{n}(\mathbf{x}))}\,\mathrm{d}s_{\mathbf{y}} \\
&-\mu\lim_{\varepsilon\to 0}\int\limits_{\mathbf{y}\in\Gamma:|\mathbf{y}-\mathbf{x}|>\varepsilon}[\mathcal{M}_{\mathbf{x}}\cdot(\mathcal{M}_{\mathbf{y}}\Delta_{\mathbf{y}}\chi)]^{\top}\cdot\mathbf{u}(\mathbf{y})\,\mathrm{d}s_{\mathbf{y}} \\
&-\lim_{\varepsilon\to 0}\int\limits_{\mathbf{y}\in\Gamma:|\mathbf{y}-\mathbf{x}|>\varepsilon}\left[\mathcal{M}_{\mathbf{x}}\cdot\left(4\mu^2\mathbf{U}-2\mu\Delta_{\mathbf{y}}\chi\mathbf{I}\right)\right]\cdot(\mathcal{M}_{\mathbf{y}}\cdot\mathbf{u}(\mathbf{y}))\,\mathrm{d}s_{\mathbf{y}} \\
&+\lim_{\varepsilon\to 0}\int\limits_{\mathbf{y}\in\Gamma:|\mathbf{y}-\mathbf{x}|>\varepsilon}[\lambda\mathbf{n}(\mathbf{x})\,\mathbf{n}(\mathbf{y})\cdot\mathbf{u}(\mathbf{y})+\mu\mathbf{n}(\mathbf{y})\,\mathbf{n}(\mathbf{x})\cdot\mathbf{u}(\mathbf{y}) \\
&\qquad\qquad +\mu\mathbf{n}(\mathbf{x})\cdot\mathbf{n}(\mathbf{y})\,\mathbf{u}(\mathbf{y})]\Delta_{\mathbf{y}}^2\chi\,\mathrm{d}s_{\mathbf{y}}\,.
\end{aligned}
\tag{4.86}
$$

For simplicity the hypersingular bilinear form is split into parts

$$
\langle\widehat{\mathcal{D}}\mathbf{u},\mathbf{v}\rangle_{\Gamma}=\sum_{i=1}^{4}\langle\widehat{\mathcal{D}}_i\mathbf{u},\mathbf{v}\rangle_{\Gamma}\,,
\tag{4.87}
$$

which correspond to every single integral in (4.86). Their definitions are given below

$$
\begin{aligned}
\langle\widehat{\mathcal{D}}_1\mathbf{u},\mathbf{v}\rangle_{\Gamma} :=& -\mu\int_{\Gamma}\mathbf{v}(\mathbf{x})\cdot\lim_{\varepsilon\to 0}\int\limits_{\mathbf{y}\in\Gamma:|\mathbf{y}-\mathbf{x}|>\varepsilon}\left[\frac{\partial}{\partial\mathbf{S}(\partial_{\mathbf{y}},\mathbf{n}(\mathbf{y}))}\otimes\mathbf{u}(\mathbf{y})\right]^{\top}\cdot\frac{\partial\Delta_{\mathbf{y}}\chi}{\partial\mathbf{S}(\partial_{\mathbf{x}},\mathbf{n}(\mathbf{x}))}\,\mathrm{d}s_{\mathbf{y}}\,\mathrm{d}s_{\mathbf{x}} \\
\langle\widehat{\mathcal{D}}_2\mathbf{u},\mathbf{v}\rangle_{\Gamma} :=& -\mu\int_{\Gamma}\mathbf{v}(\mathbf{x})\cdot\lim_{\varepsilon\to 0}\int\limits_{\mathbf{y}\in\Gamma:|\mathbf{y}-\mathbf{x}|>\varepsilon}[\mathcal{M}_{\mathbf{x}}\cdot(\mathcal{M}_{\mathbf{y}}\Delta_{\mathbf{y}}\chi)]^{\top}\cdot\mathbf{u}(\mathbf{y})\,\mathrm{d}s_{\mathbf{y}}\,\mathrm{d}s_{\mathbf{x}} \\
\langle\widehat{\mathcal{D}}_3\mathbf{u},\mathbf{v}\rangle_{\Gamma} :=& -\mu\int_{\Gamma}\mathbf{v}(\mathbf{x})\cdot\lim_{\varepsilon\to 0}\int\limits_{\mathbf{y}\in\Gamma:|\mathbf{y}-\mathbf{x}|>\varepsilon}[\mathcal{M}_{\mathbf{x}}\cdot(4\mu\mathbf{U}-2\Delta_{\mathbf{y}}\chi\mathbf{I})]\cdot(\mathcal{M}_{\mathbf{y}}\cdot\mathbf{u}(\mathbf{y}))\,\mathrm{d}s_{\mathbf{y}}\,\mathrm{d}s_{\mathbf{x}} \\
\langle\widehat{\mathcal{D}}_4\mathbf{u},\mathbf{v}\rangle_{\Gamma} :=& \mu\int_{\Gamma}\mathbf{v}(\mathbf{x})\cdot\lim_{\varepsilon\to 0}\int\limits_{\mathbf{y}\in\Gamma:|\mathbf{y}-\mathbf{x}|>\varepsilon}[\frac{\lambda}{\mu}\mathbf{n}(\mathbf{x})\,\mathbf{n}(\mathbf{y})\cdot\mathbf{u}(\mathbf{y})+\mathbf{n}(\mathbf{y})\,\mathbf{n}(\mathbf{x})\cdot\mathbf{u}(\mathbf{y}) \\
&\qquad\qquad +\mathbf{n}(\mathbf{x})\cdot\mathbf{n}(\mathbf{y})\,\mathbf{u}(\mathbf{y})]\Delta_{\mathbf{y}}^2\chi\,\mathrm{d}s_{\mathbf{y}}\,\mathrm{d}s_{\mathbf{x}}\,.
\end{aligned}
\tag{4.88}
$$

Of course, those bilinear forms depict not the final regularization step since they exhibit still derivatives with respect to the fundamental solution $\mathbf{U}$ or $\Delta\chi$, respectively. Hence, the goal is the further regularization of the bilinear forms above. By use of the auxiliary matrix

$$
\mathbf{A}(\mathbf{u}) := \frac{\partial}{\partial\mathbf{S}(\partial_{\mathbf{y}},\mathbf{n}(\mathbf{y}))}\otimes\mathbf{u}(\mathbf{y})
$$

and the auxiliary vector

$$\boldsymbol{\alpha}(\mathbf{u},\mathbf{v}) \coloneqq \mathbf{A}(\mathbf{u})\cdot\mathbf{v}(\mathbf{x})$$

the first bilinear form is simply

$$\langle\widehat{\mathcal{D}}_1\mathbf{u},\mathbf{v}\rangle_\Gamma = -\mu\lim_{\varepsilon\to 0}\int\limits_{\mathbf{y}\in\Gamma:|\mathbf{y}-\mathbf{x}|>\varepsilon}\int\limits_{\Gamma}\frac{\partial\Delta_{\mathbf{y}}\chi}{\partial\mathbf{S}(\partial_{\mathbf{x}},\mathbf{n}(\mathbf{x}))}\cdot\boldsymbol{\alpha}(\mathbf{u},\mathbf{v})\,\mathrm{d}s_{\mathbf{x}}\,\mathrm{d}s_{\mathbf{y}}\,.$$

Then, integration by parts via the identity (4.4) yields

$$\langle\widehat{\mathcal{D}}_1\mathbf{u},\mathbf{v}\rangle_\Gamma = \mu\lim_{\varepsilon\to 0}\int\limits_{\mathbf{y}\in\Gamma:|\mathbf{y}-\mathbf{x}|>\varepsilon}\int\limits_{\Gamma}\Delta_{\mathbf{y}}\chi\frac{\partial}{\partial\mathbf{S}(\partial_{\mathbf{x}},\mathbf{n}(\mathbf{x}))}\cdot\boldsymbol{\alpha}(\mathbf{u},\mathbf{v})\,\mathrm{d}s_{\mathbf{x}}\,\mathrm{d}s_{\mathbf{y}}\,. \tag{4.89}$$

The application of the surface curl to the vector $\boldsymbol{\alpha}$ can be carried out component-wise

$$\frac{\partial}{\partial\mathbf{S}(\partial_{\mathbf{x}},\mathbf{n}(\mathbf{x}))}\cdot\boldsymbol{\alpha}(\mathbf{u},\mathbf{v}) = \sum_{k=1}^{3}\frac{\partial\alpha_k}{\partial S_k(\partial_{\mathbf{x}},\mathbf{n}(\mathbf{x}))} = \sum_{k,i=1}^{3}A_{ki}(\mathbf{u})\frac{\partial v_i(\mathbf{x})}{\partial S_k(\partial_{\mathbf{x}},\mathbf{n}(\mathbf{x}))}\,.$$

Finally, with $A_{ki} = \frac{\partial u_i}{\partial S_k(\partial_{\mathbf{y}},\mathbf{n}(\mathbf{y}))}$ one obtains

$$\frac{\partial}{\partial\mathbf{S}(\partial_{\mathbf{x}},\mathbf{n}(\mathbf{x}))}\cdot\boldsymbol{\alpha}(\mathbf{u},\mathbf{v}) = \sum_{k,i=1}^{3}\frac{\partial u_i(\mathbf{y})}{\partial S_k(\partial_{\mathbf{y}},\mathbf{n}(\mathbf{y}))}\frac{\partial v_i(\mathbf{x})}{\partial S_k(\partial_{\mathbf{x}},\mathbf{n}(\mathbf{x}))}\,.$$

Inserting this expression into (4.89) gives

$$\langle\widehat{\mathcal{D}}_1\mathbf{u},\mathbf{v}\rangle_\Gamma = \mu\int\limits_{\Gamma}\lim_{\varepsilon\to 0}\int\limits_{\mathbf{y}\in\Gamma:|\mathbf{y}-\mathbf{x}|>\varepsilon}\Delta_{\mathbf{y}}\chi\sum_{k,i=1}^{3}\frac{\partial u_i(\mathbf{y})}{\partial S_k(\partial_{\mathbf{y}},\mathbf{n}(\mathbf{y}))}\frac{\partial v_i(\mathbf{x})}{\partial S_k(\partial_{\mathbf{x}},\mathbf{n}(\mathbf{x}))}\,\mathrm{d}s_{\mathbf{y}}\,\mathrm{d}s_{\mathbf{x}}. \tag{4.90}$$

The integral above contains no more derivatives with respect to the function $\Delta\chi$. No matter whether the elastostatic or the elastodynamic problem is under consideration in both cases the function χ is of order $\mathcal{O}(r)$ (cf. (4.45) and (4.49)). Therefore, $\Delta\chi$ is of order $\mathcal{O}(r^{-1})$ and the bilinear form (4.90) exhibits a weak singularity only.

Now, for the transformation of $\langle\widehat{\mathcal{D}}_2\mathbf{u},\mathbf{v}\rangle_\Gamma$ the integration order is exchanged. This yields

$$\langle\widehat{\mathcal{D}}_2\mathbf{u},\mathbf{v}\rangle_\Gamma = -\mu\lim_{\varepsilon\to 0}\int\limits_{\mathbf{y}\in\Gamma:|\mathbf{y}-\mathbf{x}|>\varepsilon}\mathbf{u}(\mathbf{y})\int\limits_{\Gamma}[\mathcal{M}_{\mathbf{x}}\cdot(\mathcal{M}_{\mathbf{y}}\Delta_{\mathbf{y}}\chi)]\cdot\mathbf{v}(\mathbf{x})\,\mathrm{d}s_{\mathbf{x}}\,\mathrm{d}s_{\mathbf{y}}$$

Then, by an application of (4.19) the bilinear form becomes

$$\langle\widehat{\mathcal{D}}_2\mathbf{u},\mathbf{v}\rangle_\Gamma = \mu\sum_{i,j,\ell=1}^{3}\lim_{\varepsilon\to 0}\int\limits_{\mathbf{y}\in\Gamma:|\mathbf{y}-\mathbf{x}|>\varepsilon}u_\ell(\mathbf{y})\int\limits_{\Gamma}\left[\mathcal{M}_{ij}(\partial_{\mathbf{y}},\mathbf{n}(\mathbf{y}))\Delta_{\mathbf{y}}\chi\right]\left[\mathcal{M}_{\ell i}(\partial_{\mathbf{x}},\mathbf{n}(\mathbf{x}))v_j(\mathbf{x})\right]\mathrm{d}s_{\mathbf{x}}\,\mathrm{d}s_{\mathbf{y}}\,.$$

Again, reversing the integration order and using the identity (4.14) gives

$$\langle \widehat{\mathcal{D}}_2 \mathbf{u}, \mathbf{v} \rangle_\Gamma = -\mu \sum_{i,j,\ell=1}^{3} \int_\Gamma \left[\mathcal{M}_{\ell i}(\partial_{\mathbf{x}}, \mathbf{n}(\mathbf{x})) v_j(\mathbf{x}) \right] \lim_{\varepsilon \to 0} \int_{\mathbf{y} \in \Gamma : |\mathbf{y}-\mathbf{x}| > \varepsilon} \Delta_{\mathbf{y}} \chi \left[\mathcal{M}_{ij}(\partial_{\mathbf{y}}, \mathbf{n}(\mathbf{y})) u_\ell(\mathbf{y}) \right] \mathrm{d}s_{\mathbf{y}} \, \mathrm{d}s_{\mathbf{x}} \, . \quad (4.91)$$

Like before, this bilinear form exhibit no more derivatives with respect to $\Delta_{\mathbf{y}} \chi$ and, therefore, consists of a weakly singular integral kernel only. Although this bilinear form is sufficient for a numerical treatment it can be subjected to a further simplification. According to to the definition of the Günter derivatives (4.8) a single entry of them is given by

$$\mathcal{M}_{ij}(\partial_{\mathbf{y}}, \mathbf{n}(\mathbf{y})) = \sum_{k=1}^{3} \epsilon_{jik} \frac{\partial}{\partial S_k(\partial_{\mathbf{y}}, \mathbf{n}(\mathbf{y}))} \quad (4.92)$$

where ϵ denotes the *Levi-Cività* or *Permutation* symbol. Its definition is

$$\epsilon_{ijk\ldots} := \begin{cases} +1 & \text{if } (i,j,k,\ldots) \text{ is an even permutation} \\ -1 & \text{if } (i,j,k,\ldots) \text{ is an odd permutation} \\ 0 & \text{otherwise, i.e., at least one index occurs twice} \end{cases} .$$

The Levi-Cività symbol reveals the useful identity

$$\sum_{i=1}^{3} \epsilon_{i\ell k} \epsilon_{imj} = \delta_{\ell m} \delta_{kj} - \delta_{\ell j} \delta_{km} \quad (4.93)$$

where δ denotes the Kronecker delta (4.41). Hence, inserting (4.92) into (4.91) yields

$$\langle \widehat{\mathcal{D}}_2 \mathbf{u}, \mathbf{v} \rangle_\Gamma = -\mu \sum_{i,\ell,k,j,m=1}^{3} \int_\Gamma \int_\Gamma \left[\epsilon_{i\ell k} \frac{\partial v_j(\mathbf{x})}{\partial S_k(\partial_{\mathbf{x}}, \mathbf{n}(\mathbf{x}))} \right] \left[\epsilon_{jim} \frac{\partial u_\ell(\mathbf{y})}{\partial S_m(\partial_{\mathbf{y}}, \mathbf{n}(\mathbf{y}))} \right] \Delta_{\mathbf{y}} \chi \, \mathrm{d}s_{\mathbf{y}} \, \mathrm{d}s_{\mathbf{x}} \, .$$

Since $\epsilon_{jim} \equiv \epsilon_{imj}$ holds the identity (4.93) can be employed such that

$$\langle \widehat{\mathcal{D}}_2 \mathbf{u}, \mathbf{v} \rangle_\Gamma = \mu \sum_{k,\ell=1}^{3} \int_\Gamma \int_\Gamma \left[\frac{\partial v_\ell(\mathbf{x})}{\partial S_k(\partial_{\mathbf{x}}, \mathbf{n}(\mathbf{x}))} \frac{\partial u_\ell(\mathbf{y})}{\partial S_k(\partial_{\mathbf{y}}, \mathbf{n}(\mathbf{y}))} - \frac{\partial v_k(\mathbf{x})}{\partial S_k(\partial_{\mathbf{x}}, \mathbf{n}(\mathbf{x}))} \frac{\partial u_\ell(\mathbf{y})}{\partial S_\ell(\partial_{\mathbf{y}}, \mathbf{n}(\mathbf{y}))} \right] \Delta_{\mathbf{y}} \chi \, \mathrm{d}s_{\mathbf{y}} \, \mathrm{d}s_{\mathbf{x}}$$

is finally achieved.

Considerably more simple is the transformation of the bilinear form $\langle \widehat{\mathcal{D}}_3 \mathbf{u}, \mathbf{v} \rangle_\Gamma$ from (4.88). As before, the integration order is exchanged such that the bilinear form reads as

$$\langle \widehat{\mathcal{D}}_3 \mathbf{u}, \mathbf{v} \rangle_\Gamma = -\mu \lim_{\varepsilon \to 0} \int_{\mathbf{y} \in \Gamma : |\mathbf{y}-\mathbf{x}| > \varepsilon} (\mathcal{M}_{\mathbf{y}} \cdot \mathbf{u}(\mathbf{y})) \cdot \int_\Gamma \left[\mathcal{M}_{\mathbf{x}} \cdot (4\mu \mathbf{U} - 2\Delta_{\mathbf{y}} \chi \mathbf{I}) \right]^\top \cdot \mathbf{v}(\mathbf{x}) \, \mathrm{d}s_{\mathbf{x}} \, \mathrm{d}s_{\mathbf{y}}$$

This expression is immediately adequate to be integrated by parts. According to (4.18) it is

$$\langle \widehat{\mathcal{D}}_3 \mathbf{u}, \mathbf{v} \rangle_\Gamma = -\mu \int_\Gamma (\mathcal{M}_\mathbf{x} \mathbf{v}(\mathbf{x})) \cdot \lim_{\varepsilon \to 0} \int_{\mathbf{y} \in \Gamma : |\mathbf{y}-\mathbf{x}| > \varepsilon} (4\mu \mathbf{U} - 2\Delta_\mathbf{y} \chi \mathbf{I}) \cdot (\mathcal{M}_\mathbf{y} \cdot \mathbf{u}(\mathbf{y})) \, \mathrm{d}s_\mathbf{y} \, \mathrm{d}s_\mathbf{x} \, . \tag{4.94}$$

As before, there are no more derivatives associated with the singular kernel functions $\mathbf{U}$ and $\Delta_\mathbf{y}\chi$. Thus, (4.94) is also of weakly singular type.

Finally, the complete hypersingular bilinear form corresponding to (4.87) is

$$\begin{aligned} \langle \widehat{\mathcal{D}} \mathbf{u}, \mathbf{v} \rangle_\Gamma =& 2\mu \int_\Gamma \int_\Gamma \Delta_\mathbf{y} \chi \sum_{k,i=1}^{3} \frac{\partial u_i(\mathbf{y})}{\partial S_k(\partial_\mathbf{y}, \mathbf{n}(\mathbf{y}))} \frac{\partial v_i(\mathbf{x})}{\partial S_k(\partial_\mathbf{x}, \mathbf{n}(\mathbf{x}))} \, \mathrm{d}s_\mathbf{y} \, \mathrm{d}s_\mathbf{x} \\ & - \mu \int_\Gamma \int_\Gamma \Delta_\mathbf{y} \chi \frac{\partial}{\partial \mathbf{S}(\partial_\mathbf{y}, \mathbf{n}(\mathbf{y}))} \cdot \mathbf{u}(\mathbf{y}) \frac{\partial}{\partial \mathbf{S}(\partial_\mathbf{x}, \mathbf{n}(\mathbf{x}))} \cdot \mathbf{v}(\mathbf{x}) \, \mathrm{d}s_\mathbf{y} \, \mathrm{d}s_\mathbf{x} \\ & - \mu \int_\Gamma \int_\Gamma (\mathcal{M}_\mathbf{x} \cdot \mathbf{v}(\mathbf{x})) \cdot (4\mu \mathbf{U} - 2\Delta_\mathbf{y} \chi \mathbf{I}) \cdot (\mathcal{M}_\mathbf{y} \cdot \mathbf{u}(\mathbf{y})) \, \mathrm{d}s_\mathbf{y} \, \mathrm{d}s_\mathbf{x} \\ & + \langle \widehat{\mathcal{D}}_4 \mathbf{u}, \mathbf{v} \rangle_\Gamma \, . \end{aligned} \tag{4.95}$$

With the formulation above the regularization of the elastic hypersingular bilinear forms is almost completed. There are just two additional steps to perform. Firstly, the last bilinear form $\langle \widehat{\mathcal{D}}_4 \mathbf{u}, \mathbf{v} \rangle_\Gamma$ has to be determined clearly. Since it contains the Biharmonic operator of the characteristic function χ the elastostatic or elastodynamic case has to be specified. In case of the elastostatic system the function $\chi = \chi^{ES}$ fulfills equation (4.44), i.e., $\Delta^2 \chi^{ES} = 0$ holds due to $\mathbf{x} \neq \mathbf{y}$. Hence, the last bilinear form vanishes and the complete elastostatic hypersingular bilinear form reads as

$$\begin{aligned} \langle \widehat{\mathcal{D}}^{ES} \mathbf{u}, \mathbf{v} \rangle_\Gamma =& 2\mu \int_\Gamma \int_\Gamma \Delta_\mathbf{y} \chi^{ES} \sum_{k,i=1}^{3} \frac{\partial u_i(\mathbf{y})}{\partial S_k(\partial_\mathbf{y}, \mathbf{n}(\mathbf{y}))} \frac{\partial v_i(\mathbf{x})}{\partial S_k(\partial_\mathbf{x}, \mathbf{n}(\mathbf{x}))} \, \mathrm{d}s_\mathbf{y} \, \mathrm{d}s_\mathbf{x} \\ & - \mu \int_\Gamma \int_\Gamma \Delta_\mathbf{y} \chi^{ES} \frac{\partial}{\partial \mathbf{S}(\partial_\mathbf{y}, \mathbf{n}(\mathbf{y}))} \cdot \mathbf{u}(\mathbf{y}) \frac{\partial}{\partial \mathbf{S}(\partial_\mathbf{x}, \mathbf{n}(\mathbf{x}))} \cdot \mathbf{v}(\mathbf{x}) \, \mathrm{d}s_\mathbf{y} \, \mathrm{d}s_\mathbf{x} \\ & - \mu \int_\Gamma \int_\Gamma (\mathcal{M}_\mathbf{x} \cdot \mathbf{v}(\mathbf{x})) \cdot \left(4\mu \mathbf{U}^{ES} - 2\Delta_\mathbf{y} \chi^{ES} \mathbf{I} \right) \cdot (\mathcal{M}_\mathbf{y} \cdot \mathbf{u}(\mathbf{y})) \, \mathrm{d}s_\mathbf{y} \, \mathrm{d}s_\mathbf{x} \, . \end{aligned} \tag{4.96}$$

Apart from a slightly modified representation, this expression matches exactly the regularization which has been already deduced by Han [58]. Contrary to elastostatics, in elastodynamics the function $\chi = \chi^{ED}$ fulfills equation (4.48) and, thus, for $\mathbf{x} \neq \mathbf{y}$ the Biharmonic operator becomes

$$\Delta_\mathbf{y}^2 \chi^{ED} = \left(k_1^2 + k_2^2 \right) \Delta_\mathbf{y} \chi^{ED} - k_1^2 k_2^2 \chi^{ED} \, .$$

This expression reveals the weak singularity of $\Delta^2\chi^{ED}$ since it is composed of the regular function χ^{ED} and the Laplacian $\Delta\chi^{ED}$. Hence, $\langle\widehat{\mathcal{D}}_4\mathbf{u},\mathbf{v}\rangle_\Gamma = \langle\widehat{\mathcal{D}}_4^{ED}\mathbf{u},\mathbf{v}\rangle_\Gamma$ from (4.88) reads as

$$\langle\widehat{\mathcal{D}}_4^{ED}\mathbf{u},\mathbf{v}\rangle_\Gamma = \mu\int_\Gamma\int_\Gamma\Bigg[\left(\frac{k_2^2}{k_1^2}-2\right)\langle\mathbf{v}(\mathbf{x}),\mathbf{n}(\mathbf{x})\rangle\langle\mathbf{u}(\mathbf{y}),\mathbf{n}(\mathbf{y})\rangle + \langle\mathbf{v}(\mathbf{x}),\mathbf{n}(\mathbf{y})\rangle\langle\mathbf{u}(\mathbf{y}),\mathbf{n}(\mathbf{x})\rangle + \langle\mathbf{u}(\mathbf{y}),\mathbf{v}(\mathbf{x})\rangle\langle\mathbf{n}(\mathbf{y}),\mathbf{n}(\mathbf{x})\rangle\Bigg]\Delta_y^2\chi^{ED}\,\mathrm{d}s_\mathbf{y}\,\mathrm{d}s_\mathbf{x}\,.$$

Now, the final step is the incorporation of the fundamental solution's $\mathbf{U}^{ED}$ additional term from (4.50) which results in the evaluation of

$$\langle\widehat{\mathcal{D}}_5\mathbf{u},\mathbf{v}\rangle_\Gamma := -\left(-\int_\Gamma\mathbf{v}(\mathbf{x})\cdot\int_\Gamma\frac{k_1^2}{\mu}\mathcal{T}_\mathbf{x}\left(\mathcal{T}_\mathbf{y}\chi^{ED}\mathbf{I}\right)^\top\cdot\mathbf{u}(\mathbf{y})\,\mathrm{d}s_\mathbf{y}\,\mathrm{d}s_\mathbf{x}\right)\,. \tag{4.97}$$

Recalling the application of the stress operator according to (4.68)

$$(\mathcal{T}_\mathbf{y}\chi^{ED}\mathbf{I})^\top = \mu\left(\frac{\lambda}{\mu}\mathcal{M}_\mathbf{y}+\left(\frac{\lambda}{\mu}+1\right)\mathcal{U}_\mathbf{y}^\top+\frac{\partial}{\partial\mathbf{n}(\mathbf{y})}\mathbf{I}\right)\chi^{ED}$$

and introducing the abbreviation

$$\theta := \frac{\lambda}{\mu} = \frac{k_2^2}{k_1^2}-2$$

one obtains

$$\mathcal{T}_\mathbf{x}\left(\mathcal{T}_\mathbf{y}\chi^{ED}\mathbf{I}\right)^\top = \mu^2\left(-\theta\mathcal{M}_\mathbf{x}+(\theta+1)\mathcal{U}_\mathbf{x}+\frac{\partial}{\partial\mathbf{n}(\mathbf{x})}\mathbf{I}\right)\cdot \left(\theta\mathcal{M}_\mathbf{y}+(\theta+1)\mathcal{U}_\mathbf{y}^\top+\frac{\partial}{\partial\mathbf{n}(\mathbf{y})}\mathbf{I}\right)\chi^{ED}\,.$$

Thus, the bilinear form (4.97) becomes

$$\langle\widehat{\mathcal{D}}_5\mathbf{u},\mathbf{v}\rangle_\Gamma = k_1^2\mu\int_\Gamma\int_\Gamma\mathbf{v}(\mathbf{x})\cdot\Bigg[-\theta^2\Delta_\mathbf{y}\chi^{ED}\mathbf{n}(\mathbf{x})\otimes\mathbf{n}(\mathbf{y})+2\theta\left(\mathcal{U}_\mathbf{x}^\top\frac{\partial\chi^{ED}}{\partial\mathbf{n}(\mathbf{y})}+\mathcal{U}_\mathbf{y}\frac{\partial\chi^{ED}}{\partial\mathbf{n}(\mathbf{x})}\right) - (\nabla_\mathbf{y}\nabla_\mathbf{y}\chi^{ED})\mathbf{n}(\mathbf{y})\cdot\mathbf{n}(\mathbf{x})+\mathcal{U}_\mathbf{x}\frac{\partial\chi^{ED}}{\partial\mathbf{n}(\mathbf{y})}+\mathcal{U}_\mathbf{y}^\top\frac{\partial\chi^{ED}}{\partial\mathbf{n}(\mathbf{x})}+\frac{\partial^2\chi^{ED}}{\partial\mathbf{n}(\mathbf{y})\partial\mathbf{n}(\mathbf{x})}\mathbf{I}\Bigg]\cdot\mathbf{u}(\mathbf{y})\,\mathrm{d}s_\mathbf{y}\,\mathrm{d}s_\mathbf{x}\,. \tag{4.98}$$

Note that the expression above is achieved just by an insertion of the differential operators' definitions from section 4.1. In principle, the work is done since the complete bilinear form is obtained simply by adding (4.98) to the expression (4.95) with the substitutions

$\mathbf{U} = \mathbf{U}(\chi^{ED})$ and $\chi = \chi^{ED}$. Nevertheless, to be consistent with the previous regularizations it would be preferable to exchange the function $\mathbf{U}(\chi^{ED})$ with the elastodynamic fundamental solution $\mathbf{U}^{ED}$ from (4.50). Therefore, in the bilinear form (4.95) the term $\mathbf{U}$ is replaced by

$$\mathbf{U}(\chi^{ED}) = \mathbf{U}^{ED} + \frac{k_1^2}{\mu}\chi^{ED}\mathbf{I}\,.$$

and the according term becomes

$$\begin{aligned}
-4\mu^2 \int_\Gamma \int_\Gamma (\mathcal{M}_\mathbf{x}\cdot\mathbf{v}(\mathbf{x}))\cdot\left[\mathbf{U}^{ED} + \frac{k_1^2}{\mu}\chi^{ED}\mathbf{I}\right]\cdot(\mathcal{M}_\mathbf{y}\cdot\mathbf{u}(\mathbf{y}))\,\mathrm{d}s_\mathbf{y}\,\mathrm{d}s_\mathbf{x} = \\
-4\mu^2 \int_\Gamma \int_\Gamma (\mathcal{M}_\mathbf{x}\cdot\mathbf{v}(\mathbf{x}))\cdot\mathbf{U}^{ED}\cdot(\mathcal{M}_\mathbf{y}\cdot\mathbf{u}(\mathbf{y}))\,\mathrm{d}s_\mathbf{y}\,\mathrm{d}s_\mathbf{x} \\
+4k_1^2\mu \int_\Gamma \int_\Gamma \mathbf{v}(\mathbf{x})\cdot\left(\mathcal{M}_\mathbf{x}\cdot(\mathcal{M}_\mathbf{y}\chi^{ED})\right)\cdot\mathbf{u}(\mathbf{y})\,\mathrm{d}s_\mathbf{y}\,. \qquad (4.99)
\end{aligned}$$

Thereby, the differential operators $\mathcal{M}_\mathbf{x}$ and $\mathcal{M}_\mathbf{y}$ have been shifted back to the function χ^{ED}. Now, in conjunction with the identities

$$\begin{aligned}
\mathcal{M}_\mathbf{x}\cdot(\mathcal{M}_\mathbf{y}\chi^{ED}) = \mathcal{U}_\mathbf{y}\frac{\partial\chi^{ED}}{\partial\mathbf{n}(\mathbf{x})} + \mathcal{U}_\mathbf{x}^\top\frac{\partial\chi^{ED}}{\partial\mathbf{n}(\mathbf{y})} \\
+\left(\nabla_\mathbf{y}\nabla_\mathbf{y}\chi^{ED}\right)\mathbf{n}(\mathbf{y})\cdot\mathbf{n}(\mathbf{x}) + \Delta_\mathbf{y}\chi^{ED}\,(\mathbf{n}(\mathbf{x})\otimes\mathbf{n}(\mathbf{y}))
\end{aligned}$$

and

$$\left[\mathcal{M}_\mathbf{x}\cdot(\mathcal{M}_\mathbf{y}\chi^{ED})\right]^\top = \mathcal{M}_\mathbf{y}\cdot(\mathcal{M}_\mathbf{x}\chi^{ED})$$

the bilinear form (4.98) reads without variants of the operator $\mathcal{U}$ as

$$\begin{aligned}
\langle\widehat{\mathcal{D}}_5\mathbf{u},\mathbf{v}\rangle_\Gamma = \mu\int_\Gamma\int_\Gamma \mathbf{v}(\mathbf{x})\cdot\Bigg[-k_2^2\left(\frac{k_2^2}{k_1^2}-2\right)\Delta_\mathbf{y}\chi^{ED}\mathbf{n}(\mathbf{x})\otimes\mathbf{n}(\mathbf{y}) - k_1^2\Delta_\mathbf{y}\chi^{ED}\mathbf{n}(\mathbf{y})\otimes\mathbf{n}(\mathbf{x}) \\
+2(k_1^2-k_2^2)\left(\nabla_\mathbf{y}\nabla_\mathbf{y}\chi^{ED}\right)\mathbf{n}(\mathbf{y})\cdot\mathbf{n}(\mathbf{x}) + k_1^2\frac{\partial^2\chi^{ED}}{\partial\mathbf{n}(\mathbf{y})\partial\mathbf{n}(\mathbf{x})}\mathbf{I} \\
+2(k_2^2-2k_1^2)\mathcal{M}_\mathbf{x}\cdot(\mathcal{M}_\mathbf{y}\chi^{ED}) + k_1^2\mathcal{M}_\mathbf{y}\cdot(\mathcal{M}_\mathbf{x}\chi^{ED})\Bigg]\cdot\mathbf{u}(\mathbf{y})\,\mathrm{d}s_\mathbf{y}\,\mathrm{d}s_\mathbf{x}
\end{aligned}$$

Finally, combining the last term of (4.99) with the expression above and adding the result

to (4.95) yields the complete regularized elastodynamic bilinear form

$$
\begin{aligned}
\langle \widehat{\mathcal{D}}^{ED}\mathbf{u},\mathbf{v}\rangle_\Gamma = 2\mu \int_\Gamma\int_\Gamma \Delta_{\mathbf{y}}\chi^{ED} \sum_{k,i=1}^{3} \frac{\partial u_i(\mathbf{y})}{\partial S_k(\partial_{\mathbf{y}},\mathbf{n}(\mathbf{y}))}\frac{\partial v_i(\mathbf{x})}{\partial S_k(\partial_{\mathbf{x}},\mathbf{n}(\mathbf{x}))}\,\mathrm{d}s_{\mathbf{y}}\,\mathrm{d}s_{\mathbf{x}} \\
-\mu \int_\Gamma\int_\Gamma \Delta_{\mathbf{y}}\chi^{ED} \frac{\partial}{\partial \mathbf{S}(\partial_{\mathbf{y}},\mathbf{n}(\mathbf{y}))}\cdot\mathbf{u}(\mathbf{y})\,\frac{\partial}{\partial \mathbf{S}(\partial_{\mathbf{x}},\mathbf{n}(\mathbf{x}))}\cdot\mathbf{v}(\mathbf{x})\,\mathrm{d}s_{\mathbf{y}}\,\mathrm{d}s_{\mathbf{x}} \\
-\mu \int_\Gamma\int_\Gamma (\mathcal{M}_{\mathbf{x}}\cdot\mathbf{v}(\mathbf{x}))\cdot\left(4\mu\mathbf{U}^{ED}-2\Delta_{\mathbf{y}}\chi^{ED}\mathbf{I}\right)\cdot(\mathcal{M}_{\mathbf{y}}\cdot\mathbf{u}(\mathbf{y}))\,\mathrm{d}s_{\mathbf{y}}\,\mathrm{d}s_{\mathbf{x}} \\
+\mu \int_\Gamma\int_\Gamma \mathbf{v}(\mathbf{x})\cdot\left[(k_2^2-2k_1^2)\left(\Delta_{\mathbf{y}}\chi^{ED}-k_2^2\chi^{ED}\right)\mathbf{n}(\mathbf{x})\otimes\mathbf{n}(\mathbf{y})\right]\cdot\mathbf{u}(\mathbf{y})\,\mathrm{d}s_{\mathbf{y}}\,\mathrm{d}s_{\mathbf{x}} \\
+\mu \int_\Gamma\int_\Gamma \mathbf{v}(\mathbf{x})\cdot\left[k_2^2\left(\Delta_{\mathbf{y}}\chi^{ED}-k_1^2\chi^{ED}\right)\mathbf{n}(\mathbf{y})\otimes\mathbf{n}(\mathbf{x})\right]\cdot\mathbf{u}(\mathbf{y})\,\mathrm{d}s_{\mathbf{y}}\,\mathrm{d}s_{\mathbf{x}} \\
+\mu \int_\Gamma\int_\Gamma \mathbf{v}(\mathbf{x})\cdot\left[\left(2(k_1^2-k_2^2)\nabla_{\mathbf{y}}\nabla_{\mathbf{y}}\chi^{ED}+\Delta_{\mathbf{y}}^2\chi^{ED}\mathbf{I}\right)\mathbf{n}(\mathbf{y})\cdot\mathbf{n}(\mathbf{x})\right]\cdot\mathbf{u}(\mathbf{y})\,\mathrm{d}s_{\mathbf{y}}\,\mathrm{d}s_{\mathbf{x}} \\
+\mu \int_\Gamma\int_\Gamma \mathbf{v}(\mathbf{x})\cdot\left[2k_2^2\mathcal{M}_{\mathbf{x}}\cdot\left(\mathcal{M}_{\mathbf{y}}\chi^{ED}\right)+k_1^2\mathcal{M}_{\mathbf{y}}\cdot\left(\mathcal{M}_{\mathbf{x}}\chi^{ED}\right)\right]\cdot\mathbf{u}(\mathbf{y})\,\mathrm{d}s_{\mathbf{y}}\,\mathrm{d}s_{\mathbf{x}} \\
+\mu \int_\Gamma\int_\Gamma k_1^2\frac{\partial^2\chi^{ED}}{\partial\mathbf{n}(\mathbf{y})\partial\mathbf{n}(\mathbf{x})}\mathbf{v}(\mathbf{x})\cdot\mathbf{u}(\mathbf{y})\,\mathrm{d}s_{\mathbf{y}}\,\mathrm{d}s_{\mathbf{x}}\,.
\end{aligned}
\tag{4.100}
$$

With view to the later proposed Boundary Element formulation one remark must be given. The presented fundamental solutions as well as the stated operators with their corresponding bilinear forms are the backbone of the numerical scheme which will be described in section 5. There, for time-dependent problems the so-called *Convolution Quadrature Method* (see. section 5.4) will be presented which utilizes the Laplace transforms of the herein deduced quantities to generate solutions in the time-domain. For instance an elastodynamic problem is solved with the help of the respective elastodynamic expressions formulated in the Laplace domain. Equivalently, a viscoelastodynamic problem is solved, but with the difference of incorporating the elastic-viscoelastic correspondence principle (2.51) into the respective operators.

5 BOUNDARY ELEMENT FORMULATION

The boundary integral equations stated in chapter 3.2 admit analytical solutions for very few and exclusive problems only. In general, they do not feature analytical solutions such that approximate solutions become evident. This chapter is devoted to the formulation of an numerical solution scheme which is based on an appropriate discretization of those boundary integral equations.

For arbitrary geometries the numerical solution is based on a parametrization of the boundary Γ and on the use of *finite elements* defined in the parameter domain. The term finite element is somehow misleading since it is commonly preserved for the use within the Finite Element Method. Therefore, these elements are usually denoted as *boundary elements* which, additionally, emphasizes their location on the boundary Γ.

The remainder of this chapter is organized as follows. At first, the spatial approximations are given which form the basis of the afterwards proposed Boundary Element Method for elliptic problems. The subsequent section is devoted to the numerical treatment of the occuring singular integrals. Then, the Convolution Quadrature Method is utilized in order to establish the time-domain Boundary Element Method. Finally, this chapter closes with an approach of dealing also with semi-infinite domains.

5.1 Boundary approximation

Boundary elements τ are commonly based on a *triangulation* G of the boundary Γ. A synonymous labeling is the term *mesh* which is used equivalent in the following. In general, this triangulation is not an exact representation of the boundary Γ but just an approximation Γ_h. With $\tau \subset \Gamma_h$ the boundary's approximation is given by the union of J disjoint boundary elements τ_j such that

$$\Gamma \approx \Gamma_h = \bigcup_{j=1}^{J} \overline{\tau}_j$$

holds. Thereby, the overline state that G is a cover of Γ_h, i.e., the union of all subsets $\tau \in G$ is the whole approximate boundary Γ_h. With this approximation any boundary integral for a kernel function $k(\mathbf{x})$ can be given by

$$\int_{\Gamma} k(\bar{\mathbf{x}}) \, \mathrm{d}s_{\bar{\mathbf{x}}} \approx \int_{\Gamma_h} k(\mathbf{x}) \, \mathrm{d}s_{\mathbf{x}} = \sum_{j=1}^{J} \int_{\tau_j} k(\mathbf{x}) \, \mathrm{d}s_{\mathbf{x}} \qquad \forall \bar{\mathbf{x}} \in \Gamma, \mathbf{x} \in \Gamma_h \, . \tag{5.1}$$

For the integration over the boundary elements τ_j a parametrization is introduced such that every boundary element τ is the image of an reference element $\hat{\tau}$ under the mapping

$$\chi_\tau \colon \hat{\tau} \to \tau \,. \tag{5.2}$$

Every boundary element τ is a two-dimensional surface patch which is embedded into the three-dimensional space. Thus, the mapping $\chi_\tau \colon \mathbb{R}^2 \to \mathbb{R}^3$ maps from the two- into the three-dimensional Euclidean space. The boundary elements τ consist either of triangles or quadrilaterals. Therefore, the reference elements according to these surfaces are chosen to be either the unit triangle $\hat{\tau}_\triangle$ or the unit square $\hat{\tau}_\square$ (cf. Fig. 5.1) being defined as

$$\begin{aligned} \hat{\tau}_\triangle &\coloneqq \{(\hat{x}_1, \hat{x}_2) \in \mathbb{R}^2 \colon 0 \leq \hat{x}_2 < \hat{x}_1 \leq 1\} \\ \hat{\tau}_\square &\coloneqq \{(\hat{x}_1, \hat{x}_2) \in \mathbb{R}^2 \colon 0 \leq (\hat{x}_1, \hat{x}_2) \leq 1\} \,. \end{aligned} \tag{5.3}$$

Depending on the unique shape of a boundary element τ the reference element $\hat{\tau}$ features of a set of local points $\hat{\mathbf{p}}_i$ with $i = 1, \ldots, N$. The total number N of those points matches the number of points a boundary element consists of. The geometry of every boundary element τ is uniquely defined by the set

$$E_N \coloneqq \bigcup_{i=1}^{N} \mathbf{p}_i$$

of several points $\mathbf{p}_i \in \mathbb{R}^3$. The more common notion for those points is the term *nodes* or, more precisely, *boundary nodes*. The most simple geometry is a straight-lined triangle which consists of the set of the three nodes $E_3 = \{\mathbf{p}_1, \mathbf{p}_2, \mathbf{p}_3\}$. Similarly, a straight-lined quadrilateral is made up of four nodes $E_4 = \{\mathbf{p}_1, \ldots, \mathbf{p}_4\}$. These two types of elements are usually denoted as *flat elements*. Contrary, also *curved elements* exist which consists at least of six nodes $E_6 = \{\mathbf{p}_1, \ldots, \mathbf{p}_6\}$ for triangles and of nine nodes $E_9 = \{\mathbf{p}_1, \ldots, \mathbf{p}_9\}$ in the case of regular quadrilaterals. Contrary to the regular quadrilaterals there exist also irregular and so-called serependity elements which feature less nodes than are actually needed from a mathematical point of view. These elements are not used within this thesis and the reader is referred to standard textbooks [127] for more details on that topic.

The mapping χ_τ relates the reference, or local, coordinates $\hat{\mathbf{x}} \in \hat{\tau}$ to a point $\mathbf{x} \in \tau$. By choosing a polynomial ansatz with N polynomial functions $\varphi_i^\alpha(\hat{\mathbf{x}}) \in \mathbb{R}$ this yields

$$\mathbf{x}(\hat{\mathbf{x}}) = \chi_\tau(\hat{\mathbf{x}}) = \sum_{i=1}^{N} \varphi_i^\alpha(\hat{\mathbf{x}}) \mathbf{p}_i \,, \quad \alpha \in \mathbb{N} \setminus \{0\} \,. \tag{5.4}$$

The parameter α denotes the polynomial degree, e.g., $\alpha = 1$ represents linear polynomials. Now, every node $\mathbf{p}_j$ is related to a distinct local point $\hat{\mathbf{p}}_j$ such that

$$\mathbf{p}_j = \chi_\tau(\hat{\mathbf{p}}_j)$$

holds. Inserting this constraint into (5.4) yields the polynomials' fundamental property

$$\varphi_i^\alpha(\hat{\mathbf{p}}_j) = \delta_{ij} \,. \tag{5.5}$$

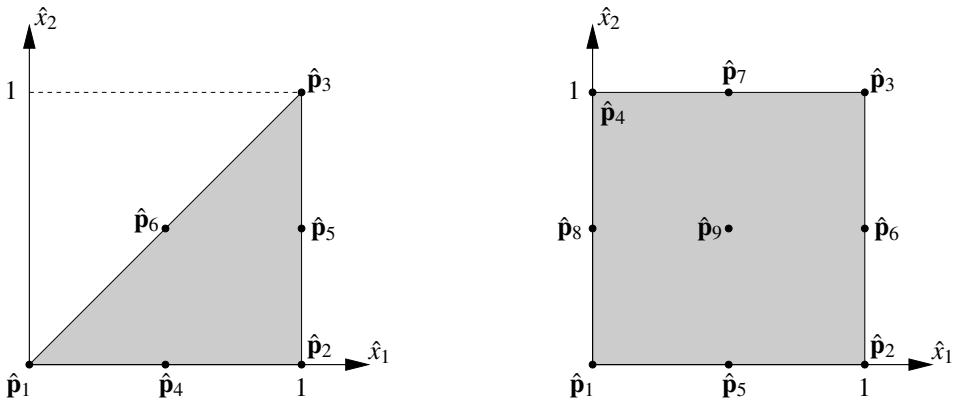

(a) Unit triangle (b) Unit square

Figure 5.1: Reference elements with local points $\hat{\mathbf{p}}_i$

The polynomials which are related to the boundary elements obey some characteristics. All triangular elements are based on polynomials of the form

$$\varphi^{\alpha}_{i,\triangle}(\hat{\mathbf{x}}) := \sum_{\substack{k+\ell\leq\alpha \\ k,\ell\geq 0}} C_{k\ell,i}\,\hat{x}_1^k\hat{x}_2^\ell\,, \tag{5.6}$$

whereas the polynomials according to the quadrilaterals are given by

$$\varphi^{\alpha}_{i,\square}(\hat{\mathbf{x}}) := \sum_{0\leq k,\ell\leq\alpha} C_{k\ell,i}\,\hat{x}_1^k\hat{x}_2^\ell\,. \tag{5.7}$$

The polynomials which build the basis for the triangular elements are denoted as *complete polynomials* [121] while the quadrilaterals are constructed by using functions from the family of polynomials with tensor products [21]. In the definitions (5.6) and (5.7), the constants $C_{k\ell,i}$ can be obtained with the help of the property (5.5). Collecting all polynomials being specific for an N-node element into the vector $\boldsymbol{\varphi}^{\alpha}_N := [\varphi^{\alpha}_1,\ldots,\varphi^{\alpha}_N]$ and interpreting the sums in (5.6) and (5.7) as multiplications of a vector of monomials $\boldsymbol{\psi}(\hat{\mathbf{x}}) := [1,\hat{x}_1,\hat{x}_2,\ldots]$ with coefficient vectors C_i one gets

$$\boldsymbol{\varphi}^{\alpha}_N(\hat{\mathbf{x}}) = \boldsymbol{\psi}(\hat{\mathbf{x}})\cdot\underbrace{[\mathsf{C}_1,\ldots,\mathsf{C}_N]}_{=:\mathsf{C}}$$

with the coefficient matrix $\mathsf{C}\in\mathbb{R}^{N\times N}$. Next, taking the property (5.5) into account gives the condition $\boldsymbol{\varphi}^{\alpha}_N(\hat{\mathbf{p}}_i) = \mathsf{e}_i^\top$ with e_i being the i-th unit vector. By use of the matrix $\mathsf{X} := [\boldsymbol{\psi}(\hat{\mathbf{p}}_1),\ldots,\boldsymbol{\psi}(\hat{\mathbf{p}}_N)]^\top$ which contains the monomials evaluated at the distinct coordinates $\hat{\mathbf{p}}_i$ one obtains

$$\mathsf{X}\cdot\mathsf{C} = \mathsf{I} \quad\Longrightarrow\quad \mathsf{C} = \mathsf{X}^{-1}\,.$$

Thus, the set of functions φ^{α}_i is given by

$$\boldsymbol{\varphi}^{\alpha}_N = \boldsymbol{\psi}(\hat{\mathbf{x}})\cdot\mathsf{X}^{-1}\,.$$

To illustrate this procedure the flat triangle is considered. This element requires polynomials of order $\alpha = 1$. Therefore, the vector of monomials reads as $\boldsymbol{\psi}(\hat{\mathbf{x}}) = [1\ \hat{x}_1\ \hat{x}_2]$ and the matrix X and its inverse are

$$\mathsf{X} = \begin{bmatrix} \boldsymbol{\psi}(\left[\begin{smallmatrix}0\\0\end{smallmatrix}\right]) \\ \boldsymbol{\psi}(\left[\begin{smallmatrix}1\\0\end{smallmatrix}\right]) \\ \boldsymbol{\psi}(\left[\begin{smallmatrix}1\\1\end{smallmatrix}\right]) \end{bmatrix} = \begin{bmatrix} 1 & 0 & 0 \\ 1 & 1 & 0 \\ 1 & 1 & 1 \end{bmatrix} \quad \Longrightarrow \quad \mathsf{X}^{-1} = \begin{bmatrix} 1 & 0 & 0 \\ -1 & 1 & 0 \\ 0 & -1 & 1 \end{bmatrix} .$$

Finally, the set of functions φ_i^1 reads as

$$\boldsymbol{\varphi}_3^1(\hat{\mathbf{x}}) = \begin{bmatrix} 1 & \hat{x}_1 & \hat{x}_2 \end{bmatrix} \cdot \begin{bmatrix} 1 & 0 & 0 \\ -1 & 1 & 0 \\ 0 & -1 & 1 \end{bmatrix} = \begin{bmatrix} 1-\hat{x}_1 & \hat{x}_1-\hat{x}_2 & \hat{x}_2 \end{bmatrix}$$

and the mapping χ_τ is simply

$$\mathbf{x} = \chi_\tau(\hat{\mathbf{x}}) = (1-\hat{x}_1)\mathbf{p}_1 + (\hat{x}_1-\hat{x}_2)\mathbf{p}_2 + \hat{x}_2\mathbf{p}_3 \, . \tag{5.8}$$

Since the construction of more complex elements follows the same procedure their detailed derivation is omitted herein. Nevertheless, the functions for quadrilaterals and higher order elements are listed in appendix A.2.

For the transformation of the integral (5.1) to local coordinates it remains to express the differential surface element $\mathrm{d}s_{\mathbf{x}}$ in local coordinates. Therefore, the *Jacobian matrix* $\mathbf{J}_\tau \in \mathbb{R}^{3\times 2}$ is introduced

$$\mathbf{J}_\tau(\hat{\mathbf{x}}) \coloneqq \begin{bmatrix} \frac{\partial \mathbf{x}}{\partial \hat{x}_1} & \frac{\partial \mathbf{x}}{\partial \hat{x}_2} \end{bmatrix} , \tag{5.9}$$

which represents a linear approximation of the vector field $\mathbf{x}$ in a neighborhood of $\hat{\mathbf{x}}$. Then the deformation of the infinitesimal surface element $\mathrm{d}s_{\mathbf{x}}$ is given by

$$\mathrm{d}s_{\mathbf{x}} = \sqrt{\det(\mathbf{J}_\tau^\top(\hat{\mathbf{x}}) \cdot \mathbf{J}_\tau(\hat{\mathbf{x}}))}\, \mathrm{d}\hat{\mathbf{x}} \, .$$

Above, the expression within the square root is the *Gram determinant*

$$g_\tau(\hat{\mathbf{x}}) \coloneqq \det(\mathbf{J}_\tau^\top(\hat{\mathbf{x}}) \cdot \mathbf{J}_\tau(\hat{\mathbf{x}}))$$

by what means the surface integral (5.1) finally reads as

$$\int_\Gamma k(\bar{\mathbf{x}})\, \mathrm{d}s_{\bar{\mathbf{x}}} \approx \int_{\Gamma_h} k(\mathbf{x})\, \mathrm{d}s_{\mathbf{x}} = \sum_{j=1}^{J} \int_{\hat{\tau}} k(\chi_{\tau_j}(\hat{\mathbf{x}})) \sqrt{g_{\tau_j}(\hat{\mathbf{x}})}\, \mathrm{d}\hat{\mathbf{x}} \, . \tag{5.10}$$

Although in general dependent on $\hat{\mathbf{x}}$ the Jacobi matrix as well as the Gram determinant boil down to constant quantities for some special but very popular element types. For instance, the Jacobi matrix according to the mapping (5.8) which represents a flat 3-node triangle (cf. Fig. 5.2) is just given by

$$\mathbf{J}_\tau = \begin{bmatrix} \mathbf{p}_2 - \mathbf{p}_1 & \mathbf{p}_3 - \mathbf{p}_2 \end{bmatrix} .$$

Introducing the abbreviations $\mathbf{a} \coloneqq \mathbf{p}_2 - \mathbf{p}_1$ and $\mathbf{b} \coloneqq \mathbf{p}_3 - \mathbf{p}_2$ as well as $a = |\mathbf{a}|$ and $b = |\mathbf{b}|$ the Gram determinant becomes

$$g_\tau = \det \begin{bmatrix} \langle \mathbf{a}^\top, \mathbf{a} \rangle & \langle \mathbf{a}^\top, \mathbf{b} \rangle \\ \langle \mathbf{b}^\top, \mathbf{a} \rangle & \langle \mathbf{b}^\top, \mathbf{b} \rangle \end{bmatrix} = a^2 b^2 - a^2 b^2 \cos^2 \theta = a^2 b^2 \sin^2 \theta \; .$$

With $\sin\theta = \frac{h_a}{b}$ the determinant is $g_\tau = a^2 h_a^2$ and, thus, the integration over the reference element becomes simply

$$\int_{\hat{\tau}} k(\chi_\tau(\hat{\mathbf{x}})) \sqrt{g_\tau(\hat{\mathbf{x}})} \, \mathrm{d}\hat{\mathbf{x}} = 2A_\triangle \int_{\hat{\tau}} k(\chi_\tau(\hat{\mathbf{x}})) \, \mathrm{d}\hat{\mathbf{x}}$$

with $A_\triangle$ being the triangle's area. If the element τ is a parallelogram the Gram determinant is also constant and equals the parallelogram's area. For all other element types, g_τ exhibits the dependency on the local coordinate vector $\hat{\mathbf{x}}$.

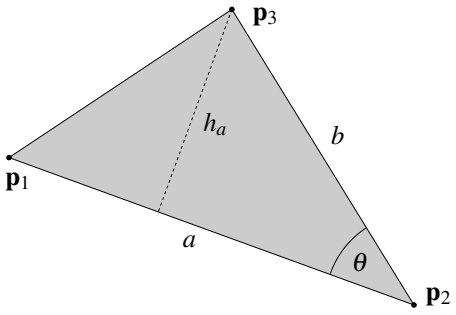

Figure 5.2: Flat 3-node triangle

With (5.10) the approximation of the surface integral by a finite number of boundary elements is done. More information about this approximation as well as on some geometrical requirements concerning the boundary elements is given in [107, 120].

There are two more quantities which demand a representation in reference coordinates. Both the normal vector and the surface curl contain geometry information. Thus, they are also subjected to the mapping (5.2). The normal vector reads in local coordinates as

$$\mathbf{n}(\hat{\mathbf{x}}) \coloneqq \frac{1}{\sqrt{g_\tau(\hat{\mathbf{x}})}} \left(\frac{\partial \mathbf{x}}{\partial \hat{x}_1} \times \frac{\partial \mathbf{x}}{\partial \hat{x}_2} \right) . \tag{5.11}$$

Now, recalling the surface curl's definition from (4.2)

$$\frac{\partial}{\partial \mathbf{S}(\partial_\mathbf{x}, \mathbf{n}(\mathbf{x}))} = \mathbf{n}(\mathbf{x}) \times \nabla_\mathbf{x}$$

and inserting (5.11) gives

$$\mathbf{n}(\mathbf{x}) \times \nabla_\mathbf{x} = -\nabla_\mathbf{x} \times \mathbf{n}(\mathbf{x}) = -\frac{1}{\sqrt{g_\tau(\hat{\mathbf{x}})}} \nabla_\mathbf{x} \times \left(\frac{\partial \mathbf{x}}{\partial \hat{x}_1} \times \frac{\partial \mathbf{x}}{\partial \hat{x}_2} \right) .$$

Next, using the vector identity $\mathbf{a}\times(\mathbf{b}\times\mathbf{c}) = \mathbf{b}(\mathbf{a}\cdot\mathbf{c}) - \mathbf{c}(\mathbf{a}\cdot\mathbf{b})$ that expression is equivalent to

$$-\frac{1}{\sqrt{g_\tau(\hat{\mathbf{x}})}}\nabla_{\mathbf{x}}\times\left(\frac{\partial\mathbf{x}}{\partial\hat{x}_1}\times\frac{\partial\mathbf{x}}{\partial\hat{x}_2}\right) = -\frac{1}{\sqrt{g_\tau(\hat{\mathbf{x}})}}\left[\frac{\partial\mathbf{x}}{\partial\hat{x}_1}\left(\nabla_{\mathbf{x}}\cdot\frac{\partial\mathbf{x}}{\partial\hat{x}_2}\right) - \frac{\partial\mathbf{x}}{\partial\hat{x}_2}\left(\nabla_{\mathbf{x}}\cdot\frac{\partial\mathbf{x}}{\partial\hat{x}_1}\right)\right] .$$

Above the terms in parenthesis can be identified with local derivatives since

$$\nabla_{\mathbf{x}}\cdot\frac{\partial\mathbf{x}}{\partial\hat{x}_i} = \sum_{k=1}^{3}\frac{\partial}{\partial x_k}\frac{\partial x_k}{\partial\hat{x}_i} = \frac{\partial}{\partial\hat{x}_i}$$

holds due to the chain rule. Thus, the surface curl reads in local coordinates as

$$\frac{\partial}{\partial\mathbf{S}(\partial_{\hat{\mathbf{x}}},\mathbf{n}(\hat{\mathbf{x}}))} = -\frac{1}{\sqrt{g_\tau(\hat{\mathbf{x}})}}\left[\frac{\partial\mathbf{x}}{\partial\hat{x}_1}\frac{\partial}{\partial\hat{x}_2} - \frac{\partial\mathbf{x}}{\partial\hat{x}_2}\frac{\partial}{\partial\hat{x}_1}\right] .$$

Finally, with the definition of the Jacobi matrix (5.9) and the operator

$$\nabla_{\hat{\mathbf{x}}}^{\perp} := \begin{bmatrix}\frac{\partial}{\partial\hat{x}_2}\\ -\frac{\partial}{\partial\hat{x}_1}\end{bmatrix}$$

the surface curl can be written more compact as

$$\frac{\partial}{\partial\mathbf{S}(\partial_{\hat{\mathbf{x}}},\mathbf{n}(\hat{\mathbf{x}}))} = -\frac{1}{\sqrt{g_\tau(\hat{\mathbf{x}})}}\mathbf{J}_\tau(\hat{\mathbf{x}})\cdot\nabla_{\hat{\mathbf{x}}}^{\perp} . \tag{5.12}$$

For later purpose, it is useful to define some characteristics related to the triangulation G. At first, the element size h_τ of the boundary element τ is defined as

$$h_\tau := \sup_{\mathbf{y},\mathbf{x}\in\tau}|\mathbf{y}-\mathbf{x}| .$$

Then, the triangulation's mesh size is given by

$$h_G := \max\{h_\tau\colon\ \tau\in G\} .$$

Finally, the constant q_G denotes the mesh's *quasiuniformity* defined as the ratio between the maximal and minimal mesh sizes

$$q_G := \frac{h_G}{\min\{h_\tau\colon\ \tau\in G\}} .$$

5.2 Galerkin discretization

In general, the discrete Galerkin scheme is nothing but a spatial discretization of the variational forms stated in section 3.3. Here, it should be deduced by means of the variational

form (3.33) which corresponds to the elliptic mixed boundary value problem given in section 2.4. While the Galerkin discretization is introduced for an elliptic problem it equivalently can be applied to the time-dependent case resulting in a semi-discrete system which still obeys the convolution integrals in time. The discretization of theses integrals is treated in section 5.4.

Recalling the variational form concerning the elliptic mixed boundary value problem reads as:

Find $(\tilde{q},\tilde{u})$ *such that*

$$\begin{aligned}\langle\widehat{\mathcal{V}}\tilde{q},w\rangle_{\Gamma_D}-\langle\widehat{\mathcal{K}}\tilde{u},w\rangle_{\Gamma_D}&=\langle(\tfrac{1}{2}\widehat{\mathcal{I}}+\widehat{\mathcal{K}})\tilde{g}_D-\widehat{\mathcal{V}}\tilde{g}_N-\widehat{\mathcal{N}}_0 f,w\rangle_{\Gamma_D}\\ \langle\widehat{\mathcal{K}}'\tilde{q},v\rangle_{\Gamma_N}+\langle\widehat{\mathcal{D}}\tilde{u},v\rangle_{\Gamma_N}&=\langle(\tfrac{1}{2}\widehat{\mathcal{I}}-\widehat{\mathcal{K}}')\tilde{g}_N-\widehat{\mathcal{D}}\tilde{g}_D-\widehat{\mathcal{N}}_1 f,v\rangle_{\Gamma_N}\end{aligned} \tag{5.13}$$

is fulfilled for all test functions (w,v).

Now, the Boundary Element Method defines an approximation of the unknown boundary data $(\tilde{q},\tilde{u})$. Thereby, the unknown data have to be approximated by a finite number of parameters. The realization of such an approximation is usually done by the choice of polynomial basis functions. To define those functions, first, appropriate finite-dimensional subspaces

$$\begin{aligned}S_h^\gamma(\Gamma_{D,h})&\coloneqq\operatorname{span}\{\varphi_k^\gamma\}_{k=1}^N && \gamma\in\mathbb{N}\\ S_h^\beta(\Gamma_{N,h})&\coloneqq\operatorname{span}\{\psi_\ell^\beta\}_{\ell=1}^M && \beta\in\mathbb{N}\setminus\{0\}\end{aligned} \tag{5.14}$$

are introduced with the basis functions φ_k^γ and ψ_ℓ^β. These subspaces have to be constructed in such a manner that appropriate linear combinations of their basis functions reflect the correct solution behavior of $(\tilde{q},\tilde{u})$. Their dimensions N and M correspond to the number of unknown parameters on the boundary $\Gamma_h=\Gamma_{D,h}\cup\Gamma_{N,h}$. According to the stated boundary value problems in section 2.4, on the Dirichlet boundary $\Gamma_{D,h}$ the Neumann datum $\tilde{q}$ is unknown while on the Neumann boundary it is the Dirichlet datum $\tilde{u}$ which is sought after. Since the Neumann data are related to the normal vector as it is stated in Eqns. (2.67) & (2.68) its distribution is not necessarily continuous. Thus, it is sufficient that the space $S_h^\gamma(\Gamma_{D,h})$ consists of N piecewise continuous functions φ_k^γ of order γ. Contrary, the Dirichlet data have to be continuous and, therefore, the subspace $S_h^\beta(\Gamma_{N,h})$ comprises the set of M continuous functions ψ_ℓ^β of order β. More mathematical details concerning the choice of the appropriate subspaces may be found in the textbooks of Hackbusch [54], Sauter & Schwab [107], Steinbach [120], and Hsiao & Wendland [63].

Next, approximating the unknown Dirichlet and Neumann data by linear combinations of φ_k^γ and ψ_ℓ^β yields

$$\begin{aligned}\tilde{q}\approx q_h^\gamma(\mathbf{x})&\coloneqq\sum_{k=1}^N q_k\varphi_k^\gamma(\mathbf{x}) && \in S_h^\gamma(\Gamma_{D,h})\\ \tilde{u}\approx u_h^\beta(\mathbf{x})&\coloneqq\sum_{\ell=1}^M u_\ell\psi_\ell^\beta(\mathbf{x}) && \in S_h^\beta(\Gamma_{N,h})\,.\end{aligned} \tag{5.15}$$

Inserting these approximations into the variational formulation (5.13) results in two equations with N unknown parameters q_k for the first one and M unknown parameters u_ℓ for the second one, respectively. To determine those $N+M$ unknowns q_k and u_ℓ an equivalent number of constraints is essential. For this purpose, the variational formulation (5.13) is passed through the respective subspace's basis (5.14). This yields the discretized variational Galerkin formulation which now reads as:

Find (q_h^γ, u_h^β) *such that*

$$\begin{aligned}\langle\widehat{\mathcal{V}}q_h^\gamma, w_h^\gamma\rangle_{\Gamma_{D,h}} - \langle\widehat{\mathcal{K}}u_h^\beta, w_h^\gamma\rangle_{\Gamma_{D,h}} &= \langle(\tfrac{1}{2}\widehat{\mathcal{I}}+\widehat{\mathcal{K}})g_{D,h}^\beta - \widehat{\mathcal{V}}g_{N,h}^\gamma - \widehat{\mathcal{N}}_0 f_h, w_h^\gamma\rangle_{\Gamma_{D,h}}\\ \langle\widehat{\mathcal{K}}'q_h^\gamma, v_h^\beta\rangle_{\Gamma_{N,h}} + \langle\widehat{\mathcal{D}}u_h^\beta, v_h^\beta\rangle_{\Gamma_{N,h}} &= \langle(\tfrac{1}{2}\widehat{\mathcal{I}}-\widehat{\mathcal{K}}')g_{N,h}^\gamma - \widehat{\mathcal{D}}g_{D,h}^\beta - \widehat{\mathcal{N}}_1 f_h, v_h^\beta\rangle_{\Gamma_{N,h}}\end{aligned}$$

is satisfied for all $w_h^\gamma \in S_h^\gamma(\Gamma_{D,h})$ *and* $v_h^\beta \in S_h^\beta(\Gamma_{N,h})$.

Note that also the given data has to be approximated by making use of $S_h^\gamma(\Gamma_{D,h})$ and $S_h^\beta(\Gamma_{N,h})$, respectively.

The discretized variational form is equivalent to the linear system of equations

$$\begin{bmatrix}\widehat{\mathsf{V}}_h & -\widehat{\mathsf{K}}_h\\ \widehat{\mathsf{K}}_h^\top & \widehat{\mathsf{D}}_h\end{bmatrix}\cdot\begin{bmatrix}\mathsf{q}_h\\ \mathsf{u}_h\end{bmatrix} = \begin{bmatrix}\widehat{\mathsf{f}}_D\\ \widehat{\mathsf{f}}_N\end{bmatrix} \tag{5.16}$$

where $\widehat{\mathsf{V}}$ denotes the discrete single layer matrix, $\widehat{\mathsf{K}}_h$ and $\widehat{\mathsf{K}}_h^\top$ are the discrete double and adjoint double layer matrices, and $\widehat{\mathsf{D}}_h$ reflects the discrete hypersingular operator matrix, respectively. Moreover, the given data are collected into the vectors $\widehat{\mathsf{f}}_D$ and $\widehat{\mathsf{f}}_N$, and the unknown Cauchy data are represented by the vector of unknowns $[\mathsf{q}_h\ \mathsf{u}_h]^\top$. In detail, the entries of the system matrices are given by

$$\begin{aligned}\widehat{\mathsf{V}}_h[i,k] &= \langle\widehat{\mathcal{V}}\varphi_k^\gamma, \varphi_i^\gamma\rangle_{\Gamma_{D,h}} = \int\limits_{\mathrm{supp}(\varphi_i^\gamma)} \varphi_i^\gamma(\mathbf{x}) \int\limits_{\mathrm{supp}(\varphi_k^\gamma)} U(\mathbf{y}-\mathbf{x})\varphi_k^\gamma(\mathbf{y})\,\mathrm{d}s_\mathbf{y}\,\mathrm{d}s_\mathbf{x}\\ \widehat{\mathsf{K}}_h[i,\ell] &= \langle\widehat{\mathcal{K}}\psi_\ell^\beta, \varphi_i^\gamma\rangle_{\Gamma_{D,h}} = \int\limits_{\mathrm{supp}(\varphi_i^\gamma)} \varphi_i^\gamma(\mathbf{x}) \int\limits_{\mathrm{supp}(\psi_\ell^\beta)} (\mathcal{T}_\mathbf{y}U)^\top(\mathbf{y}-\mathbf{x})\psi_\ell^\beta(\mathbf{y})\,\mathrm{d}s_\mathbf{y}\,\mathrm{d}s_\mathbf{x}\\ \widehat{\mathsf{D}}_h[j,\ell] &= \langle\widehat{\mathcal{D}}\psi_\ell^\beta, \psi_j^\beta\rangle_{\Gamma_{N,h}} = -\int\limits_{\mathrm{supp}(\psi_j^\beta)} \psi_j^\beta(\mathbf{x})\mathcal{T}_\mathbf{x} \int\limits_{\mathrm{supp}(\psi_\ell^\beta)} (\mathcal{T}_\mathbf{y}U)^\top(\mathbf{y}-\mathbf{x})\psi_\ell^\beta(\mathbf{y})\,\mathrm{d}s_\mathbf{y}\,\mathrm{d}s_\mathbf{x}\end{aligned} \tag{5.17}$$

where $\mathrm{supp}(\phi)$ denotes the support of the function ϕ. The support of a function is the domain on which the function ϕ is evaluated to non-zero values. Analogously, the entries of the right hand side are

$$\begin{aligned}\widehat{\mathsf{f}}_D[i] &= \langle(\tfrac{1}{2}\widehat{\mathcal{I}}+\widehat{\mathcal{K}})g_{D,h}^\beta - \widehat{\mathcal{V}}g_{N,h}^\gamma - \widehat{\mathcal{N}}_0 f_h, \varphi_i^\gamma\rangle_{\Gamma_{D,h}}\\ \widehat{\mathsf{f}}_N[j] &= \langle(\tfrac{1}{2}\widehat{\mathcal{I}}-\widehat{\mathcal{K}}')g_{N,h}^\gamma - \widehat{\mathcal{D}}g_{D,h}^\beta - \widehat{\mathcal{N}}_1 f_h, \psi_j^\beta\rangle_{\Gamma_{N,h}}\,.\end{aligned}$$

Thereby, the entries according to the identity operator are computed by

$$\mathsf{I}[m,n] = \int\limits_{\mathrm{supp}(\psi_m^\beta)} \psi_m^\beta(\mathbf{x})\varphi_n^\gamma(\mathbf{x})\,\mathrm{d}s_{\mathbf{x}}$$

which is nothing but the classical mass matrix. Due to the Galerkin discretization the matrices $\widehat{\mathsf{V}}_h$ and $\widehat{\mathsf{D}}_h$ are symmetric (see (5.17)). Thus, the system (5.16) is block skew-symmetric. Additionally, the discretization of static problems results in a positive definite $\widehat{\mathsf{V}}_h$ whereas in the time harmonic case the situation slightly changes. There, the fundamental solution is of the form $U = U(\mathbf{y}-\mathbf{x},\omega)$ and the system (5.16) is positive definite only under the constraint that the frequency ω is not an eigenfrequency of the problem. Moreover, the linear system (5.16) consists of real entries in the static case and of complex entries for time harmonic problems.

To develop an appropriate solution algorithm for the system (5.16), first, a closer look should be given on the physics behind it. In almost all engineering applications the Dirichlet boundary is small compared to the Neumann part, i.e., there are usually much more Neumann data than Dirichlet data prescribed. Hence, the number N of unknown Neumann data is considerably smaller than the number M of unknown Dirichlet data. With the assumption $N \ll M$ and the knowledge that $\widehat{\mathsf{V}}_h$ is positive definite the first equation of (5.16) could be solved for the first unknown

$$\mathsf{q}_h = \widehat{\mathsf{V}}_h^{-1}\widehat{\mathsf{K}}_h\mathsf{u}_h + \widehat{\mathsf{V}}_h^{-1}\widehat{\mathsf{f}}_D\,.$$

Inserting this into the second equation of (5.16) gives the *Schur complement system*

$$\widehat{\mathsf{S}}_h\mathsf{u}_h = \widehat{\mathsf{f}}_N - \widehat{\mathsf{K}}_h^\top\widehat{\mathsf{V}}_h^{-1}\widehat{\mathsf{f}}_D \tag{5.18}$$

with the symmetric and positive definite *Schur complement matrix* [120]

$$\widehat{\mathsf{S}}_h := \widehat{\mathsf{D}}_h + \widehat{\mathsf{K}}_h^\top\widehat{\mathsf{V}}_h^{-1}\widehat{\mathsf{K}}_h\,. \tag{5.19}$$

In principle, there exist two approaches to obtain an explicit solution of (5.18). One is based on iterative solution methods and the other one uses classical direct solver algorithms. Within this thesis direct solvers are used as they are, for instance, described in the standard textbook of Golub & van Loan [46] concerning linear algebra. The use of a direct solver scheme restricts this formulation to rather small or medium sized problems since those solvers obey the complexity $\mathcal{O}(M^3)$ contrary to the complexity $\mathcal{O}(M^2)$ for iterative methods. Nevertheless, as the emphasis of this thesis is the solution of time-dependent problems this restriction becomes less evident, since in that case the storage of the system matrices for every time step is required. The forthcoming section will clarify this issue.

Now, to sketch the solution of (5.18) briefly one has to distinct between the static and the time-harmonic case. In statics the situation is simple. The matrix $\widehat{\mathsf{V}}_h$ can be inverted using the Cholesky factorization [46], i.e., the discrete single layer potential matrix is decomposed into $\widehat{\mathsf{V}}_h = \mathsf{L}\mathsf{L}^\top$ where $\mathsf{L} \in \mathbb{R}^{N\times N}$ is an upper or lower triangular matrix. Analogously, the Schur complement matrix can be decomposed via the Cholesky factorization.

In frequency-dependent problems the matrices are complex valued, symmetric, but not Hermitian. Thus, the classical Cholesky algorithm fails and one has to be content with a slightly modified factorization. The so-called $LDL^\top$-factorization [46] decomposes $\widehat{\mathsf{V}}_h$ into a lower triangular matrix $\mathsf{L} \in \mathbb{C}^{N\times N}$ and a diagonal matrix $\mathsf{D} \in \mathbb{C}^{N\times N}$, i.e., $\widehat{\mathsf{V}}_h = \mathsf{L}\mathsf{D}\mathsf{L}^\top$. Finally, also the decomposition of the Schur complement matrix is done by making use of the $LDL^\top$-factorization.

5.3 Numerical integration

Probably the most challenging part within any Boundary Element formulation is the accurate evaluation of the matrix entries according to (5.16). As mentioned at the beginning of chapter 4 the analytical integration of the integral kernels is impossible in general and numerical integration schemes have to be used instead. An insufficient numerical integration scheme is sometimes categorized as *variational crime*, a term which has been coined by Strang & Fix [121]. To exclude such an issue as far as possible some investigations concerning the computation of the matrix entries (5.17) must be given.

During this section the integral kernel is just denoted as $K(\mathbf{y}-\mathbf{x})$ whereas K represent any of the stated fundamental solutions. Applying a numerical scheme onto this kernel function means that the integral $I[K]$ is replaced by a quadrature $Q_{nm}[K]$. For two points $\mathbf{x} \in \tau_\mathbf{x}$ and $\mathbf{y} \in \tau_\mathbf{y}$ being defined on two elements $\tau_\mathbf{x}$ and $\tau_\mathbf{y}$, respectively, the general form of a boundary integral's kernel in local coordinates $\hat{\mathbf{x}}$ and $\hat{\mathbf{y}}$ reads as

$$\hat{K}(\hat{\mathbf{y}},\hat{\mathbf{x}}) := \phi(\hat{\mathbf{x}})\, K(\chi_{\tau_\mathbf{y}}(\hat{\mathbf{y}}) - \chi_{\tau_\mathbf{x}}(\hat{\mathbf{x}}))\, \psi(\hat{\mathbf{y}}) \sqrt{g_{\tau_\mathbf{x}}(\hat{\mathbf{x}})}\sqrt{g_{\tau_\mathbf{y}}(\hat{\mathbf{y}})}\,. \tag{5.20}$$

Thereby, the functions ϕ and ψ denote the respective test- and trial-functions according to the Galerkin scheme. The quadrature of the four-dimensional integral is given by

$$I[K] = \int_{\hat{\tau}_\mathbf{x}} \int_{\hat{\tau}_\mathbf{y}} \hat{K}(\hat{\mathbf{y}},\hat{\mathbf{x}})\, \mathrm{d}\hat{\mathbf{y}}\, \mathrm{d}\hat{\mathbf{x}} \approx \sum_{i=1}^{n}\sum_{j=1}^{m} \omega_i \omega_j\, \hat{K}(\boldsymbol{\xi}_i, \boldsymbol{\eta}_j) = Q_{nm}[K]\,. \tag{5.21}$$

Note that the quadrature rule has to be chosen according to the two different element types defined in (5.3). In this work, all regular numerical integrations concerning the reference triangle are done by using quadrature rules developed by Dunavant [36] while in case of quadrilaterals the regular integrations are performed by using the tensor product of the classical *Gauss-Legendre quadrature*. At least, this fundamental numerical integration scheme can be found in almost every textbook on Finite Elements, e.g., in the textbook of Bathe [8].

The quadrature (5.21) shows already one important drawback of the proposed Boundary Element Method. Contrary to the classical Finite Element Methods, here, the integral kernel is not a polynomial of fixed degree but rather a rational function of the form

$$\hat{K}(\hat{\mathbf{x}},\hat{\mathbf{y}}) = \frac{f(\hat{\mathbf{x}},\hat{\mathbf{y}})}{\chi_{\tau_\mathbf{y}}(\hat{\mathbf{y}}) - \chi_{\tau_\mathbf{x}}(\hat{\mathbf{x}})}$$

with some sufficient smooth function $f(\hat{\mathbf{x}},\hat{\mathbf{y}})$. Therefore, it is not possible to determine the number of Gauss points n and m such that the quadrature is exact. It is even challenging to answer the question on the number of Gauss points which is necessary to go below a certain error bound ε. In other words, the control of the absolute integration error

$$E_{nm}[K] := |(I - Q_{nm})[K]| \tag{5.22}$$

such that $E_{nm}[K] < \varepsilon$ is a large problem within every Boundary Element Method which relies on numerical integration schemes. Unfortunately, this method is still lacking of appropriate error estimates such that one has to be content with a rather heuristic choice concerning the number of appropriate Gauss points. The fact that the kernel functions depend basically on the reciprocal distance $1/|\mathbf{y}-\mathbf{x}|$ motivates the use of the distance between two elements $\tau_{\mathbf{x}}$ and $\tau_{\mathbf{y}}$ as a main criterion to fix the number of Gauss points. Qualitative this criterion is formulated as: The larger the distance between two elements become the fewer Gauss points need to be chosen. The distance's definition between two elements is taken from [107]

$$\operatorname{dist}(\tau_{\mathbf{x}},\tau_{\mathbf{y}}) := \inf_{\substack{\mathbf{x}\in\tau_{\mathbf{x}}\\ \mathbf{y}\in\tau_{\mathbf{y}}}} |\mathbf{y}-\mathbf{x}| \; .$$

Obviously, this distance is difficult to measure so that the following approximation serves as a sufficiently good enough estimate

$$\operatorname{dist}(\tau_{\mathbf{x}},\tau_{\mathbf{y}}) \approx \widetilde{\operatorname{dist}}(\tau_{\mathbf{x}},\tau_{\mathbf{y}}) := |\mathbf{s}_{\mathbf{y}}-\mathbf{s}_{\mathbf{x}}| - \frac{1}{2}\left(h_{\mathbf{y}}+h_{\mathbf{x}}\right) \; .$$

Above, the points $\mathbf{s}_{\mathbf{x}}$ and $\mathbf{s}_{\mathbf{y}}$ denote the centers of the respective boundary elements and $h_{\mathbf{x}}$ as well as $h_{\mathbf{y}}$ are their mesh sizes. As mentioned before, the choice of the Gauss points' number depends on an heuristic approach and has no rigorous mathematical background. The number of Gauss points which are used for the numerical examples in chapter 6 is given in Tab. 5.1. There, the dimensionless distance $\widetilde{\delta}(\tau_{\mathbf{x}},\tau_{\mathbf{y}}) := \widetilde{\operatorname{dist}}(\tau_{\mathbf{x}},\tau_{\mathbf{y}})/h_G$ is introduced. Further, the number of Gauss points per element is given by $n_{\triangle}$ for triangles and by $n_{\square}$ for quadrilaterals, respectively.

$\widetilde{\delta}(\tau_{\mathbf{x}},\tau_{\mathbf{y}})$	$n_{\triangle}$	$n_{\square}$
0	-	5^2
$0\ldots1$	6	5^2
$1\ldots5$	4	3^2
>5	3	2^2

Table 5.1: Quadrature rule dependent on $\widetilde{\delta}$

A real error estimate from a mathematical point of view is given by Sauter & Schwab in [107, p. 266]. Contrary to the presented approach that estimate's aim is to guarantee the convergence of the Galerkin scheme, i.e., it controls the discretization error instead

of the integration error. Although being much more powerful at the end it is not used for the numerical examples which will be presented in chapter 6. Those examples are primary intended to confirm the herein presented Boundary Element Method. Therefore, the numerical tests will be done by means of simple geometries with coarser meshes which demand accurate integration schemes in order to give reasonable results.

The numerical integration scheme discussed so far is in some sense only the prelude of the probably most challenging numerical task. If the distance between two elements becomes zero, i.e., if the point $\mathbf{x}$ reaches the point $\mathbf{y}$ the integral kernel gets singular. Fortunately, due to the former stated regularization of the strong- and hypersingular integral kernels this singularity is always of a weak type such that the integral exists in an improper sense. Nevertheless, the application of Gaussian quadrature is inadequate since the kernel is not regular enough. One approach to handle weak singularities is the transformation by special coordinate transformations which remove the singularity by help of the transformation's Gram determinant. Although those coordinate transformations go back to the work of Lachat & Watson [71] they are commonly better known as *Duffy transformations* [35]. The method is illustrated on the basis of a two-dimensional function f being defined as

$$f(\hat{\mathbf{x}}) := \frac{\hat{x}_1\,(1-\hat{x}_2)}{\sqrt{\hat{x}_1^2+\hat{x}_2^2}}\,, \qquad 0 \le (\hat{x}_1,\hat{x}_2) \le 1\ .$$

The function f has a singularity at the point $(\hat{x}_1,\hat{x}_2) = (0,0)$ but the integral exists as an improper integral with

$$I[f] = \lim_{\substack{\varepsilon\to 0\\ \varepsilon>0}} \int_{\varepsilon}^{1}\int_{\varepsilon}^{1} f(\hat{\mathbf{x}})\,\mathrm{d}\hat{x}_2\,\mathrm{d}\hat{x}_1 = \frac{1}{6}\left(1-\sqrt{2}+3\log(1+\sqrt{2})\right)\ . \tag{5.23}$$

Although an application of the Gauss-Legendre quadrature to that integral yields not a completely wrong result, the quadrature's convergence rate is by far too slow. For an acceleration of the convergence a regularization is mandatory in order to remove the singularity at the origin. In Fig. 5.3, the main steps of this regularization process are depicted.

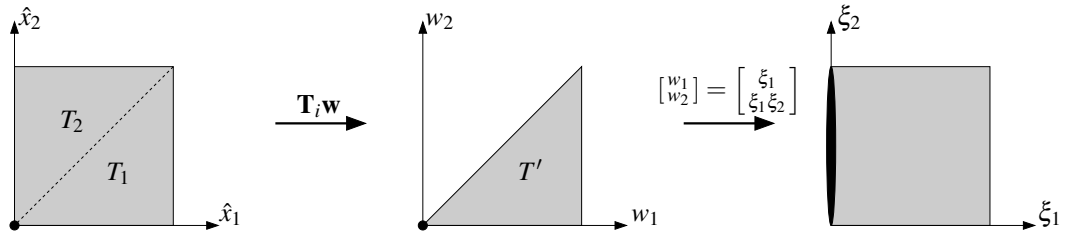

Figure 5.3: Regularization via coordinate transformations

At first, the domain of integration is split into two triangles both exhibiting the singularity at the origin. With the lower triangle $T_1 := \{(\hat{x}_1,\hat{x}_2) \in \mathbb{R}^2 \colon 0 < \hat{x}_2 < \hat{x}_1 < 1\}$ and the upper

triangle $T_2 := \{(\hat{x}_1, \hat{x}_2) \in \mathbb{R}^2 \colon 0 < \hat{x}_1 < \hat{x}_2 < 1\}$, respectively, the integration becomes

$$I[f] = \int_0^1 \int_0^{\hat{x}_1} f(\hat{\mathbf{x}}) \, \mathrm{d}\hat{x}_2 \, \mathrm{d}\hat{x}_1 + \int_0^1 \int_{\hat{x}_1}^1 f(\hat{\mathbf{x}}) \, \mathrm{d}\hat{x}_2 \, \mathrm{d}\hat{x}_1 \, . \tag{5.24}$$

Next, two linear mappings $\chi_{T_i} \colon T' \to T_i$ with $i = 1, 2$ are introduced which map the reference triangle T' to the images T_1 and T_2, respectively. The mapping χ_{T_1} is, obviously, just the identity

$$\chi_{T_1} \colon \begin{bmatrix} \hat{x}_1 \\ \hat{x}_2 \end{bmatrix} = \begin{bmatrix} 1 & 0 \\ 0 & 1 \end{bmatrix} \cdot \begin{bmatrix} w_1 \\ w_2 \end{bmatrix} =: \mathbf{T}_1 \mathbf{w} \, . \tag{5.25}$$

To obtain $\chi_{T_2} \colon T' \to T_2$ one simply use (5.8) with $\mathbf{p}_1 = [0, 0]^\top$, $\mathbf{p}_2 = [1, 1]^\top$, and with $\mathbf{p}_3 = [0, 1]^\top$, respectively. This yields

$$\chi_{T_2} \colon \begin{bmatrix} \hat{x}_1 \\ \hat{x}_2 \end{bmatrix} = \begin{bmatrix} 1 & -1 \\ 1 & 0 \end{bmatrix} \cdot \begin{bmatrix} w_1 \\ w_2 \end{bmatrix} =: \mathbf{T}_2 \mathbf{w} \, . \tag{5.26}$$

Due to $\det(\mathbf{T}_i) = 1$ with $i = 1, 2$ the integral (5.24) is given in (w_1, w_2)-coordinates by

$$I[f] = \sum_{i=1}^{2} \int_0^1 \int_0^{w_1} f(\mathbf{T}_i \mathbf{w}) \, \mathrm{d}w_2 \, \mathrm{d}w_1 \, .$$

Note that until now, no regularization has taken place and that the original singularity is still existent. But in contrast to (5.23), the expression above is appropriate for a regularization via the Duffy transformation. With the simplex coordinates

$$\begin{bmatrix} w_1 \\ w_2 \end{bmatrix} = \begin{bmatrix} \xi_1 \\ \xi_1 \xi_2 \end{bmatrix}$$

and together with the Gram determinant $g = \xi_1$ the integral is, finally, given by

$$I[f] = \sum_{i=1}^{2} \int_0^1 \int_0^1 f(\mathbf{T}_i \begin{bmatrix} \xi_1 \\ \xi_1 \xi_2 \end{bmatrix}) \, \xi_1 \, \mathrm{d}\xi_2 \, \mathrm{d}\xi_1 \, . \tag{5.27}$$

This expression is appropriate for the use within the standard Gauss-Legendre quadrature since the singularity has been removed. The kernel's regularity can either be proofed by the limiting process which yields

$$\lim_{\substack{\xi_1 \to 0 \\ \xi_1 > 0}} \left(f(\mathbf{T}_i \begin{bmatrix} \xi_1 \\ \xi_1 \xi_2 \end{bmatrix}) \, \xi_1 \right) = 0 \, , \qquad i = 1, 2$$

or simply by calculating the kernel's explicit form which gives

$$\sum_{i=1}^{2} f(\mathbf{T}_i \begin{bmatrix} \xi_1 \\ \xi_1 \xi_2 \end{bmatrix}) \, \xi_1 = \frac{\xi_1 \, (1 - \xi_1 \xi_2)}{\sqrt{1 + \xi_2^2}} + \frac{\xi_1 \, (1 - \xi_1) \, (1 - \xi_2)}{\sqrt{1 + (1 - \xi_2)^2}} \, .$$

This kind of regularization is advantageous due to the fact that it relies only on appropriate coordinate transformations. Hence, there are only few requirements concerning the integral kernel. Beside the knowledge of the singularity's type the only necessary information is the singularity's location which is always known. Further, it is extremely simple from an implementation point of view since the integral kernel itself is left unchanged. According to (5.27) only the transformed coordinates have to be plugged into the kernel function. To verify this integration scheme, in Tab. 5.2 and in Fig. 5.4 the integration errors for an increasing number of Gauss points are depicted. The integration error's definition is based on (5.22). The values E_n^{std} refer to an application of the Gauss-Legendre quadrature to the unmodified kernel whereas the last column represents the integration error E_n^{reg} based on an evaluation of the regularized kernel (5.27).

$\sqrt{n}$	$E_n^{std}[f]$	$E_n^{reg}[f]$
1	3.7e-01	3.7e-01
2	1.8e-02	7.6e-02
3	9.2e-03	4.1e-04
4	2.8e-03	2.4e-05
5	1.1e-03	6.6e-07
⋮	⋮	⋮
30	6.5e-07	6.7e-16

Table 5.2: Non-regularized and regularized Quadrature

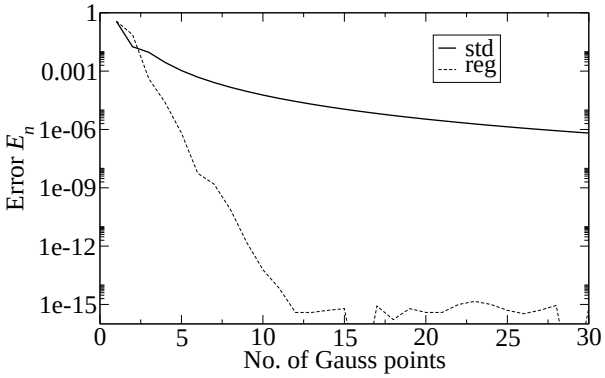

Figure 5.4: Error plot

As assumed the absolute integration error decreases considerably faster for the regularized kernel than for the unmodified one. For the regularized approach an accuracy of $E_n[f] \approx 10^{-7}$ is achieved for 5^2 Gauss points. In contrast, about 30^2 Gauss points are necessary to achieve a similar accuracy in case of the non-regularized quadrature. Thus, it is obviously more efficient to apply certain coordinate transformations resulting in a removal of the kernel's singularity.

Until now, the presented regularization is only stated by means of a two-dimensional example. Obviously, this regularization is not suitable for use within the numerical treatment of (5.21), since there the occurring integrals are defined on a four-dimensional reference domain. To handle this case, quadrature rules as they are stated in the works of Sauter [37, 106, 107] are used within this work. Their detailed derivation is very laborious and is omitted herein. Nevertheless, with view to section 5.5 it is important to sketch at least the outline of their deduction in the following. In principle, the regularization of the four-dimensional integral kernels given by Sauter follows the same rules as in the two-dimensional case except one essential difference. Contrary to the stated example the singularity in Galerkin methods is not necessarily concentrated at a single point. Depending on the location of two boundary elements $\tau_{\mathbf{x}}$ and $\tau_{\mathbf{y}}$ one has to distinguish four different cases:

- Boundary elements with positive distance: $\operatorname{dist}(\tau_{\mathbf{x}}, \tau_{\mathbf{y}}) > 0$
- Identical boundary elements $\tau_{\mathbf{x}} = \tau_{\mathbf{y}}$
- The elements $\tau_{\mathbf{x}}$ and $\tau_{\mathbf{y}}$ share a common edge
- The elements $\tau_{\mathbf{x}}$ and $\tau_{\mathbf{y}}$ share a common point

Fig. 5.5 illustrates these four cases more strikingly. The regular integrations are not considered at this point so that it remains to investigate the remaining three cases. Obviously, only if two elements share one common point there exist a point singularity. Let $\chi_{\tau_{\mathbf{x}}} \colon \hat{\tau} \to \tau_{\mathbf{x}}$ be the mapping onto the element $\tau_{\mathbf{x}}$, and let $\chi_{\tau_{\mathbf{y}}} \colon \hat{\tau} \to \tau_{\mathbf{y}}$ be the mapping according to the element $\tau_{\mathbf{y}}$. Then, it is assumed that both mappings are given such that in the vertex-adjacent case

$$\chi_{\tau_{\mathbf{x}}}(\left[\begin{smallmatrix}0\\0\end{smallmatrix}\right]) = \chi_{\tau_{\mathbf{y}}}(\left[\begin{smallmatrix}0\\0\end{smallmatrix}\right])$$

holds. In the edge-adjacent case the mappings are chosen such that the singularity can be expressed by the line

$$\chi_{\tau_{\mathbf{x}}}(\left[\begin{smallmatrix}s\\0\end{smallmatrix}\right]) = \chi_{\tau_{\mathbf{y}}}(\left[\begin{smallmatrix}s\\0\end{smallmatrix}\right]) \qquad \forall s \in [0,1] \,.$$

Finally, in the coincident case the singularity is a plane within the four-dimensional reference domain

$$\chi_{\tau_{\mathbf{x}}}(\left[\begin{smallmatrix}s\\t\end{smallmatrix}\right]) = \chi_{\tau_{\mathbf{y}}}(\left[\begin{smallmatrix}s\\t\end{smallmatrix}\right]) \qquad \forall (s,t) \in [0,1]^2 \,. \tag{5.28}$$

In the end, the regularization relies on an application of a Duffy transformation which demand a point singularity at the origin. Hence, as a preliminary work the singularities above have to be fixed at the origin. To achieve this goal relative coordinates are introduced. After this is done, the region of integration can be divided into several sub-regions such that the already described procedure of regularization can be applied (cf. Fig. 5.3).

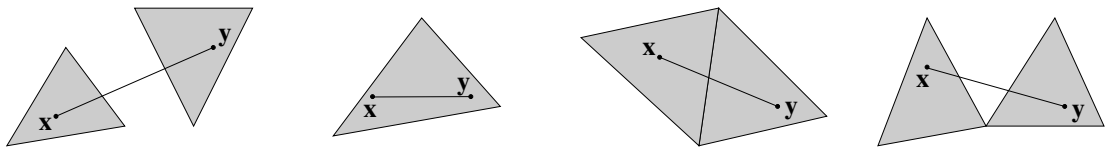

(a) Regular case (b) Coincident case (c) Edge adjacent case (d) Vertex adjacent case

Figure 5.5: Possible element correlations

To illustrate the use of relative coordinates very briefly, the coincident case is considered exemplary. Let $\tau_{\mathbf{x}}$ and $\tau_{\mathbf{y}}$ be two coincident quadrilateral elements. Then, the integral kernel reads as

$$I[K] = \int_0^1 \int_0^1 \int_0^1 \int_0^1 \hat{K}(\hat{\mathbf{x}}, \hat{\mathbf{y}}) \, \mathrm{d}\hat{\mathbf{y}} \, \mathrm{d}\hat{\mathbf{x}}$$

with a kernel function $\hat{K}$ of the form (5.20). Next, due to the singularity (5.28) relative coordinates $\hat{\mathbf{z}}$ are introduced such that the new coordinates $(\hat{\mathbf{x}}, \hat{\mathbf{z}}) = (\hat{\mathbf{x}}, \hat{\mathbf{y}} - \hat{\mathbf{x}})$ fix the singularity at $\hat{\mathbf{z}} = \mathbf{0}$. This yields the modified integral

$$I[K] = \int_0^1 \int_0^1 \int_{-\hat{x}_1}^{1-\hat{x}_1} \int_{-\hat{x}_2}^{1-\hat{x}_2} \hat{K}(\hat{\mathbf{x}}, \hat{\mathbf{z}} + \hat{\mathbf{x}}) \, \mathrm{d}\hat{\mathbf{z}} \, \mathrm{d}\hat{\mathbf{x}} \, .$$

Afterwards, a splitting of the integration domain into eight subdomains leads to analogous integration domains as they are given for the two-dimensional case in (5.24). With the four-dimensional unit simplex

$$T_4' := \{(w_1, w_2, w_3, w_4) \in \mathbb{R}^4 \colon 0 \leq w_4 \leq w_3 \leq w_2 \leq w_1 \leq 1\}$$

mappings are introduced such that those domains are images of the reference simplex T_4'. Finally, simplex coordinates $w_i = \prod_{k=1}^{i} \xi_k$ with $i = 1 \ldots 4$ are used to remove the singularity at the origin and to end up with an analytical kernel function. All of these steps are given in detail in [107] and, therefore, are omitted herein. Nevertheless, one closing remark must be given concerning the derivation stated here and the one stated in [107]. There, the aim is the regularization of kernel functions which feature not only a weak singularity but which may exhibit also a strong singularity. To regularize the latter type of singularity one has to perform two additional steps. First, the order of integration is reversed and, secondly, some antisymmetric properties of the fundamental solutions derivatives are used by what the strong singularities are eliminated.

To close this section the main results may be summarized. At first, a numerical scheme is applied for all integrations. The regular, i.e., non-singular, integrations over the reference triangle are done by use of a special triangular quadrature. All quadrilaterals and singular integrals are computed by the standard Gauss-Legendre quadrature. Additionally, in the singular case the quadrature is preceded by a regularization of the integral kernel. This regularization is mainly based on the use of relative coordinates and an application of the Duffy transformation to remove the singularity.

5.4 Convolution Quadrature Method

As mentioned at the outset of section 5.2, the Galerkin discretization can be applied also to hyperbolic problems and their variational formulations as they are given in section 3.3. Exemplary, the variational formulation according to a mixed hyperbolic boundary value problem reads as:

Find $(\tilde{q}, \tilde{u})$ *such that*

$$\begin{aligned} \langle \mathcal{V} * \tilde{q}, w \rangle_{\Gamma_D} - \langle \mathcal{K} * \tilde{u}, w \rangle_{\Gamma_D} &= \langle f_D, w \rangle_{\Gamma_D} \\ \langle \mathcal{K}' * \tilde{q}, v \rangle_{\Gamma_N} + \langle \mathcal{D} * \tilde{u}, v \rangle_{\Gamma_N} &= \langle f_N, v \rangle_{\Gamma_N} \, . \end{aligned} \tag{5.29}$$

is fulfilled for all test-functions (w,v).

In the statement above, the right hand-sides are abbreviated. Their explicit form is given in Eqn. (3.31).

In contrast to the elliptic cases the unknown data exhibit a time-dependency such that $\tilde{q} = \tilde{q}(\mathbf{y},t)$ and $\tilde{u} = \tilde{u}(\mathbf{y},t)$, respectively, holds. For this data, an approximation can be given by decoupling the time dependency from the spatial dependency. In accordance to the elliptic approximation (5.15) this yields

$$\begin{aligned} \tilde{q} \approx q_h^\gamma(\mathbf{x},t) &:= \sum_{k=1}^{N} q_k(t)\varphi_k^\gamma(\mathbf{x}) \qquad \in S_h^\gamma(\Gamma_{D,h}) \\ \tilde{u} \approx u_h^\beta(\mathbf{x},t) &:= \sum_{\ell=1}^{M} u_\ell(t)\psi_\ell^\beta(\mathbf{x}) \qquad \in S_h^\beta(\Gamma_{N,h})\,. \end{aligned} \tag{5.30}$$

Note that the functional spaces above coincide with those for the elliptic case (cf. Eqn. (5.14)). Inserting (5.30) into (5.29) yields the semi-discrete variational problem

$$\begin{aligned} \langle \mathcal{V} * q_h^\gamma, w_h^\gamma\rangle_{\Gamma_{D,h}} - \langle \mathcal{K} * u_h^\beta, w_h^\gamma\rangle_{\Gamma_{D,h}} &= \langle f_{D,h}, w_h^\gamma\rangle_{\Gamma_{D,h}} \\ \langle \mathcal{K}' * q_h^\gamma, v_h^\beta\rangle_{\Gamma_{N,h}} + \langle \mathcal{D} * u_h^\beta, v_h^\beta\rangle_{\Gamma_{N,h}} &= \langle f_{N,h}, v_h^\beta\rangle_{\Gamma_{N,h}} \end{aligned} \tag{5.31}$$

for all test-functions $w_h^\gamma(\mathbf{x}) \in S_h^\gamma(\Gamma_{D,h})$ and $v_h^\beta(\mathbf{x}) \in S_h^\beta(\Gamma_{N,h})$. The test-functions w_h and v_h exhibit no time-dependency by what the Galerkin discretization is a discretization scheme for the spatial dimensionality only. Therefore, in order to arrive at a purely algebraic set of equations, the remaining goal within this section is the numerical treatment of the time convolution integrals of type

$$(f * g)(t) := \int_0^t f(t-\tau)g(\tau)\,\mathrm{d}\tau \quad \forall t > 0\,. \tag{5.32}$$

Costabel [29] gives a comprehensive overview concerning time stepping procedures within Boundary Element Methods where, in principle, three possibilities of treating the time-dependency in boundary integral equation methods are distinguished. The so-called class of *time-stepping methods* avoid the time convolution integrals (5.32) completely since there are no space-time boundary integral equations involved at all. These methods incorporate the time-discretization already in the earliest possible stage, namely at the level of the associated initial boundary value problem. Applying a time-stepping scheme onto the initial boundary value problem yields a sequence of elliptic boundary value problems parametrized by the time-variable. Then, this sequence of boundary value problems is treated by the use of boundary integral equations as they are stated for elliptic problems. An application of this idea may be found, e.g., in [24]. The drawback of this method consist mainly in inhomogeneities resulting from the time-discretization. Those inhomogeneities are rather cumbersome to deal with since they result in domain integrals within the boundary integral equations.

Contrary to that, the *space-time integral equations methods* can be regarded as the opponents to the former method since here, the time-discretization is invoked very lately. This method has been mainly established by Mansur [80] for the acoustic fluid and for elastodynamics in two space dimensions. For elasticity problems, an extension to three dimensions has been proposed by Antes [5]. The method's main idea is the discretization of the time-dependent coefficients $q_k(t)$ and $u_\ell(t)$ in (5.30) via appropriate polynomial trial-functions. Afterwards, these functions are inserted into the time convolution integrals of type (5.32) and the integrations are performed analytically. Obviously, this analytical treatment demands the knowledge of the time-domain fundamental solution which is not known for every physical problem. Actually, the time-domain fundamental solution for viscoelastic continua is unknown in closed form and, thus, the method is not applicable in this case. Another drawback of this method is the fact that the stability properties are occasionally problematic. Due to these weaknesses this approach is not followed any longer. For more details the works of Mansur [80] and of Ha-Duong [53] are recommended.

The method presented here can be generally classified into the group of *Laplace transform methods* [29]. As the name already induces those time-stepping schemes utilize the Laplace transformation to approximate the time convolution integral (5.32). In particular, the time-stepping scheme presented here is commonly denoted as *convolution*, or *operational quadrature method*. In the following, the method's name is abbreviated by CQM. Its use is advantageous since the CQM is capable to treat problems where the fundamental solution is known in the Laplace-domain only. This method has been developed by Lubich [76–78] and has been succesfully applied to parabolic problems [79] as well as to viscoelastic [112] and poroelastic [111] Boundary Element Formulations being based on a collocation scheme in space. Nowadays, the method is well-known and should be sketched out only briefly in the following. Its detailed derivation can either be found in the original work of Lubich [76, 77] or in the book of Schanz [111]. Here, Schanz's deduction is followed and whenever details are omitted the reader is referred to [111].

As a starting point serves the inverse Laplace transformation [33]

$$f(t) = \lim_{Y\to\infty} \frac{1}{2\pi\mathrm{i}} \int_{c-\mathrm{i}Y}^{c+\mathrm{i}Y} \hat{f}(s)\exp(ts)\,\mathrm{d}s\,, \quad t>0 \tag{5.33}$$

which defines the original time-domain solution $f(t)$ by its Laplace-transform $\hat{f}(s)$. In (5.33) the path integral is performed along a line which runs parallel to the imaginary axis and crosses the abscissa $c\in\mathbb{R}$. In order to be well posed, c must be chosen to be larger than the largest real part of all poles of the Laplace transform $\hat{f}(s)$. Inserting (5.33) into the convolution integral (5.32) yields

$$(f*g)(t) = \frac{1}{2\pi\mathrm{i}} \lim_{Y\to\infty} \int_{c-\mathrm{i}Y}^{c+\mathrm{i}Y} \hat{f}(s) \underbrace{\int_0^t g(\tau)\exp(s(t-\tau))\,\mathrm{d}\tau}_{:=h(t,s)}\mathrm{d}s\,. \tag{5.34}$$

Note, above the integrations have been exchanged which enables the definition of a function $h(t,s)$. For a further treatment of (5.34) it would be advantageous to separate the complex variable s from the time-variable t such that $h(t,s)$ can be decomposed into two functions depending either on s or on t. Then, such a decomposition can be used to perform the complex integration analytical. Of course, this cannot be done completely analytical but semi-analytical. At first, it turns out that $h(t,s)$ is the solution of the ordinary differential equation of first order

$$\left(\frac{\mathrm{d}}{\mathrm{d}t} - s\right) h(t,s) = g(t) \tag{5.35}$$

with the homogeneous initial condition

$$h(0,s) = 0\,.$$

The representation (5.35) gives a hint to the solution scheme. An inversion of the differential operator $\mathrm{d}/\mathrm{d}t - s$ yields the solution for $h(t,s)$. Now, having a numerical scheme in mind this inversion is not performed analytically (which would lead to the integral definition in (5.34)) but by using a classical multistep method [122]. For this, the continuous function $h(t,s)$ is evaluated at distinct times $t_n = n\Delta t$ with $n \in \mathbb{N}$ and a constant time step size Δt. In the following, as an abbreviation all time dependent quantities $f(t_n,\cdot)$ will be noted as f_n. The incorporation of the multistep method is rather cumbersome and is omitted in this work. It is sufficient to note that within the multistep method it is not possible to isolate h_n such that $h_n = F(g_n)$ holds for some known function F. Nevertheless, at the end the power series

$$\sum_{n=0}^{\infty} h_n z^n = \frac{1}{\frac{\theta(z)}{\Delta t} - s} \sum_{n=0}^{\infty} g_n z^n \tag{5.36}$$

is obtained for some complex number $z \in \mathbb{C}$. The above expression is deduced under the restriction that the k-step method uses k zero starting values, i.e., the function h_n features k homogeneous initial conditions $h_0 = h_1 = \ldots = h_{k-1} = 0$. The function

$$\theta(z) \coloneqq \frac{\rho(z)}{\sigma(z)}$$

is defined as the quotient of two polynomials $\rho(z)$ and $\sigma(z)$ characterizing the underlying multistep method [73]. Therefore, the quotient $\theta(z)$ will be denoted as characteristic function throughout the rest of this section. A comparison of (5.36) with the differential equation (5.35) reveals the similarity of both expressions. The factor on the right-hand side of (5.36) may be interpreted as a discrete version of the inverse of the differential operator $\mathrm{d}/\mathrm{d}t - s$. Moreover, in (5.36) the time-variable t_n is separated from the Laplace parameter s such that this expression is suitable to be re-inserted into (5.34). For this, (5.34) has to

be multiplied with z^n and summed up over all n. This gives

$$\begin{aligned}\sum_{n=0}^{\infty}(f*g)_n z^n &= \frac{1}{2\pi\mathrm{i}}\lim_{Y\to\infty}\int_{c-\mathrm{i}Y}^{c+\mathrm{i}Y}\hat{f}(s)\sum_{n=0}^{\infty}h_n z^n\,\mathrm{d}s \\ &= \frac{1}{2\pi\mathrm{i}}\lim_{Y\to\infty}\int_{c-\mathrm{i}Y}^{c+\mathrm{i}Y}\hat{f}(s)\frac{1}{\frac{\theta(z)}{\Delta t}-s}\,\mathrm{d}s\sum_{n=0}^{\infty}g_n z^n\,.\end{aligned} \tag{5.37}$$

Now, the complex integration can be performed by using the residue theorem [114]. The Laplace transform has by definition no more poles for $\mathrm{Re}(s)\geq c$. Hence, the integral has a single pole at $s=\theta(z)/\Delta t$ which gives

$$\frac{1}{2\pi\mathrm{i}}\lim_{Y\to\infty}\int_{\mathcal{S}_Y(c)}\hat{f}(s)\frac{1}{\frac{\theta(z)}{\Delta t}-s}\,\mathrm{d}s=\hat{f}\left(\frac{\theta(z)}{\Delta t}\right)\,. \tag{5.38}$$

Note that the application of the residue theorem demands a closed contour path. Here, $\mathcal{S}_Y(c):=\{s\in\mathbb{C}\colon(\mathrm{Re}(s)=c\wedge|s|\leq Y)\vee(\mathrm{Re}(s)>c\wedge|s-c|=Y)\}$ denotes the union of the line parallel to the imaginary axis with a half circle in the complex plane of radius Y centered at c. Since the integral above must equal that integral in (5.37) the Laplace transform $\hat{f}$ has to fulfill the additional constraint $\lim_{|s|\to\infty}|\hat{f}(s)|=0$. Next, inserting the result (5.38) into (5.37) yields

$$\sum_{n=0}^{\infty}(f*g)_n z^n=\hat{f}\left(\frac{\theta(z)}{\Delta t}\right)\sum_{n=0}^{\infty}g_n z^n\,. \tag{5.39}$$

Of course, the aim is not to find an expression for the sum $\sum_{n=0}^{\infty}(f*g)_n z^n$ but for the convolution integral $(f*g)_n$ itself. For this purpose, the function $\hat{f}(\theta(z)/\Delta t)$ is developed in a power series

$$\hat{f}\left(\frac{\theta(z)}{\Delta t}\right)=\sum_{n=0}^{\infty}\omega_n(\hat{f})z^n\,.$$

Inserting this into (5.39) yields a double sum which can be simplified using the Cauchy product of two power series [55]

$$\hat{f}\left(\frac{\theta(z)}{\Delta t}\right)\sum_{n=0}^{\infty}g_n z^n=\sum_{n=0}^{\infty}\omega_n(\hat{f})z^n\sum_{n=0}^{\infty}g_n z^n=\sum_{n=0}^{\infty}\sum_{k=0}^{n}\omega_{n-k}(\hat{f})g_k z^n\,. \tag{5.40}$$

Finally, by inserting (5.40) into (5.39) and by comparing the coefficients a quadrature rule for the convolution integral (5.32) is obtained

$$(f*g)_n\approx\sum_{k=0}^{n}\omega_{n-k}(\hat{f},\Delta t,\theta)\,g_k\,,\quad\forall n\in\mathbb{N}\,. \tag{5.41}$$

The terms in parenthesis should emphasize on the weights' main dependencies which are the Laplace transform $\hat{f}$, the time step size Δt, and the characteristic function θ, respectively. Now, it remains to give a detailed representation of those. If the series expansion of

the Laplace transform $\hat{f}$ is explicitly known the weights can be determined analytical. But since this is in general not the case the calculation of the weights ω_n is based on Cauchy's integral formula [114]

$$\omega_n(\hat{f},\Delta t,\theta) = \frac{1}{2\pi \mathrm{i}} \int\limits_{\partial B_R} \hat{f}\left(\frac{\theta(z)}{\Delta t}\right) z^{-n-1}\,\mathrm{d}z\,. \tag{5.42}$$

The contour $\partial B_R := \{z \in \mathbb{C}\colon |z| = R\}$ denotes the circle in the domain of analyticity of the function $\hat{f}(\theta(z)/\Delta t)$. A numerical treatment of (5.42) can be achieved by using the trapezoidal rule. Again, a detailed derivation is omitted and just the final form is recalled

$$\omega_n(\hat{f},\Delta t,\theta) \approx \frac{1}{L}\sum_{\ell=0}^{L-1} \hat{f}\left(\frac{\theta(\zeta_\ell)}{\Delta t}\right)\zeta_\ell^{-n}, \quad \zeta_\ell := R\exp(\mathrm{i}\ell\tfrac{2\pi}{L})\,. \tag{5.43}$$

With the expression above at least two approximations have been introduced during the deduction of the CQM. Beside the approximation above a linear multistep method is used which demands some requirements that have not been mentioned yet. The multistep method has to meet certain stability criteria which limit the class of sufficient methods [76]. Within this thesis a BDF of order 2 (BDF2) is used which is known to suffice the stability criteria. The method's underlying characteristic polynomial is given by

$$\theta(z) = \frac{3}{2} - 2z + \frac{1}{2}z^2\,.$$

Finally, the parameters L and R from (5.43) need to be specified. While the parameter R simply denotes the radius of the circle ∂B_R the parameter L represents the number of intervals the circle ∂B_R is split into within the numerical approximation of the integral (5.42). Now, let N be the number of total time steps for which the convolution (5.41) has to be approximated and let ε be a prescribed error bound for the computation of $\hat{f}$ in (5.43), then the choice of $R^N = \sqrt{\varepsilon}$ and $L = N$ yields an error in the weight ω_n of order $\mathcal{O}(\sqrt{\varepsilon})$ [77, 111]. The choice of $L = N$ is mainly motivated by efficiency reasons since it allows the computation of the weights ω_n by a technique similar to the Fast Fourier Transformation (FFT). Numerical studies concerning the choice of parameters can be also found in the work of Schanz [111].

Now, it remains to adopt the CQM for the use within the present Boundary Element Method. Therefore, the time-convolution integrals of the semi-discrete variational formulation (5.31) are simply plugged into (5.41). As a preliminary, a time grid is introduced in order to divide the time period of interest $[0,T]$ with $T > 0$ in N intervals of constant size Δt, i.e., the variational form (5.31) will be approximated at distinct sampling points $t_n = n\Delta t$ with $n = 0,1,\ldots,N$. Then, for a time t_n an application of the single layer operator

in (5.31) gives

$$\begin{aligned}\langle(\mathcal{V}*q_h^\gamma)(t_n),w_h^\gamma\rangle_{\Gamma_D} &= \int_{\Gamma_D} w_h^\gamma(\mathbf{x}) \int_{\Gamma_D}\int_0^{t_n} U(\mathbf{y}-\mathbf{x},t_n-\tau)q_h^\gamma(\mathbf{y},\tau)\,\mathrm{d}\tau\,\mathrm{d}s_\mathbf{y}\,\mathrm{d}s_\mathbf{x} \\ &\approx \int_{\Gamma_D} w_h^\gamma(\mathbf{x}) \int_{\Gamma_D} \sum_{m=0}^{n} \omega_{n-m}\left(\hat{U},\Delta t,\theta\right) q_h^\gamma(\mathbf{y},t_m)\,\mathrm{d}s_\mathbf{y}\,\mathrm{d}s_\mathbf{x}\,.\end{aligned} \tag{5.44}$$

Above, $\hat{U}$ denotes the Laplace transformed fundamental solution. Thus, it becomes once more obvious that the approximation of the time convolution integral is done by using the Laplace transformed fundamental solution only. This fact makes the knowledge of any time-dependent fundamental solution obsolete by what means the method fits perfectly for applications to problems where fundamental solutions in the time-domain are unknown.

Now, inserting the definitions for q_h^γ and w_h from (5.30) into the expression (5.44) the convolution becomes

$$\left(\mathsf{V}*\mathsf{q}\right)(t_n) = \sum_{m=0}^{n} \omega_{n-m}(\hat{\mathsf{V}},\Delta t,\theta)\mathsf{q}(t_m)\,.$$

Of course, the discretizations of the remaining operators $\mathcal{K}$, $\mathcal{K}'$, and $\mathcal{D}$ as well as the discretization of the right hand-side are subjected to the same numerical scheme. With the definitions

$$\begin{aligned}\mathsf{V}_n &\coloneqq \omega_n(\hat{\mathsf{V}},\Delta t,\theta) & \mathsf{q}_n &\coloneqq \mathsf{q}(t_n)\\ \mathsf{K}_n &\coloneqq \omega_n(\hat{\mathsf{K}},\Delta t,\theta) & \mathsf{u}_n &\coloneqq \mathsf{u}(t_n)\\ \mathsf{K}'_n &\coloneqq \omega_n(\hat{\mathsf{K}}',\Delta t,\theta) & \mathsf{f}_{D,n} &\coloneqq \mathsf{f}_D(t_n)\\ \mathsf{D}_n &\coloneqq \omega_n(\hat{\mathsf{D}},\Delta t,\theta) & \mathsf{f}_{N,n} &\coloneqq \mathsf{f}_N(t_n)\end{aligned}$$

a sequence of linear systems of equations for every time step $n=0,\dots,N$ is obtained

$$\begin{bmatrix}\mathsf{V}_0 & -\mathsf{K}_0\\ \mathsf{K}_0^\top & \mathsf{D}_0\end{bmatrix}\cdot\begin{bmatrix}\mathsf{q}_n\\ \mathsf{u}_n\end{bmatrix} = \underbrace{\begin{bmatrix}\mathsf{f}_{D,n}\\ \mathsf{f}_{N,n}\end{bmatrix} - \sum_{m=0}^{n-1}\begin{bmatrix}\mathsf{V}_{n-m}\cdot\mathsf{q}_m - \mathsf{K}_{n-m}\cdot\mathsf{u}_m\\ \mathsf{K}_{n-m}^\top\cdot\mathsf{q}_m + \mathsf{D}_{n-m}\cdot\mathsf{u}_m\end{bmatrix}}_{=:\begin{bmatrix}\tilde{\mathsf{f}}_{D,n}\\ \tilde{\mathsf{f}}_{N,n}\end{bmatrix}}\,. \tag{5.45}$$

Above, the given right hand-side reveals the usual structure of a typical Boundary Element Method's time stepping technique since it consists of two parts. While all prescribed boundary data up to the actual time t_n are stored in the vector $[\mathsf{f}_{D,n}\ \mathsf{f}_{N,n}]^\top$ the last term comprises the complete time-history according to the already computed Cauchy data $[\mathsf{q}_n\ \mathsf{u}_n]^\top$ for the times $t_0,\dots,t_{n-1}$. Corresponding to the variational form's load vectors (3.31) the

prescribed data $[\mathsf{f}_{D,n}\ \mathsf{f}_{N,n}]^\top$ reads in discretized form as

$$\begin{bmatrix}\mathsf{f}_{D,n}\\ \mathsf{f}_{N,n}\end{bmatrix} = \begin{bmatrix}\bar{\mathsf{K}}_0\cdot\mathsf{g}_{D,n} - \mathsf{V}_0\cdot\mathsf{g}_{N,n} - \mathsf{N}_{0,0}\cdot f_{\Omega,n}\\ \bar{\mathsf{K}}_0'\cdot\mathsf{g}_{N,n} - \mathsf{D}_0\cdot\mathsf{g}_{D,n} - \mathsf{N}_{1,0}\cdot f_{\Omega,n}\end{bmatrix} + \sum_{m=0}^{n-1}\begin{bmatrix}\mathsf{K}_{n-m}\cdot\mathsf{g}_{D,m} - \mathsf{V}_{n-m}\cdot\mathsf{g}_{N,m} - \mathsf{N}_{0,n-m}\cdot f_{\Omega,m}\\ \mathsf{K}'_{n-m}\cdot\mathsf{g}_{N,m} - \mathsf{D}_{n-m}\cdot\mathsf{g}_{D,m} - \mathsf{N}_{1,n-m}\cdot f_{\Omega,m}\end{bmatrix} \tag{5.46}$$

where $\mathsf{N}_{i,\cdot}$ denotes the discretized i-th Newton potential and $\mathsf{f}_{\Omega,\cdot}$ are the discretized volume forces. The matrices $\bar{\mathsf{K}}_0 := \frac{1}{2}\mathsf{I} + \mathsf{K}_0$ and $\bar{\mathsf{K}}_0' := \frac{1}{2}\mathsf{I} - \mathsf{K}_0'$ correspond to the discrete double layer and adjoint double layer matrices for the first time step. Their definitions are due to the fact that the identity operator (3.27) contributes only to the first time step. This can be simply shown since the weights $\mathsf{I}_n := \omega_n(\hat{\mathsf{I}}, \Delta t, \theta)$ can be computed analytically. The identity operator contains the Delta distribution δ whose Laplace transform $\mathscr{L}\{\delta\}(s)$ is known to be 1. Therefore, the integration weights ω_n can directly be computed by substituting $z = R\exp(\mathrm{i}\varphi)$ in Cauchy's formula (5.42). This gives

$$\omega_n(\hat{\mathsf{I}}, \Delta t, \theta) = \frac{1}{2\pi\mathrm{i}}\int_{\partial B_R} z^{-n-1}\,\mathrm{d}z = \frac{R^{-n}}{2\pi}\int_0^{2\pi}\exp(-\mathrm{i}n\varphi)\,\mathrm{d}\varphi = \begin{cases}1 & \text{for } n=0\\ 0 & \text{for } n\neq 0\end{cases}.$$

From (5.45), it is obvious that the solution requires only the inversion of the matrix corresponding to the first time step. Thus, the solution scheme is very similar to the elliptic case. Again, a direct solver strategy is applied and the matrix V_0, which is symmetric as a result of the Galerkin discretization, is decomposed via a *Cholesky-factorization*. Afterwards, the *Schur-Complement-System* is computed by

$$\mathsf{S}_0 = \mathsf{K}_0^\top\mathsf{V}_0^{-1}\mathsf{K}_0 + \mathsf{D}_0\,. \tag{5.47}$$

Due to the symmetry of V_0 and D_0 the Schur-Complement S_0 is also symmetric and can be decomposed itself by a Cholesky-factorization. Note that the Cholesky-factorization demands a positive definite matrix [46]. While the positive definiteness is proven for elliptic systems it still remains to be proven also for hyperbolic systems. However, since the numerical examples in the following chapter are done by using this solution scheme the according system matrices must be positive definite. Otherwise, the Cholesky-factorization would fail.

Next, the Dirichlet data u_n and the Neumann data q_n can be found by solving

$$\mathsf{S}_0\mathsf{u}_n = \tilde{\mathsf{f}}_{N,n} - \mathsf{K}_0^\top\mathsf{V}_0^{-1}\tilde{\mathsf{f}}_{D,n} \tag{5.48}$$

and

$$\mathsf{q}_n = \mathsf{V}_0^{-1}\left(\tilde{\mathsf{f}}_{D,n} + \mathsf{K}_0\mathsf{u}_n\right) \tag{5.49}$$

for every time step $n = 0,\ldots,N$. In (5.48) and (5.49), the abbreviations $\tilde{\mathsf{f}}_{D,\cdot}$ and $\tilde{\mathsf{f}}_{N,\cdot}$ denote the complete right hand-side as it is defined in (5.45).

With the solver scheme above, the formulation of the symmetric Galerkin Boundary Element Method for time-dependent problems is completed. Nevertheless, the efficiency of the time-discretization algorithm can be improved in case of non-dissipative systems. Contrary to dissipative material models a non-dissipative material has no memory, i.e., there exists only a limited time-frame for which the information needs to be stored. In fact, the linear equations in (5.45) are obtained by resorting a system of lower triangular Toeplitz block matrices. For both material models the structure of these block matrix systems is depicted schematically in the Fig. 5.6. Due to causality the physical state at a distinct time can be influenced by preceding times only and is not affected by future times, i.e., until the compression wave has not arrived at a certain location all operators must be zero. Within the system matrices, this physical principle is reflected by the zero matrix blocks in their upper half. But in contrast to the dissipative model, the non-dissipative system assimilates no additional information when the shear wave has passed by, i.e., after a certain time $t_{\bar{n}}$ the operators must be zero again (cf. Fig. 5.6b). Therefore, the storage requirement of the original N system matrices can be reduced to an amount of only $\bar{n}$ matrices.

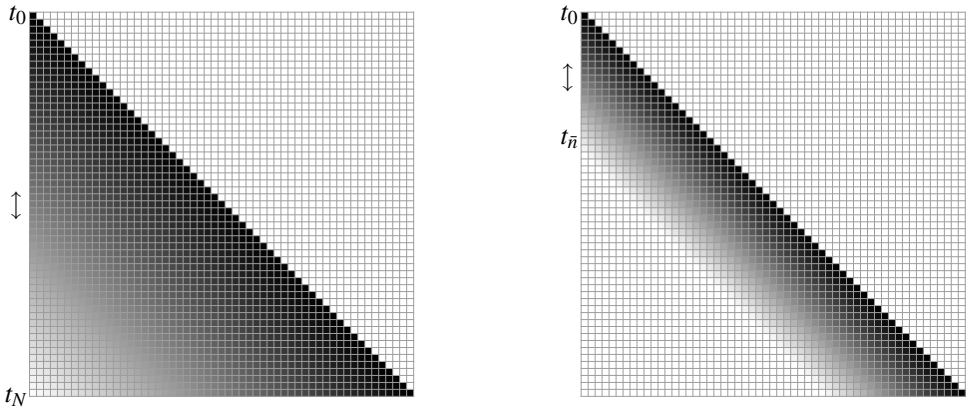

(a) Dissipative material (b) Non-dissipative material

Figure 5.6: Structure of the system matrices for different material models

Unfortunately, in contrast to the non-dissipative model, a dissipative material like, e.g., a viscoelastic material, features not the possibility of introducing an equivalent cutoff such that the complete range of time steps $0,\ldots,N$ is required (cf. Fig. 5.6a).

In the aforementioned space-time boundary integral equation methods the cutoff is a consequence of the analytical time-integration [80]. But here, one has to be content with an estimate for it [111] which is based on the asymptotic behavior of the integration weights

$$\omega_n \approx \frac{1}{n!}\left(\frac{r_{\max}}{c_2\Delta t}\right)^n \exp\left(-\tfrac{3}{2}\tfrac{r_{\max}}{c_2\Delta t}\right) .$$

In the above equation, $r_{\max}$ is the maximum distance in the discretized body, i.e., the largest distance the shear wave associated with the velocity c_2 has to travel. Moreover, for this estimate a BDF 2 as underlying multistep method is assumed. The use of other multistep methods will, of course, lead to other estimations. Hence, an upper limit $\bar{n}$ for

calculating the integration weights can be estimated so that for all $n > \bar{n}$ the integration weights can be neglected in relation to the weights $n < \bar{n}$. The use of a cutoff leads to a significant optimization due to the fact that it is dispensable to calculate and to store the system matrices for the time steps $t_k, k > \bar{n}$. So, instead of obtaining a system of lower triangular Toeplitz block matrices one ends up with a banded system (cf. Fig. 5.6b) just by replacing the sums in (5.45) and (5.46) by $\sum_{m=0}^{n-1}(\cdots) \rightarrow \sum_{m=\max(0,n-\bar{n})}^{n-1}(\cdots)$. A detailed computation scheme for this cutoff is given in the appendix A.3.

5.5 Semi-infinite domains

In section 3.4, the representation formulae's validity has been extended to unbounded domains and it has been stated that the boundary integral equations leave unchanged if certain far field conditions are assumed. Fortunately, due to the exact implication of the far field conditions within the underlying boundary integral equations the discretization scheme is not affected – at least for unbounded domains with bounded surface. For sure, this is one of the biggest advantages Boundary Element Methods have. But contrary to domains with bounded surface, there exist physical problems in which both the domain as well as the surface remain unbounded. And thus, the question arises how the discretization of an unbounded surface can be realized.

The problem is illustrated by means of the semi-infinite half-space being defined as

$$\begin{aligned}\Omega &:= \{\tilde{\mathbf{x}} \in \mathbb{R}^3 \colon \tilde{x}_3 < 0\} \\ \Gamma_\infty &= \{\mathbf{y} \in \mathbb{R}^3 \colon y_3 = 0\}\end{aligned}$$

where the boundary Γ_∞ depicts a surface with infinite extension. Typically, this kind of geometries occur in elasticity problems where the half-space is usually subjected to some stresses $\mathbf{g}$ on its surface. In the elastostatic case the according homogeneous boundary value problems reads as

$$\begin{aligned}(\mathcal{L}\mathbf{u})(\tilde{\mathbf{x}}) &= \mathbf{0} && \forall \tilde{\mathbf{x}} \in \Omega \\ \mathbf{t}(\mathbf{y}) &= \mathbf{g}(\mathbf{y}) && \forall \mathbf{y} \in \Gamma_\infty \\ \lim_{|\mathbf{x}|\to\infty} |\mathbf{x}|\mathbf{u}(\mathbf{x}) &= \mathbf{0} && \forall \mathbf{x} \in \overline{\Omega}\,.\end{aligned} \tag{5.50}$$

Hence, the bilinear form with respect to the Galerkin formulation follows to

$$\langle \widehat{\mathcal{D}}\mathbf{u}, \mathbf{v}\rangle_{\Gamma_\infty} = \langle (\tfrac{1}{2}\widehat{\mathcal{I}} - \widehat{\mathcal{K}}')\mathbf{g}, \mathbf{v}\rangle_{\Gamma_\infty}\,. \tag{5.51}$$

Equivalent, the boundary value problem in elastodynamics is given by

$$\begin{aligned}\left[\left(\mathcal{L} + \varrho_0 \frac{\partial^2}{\partial t^2}\right)\mathbf{u}\right](\tilde{\mathbf{x}}, t) &= \mathbf{0} && \forall (\tilde{\mathbf{x}}, t) \in \Omega \times (0,\infty) \\ \mathbf{t}(\mathbf{y}, t) &= \mathbf{g}(\mathbf{y}, t) && \forall (\mathbf{y}, t) \in \Gamma_\infty \times (0,\infty) \\ \mathbf{u}(\tilde{\mathbf{x}}, 0^+) &= \mathbf{0} && \forall \tilde{\mathbf{x}} \in \Omega \\ \dot{\mathbf{u}}(\tilde{\mathbf{x}}, 0^+) &= \mathbf{0} && \forall \tilde{\mathbf{x}} \in \Omega\end{aligned} \tag{5.52}$$

with its corresponding boundary integral representation

$$\langle \mathcal{D} * \mathbf{u}, \mathbf{v} \rangle_{\Gamma_\infty} = \langle (\tfrac{1}{2}\mathcal{I} - \mathcal{K}') * \mathbf{g}, \mathbf{v} \rangle_{\Gamma_\infty} \, . \tag{5.53}$$

Note that in the hyperbolic boundary value problem homogeneous initial conditions are prescribed such that the solution fulfills a radiation condition of the type (3.36) for every point $\mathbf{x} \in \overline{\Omega}$.

When considering the far field conditions above one specific feature attracts the attention. The far field conditions are not restricted to the domain Ω but also include the boundary Γ_∞. Probably, this fact affects the variational form's solvability. In contrast, the exterior problems stated in section 3.4 involve the far field conditions for the domain only.

With view to the discretization of the variational forms (5.51) and (5.53) the properties of the underlying hypersingular operators have to be recalled. Since a direct evaluation of the original hypersingularities is rather impossible, in chapter 4 a regularization process has been presented which transforms those hypersingular bilinear forms into weakly singular ones. The transformation of the hypersingularities is based on Stokes theorem and throughout the whole regularization process it has been assumed that the surface Γ is closed, i.e., $\partial\Gamma = \emptyset$. Here, the surface is obviously not closed but still unbounded. However, the radiation condition ensures that the kernel functions vanish in the limit $|\mathbf{x}| \to \infty$ for all points $\mathbf{x} \in \overline{\Omega}$. Hence, it can be assumed that the variational forms (5.51) and (5.53) hold also for the regularized hypersingular bilinear forms.

Unfortunately, the problems arise on the discrete level. There, it is a common practice to model just a truncated part of the infinite geometry, i.e., the boundary Γ_∞ is approximated by a 'sufficiently large enough' surface patch $\Gamma_h \subseteq \Gamma_\infty$. While this approximation works relatively adequate for discretization schemes which do not rely on a regularization based on Stokes theorem it will fail completely within the current setting. Here, the approximation Γ_h with its emerging truncation's borderline $\partial\Gamma_h$ would model a surface which is neither closed anymore nor can the integral kernels be assumed to vanish on $\partial\Gamma_h$. Therefore, it has to be ensured that the approximated surface is either closed or of infinite extent. While the former constraint is impossible to satisfy in case of the half-space, there exist approaches to overcome the latter constraint. Within the development of the Finite Element Method so-called *infinite elements* have gained some popularity [17] to abolish the method's restriction to bounded domains. In a certain sense the situation here is comparable. The present Boundary Element Method is restricted to bounded surfaces and the use of infinite elements is probably one possibility to get rid of this restriction.

There is another argument suggesting the use of infinite elements. According to the problem statements (5.50) and (5.52), respectively, the associated variational forms demand a discretization of the hypersingular operator. Thereby, a necessary condition for its application is the use of at least continuous test- and trial-functions. This condition is obviously violated for a truncated mesh with unknown Dirichlet data on the truncation's borderline. In this sense, infinite elements can be thought as a completion of the support for these data.

Figure 5.7a illustrates the discretization approach of an unbounded domain. Thereby, the boundary Γ_∞ is represented by the surface Γ_h which is the union of two sets of different geometrical elements

$$\Gamma_h = \bigcup_{j=1}^{J} \overline{\tau}_j \cup \bigcup_{\ell=1}^{L} \overline{\tau}_{\infty_\ell} \, .$$

Above, the J elements τ_j denote the standard (finite) boundary elements as they have been presented in section 5.1. But additionally, the boundary's far field is approximated by L infinite boundary elements whose configuration is depicted in Fig. 5.7b.

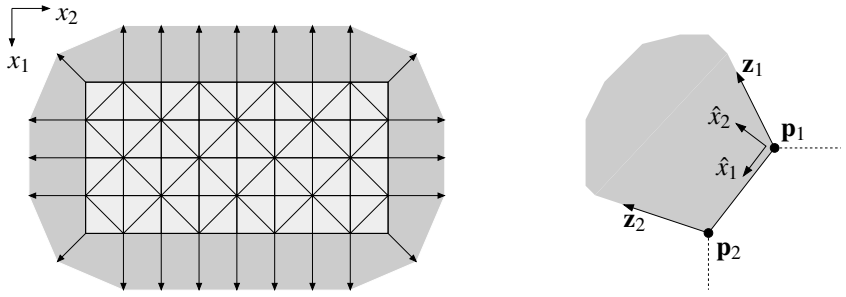

(a) Half-space with infinite elements (b) Infinite element

Figure 5.7: Discretized half-space and infinite mapping

The depicted infinite element is defined by two boundary nodes $\mathbf{p}_1$ and $\mathbf{p}_2$, and by two corresponding direction vectors $\mathbf{z}_1$ and $\mathbf{z}_2$, respectively. Analogous to the standard finite elements there exist a mapping $\chi_{\tau_\infty} \colon \hat{\tau}_\infty \to \tau_\infty$ from a reference element $\hat{\tau}_\infty$ to an infinite element τ_∞. In principle, there exist two classes of mappings for infinite elements [17]. One class are the so-called *decay function infinite elements* while the other class is usually denoted as *mapped infinite elements*. The fundamental difference between both types is the definition of the two-dimensional reference domain. The decay function infinite element depicts a very natural approach since there the reference domain is, equivalent to the image's τ_∞ domain, of infinite extent. Thus, the reference element is given by

$$\hat{\tau}_\infty^{dec} := \{(\hat{x}_1, \hat{x}_2) \in \mathbb{R}^2 \colon (\hat{x}_1, \hat{x}_2) \in [0,1] \times [0,\infty)\} \, .$$

Contrary, the mapped infinite element consists of a finite reference domain whose definition is strongly related to that of an quadrilateral element (cf. (5.3)). For a mapped infinite element it reads as

$$\hat{\tau}_\infty^{map} := \{(\hat{x}_1, \hat{x}_2) \in \mathbb{R}^2 \colon (\hat{x}_1, \hat{x}_2) \in [0,1] \times [0,1)\} \, . \tag{5.54}$$

Having a numerical integration scheme in mind the term decay function infinite element becomes clear. Obviously, the quadrature on semi-infinite intervals demand special decay weighting functions, usually in form of exponential functions. Then, the integrals of type $\int_0^\infty f(x) \exp(-x) \, \mathrm{d}x$ can be solved by using a *Gauss-Laguerre quadrature* [1]. For reasons that will become clear later this type of mapping is not used any further so that for more insight on this the reader is referred to the literature [17, 43]. Instead of the decay function

element the mapped infinite element will be used in the following. Thus, the reference element $\hat{\tau}_\infty$ has to be identified with $\hat{\tau}_\infty^{map}$. The mapped infinite element uses a singular mapping function. According to the element's configuration (Fig. 5.7b) this mapping is given by

$$\mathbf{x}_\infty = \chi_{\tau_\infty}(\hat{\mathbf{x}}) := \sum_{i=1}^{2} \varphi_i^1(\hat{x}_1)\mathbf{p}_i + \frac{\hat{x}_2}{1-\hat{x}_2}\alpha \sum_{i=1}^{2} \varphi_i^1(\hat{x}_1)\mathbf{z}_i\,, \qquad \alpha > 0\,. \tag{5.55}$$

In (5.55), the points $\mathbf{p}_i$ are the fixed vertex points of the infinite element as it is depicted in Fig. 5.7b and the $\mathbf{z}_i$ are the two corresponding directions. Restricting the nodes $\mathbf{p}_i$ to two points implicates a linear mapping in the element's finite extension. Thus, the infinite element can be referred to as *flat infinite element* which is somehow comparable to the flat elements of section 5.1. In principle, curved infinite elements are also possible but are omitted herein since the main goal is a sufficient representation of the half-space which is, finally, a flat geometry. The functions φ_i^1 denote the linear mapping functions which are simply

$$\boldsymbol{\varphi}^1(s) = \begin{bmatrix} 1-s \\ s \end{bmatrix} \qquad \forall s \in [0,1]\,.$$

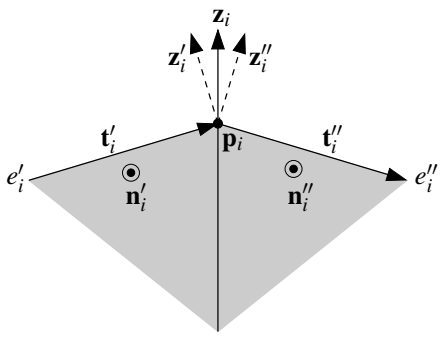

Figure 5.8: Construction of the direction vector $\mathbf{z}_i$

The directions $\mathbf{z}_i$ are determined by two edges e_i' and e_i'' which are associated to the corresponding node $\mathbf{p}_i$ (cf. Fig. 5.8). Let $\mathbf{t}_i'$ and $\mathbf{n}_i'$ be the tangent vector along the edge e_i' as well as the normal vector which is attached to the boundary element that particular edge e_i' belongs to. Then, a direction $\mathbf{z}_i'$ is given by

$$\mathbf{z}_i' := \frac{\bar{\mathbf{z}}_i'}{|\bar{\mathbf{z}}_i'|} \qquad \bar{\mathbf{z}}_i' := \mathbf{n}_i' \times \mathbf{t}_i'\,. \tag{5.56}$$

In the same manner, the vector $\mathbf{z}_i''$ connected to the second edge e_i'' can be deduced. Finally, the direction $\mathbf{z}_i$ is given by

$$\mathbf{z}_i := \frac{\bar{\mathbf{z}}_i}{|\bar{\mathbf{z}}_i|} \qquad \bar{\mathbf{z}}_i := \mathbf{z}_i' + \mathbf{z}_i'' \tag{5.57}$$

such that final directions $\mathbf{z}_i$ lie on a bisecting line between the edges e_i' and e_i''. Note that the directions $\mathbf{z}_i$ are normalized, i.e., $\langle \mathbf{z}_i, \mathbf{z}_i \rangle = 1$ holds, so that their total lengths are defined

by the scalar parameter α in (5.55). This parameter is equally chosen for the complete set of infinite elements.

This definition of the directions $\mathbf{z}_i$ is not mandatory. It is also common practice to choose the infinite directions with respect to some fixed point $\mathbf{c}$ somewhere *(usually the center)* within the discretized surface patch. Then, every direction is simply given by

$$\mathbf{z}_i = \frac{\bar{\mathbf{z}}_i}{|\bar{\mathbf{z}}_i|} \qquad \bar{\mathbf{z}}_i \coloneqq \mathbf{p}_i - \mathbf{c} \,. \tag{5.58}$$

While in the first method the directions are determined by the finite boundary elements at the truncation's borderline, in (5.58) the directions are constructed with the help of some point $\mathbf{c}$ which has to be prescribed by the user. Fig. 5.9 depicts the difference in the construction of $\mathbf{z}_i$ by these two methods schematically. In the next chapter both methods are compared numerically.

(a) Definition by finite elements (b) Definition by a point

Figure 5.9: Two methods to define the directions to infinity

Independent of the particular choice of the directions the singular mapping itself is actually given by the term $\hat{x}_2/(1-\hat{x}_2)$ which tends to infinity when $\hat{x}_2$ tends to 1. Therefore, in this limit the mapping (5.55) yields

$$\lim_{\substack{\hat{x}_2 \to 1 \\ \hat{x}_2 < 1}} |\chi_{\tau_\infty}(\hat{\mathbf{x}})| = \infty \,. \tag{5.59}$$

Now, with the mapping (5.55) a closer lock on the local representations of the integral kernels is necessary. Up to this point, the regular as well as the singular integrals converge. And this convergence must hold also for the infinite elements. However, due to the behavior (5.59) this convergence is not ensured. To investigate this more detailed the asymptotics of the mapping (5.55) must be given. Recalling the Jacobi matrix's definition

$$\mathbf{J}_{\tau_\infty}(\hat{\mathbf{x}}) = \begin{bmatrix} \frac{\partial \mathbf{x}_\infty}{\partial \hat{x}_1} & \frac{\partial \mathbf{x}_\infty}{\partial \hat{x}_2} \end{bmatrix} =: \begin{bmatrix} \mathbf{J}_1 & \mathbf{J}_2 \end{bmatrix}$$

one obtains that $\mathbf{J}_1$ and $\mathbf{J}_2$ behave like

$$\mathbf{J}_1 \in \mathcal{O}(|\hat{x}_2 - 1|^{-1}) \quad \text{and} \quad \mathbf{J}_2 \in \mathcal{O}(|\hat{x}_2 - 1|^{-2}) \,.$$

Hence, the associated Gram determinant's root becomes

$$\sqrt{g_{\tau_\infty}(\hat{\mathbf{x}})} = \sqrt{\det(\mathbf{J}_{\tau_\infty}(\hat{\mathbf{x}})^\top \mathbf{J}_{\tau_\infty}(\hat{\mathbf{x}}))} = \sqrt{\langle \mathbf{J}_1, \mathbf{J}_1 \rangle \langle \mathbf{J}_2, \mathbf{J}_2 \rangle - \langle \mathbf{J}_1, \mathbf{J}_2 \rangle^2} \in \mathcal{O}(|\hat{x}_2 - 1|^{-3}) \,.$$

Note that equivalent, the distance function (4.51) can be used also to express the asymptotic behavior. The distance $r(\mathbf{y},\mathbf{x}_\infty)$ is of order $\mathcal{O}(|\hat{x}_2-1|^{-1})$ such that vice versa the inverse $\hat{x}_2(r)\in\mathcal{O}(r^{-1})$ holds.

The only possibility of compensating this behavior, i.e., of ensuring the integrations' convergence, is an appropriate modeling of the trial- and test-functions. For this, the trial- and test-functions ψ and ϕ are assumed to behave like $\mathcal{O}(|\hat{x}_2-1|^n)$ with $n>0$. Now the question arises on how the exponent n has to be selected in order to make the integrations bounded. For reasons that will become immediately clear the answer to this question demands a separate treatment of the static and the dynamic problem.

Just for sake of simplicity the static problem is covered by means of the boundary value problem according to the Laplace equation. The regularized hypersingular operator is given in (4.27) and an integral entry $\mathsf{D}[m,\ell]$ reads as

$$\mathsf{D}[m,\ell]=\int\limits_{\operatorname{supp}(\phi_m)}\int\limits_{\operatorname{supp}(\psi_\ell)}\frac{\partial\phi_m(\mathbf{x})}{\partial\mathbf{S}(\partial_{\mathbf{x}},\mathbf{n}(\mathbf{x}))}\cdot\frac{\partial\psi_\ell(\mathbf{y})}{\partial\mathbf{S}(\partial_{\mathbf{y}},\mathbf{n}(\mathbf{y}))}U^L(\mathbf{y}-\mathbf{x})\,\mathrm{d}s_{\mathbf{y}}\,\mathrm{d}s_{\mathbf{x}}\,. \tag{5.60}$$

Using the local representation of the surface curl from (5.12) that integral reads in local coordinates as

$$\begin{aligned}\mathsf{D}[m,\ell]=\sum_{\tau_i\in\operatorname{supp}(\phi_m)}\sum_{\tau_j\in\operatorname{supp}(\psi_\ell)}\int\limits_{\hat{\tau}}\int\limits_{\hat{\tau}}\Big(\mathbf{J}_{\tau_i}(\hat{\mathbf{x}})\cdot\nabla^{\perp}_{\hat{\mathbf{x}}}\phi_{im}(\hat{\mathbf{x}})\Big)\cdot\\ \Big(\mathbf{J}_{\tau_j}(\hat{\mathbf{y}})\cdot\nabla^{\perp}_{\hat{\mathbf{y}}}\psi_{j\ell}(\hat{\mathbf{y}})\Big)\,U^L(\chi_{\tau_j}(\hat{\mathbf{y}})-\chi_{\tau_i}(\hat{\mathbf{x}}))\,\mathrm{d}\hat{\mathbf{y}}\,\mathrm{d}\hat{\mathbf{x}}\,.\end{aligned} \tag{5.61}$$

Above, the fundamental solution is of order $U^L=\mathcal{O}(r^{-1})=\mathcal{O}(|\hat{x}_2-1|^1)$. Now, supposing that at least one of the involved elements is of infinite type the application of the partial derivatives $\partial/\partial\hat{x}_i$ to a function $\varphi(\hat{\mathbf{x}})\in\mathcal{O}(|\hat{x}_2-1|^n)$ yields

$$\frac{\partial}{\partial\hat{x}_1}\varphi(\hat{\mathbf{x}})\in\mathcal{O}(|\hat{x}_2-1|^n)\quad\text{and}\quad\frac{\partial}{\partial\hat{x}_2}\varphi(\hat{\mathbf{x}})\in\mathcal{O}(|\hat{x}_2-1|^{n-1})\,.$$

Taking the behavior of the Jacobi matrix into account yields the asymptotics of the surface curl

$$\mathbf{J}_\infty(\hat{\mathbf{x}})\cdot\nabla^{\perp}_{\hat{\mathbf{x}}}\varphi(\hat{\mathbf{x}})\in\mathcal{O}(|\hat{x}_2-1|^{n-2})\,. \tag{5.62}$$

Obviously an order of $n\geq 2$ needs to be chosen to ensure the integral's (5.60) convergence. Clearly, the regularized hypersingular bilinear form according to elastostatics (4.96) exhibit the same characteristics as the hypersingular form concerning the Laplace equation. Thus, the exponent n can be chosen of the same size, i.e., $n\geq 2$ holds for every single static problem.

Now, turning over to the dynamic problems the difference compared to the static problems becomes obvious. At first, according to (5.61) it can be considered that the surface curls features the nice property of canceling out the Gram determinant. While in the static case the integral kernels involve the surface curls only this holds not for dynamic problems.

As before, exemplary the regularized hypersingular bilinear form corresponding to the Helmholtz equation is given

$$\begin{aligned}\mathsf{D}_k[m,\ell] = \sum_{\tau_i\in\mathrm{supp}(\phi_m)}\sum_{\tau_j\in\mathrm{supp}(\psi_\ell)} \Bigg\{ & \int_{\hat\tau}\int_{\hat\tau} \left(\mathbf{J}_{\tau_i}(\hat{\mathbf{x}})\cdot\nabla^{\perp}_{\hat{\mathbf{x}}}\phi^{(n)}_{im}(\hat{\mathbf{x}})\right)\cdot\left(\mathbf{J}_{\tau_j}(\hat{\mathbf{y}})\cdot\nabla^{\perp}_{\hat{\mathbf{y}}}\psi^{(n)}_{j\ell}(\hat{\mathbf{y}})\right) U^W_k(\chi_{\tau_j}(\hat{\mathbf{y}})-\chi_{\tau_i}(\hat{\mathbf{x}}))\,\mathrm{d}\hat{\mathbf{y}}\,\mathrm{d}\hat{\mathbf{x}} \\ & +k^2\int_{\hat\tau}\int_{\hat\tau}\phi^{(n)}_{im}(\hat{\mathbf{x}})\psi^{(n)}_{j\ell}(\hat{\mathbf{y}})U^W_k(\chi_{\tau_j}(\hat{\mathbf{y}})-\chi_{\tau_i}(\hat{\mathbf{x}}))\mathbf{n}(\hat{\mathbf{x}})\cdot\mathbf{n}(\hat{\mathbf{y}})\sqrt{g_{\tau_{\mathbf{y}}}(\hat{\mathbf{y}})}\sqrt{g_{\tau_{\mathbf{x}}}(\hat{\mathbf{x}})}\,\mathrm{d}\hat{\mathbf{y}}\,\mathrm{d}\hat{\mathbf{x}}\Bigg\}\,.\end{aligned}$$

Of course, the exponent n equals 1 if the considered boundary element is of finite extent. The additional term within the regularized hypersingular bilinear form is actually of the general form (5.20) by what the necessary exponent's order increases by one. Hence, $n \geq 3$ has to be demanded in the time-dependent case.

The fact that the exponents n vary for different types of analysis is, of course, a blemish at this point since it contradicts in a way the far field conditions given in section 3.4. Additionally, the choice of the exponent n is justified only in a mathematical manner but it does not coincide with the decay behavior that is predicted by physical principles.

Nevertheless, continuing the deduction of the infinite elements it remains to formulate explicit expressions for the test- and trial-functions on these elements. Due to the prescribed homogeneous far field conditions it is sufficient to recall the approximation for the Dirichlet data from (5.15). For a linear approximation these data were given by

$$u^1_h(\mathbf{x}) = \sum_{\ell=1}^{M} u_\ell\psi^1_\ell(\mathbf{x})\,.$$

As long as the support $\mathrm{supp}(\psi_\ell)$ contains finite boundary elements only the functions are chosen corresponding to those being given in section 5.2. But if it is connected to an infinite element the functions $\psi^{(n)}_\ell$ are given by the composition

$$\psi^{(n)}_\ell(\mathbf{x}) = \chi_{\tau_{\infty_j}}\circ\psi^{(n)}_{i(\ell)}(\hat{\mathbf{x}}) \quad \text{with} \quad \tau_{\infty_j}\in\mathrm{supp}(\psi_\ell)$$

and with $\psi^{(n)}_{i(\ell)}(\hat{\mathbf{x}})$ being the appropriate component $i(\ell)$ of the vector function

$$\boldsymbol{\psi}^{(n)}(\hat{\mathbf{x}}) := \begin{bmatrix}1-\hat{x}_1\\ \hat{x}_1\end{bmatrix}(1-\hat{x}_2)^n\,. \tag{5.63}$$

Beside this definition there exist another possible choice for the test- and trial-functions which, somehow, takes the truncation's borderline into account. Thereby, the definition is based on the ratio between the distances $\hat{r}$ from a point $\mathbf{x}_\infty\in\tau_\infty$ and the projection from this point to the truncation's borderline with its distance $\hat{r}_0$. For both $\hat{r}$ as well as $\hat{r}_0$ the

distances are measured with respect to a fixed origin **o**. Thus, the corresponding test- and trial-functions are given by

$$\boldsymbol{\psi}^{(n)}(\hat{\mathbf{x}}) := \begin{bmatrix} 1-\hat{x}_1 \\ \hat{x}_1 \end{bmatrix} \left(\frac{\hat{r}(\hat{x}_1,\hat{x}_2)}{\hat{r}_0(\hat{x}_1)} \right)^n = \begin{bmatrix} 1-\hat{x}_1 \\ \hat{x}_1 \end{bmatrix} \left(\frac{r(\mathbf{o}, \chi_{\tau_\infty}(\begin{bmatrix} \hat{x}_1 \\ \hat{x}_2 \end{bmatrix}))}{r(\mathbf{o}, \chi_{\tau_\infty}(\begin{bmatrix} \hat{x}_1 \\ 0 \end{bmatrix}))} \right)^n . \tag{5.64}$$

Fig. 5.10 depicts the construction of this type of functions more clearly. In chapter 6, numerical studies compare the approach (5.63) with the approach (5.64).

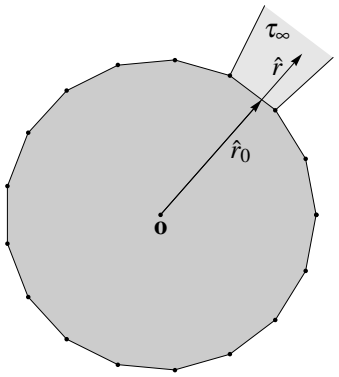

Figure 5.10: Test- and trial-functions of order $\left(\frac{\hat{r}}{\hat{r}_0}\right)^n$

With the definition of the trial- and test-functions the Boundary Element formulation for open domains is completed. As mentioned at the beginning of this section the infinite elements can be interpreted as the support's completion on the borderline of a finite surface patch. And probably this is the best way to handle them. Contrary to the infinite elements being used in the Finite Element Method the infinite boundary elements are something like the geometrical condensation of the infinite domain, i.e., they serve as geometrical mapping only. In Finite Element Methods the infinite elements have to incorporate the far field conditions. Since these conditions differ for static and frequency domain problems special infinite elements need to be developed for the different types of analysis [17]. Here, the fulfillment of the far field conditions is left to the respective fundamental solutions such that there is no need for the development of *static infinite boundary elements* or *time-harmonic infinite boundary elements*. Except the different required order of the trial- and test-functions the infinite element stated here is used for every physical problem.

However, one important task has been suppressed completely so far. This concerns the singular integrations which actually demand a comment. In fact, the singular integrations are the main reason for using the mapped infinite elements instead of the decay function infinite elements. As mentioned earlier the infinite reference element from (5.54) is similar to the quadrilateral element's definition from (5.3). The only difference between both reference elements consists in the singularity for $\hat{x}_2 \to \infty$ in case of the infinite boundary element. On the other hand this singularity is removable by an appropriate choice of the trial- and test-functions. This motivates the direct use of the singular quadrature rules

developed by Sauter [107] also for this element type. Unfortunately, Sauter's proof of the singular quadrature rules does not include this type of element since it does not feature the regularity requirements which are demanded there. Nevertheless, those formulae are also applied to the infinite elements without changes. This is due to the fact that the geometrical singularity is removed by an appropriate choice of the trial- and test-functions. Thus, the remaining kernels feature only a singularity for $|\mathbf{y}-\mathbf{x}| \to 0$, just as it is the case for the finite boundary elements.

In the following, the use of the singular quadrature is exemplary illustrated by means of a function $f_{h_\mathbf{x},h_\mathbf{y}}$. This kernel function serves as a two-dimensional counterpart to the three-dimensional case. Of course, the intention is to substantiate the former motivation of using the special singular quadrature. In Fig. 5.11, two infinite element combinations are depicted. The first combination is made up of one infinite element in conjunction with a finite element (cf. Fig. 5.11a) while the latter depicts two infinite elements (cf. Fig. 5.11b).

(a) Inf. element connected to fin. element

(b) Inf. element connected to inf. element

Figure 5.11: Singular integration on infinite elements: Two-dimensional examples

In both cases the point $\mathbf{p}_0 = [0\ 0]^\top$ lies at the origin. The finite element $\tau_\mathbf{x}$ contains a second point $\mathbf{p}_1 = [1\ 0]^\top$. Thus, its mapping is given by $\chi_{\tau_\mathbf{x}}(\hat{x}_1) = (1-\hat{x}_1)\mathbf{p}_0 + \hat{x}_1\mathbf{p}_1 = [\hat{x}_1\ 0]^\top$ and the according Gram determinant follows to $g_{\tau_\mathbf{x}}(\hat{x}_1) = |\partial\chi_{\tau_\mathbf{x}}(\hat{x}_1)/\partial\hat{x}_1| = 1$. The infinite element $\tau_{\infty,\mathbf{y}}$ is determined by the direction vector $\mathbf{u}_\mathbf{y} = [-1\ 0]^\top$. Thus, the infinite mapping reads simply as $\chi_{\tau_{\infty,\mathbf{y}}}(\hat{x}_2) = \hat{x}_2/(1-\hat{x}_2)\mathbf{u}_\mathbf{y} = [-\hat{x}_2/(1-\hat{x}_2)\ 0]^\top$. The Gram determinant of this mapping is given by $g_{\tau_{\infty,\mathbf{y}}}(\hat{x}_2) = 1/(1-\hat{x}_2)^2$ such that a trial-function $\varphi(\hat{x}_2) = (1-\hat{x}_2)^2$ is introduced in order to compensate the geometrical singularity. With this data and an additional test-function $\psi(\hat{x}_1) = 1-\hat{x}_1$ the kernel function can be defined as

$$f_{1,\infty}(\hat{x}_1,\hat{x}_2) \coloneqq \frac{1}{|\chi_{\tau_{\infty,\mathbf{y}}}(\hat{x}_2) - \chi_{\tau_\mathbf{x}}(\hat{x}_1)|} g_{\tau_{\infty,\mathbf{y}}}(\hat{x}_2) g_{\tau_\mathbf{x}}(\hat{x}_1) \varphi(\hat{x}_2)\psi(\hat{x}_1)$$
$$= \frac{(1-\hat{x}_1)(1-\hat{x}_2)}{\hat{x}_1 - \hat{x}_1\hat{x}_2 + \hat{x}_2} \qquad \forall (\hat{x}_1,\hat{x}_2) \in [0,1]^2 \,.$$

The second kernel $f_{\infty,\infty}$ can be constructed equivalent. By using the direction vector $\mathbf{u}_\mathbf{x} = [1\ 0]^\top$ the mapping is $\chi_{\tau_{\infty,\mathbf{x}}}(\hat{x}_1) = [\hat{x}_1/(1-\hat{x}_1)\ 0]^\top$. Again, choosing appropriate functions φ and ψ for the compensation of the singularities induced by the Gram determinants

$g_{\tau_{\infty,\mathbf{x}}}$ and $g_{\tau_{\infty,\mathbf{y}}}$ the kernel $f_{\infty,\infty}$ reads as

$$f_{\infty,\infty}(\hat{x}_1,\hat{x}_2) := \frac{(1-\hat{x}_1)(1-\hat{x}_2)}{\hat{x}_1 - 2\hat{x}_1\hat{x}_2 + \hat{x}_2} \qquad \forall\,(\hat{x}_1,\hat{x}_2) \in [0,1]^2\,.$$

Both kernel functions exhibit a singularity at the origin but, additionally, the denominator of $f_{\infty,\infty}$ becomes zero for $(\hat{x}_1,\hat{x}_2) = (1,1)$. On the other hand, the numerator tends also to zero in this case and the singularity at this point is removable. Now, performing the integrations yields

$$I[f_{1,\infty}] = \int_0^1 \int_0^1 f_{1,\infty}(\hat{x}_1,\hat{x}_2)\,\mathrm{d}\hat{x}_1\,\mathrm{d}\hat{x}_2 = \frac{\pi^2}{6} - 1$$
$$I[f_{\infty,\infty}] = \int_0^1 \int_0^1 f_{\infty,\infty}(\hat{x}_1,\hat{x}_2)\,\mathrm{d}\hat{x}_1\,\mathrm{d}\hat{x}_2 = \frac{\pi^2}{8} - \frac{1}{2}\,.$$

Plugging the transformation (5.27) with $\mathbf{T}_i$ from (5.25) and (5.26) into the kernels above yields

$$\begin{aligned} f^{reg}_{1,\infty}(\xi_1,\xi_2) &= \frac{(1-\xi_1)(1-\xi_1\xi_2)}{1+(1-\xi_1)\xi_2} + \frac{(1-\xi_1)(1-\xi_1(1-\xi_2))}{2-\xi_1(1-\xi_2)-\xi_2} \quad \forall\,(\xi_1,\xi_2) \in [0,1]^2 \\ f^{reg}_{\infty,\infty}(\xi_1,\xi_2) &= \frac{(1-\xi_1)(1-\xi_1\xi_2)}{1+(1-2\xi_1)\xi_2} + \frac{(1-\xi_1)(1-\xi_1(1-\xi_2))}{2-2\xi_1(1-\xi_2)-\xi_2} \quad \forall\,(\xi_1,\xi_2) \in [0,1]^2\,. \end{aligned} \tag{5.65}$$

Clearly, the regularization ensures the regularity at the point $(\xi_1,\xi_2) \in [0,1]^2$ and a numerical test for the integration of the first kernel $f_{1,\infty}$ confirms the assumption of using a regularization also for the infinite elements.

$\sqrt{n}$	$E_n^{std}[f_{1,\infty}]$	$E_n^{reg}[f_{1,\infty}]$
1	6.4e-01	6.4e-01
2	3.1e-01	4.5e-02
3	1.2e-01	9.1e-04
4	6.4e-02	2.0e-05
5	3.9e-02	4.6e-07
⋮	⋮	⋮
30	9.2e-04	5.6e-16

Table 5.3: Non-regularized and regularized Quadrature

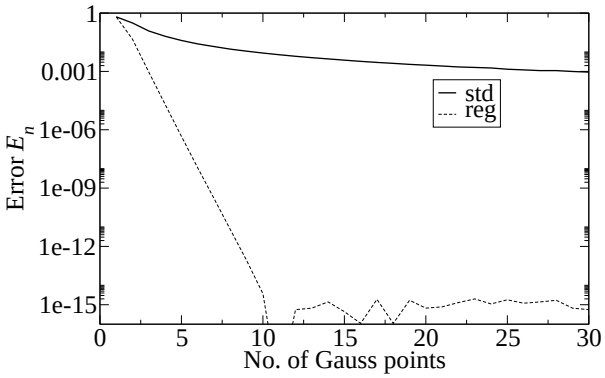

Figure 5.12: Error plot for $E_n[f_{1,\infty}]$

In Tab. 5.3 and Fig. 5.12, the results for this numerical test are shown and one obtains a much higher convergence rate for the regularized kernels than for the original ones.

Unfortunately, the numerical results for the second kernel function $f_{\infty,\infty}$ are less compelling. These results are depicted in Tab. 5.4 and Fig. 5.13 and they clearly feature the quadrature's weakness when infinite elements are involved.

$\sqrt{n}$	$E_n^{std}[f_{\infty,\infty}]$	$E_n^{reg}[f_{\infty,\infty}]$
1	7.3e-01	7.3e-01
2	2.3e-01	1.6e-02
3	1.1e-01	1.5e-03
4	6.0e-02	2.8e-04
5	3.8e-02	7.1e-05
⋮	⋮	⋮
30	9.2e-04	1.1e-09

Table 5.4: Non-regularized and regularized Quadrature

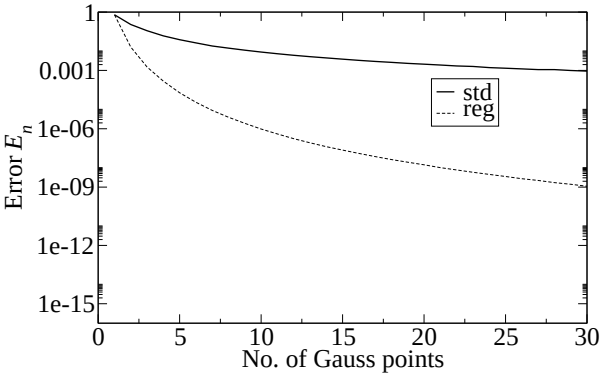

Figure 5.13: Error plot for $E_n[f_{\infty,\infty}]$

In fact, the regularization is designed to remove a singularity at a distinct point under the assumption that the singularity function is well-defined elsewhere. Contrary, the examples stated here show that although the singularity at the distinct point is removed the convergence rate might decrease. This is due to the removable singularities at the endpoints of the infinite elements' local intervals. Those removable singularities occur also in the transformed kernel (cf. (5.65)). Of course, the regularity of such a function is of a lower order than a finite boundary element's one.

Nevertheless, since no special quadrature rules are available for infinite elements so far, and since the results at least for this example are acceptable the rules of Sauter [37, 106, 107] are applied also to this type of element.

6 NUMERICAL RESULTS

In this chapter, the previously introduced Symmetric Galerkin Boundary Element Method is applied to some numerical examples. For verification purposes, this chapter deals with examples which are comparable to analytical solutions.

Primarily, the necessary implementation details should be given. Unless mentioned otherwise the integrations are performed by using the number of Gauss points as they are stated in Tab. 5.1. In case of infinite elements, nine Gauss points per direction are used for every infinite-infinite or infinite-finite boundary element combination, respectively. Moreover, all time-domain computations are done by help of the FFTW routine [40] and the direct solver routines are implemented using the standard LAPACK library [4]. Also, all given condition numbers are LAPACK implementations. They are given as estimates in the L_1-norm and their computation is based on the algorithm of Higham [61].

This thesis comprises more than one material model and it features static analysis as well as time-harmonic and time-dependent analysis. Additionally, the Boundary Element discretization allows the use of different types of elements with trial and test-functions varying in their polynomial degrees. Thus, the organization of this demands some preliminary definitions and abbreviations. Concerning the discretization, the boundary element mesh for bounded surfaces is constructed by using triangles or quadrilaterals (or a mixture of them). Table 6.1 depicts the abbreviations for the used combinations of boundary elements and the appropriate choice of approximation orders concerning the Dirichlet and Neumann data.

		Approximation of Dirichlet/Neumann data	
		(bi-)linear/constant	quadratic/(bi-)linear
Element type	Triangle	**TLC**	**TQL**
	Quadrilateral	**QLC**	**QQL**

Table 6.1: Shortcuts for element- and approximation-type combinations

Thereby, the abbreviations are constructed by three letters. The first letter denotes the underlying element type while the both remaining letters represent the type of approximation being used for the boundary data. Moreover, the geometry approximation is directly linked to the discretization of the Dirichlet data. For instance, the abbreviation *TQL* denotes a curved 6-point triangle with a quadratic distribution of the Dirichlet data and a piecewise linear approximation of the Neumann data.

The material data corresponding to acoustics is given in Tab. 6.2a. The material data for the considered elastic solids are depicted in Tab. 6.2b. For the verification of the numerical

results against 1-dimensional solutions the material data of *Steel* are slightly manipulated. The respective Lamé constants are given such that they correspond to an artificial Poisson's ratio of $\nu = 0$.

Material name	ϱ_0 $[\mathrm{kg/m^3}]$	K $[\mathrm{N/m^2}]$	c $[\mathrm{m/s}]$
Air	1.2	$1.4153 \cdot 10^5$	343.4

(a) Acoustic fluid

Material name	ϱ_0 $[\mathrm{kg/m^3}]$	λ $[\mathrm{N/m^2}]$	μ $[\mathrm{N/m^2}]$	c_1 $[\mathrm{m/s}]$	c_2 $[\mathrm{m/s}]$
Soil	1884	$1.3627 \cdot 10^8$	$1.3627 \cdot 10^8$	465.8	268.9
Steel	7850	0	$1.055 \cdot 10^{11}$	5184.5	3666.0

(b) Elastic solids

Material name	ϱ_0 $[\mathrm{kg/m^3}]$	K $[\mathrm{N/m^2}]$	μ $[\mathrm{N/m^2}]$	α $[-]$	q $[1/\mathrm{s}]$	p $[1/\mathrm{s}]$
PMMA	1184	$1.24 \cdot 10^9$	$1.86 \cdot 10^9$	1.0	0.0023	0.002

(c) Viscoelastic solid: The viscoelastic material parameters are equal for the deviatoric and the hydrostatic parts, i.e., $\alpha = \alpha_D = \alpha_H$, $q = q_D = q_H$, and $p = p_D = p_H$

Table 6.2: Material data

The viscoelastic material data are given for a perspex (PMMA) strip and is based on measurements being done at the Technical University Braunschweig, Germany. The data have been primarily used in the monograph of Schanz [111][1] and are reused here. As for the elastic material, for the comparison with some semi-analytical solutions it is necessary to force the Poisson's ratio to vanish. Thus, the bulk modulus K is artificially given by $K = 2/3\mu$. Moreover, the viscoelastic material parameters in Tab. 6.2c are obtained by data fitting techniques. Those parameters are not fixed throughout all numerical experiments. In order to illustrate their influence on the material's behavior they are modified in certain examples. However, if the viscoelastic material parameters are not explicitly mentioned, they always correspond to those from 6.2c.

A typical geometry which will be used several times in this chapter is that of a simple cuboid. The cuboid has a constant cross-sectional area of $A = 1\mathrm{m} \times 1\mathrm{m}$ and an adjustable

[1] Unfortunately, in that book a typo occurs since the Young's modulus is given as $E = 3.72 \cdot 10^{-9}\,\mathrm{N/m^2}$. Of course, this is wrong. The correct Young's modulus is $E = 3.72 \cdot 10^{9}\,\mathrm{N/m^2}$.

length of ℓm. Its domain and closure are given by

$$\begin{aligned}\Omega^{(\ell)} &:= \left\{\mathbf{x} \in \mathbb{R}^3 \colon \mathbf{x} \in (0,\ell) \times (-\tfrac{1}{2},\tfrac{1}{2})^2\right\} \\ \overline{\Omega}^{(\ell)} &:= \left\{\mathbf{x} \in \mathbb{R}^3 \colon \mathbf{x} \in [0,\ell] \times [-\tfrac{1}{2},\tfrac{1}{2}]^2\right\} .\end{aligned} \tag{6.1}$$

Then, the boundary is $\Gamma^{(\ell)} = \overline{\Omega}^{(\ell)} \setminus \Omega^{(\ell)}$. Moreover, a mixed boundary value problem is stated where the Dirichlet boundary and the Neumann boundary are defined by the two sets

$$\begin{aligned}\Gamma_D &:= \left\{\mathbf{x} \in \mathbb{R}^3 \colon x_1 \equiv 0 \wedge (x_2, x_3) \in [-\tfrac{1}{2},\tfrac{1}{2}]^2\right\} \\ \Gamma_N^{(\ell)} &= \Gamma^{(\ell)} \setminus \Gamma_D .\end{aligned} \tag{6.2}$$

Figure 6.1 depicts the geometry of a column of 3m length.

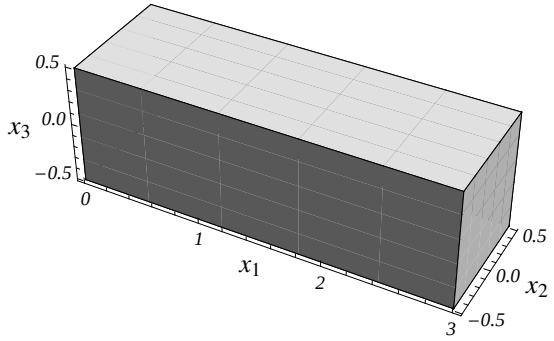

Figure 6.1: Geometry and coordinate system for $\ell = 3$

6.1 The conditioning of the system matrices in static analysis

At first, the behavior of the system matrices' condition numbers for different meshes is investigated. The knowledge of the systems' conditioning is very important with respect to the solution process since it represents the impact of round-off errors in the final solution. The conditioning of a matrix $\mathsf{A} \in \mathbb{R}^{N \times N}$ is measured by the condition number

$$\operatorname{cond}_p(\mathsf{A}) := \|\mathsf{A}\|_p \, \|\mathsf{A}^{-1}\|_p .$$

Above, $\|\mathsf{A}\|_p$ denotes the p-norm of the matrix A. The p-norm of a matrix A is defined via the induced vector norm

$$\|\mathsf{A}\|_p := \sup_{\substack{\mathsf{x} \in \mathbb{R}^N \\ \mathsf{x} \neq \mathsf{0}}} \frac{\|\mathsf{A}\mathsf{x}\|_p}{\|\mathsf{x}\|_p} .$$

The p-norm of some real vector y is given by

$$\|\mathsf{y}\|_p = \left(\sum_{i=1}^{N} |y_i|^p \right)^{1/p}, \quad p \in \mathbb{R}, p \geq 1 .$$

The mathematical theory of boundary integral equations prescribes that the condition numbers according to the Laplace equation behave like

$$\mathrm{cond}_2(\mathsf{V}_L) \leq C_L^V \frac{1}{h_G} \tag{6.3}$$

for the single layer operator and like

$$\mathrm{cond}_2(\mathsf{D}_L) \leq C_L^D \frac{1}{h_G} \tag{6.4}$$

for the hypersingular operator, respectively [107]. In (6.3) and (6.4), C_L^V and C_L^D denote two real and positive constants. In the following, these two predictions are verified by a numerical example. For this, a column of 3m is considered matching the definitions from (6.1) and (6.2). It is discretized uniformly by using the element combinations stated in Tab. 6.1. Thereby, the four different combinations TLC, TQL, QLC, and QQL are used in conjunction with five different mesh sizes. These discretizations with the corresponding number of degrees of freedom are stated in Tab. 6.3.

Approx. order	Mesh sizes	No. of Elems.		No. of degrees of freedom			
		Tria	Quad	N_D		N_N	
				Tria	Quad	Tria	Quad
LC	1.41	28	14	2	1	12	12
	0.71	112	56	8	4	49	49
	0.35	448	224	32	16	201	201
	0.18	1792	896	128	64	817	817
	0.07	11200	5600	800	400	5161	5161
QL	1.41	28	14	6	4	49	49
	0.71	112	56	24	16	201	201
	0.35	448	224	96	64	817	817
	0.18	1792	896	384	256	3297	3297
	0.07	11200	5600	2400	1600	20721	20721

Table 6.3: Discretizations of the 3m-column for the acoustic fluid: In elasticity the degrees of freedom have to be multiplied by the factor three

In Tab. 6.3, the quantities N_D and N_N denote the number of degrees of freedom on the Dirichlet boundary Γ_D and on the Neumann boundary Γ_N, respectively. Moreover, from Tab. 6.3 the relation between the number of degrees of freedoms and the mesh-sizes become obvious. A bi-sectioning of the mesh size results in a quadruplication of the number of degrees of freedom N. Thus, the relations (6.3) and (6.4) can equivalently be described as

$$\mathrm{cond}_2(\mathsf{V}_L) \leq C_L^V \sqrt{N_D} \quad \text{and} \quad \mathrm{cond}_2(\mathsf{D}_L) \leq C_L^D \sqrt{N_N}\,. \tag{6.5}$$

Although the predictions for the condition numbers are usually given in the 2-norm it is more efficient to use the 1-norm within the implementation. Since both norms are equivalent a change of the norm, finally, result in different constants C_L^V and C_L^D only, but the asymptotics will be left unchanged. Here, those constants are of minor importance so that it is absolutely justified to use the 1-norm in the following. Additionally, the considered mixed boundary value problem demands the matrices' inversions according to the single layer operator from (5.16) and of the Schur complement from (5.19). Hence, the figures 6.2 and 6.3 depicts the condition numbers according to these two matrices.

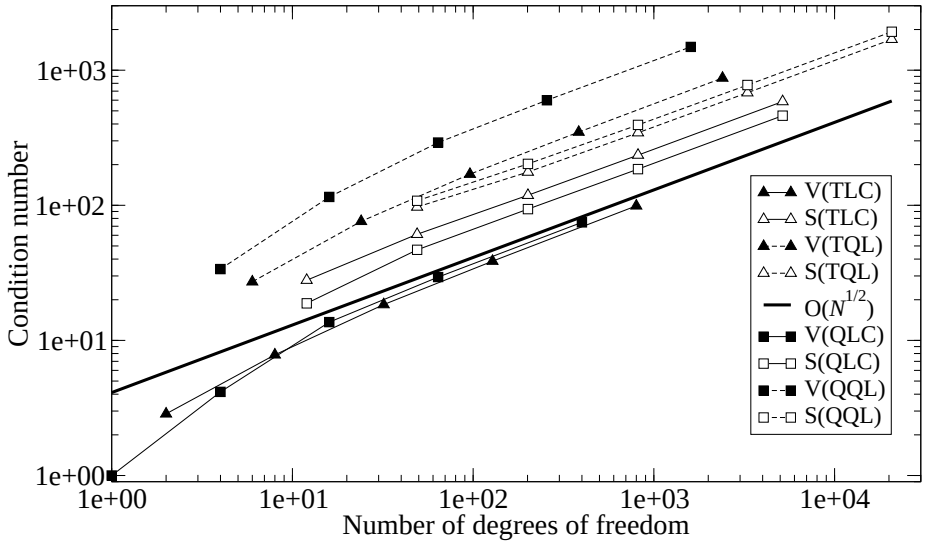

Figure 6.2: Condition numbers for the Laplace equation

The Figure 6.2 shows the results obtained by using the symmetric Galerkin Boundary Element Method for the Laplace equation in a double logarithmic scale. The continuous line without markers represents the asymptotics from (6.5). The lines with filled markers corresponds to single layer matrices whereas the lines with hollow markers depicts the condition numbers according to the Schur complements. Moreover, continuous lines with markers are based on the linear/constant approximation of Dirichlet- and Neumann-data while the dashed ones depict the quadratic/linear approximations. Finally, the markers' shapes correspond to the underlying boundary elements, i.e., triangular markers stand for triangles and quadrilateral markers identify the quadrilateral boundary element mesh.

The numerical tests approve the theoretical predictions completely. While for a lower number of degrees of freedom the conditioning is slightly better than the estimate for larger numbers of degrees of freedoms the condition numbers are straight lines parallel to the prediction line. Moreover, for the same number of degrees of freedom the quadratic/linear approximations reveal larger condition numbers than their linear/constant counterparts which induces that such systems with higher-order polynomials are in general more ill-conditioned than the systems with lower polynomial degrees. Additionally, in case of the quadratic/linear approximations the single layer operator matrices display higher condition

numbers than the corresponding Schur complement matrices. This is somehow surprising since in all other cases the single layer matrices are better conditioned than the respective Schur complements.

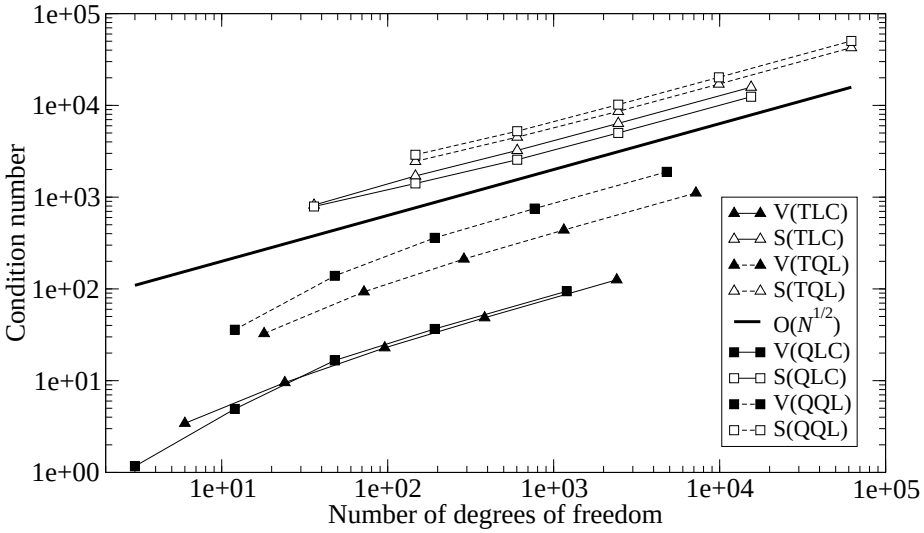

Figure 6.3: Condition numbers for elastostatics

In Figure 6.3, the observations made for the Boundary Element discretization for the Laplace equation continue. Again, the condition numbers lie parallel to the prediction line. But in contrast to the Laplace equation the single layer operator matrices reveal better condition numbers than their respective Schur complements for every single approximation type.

6.2 Cantilever beam

After the more abstract investigation of the condition numbers a more engineering example will be stated. Here, an elastostatic 3-dimensional cantilever beam of 5 m length is modeled. As before, a mixed boundary value problem is considered which means that the beam is fixed at the location $x_1 = 0\,\mathrm{m}$ and that it is loaded with a constant traction of $\mathbf{g} = [0, 0, -1]^\top \,\mathrm{N/m^2}$ at the opposite location $x_1 = 5\,\mathrm{m}$. The remaining surfaces are traction free. With the domain and boundary definitions from (6.1) and (6.2) the boundary value problem reads as

$$\begin{aligned} \left(-(\lambda+\mu)\nabla\nabla\cdot\mathbf{u} - \mu\Delta\mathbf{u}\right)(\tilde{\mathbf{x}}) &= \mathbf{0} && \forall \tilde{\mathbf{x}} \in \Omega^{(5)} \\ \mathbf{u}(\mathbf{y}) &= \mathbf{0} && \forall \mathbf{y} \in \Gamma_D \\ \mathbf{t}(\mathbf{y}) &= \tilde{\mathbf{g}}(\mathbf{y}) && \forall \mathbf{y} \in \Gamma_N^{(5)} \,. \end{aligned} \tag{6.6}$$

Above, the prescribed tractions $\tilde{\mathbf{g}}$ are given such that

$$\tilde{\mathbf{g}}(\mathbf{y}) := \begin{cases} \mathbf{g} & \forall \mathbf{y} \in \Gamma_N^{(5)} \wedge y_1 = 5 \\ \mathbf{0} & \forall \mathbf{y} \in \Gamma_N^{(5)} \wedge y_1 \neq 5 \end{cases}$$

holds. The material parameters λ and μ are that of steel from Tab. 6.2b. Unfortunately, there exist no analytical solutions to this problem. Hence, one has to be content with some convergence investigations. If there exist a solution, then for finer grids the numerical solutions must converge to the real solution. For these convergence analysis four different uniform triangular meshes as well as four corresponding uniform quadrilateral meshes are considered. The triangular meshes are depicted in Fig. 6.4 and they consist of 44 boundary elements with a mesh size of $h_G = \sqrt{2}\,\mathrm{m}$, 176 elements with $h_G = 1/\sqrt{2}\,\mathrm{m}$, 704 elements with $h_G = 1/\sqrt{8}\,\mathrm{m}$, and 4400 elements with $h_G = 1/5\sqrt{2}\,\mathrm{m}$, respectively. The quadrilateral meshes hold the same mesh sizes but, of course, they feature only half of the number of elements, i.e., those meshes consist of 22, 88, 352, and 2200 boundary elements.

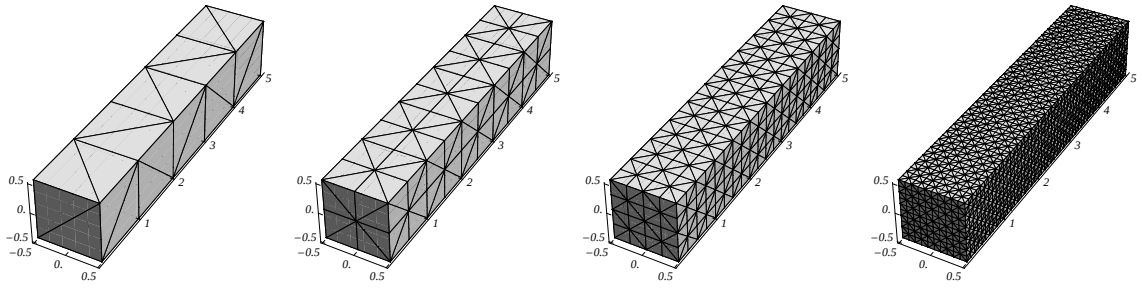

(a) 44 Elements (b) 176 Elements (c) 704 Elements (d) 4400 Elements

Figure 6.4: Triangular discretizations of the cantilever beam

The Figure 6.5 presents the vertical deflection $u_3([x_1, 1/2, 0]^\top)$ of the cantilever beam on the line $0\,\mathrm{m} \leq x_1 \leq 5\,\mathrm{m}$ for the triangular meshes with linear/constant approximations for the Dirichlet- and Neumann-data. The solution approves clearly the assumption that the finer discretizations yield better results than the coarser ones. While the result varies strongly for the coarsest mesh and the next level mesh being made up of 176 elements, the differences between the 176-element mesh and the 704-element mesh are less distinctive. Finally, the variations in the result between that mesh and the finest mesh are barely visible which induces that the final state has been almost reached. Hence, at least for this case the Boundary Element Method converges. Next, doing the same for the remaining element/approximation combinations TQL, QLC, and QQL equivalent graphs like that one in Fig. 6.5 would be obtained. But in that cases the results converge much more faster to the final state and the differences between them become practically invisible.

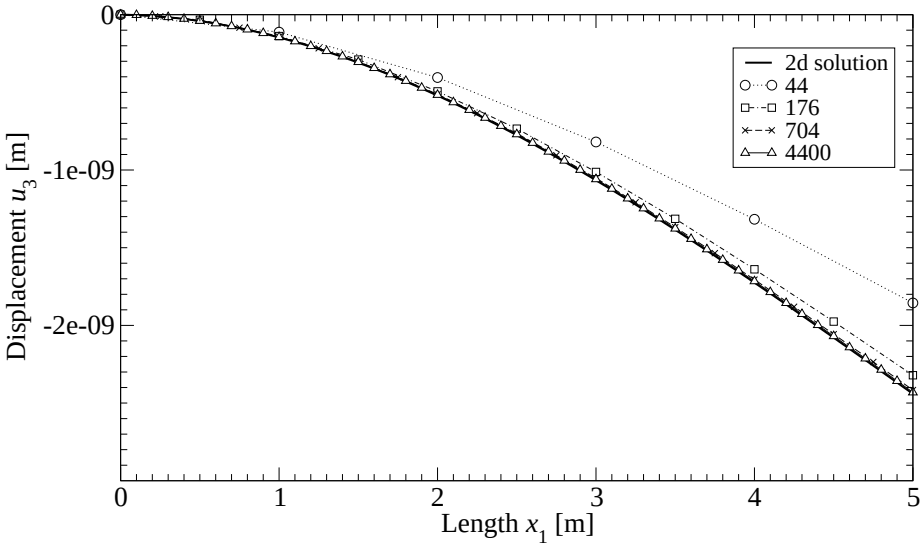

Figure 6.5: Deflection $u_3([x_1, 1/2, 0]^\top)$ of the cantilever beam (TLC combination)

6.2.1 Airy stress functions

However, to display the convergence rate graphically the solutions are compared to a 2-dimensional solution for the cantilever. Naturally, this analytical solution reflects not the present, quite complex 3-dimensional state but its use is more convenient than an application of 1-dimensional solutions like, e.g., that of Timoshenko's beam [124]. In Fig. 6.5, the 2-dimensional solution for the cantilever is already incorporated and the differences between the result obtained for the finest mesh and that solution are quite dispensable. In the following, this 2-dimensional solution should be derived briefly. The detailed derivation of it may be found, e.g., in the textbook of Szabó [123] where a solution is obtained by making use of the Airy stress functions $F = F(x_1, x_3)$. The Airy stress functions can be used only under the assumption of plane strain, i.e., the considered body exhibits no normal- and no shear-stresses in a certain direction. Here, it is assumed that there are no shear- and no normal stresses in x_2-direction. Now, the Airy stress functions are defined such that

$$\sigma_{11}(\mathbf{x}) = \frac{\partial^2 F}{\partial x_3^2}, \qquad \sigma_{33}(\mathbf{x}) = \frac{\partial^2 F}{\partial x_1^2}, \qquad \sigma_{13}(\mathbf{x}) = \sigma_{31}(\mathbf{x}) = -\frac{\partial^2 F}{\partial x_1 \partial x_3} \tag{6.7}$$

holds. Since F depends only on x_1 and x_3 all derivatives with respect to x_2 vanish and the resulting stress tensor $\boldsymbol{\sigma}(\mathbf{x})$ represents the plain strain state. Next, taking the compatibility condition (2.21) into account and expressing the strains via the stresses one obtains, finally, the expression

$$\Delta(\sigma_{11} + \sigma_{33}) = 0\,. \tag{6.8}$$

Note that the Eqn. (6.8) represents only one component of the resulting fourth order tensor in (2.21). Moreover, the plain stress state is just an approximation of the real physical state

since it injures the compatibility condition. However, inserting (6.7) into (6.8) yields the Bi-Laplace equation

$$\Delta^2 F = 0\,. \tag{6.9}$$

Thus, the strain stress problem is reduced to the solution of a *bipotential equation* which, naturally, has an infinite number of solutions.

To construct an approximate solution for the problem (6.6) the cantilever is loaded by a single force $\mathbf{P} = [0\,,0\,,P_3]^\top$ at the free end $x_1 = 5\,\mathrm{m}$ (see Fig. 6.6a). Then, the induced shear stresses are assumed to be parabolic over the cantilever's height and constant in its length direction. Additionally, the normal stresses are assumed to be linear distributed over the cantilever's height (see Fig. 6.6b).

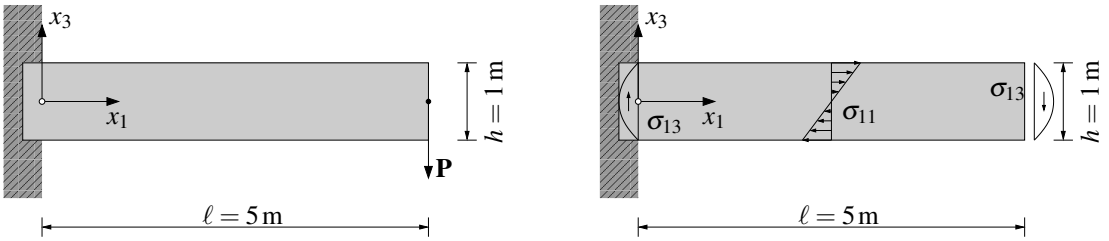

(a) Shear force loading

(b) Assumed stress distribution

Figure 6.6: Cantilever beam

The ansatz

$$F(x_1,x_3) = A(\ell - x_1)x_3^3 + Bx_1x_3 \tag{6.10}$$

with the two real constants $A,B \in \mathbb{R}$ suffices those assumptions and, simultaneously, solves the differential equation (6.9). To determine the two constants A and B one starts with the constraint that the surfaces feature no shear stresses. This yields

$$\sigma_{13}(x_1,x_3 = \pm\tfrac{h}{2}) = -\left.\frac{\partial^2 F}{\partial x_1 \partial x_3}\right|_{x_3=\pm\frac{h}{2}} = \frac{3}{4}Ah^2 - B = 0\,.$$

A second constraint is obtained at the free end. There, the surface integral over the shear stresses has to match the force P_3. With the cantilever's thickness b and with $A = {}^{4B}/_{3h^2}$ the integral yields the constant B

$$P_3 = \int_{-h/2}^{+h/2} \sigma_{13} b \,\mathrm{d}x_3 = -\frac{2}{3}Bhb \qquad \Longrightarrow \qquad B = -\frac{3}{2}\frac{P_3}{hb}\,.$$

Hence, the stresses read as

$$\sigma_{11}(\mathbf{x}) = -\frac{12P_3}{h^3 b}(\ell - x_1)x_3\,, \quad \sigma_{33}(\mathbf{x}) = 0\,, \quad \sigma_{13}(\mathbf{x}) = \frac{1}{2}\frac{12P_3}{h^3 b}\left[\left(\frac{h}{2}\right)^2 - x_3^2\right]\,. \tag{6.11}$$

By help of Hooke's law (2.27) the strain tensor's components ε_{11} and ε_3 can be deduced

$$\varepsilon_{11} = \frac{\partial u_1}{\partial x_1} = \frac{\lambda+\mu}{\mu\,(3\lambda+2\mu)}\sigma_{11}$$
$$\varepsilon_{33} = \frac{\partial u_3}{\partial x_3} = -\frac{\lambda}{2\mu\,(3\lambda+2\mu)}\sigma_{11}\,.$$

From these equations and with the additional equation $\sigma_{13} = \mu\left(\frac{\partial u_1}{\partial x_3} + \frac{\partial u_3}{\partial x_1}\right)$ the displacement field can be reconstructed. Using the boundary conditions

$$u_i(x_1 = 0, x_3 = 0) = 0\,, \quad i = 1,3 \qquad \text{and} \qquad \left.\frac{\partial u_1}{\partial x_3}\right|_{x_1=0,x_3=0} = 0 \tag{6.12}$$

the vertical displacement u_3 is finally obtained

$$u_3(x_1,x_3) = \frac{1}{2}\frac{P_3}{h^3 b\mu\,(3\lambda+2\mu)}\Big[4(\lambda+\mu)\,(3\ell-x_1)x_1^2 + 6\lambda\,(\ell-x_1)x_3^2 + 3(3\lambda+2\mu)h^2x_1\Big]\,. \tag{6.13}$$

The displacements above represents the 2-dimensional comparative solution which has been already used within Fig. 6.5 and which will be used in the following convergence examinations. It is important to mention that the boundary conditions (6.12) are prescribed point-wise. Therefore, they fail the much more complex boundary conditions at the fixed end where, in fact, $u_1(x_1 = 0, x_3) = u_3(x_1 = 0, x_3) = 0$ is demanded for all $-h/2 \le x_3 \le +h/2$. These boundary conditions cannot be satisfied with the rather simple function (6.10).

Note, that the use of the Airy stress functions is exceptional advantageous because of a second reason which consist in the knowledge of the stresses within the cantilever. Of course, the term *stress function* is not chosen arbitrary such that the title already induces this matter of fact. As mentioned earlier the Boundary Element Method is a well-known method for the approximation of the interior stress tensor field. Hence, the expressions (6.11) are useful for convergence analysis concerning the interior stress evaluation. The subsection 6.2.3 is dedicated to this topic.

6.2.2 Convergence examinations

Returning to the actual cantilever-problem (6.6), for the measurement of the convergence a residual function $\chi(x_1)$ is defined

$$\chi^{\Xi}_{h_G}(x_1) := \left|\frac{u^{\Xi}_{3,h_G}(x_1) - u_3(x_1)}{u_3(x_1)}\right|\,. \tag{6.14}$$

Above, u^{Ξ}_{3,h_G} denotes the third component of the numerical solution $\mathbf{u}^{\Xi}_{h_G}(\mathbf{x}^\star)$ evaluated for all points $\mathbf{x}^\star = [x_1\,,\tfrac{1}{2}\,,0]^\top$ while u_3 is the 2-dimensional solution (6.13) evaluated at the points $0 \leq x_1 \leq 5$ and $x_3 = -1/2$. The superscript Ξ denotes the element/approximation combination from Tab. 6.1. Note that the function (6.14) is not an error function in the way that it vanishes in the limit such that $\lim_{h_G \to 0} \chi^{\Xi}_{h_G} = 0$ holds. From the preceding chapter it is known that the function (6.13) does not satisfy the boundary conditions at the clamping. Moreover, shear stresses at the free end feature the parabolic distribution only if the force is induced in this way. Within the problem statement (6.6) this is not the case. The tractions are distributed constant at the free end. Hence, one can assume some variations at the clamping as well as at the free end. Nevertheless, in the limit $h_G \to 0$ the function $\chi^{\Xi}_{h_G}$ has to meet a certain function $\overline{\chi}$ which represents a fixed residuum between the 2-dimensional function and the 3-dimensional state.

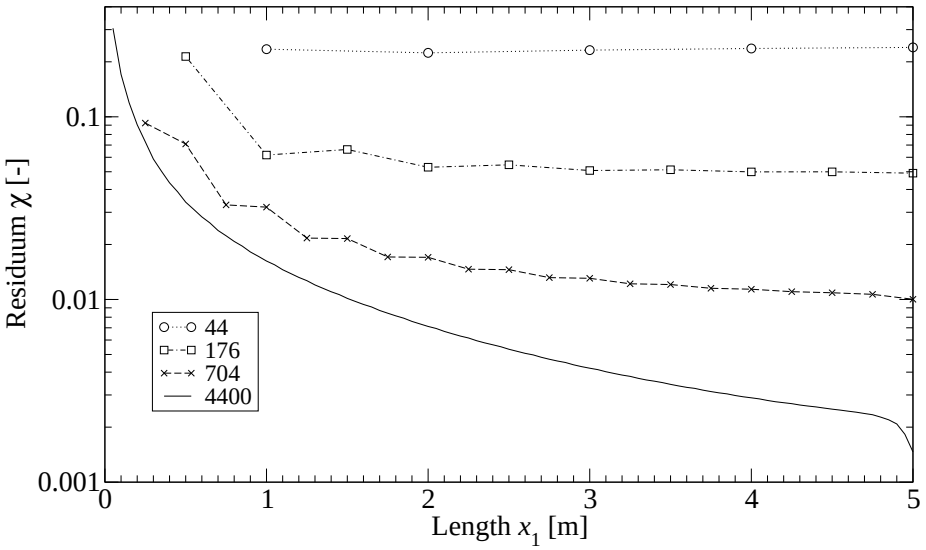

Figure 6.7: Residual function $\chi^{\mathrm{TLC}}_{h_G}$

The Figures 6.7–6.10 depict the various functions $\chi^{\Xi}_{h_G}$ for $\Xi = \mathrm{TLC}, \mathrm{TQL}, \mathrm{QLC}, \mathrm{QQL}$ and the different discretizations h_G corresponding to Fig. 6.4 in a logarithmic scale. A look on these plots reveals some commonnesses between all four graphs. At first, they seem to converge to some characteristic curve $\overline{\chi}$ and, except the coarsest QLC discretization, they converge to this curve from above. The second observation is important since it confirms the theoretical convergence behavior of the Galerkin method.

The graph 6.7 is just another representation of the results illustrated in Fig. 6.5. Again, one can clearly distinguish between the different meshes. While the coarsest mesh of 44 triangular elements obeys a constant variation of about 20% with respect to the comparative solution the three remaining discretizations feature larger variations at the fixed end and minor differences at the free end compared to the analytical solution (6.13).

In case of the triangular discretizations with quadratic approximations the observations continue. But in contrast to the constant approximations in Figure 6.7 the residual func-

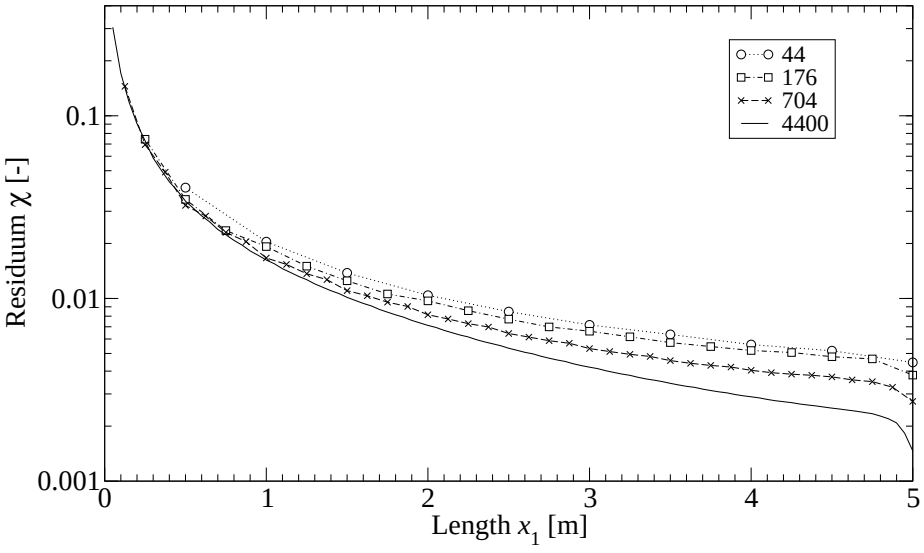

Figure 6.8: Residual function $\chi_{h_G}^{\mathrm{TQL}}$

tions $\chi_{h_G}^{\mathrm{TQL}}$ are not as scattered as before. Obviously, the convergence rate is more convenient for higher polynomial degrees than for linear/constant approximations. Of course, this conclusion is not astonishing since higher order polynomials approximate curved deflections better than linear polynomials.

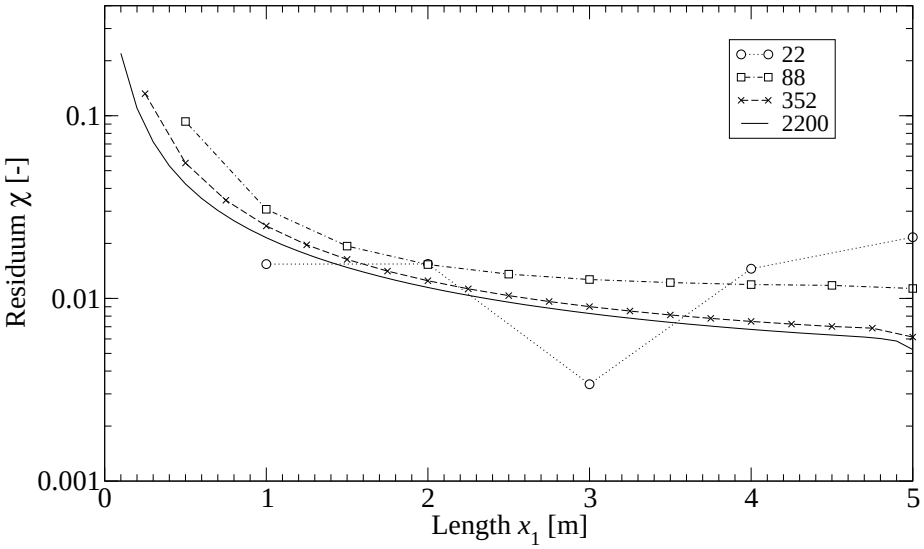

Figure 6.9: Residual function $\chi_{h_G}^{\mathrm{QLC}}$

Concerning the quadrilateral discretizations the corresponding numerical results obey better convergence rates compared to the respective triangular meshes. Except for the rather crude discretization of 22 quadrilateral boundary elements the numerical results in case of the bilinear/constant approximation are, again, converging to some characteristic curve $\overline{\chi}$

(see Fig. 6.9).

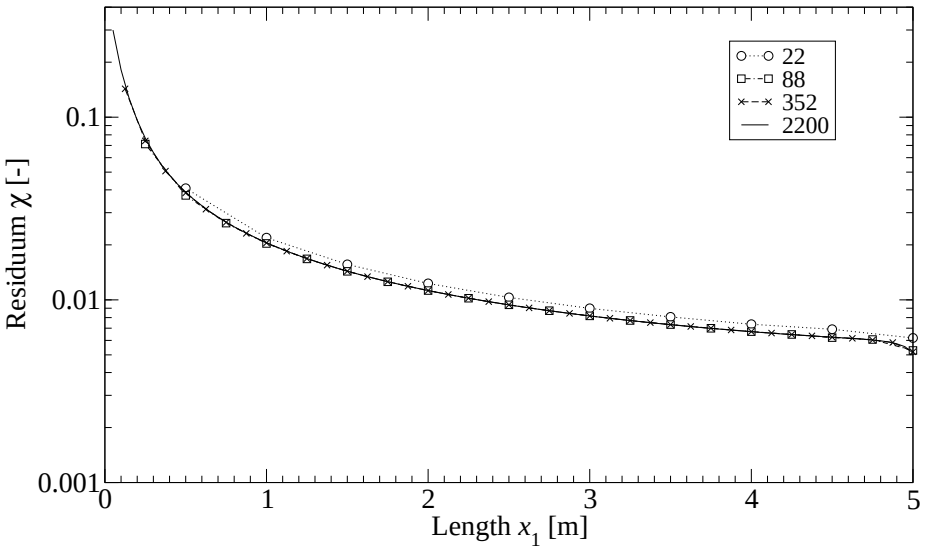

Figure 6.10: Residual function $\chi_{h_G}^{\mathrm{QQL}}$

Finally, the QQL discretizations of the cantilever feature the lowest variations. Except for the coarsest mesh differences between the numerical results for the remaining meshes are hardly measurable. Thus, at the end one can state that, already for relatively coarse discretizations, the quadrilateral elements with quadratic/linear test- and trial-functions for the Dirichlet- and Neumann data yield excellent results. In contrast, the TLC discretizations demand relative fine discretizations to obtain similar results which is due to the fact that the underlying polynomials do not feature any bilinear or quadratic terms.

6.2.3 Stress evaluation

One of the main benefits of the Boundary Element Method compared to several other numerical methods like, e.g, displacement based Finite Element Methods is the proper evaluation of the dual variables. Thus, bearing the cantilever as an elastic solid in mind, the Boundary Element Method for this case is supposed to evaluate the surface tractions as well as the interior stresses with an adequate accuracy. Therefore, the numerical results for the interior stresses should be compared to the analytical 2-dimensional solutions (6.11). From the preceding subsection it is known that the numerical results and its analytic comparative differ at the clamping. Therefore, the interior stress field must be evaluated far enough from the cantilever's fixed end. Here, the set Υ of discrete points is chosen in such a way that all points lie on a line parallel to the x_3-axis which crosses the boundary $\Gamma^{(5)}$ at the center of the upper and lower boundary planes at $[x_1, x_2, -\frac{1}{2}]$ and $[x_1, x_2, \frac{1}{2}]$, respectively. Then, for the calculation of the stress tensor field the representation formula

$$\boldsymbol{\sigma}(\tilde{\mathbf{x}}) = (\widetilde{\mathcal{S}}_1 \mathbf{t}_\Gamma)(\tilde{\mathbf{x}}) - (\widetilde{\mathcal{S}}_2 \mathbf{u}_\Gamma)(\tilde{\mathbf{x}}) \qquad \forall \tilde{\mathbf{x}} \in \Upsilon \subset \Omega^{(5)} \tag{6.15}$$

is evaluated with Υ being defined as

$$\Upsilon := \{\tilde{\mathbf{x}} \in \mathbb{R}^3 \colon (\tilde{x}_1, \tilde{x}_2) = (\tfrac{5}{2}, 0) \wedge \tilde{x}_3 = \tfrac{i}{40} - \tfrac{1}{2}, \forall\, i \in \mathbb{N} \wedge 1 \leq i \leq 39\} \,.$$

Note that the formula (6.15) is the static counterpart of (3.41) and that $\boldsymbol{\sigma}$ can only be obtained by a posterior calculation since the knowledge of the complete Cauchy data $[\mathbf{u}_\Gamma, \mathbf{t}_\Gamma]$ are required.

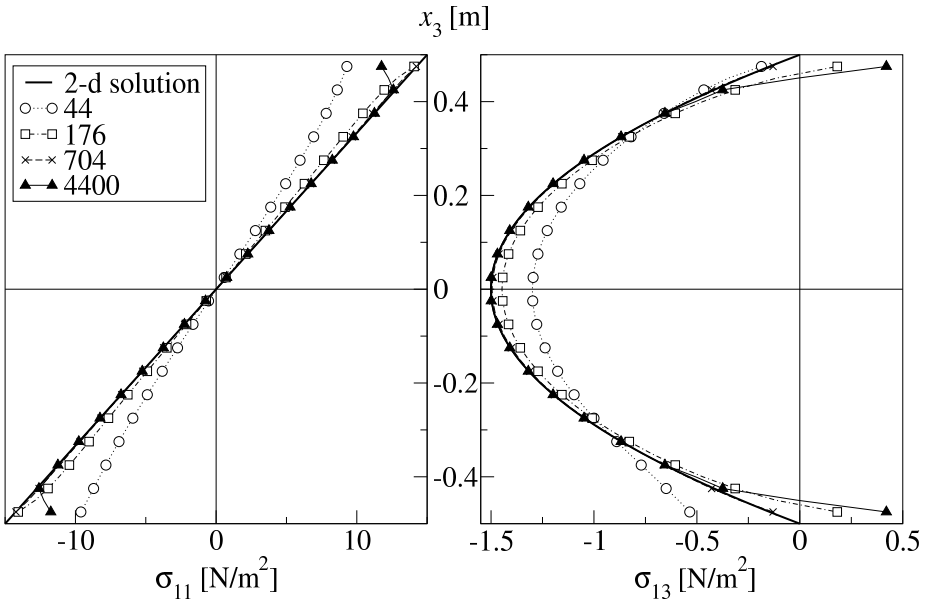

Figure 6.11: Interior stresses for the TLC combination

The Figures 6.11– 6.14 depict the normal stresses $\sigma_{11}(\tilde{\mathbf{x}})$ as well as the shear stresses $\sigma_{13}(\tilde{\mathbf{x}})$ side by side. Thereby, the vertical axes denote the x_3 coordinate while the corresponding stresses are plotted horizontally. Again, every single illustration depicts a certain element/approximation with the same set of discretizations as before.

Clearly, the numerical results show an exceptional agreement with respect to the comparative solutions (6.11). Even the TLC-elements, which are known to approximate the displacements field with an considerable error, behave more or less convincingly (see Fig. 6.11). There, already the relatively coarse discretization of 176 elements yields an adequate result. Nevertheless, it has to be mentioned that there are some mavericks in the boundary's neighborhood. Especially the triangular discretizations in Fig. 6.11 and Fig. 6.12 reveal some rather crude results nearby the boundary. Unfortunately, these numerical errors are partially more obvious for the finer grids than for the coarser discretizations which, somehow, contradicts the expected convergence behavior of the method. On the other hand the integrals in (6.15) become *almost singular*, i.e., quasi-singular, in the vicinity of the boundary. Naturally, the sufficient numerical evaluation of those integrals becomes more conspicuous in these cases such that the respective results cannot be assumed to be overwhelming.

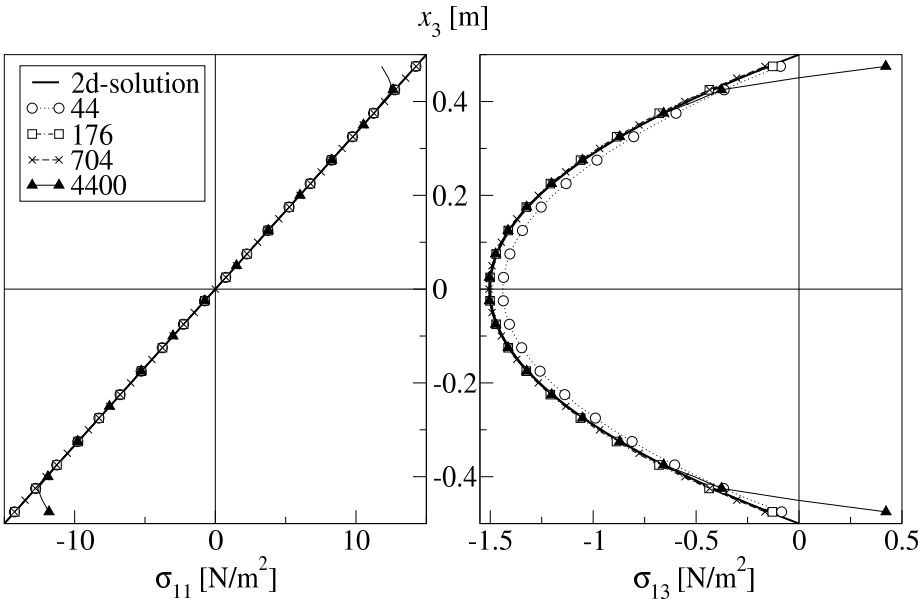

Figure 6.12: Interior stresses for the TQL combination

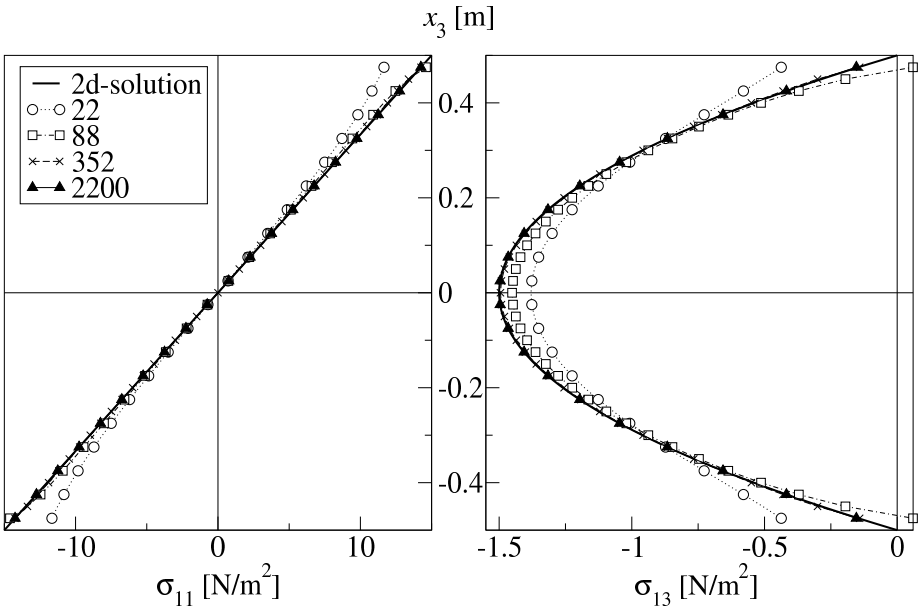

Figure 6.13: Interior stresses for the QLC combination

The numerical errors for the quadrilateral discretizations in Fig. 6.13 and Fig. 6.14 are almost not noteworthy. But it is worth to mention that those discretizations exhibit the typical convergence behavior, i.e., the results' quality increases with decreasing mesh sizes. Analogous to the displacement solution, there the QQL elements yield by far the best results. In Figure 6.14, the stresses are depicted only for the interval $0 \leq x_3 \leq 1/2$ and, except for the coarsest mesh, the numerical results are hardly distinguishable from the 2-dimensional solution.

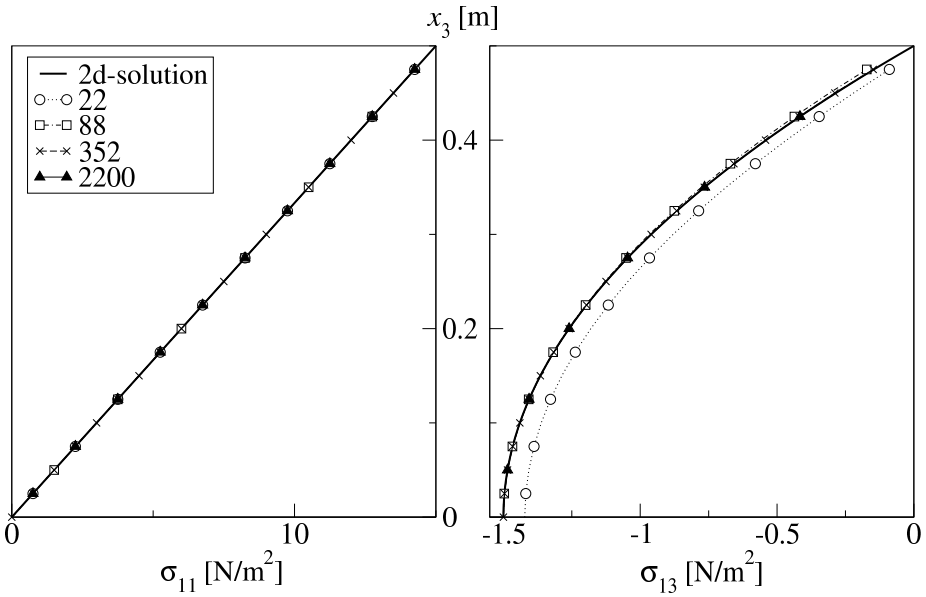

Figure 6.14: Interior stresses for the QQL combination

Finally, the stress evaluation can be regarded as being of the same quality as the displacement solution. This fact makes the Boundary Element method very competitive in cases where the numerical solution of the dual data demands a high precision.

6.3 The conditioning of the system matrices in dynamic analysis

Before any time domain solutions are presented, first, the same investigations concerning the conditioning of the system matrices as in section 6.1 are performed. There, the quintessence was the system matrices' behavior of order $\mathcal{O}(h^{-1})$, or, equivalent, of order $\mathcal{O}(\sqrt{N})$ if it is expressed via the number of degrees of freedom N. Moreover, the general behavior was independent of the element/approximation combination, i.e., the choice of the element type as well as the choice of the approximation order did not influence the system matrices' behavior considerably. Therefore, within this section the numerical examples are restricted to the TLC-elements and the aim is to focus on the influences of the time discretization. First, for an adequate comparison the dimensionless parameter

$$\beta := \frac{c\Delta t}{h} \tag{6.16}$$

is introduced which is commonly referred to as *Courant-Friedrichs-Lewy-Number* (CFL number) [31]. This number connects the time-grid size Δt with the spatial discretization h via the wave velocity c. According to the underlying material model this wave velocity has to be either identified with the acoustic fluid's wave velocity from (2.10) or, respectively, with the compressional wave speed from (2.33) in case of an elastic solid. For viscoelastic materials this number is chosen to meet the initial wave velocity of the compressional wave (2.60). The Convolution Quadrature Method demands an equidistant subdivision of the time interval into constant time step sizes Δt. Obviously, this time-uniformity is not portable to the spatial discretization. In general, a boundary element mesh consists of different sized elements such that h is chosen to be the mean size of the triangulation G, i.e., $h = \text{mean}_{\tau_i \in G}(h_i)$. Usually the CFL number is chosen such that $\beta < 1$ holds. Physically, this means that the waves pass not one complete element's length within one time step. Again, the computations are performed on the geometry of a 3m column corresponding to (6.1) with the Dirichlet- and Neumann-boundary definitions taken from (6.2). Moreover, the material data in case of the acoustic fluid as well as in case of the elastodynamic solid are that of Tab. 6.2.

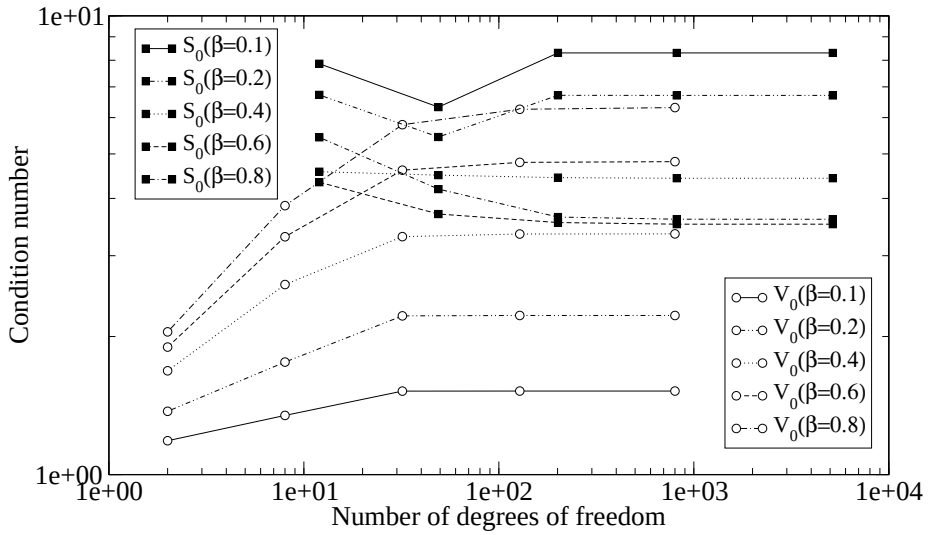

Figure 6.15: Condition numbers for the wave equation

The system of linear equations (5.45) demands the decomposition of the system matrices according to the first time step only. Hence, the Figures 6.15 and 6.16 depict the condition numbers for various CFL numbers of the single layer operator V_0 and of the Schur complement S_0 from (5.47). Analogous to section 6.1 the condition numbers are plotted against the number of degrees of freedom which correspond to the TLC-elements from Tab. 6.3.

In case of the acoustic fluid the condition numbers' behavior as it is shown in Fig. 6.15 has nothing in common with its static counterpart, the Laplace equation (see Fig. 6.2). Here, the condition numbers are extraordinary small and they seem to keep constant with an increasing number of degrees of freedoms, i.e., a dependency in form of $\mathcal{O}(\sqrt{N})$ cannot

be detected. Additionally, the condition numbers are just slightly affected by different CFL numbers. With an increasing CFL number also the condition numbers for the single layer operator increase. The situation changes for the Schur complement system. There, the condition numbers decrease with an increasing CFL number. However, for both types of matrices the system is extremely well conditioned since all condition numbers are lower than 10 up to 10^4 degrees of freedom and within a range of $0.1 \leq \beta \leq 0.8$ for the CFL number.

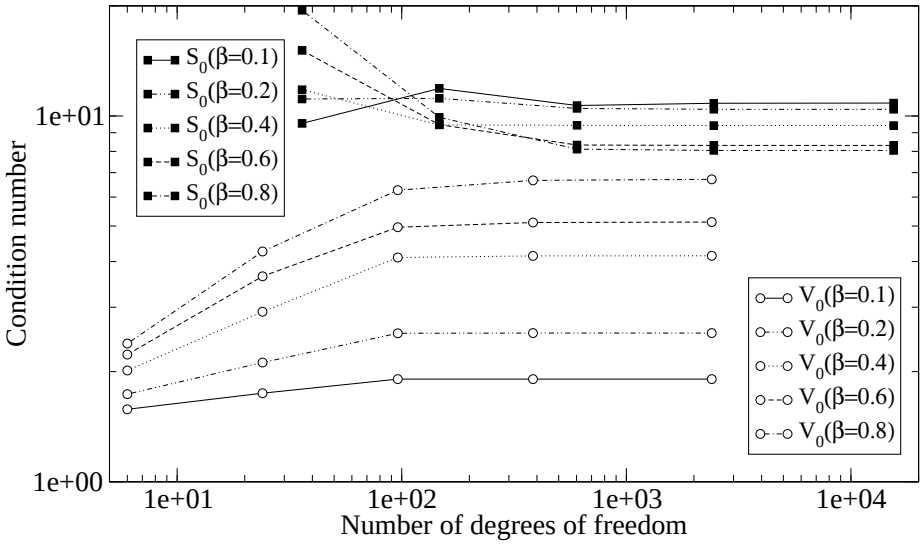

Figure 6.16: Condition numbers for elastodynamics

Next, considering the elastodynamic system in Fig. 6.16 the observations continue. Again, the condition numbers seem to converge against a constant value for an increasing number of degrees of freedom. Additionally, the condition numbers according to the single layer operator increase with an increasing CFL number, and they seem to decrease in the case of the Schur complement system matrix. Finally, both system matrices reveal quite sufficient conditioning properties since, just as before, the condition numbers are less than 20.

Note that the investigations made above are not substantiated by any theoretical predictions. Hence, the good conditioning of the system matrices in time domain can only be assumed and is not proven yet.

6.4 Elastodynamic rod with a longitudinal step load

An almost classical example concerning the verification of the Convolution Quadrature Method is a rod being stressed by a longitudinal stress load [64, 111]. With the Lamé-Navier operator $\mathcal{L}$ from (2.34) the corresponding initial boundary value problem reads

as

$$\begin{aligned}
\left[\left(\mathcal{L}+\varrho_0\frac{\partial^2}{\partial t^2}\right)\mathbf{u}\right](\tilde{\mathbf{x}},t) &= \mathbf{0} && \forall(\tilde{\mathbf{x}},t)\in\Omega^{(3)}\times(0,\infty)\\
\mathbf{u}(\mathbf{y},t) &= \mathbf{0} && \forall(\mathbf{y},t)\in\Gamma_D\times(0,\infty)\\
\mathbf{t}(\mathbf{y},t) &= \tilde{\mathbf{g}}(\mathbf{y},t) && \forall(\mathbf{y},t)\in\Gamma_N^{(3)}\times(0,\infty)\\
\mathbf{u}(\tilde{\mathbf{x}},0^+) &= \mathbf{0} && \forall\tilde{\mathbf{x}}\in\Omega\\
\dot{\mathbf{u}}(\tilde{\mathbf{x}},0^+) &= \mathbf{0} && \forall\tilde{\mathbf{x}}\in\Omega
\end{aligned} \tag{6.17}$$

with the prescribed Neumann data

$$\tilde{\mathbf{g}}(\mathbf{y},t) := \begin{cases} [1,0,0]^\top H(t) & \forall\mathbf{y}\in\Gamma_N^{(3)}\wedge y_1=3\\ \mathbf{0} & \forall\mathbf{y}\in\Gamma_N^{(3)}\wedge y_1\neq 3\,. \end{cases} \tag{6.18}$$

Again, the geometry specifications as well as the classification of Dirichlet- and Neumann boundary correspond to the definitions (6.1) and (6.2), respectively. In (6.18), the function $H(t)$ denotes the Heaviside or, respectively, Unit-Step function

$$H(t) := \begin{cases} 1 & t>0\\ 0 & t<0\,. \end{cases} \tag{6.19}$$

With the artificial value of $\lambda = 0\,\mathrm{N/m^2}$ the initial boundary value problem (6.17) results in a purely uni-axial stress state which is comparable to the 1-dimensional system of a rod with a constant cross-sectional area A and with the impact force F_0 at the free end (see Fig. A.2). The analytical solution for this 1-dimensional state is derived in the appendix A.4 and is explicitly given in (A.13). From that analytical solution it is obvious that the displacements vary linearly while the tractions are constantly distributed with respect to the spatial coordinate. Therefore, a detailed discussion of the numerical solution by means of different element/approximation combinations is skipped and only the TLC-elements will be used in the forthcoming. Nevertheless, the results' quality is investigated by using several meshes as well as several time-grids.

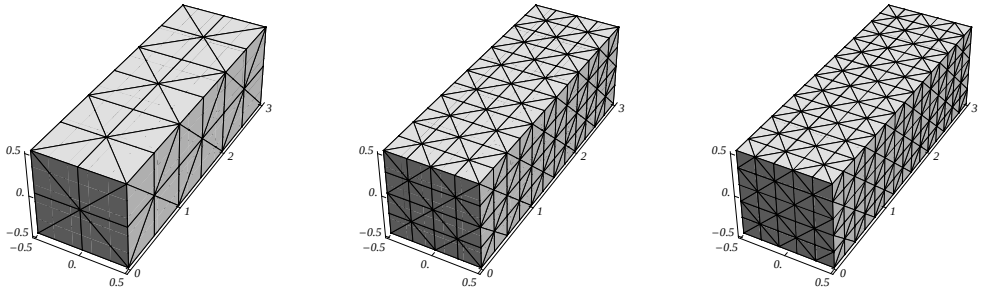

(a) 112 Elements (b) 448 Elements (c) 700 Elements

Figure 6.17: Triangular discretizations of the 3m rod

The Figure 6.17 depicts three different discretizations being used in the following. All meshes consist of regular triangular grids with mesh-sizes of $h_G = \sqrt{2}/2\,\mathrm{m}$ for the coarsest

mesh (Fig. 6.17a), $h_G = \sqrt{2}/4\,\mathrm{m}$ for the 448-element mesh (Fig. 6.17b), and $h_G = \sqrt{2}/5\,\mathrm{m}$ for the finest mesh featuring 700 elements (Fig. 6.17c).

The Figures 6.18 and 6.19 depict the numerical solutions obtained for various spatial and time discretizations. While Fig. 6.18 shows the displacements u_1 at the free end up to the time 0.01s the Fig. 6.19 shows the traction-solutions at the fixed end for the same time interval. In both figures the continuous lines without markers represent the analytical solutions (A.13), which posses kinks in case of the displacement field and jumps for the traction solution. Of course, those exceptional locations are quite challenging to approximate since kinks or discontinuities are hardly producible by the present numerical scheme. However, a rough look at the numerical solutions reveals a quite good correlation of the numerical solutions with the reference solution (A.13).

Comparing different spatial discretizations it becomes clear that the Convolution Quadrature Method has a lower bound concerning the results' stability. While the coarsest mesh provides stable results throughout the complete time interval for both the displacement as well as the traction solution this holds not for the two remaining discretizations. Moreover, a fixed CFL number obviously does not guarantee a proper solution. For instance, the coarsest mesh of 112 elements features a stable solution within the whole time interval. Contrary, the finest time discretization for the finer meshes produces unstable results. In case of the 448-element mesh the solution begins to oscillate at the time $t^* \approx 0.0064$s. With a CFL number of $\beta = 0.1$ this is equivalent to nearly 940 time steps. For the 700-element mesh the solution becomes instable at $t^* \approx 0.0046$s. This corresponds to almost 845 time steps. Thus, the decreasing number of time steps for which stable results exist induces that a constant CFL number is not a sufficient stability criteria. That the CFL number cannot satisfy such a criterion becomes immediately clear when the expression (6.16) is considered. Keeping β constant and downsizing h results in a reduced time step size Δt. Naturally, this decreased time step size affects the Convolution Quadrature Method. On the other hand a larger CFL number yields more sufficient solutions for a finer boundary element mesh than it does for a coarser one. The reason for this behavior is exactly the same as before, namely the reduced time step size Δt which goes ahead with a decreasing mesh size h. Hence, a finer boundary element mesh bears larger CFL numbers for an adequate time resolution of the solution.

A second argument concerning the stability properties of the CQM consists in the spatial quadrature's quality. Until now, all computations have been performed by using the heuristic quadrature rule proposed in Tab. 5.1. While this quadrature rule works sufficient in case of static problems it features some weaknesses in the dynamic cases. This is due to the fact that the quadrature is performed with integral kernels of complex valued arguments. Those complex arguments are responsible for a oscillatory behavior of the integral kernels by what the quadrature becomes more conspicuous. Hence, the quadrature rule from Tab. 5.1 fails for the finest time discretization in the considered time interval. As a proof for this proposition serve the numerical solutions in the Figures 6.20 and 6.21, respectively. For those results the heuristic quadrature rule has been deactivated and all

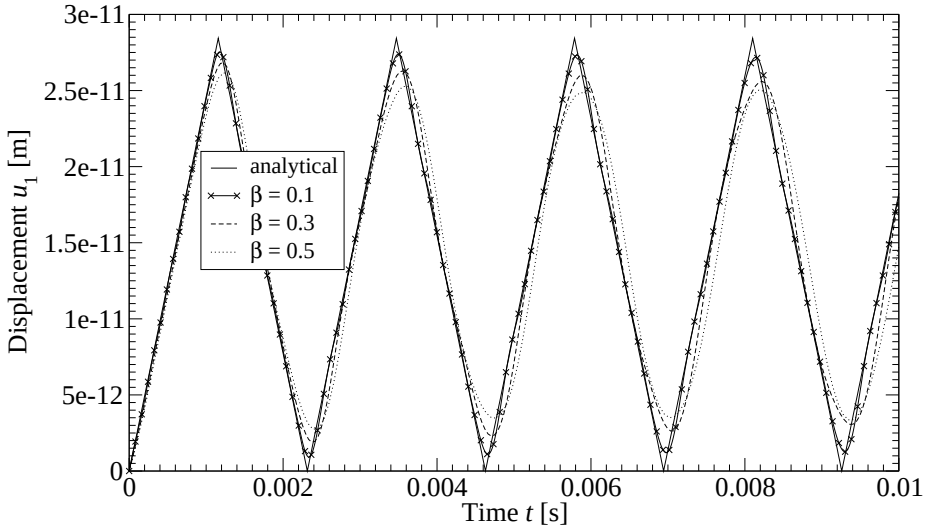

(a) 112 Elements

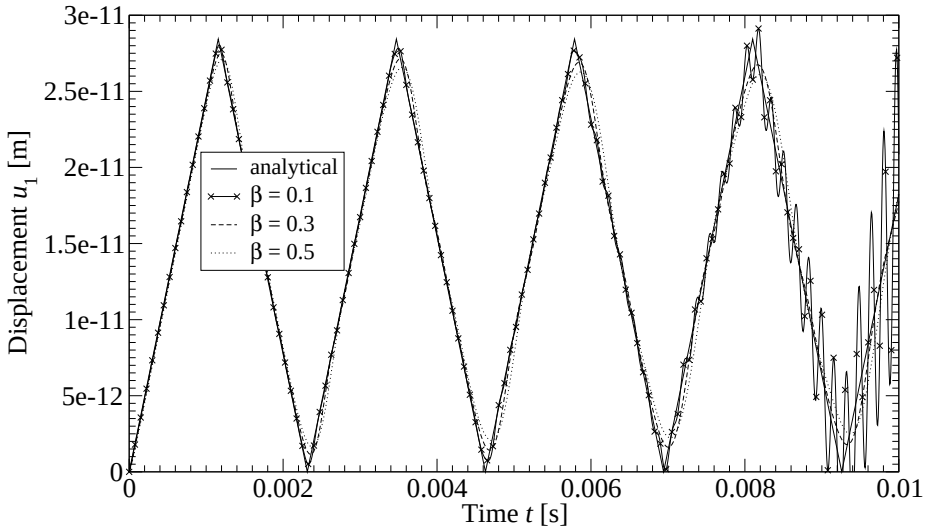

(b) 448 Elements

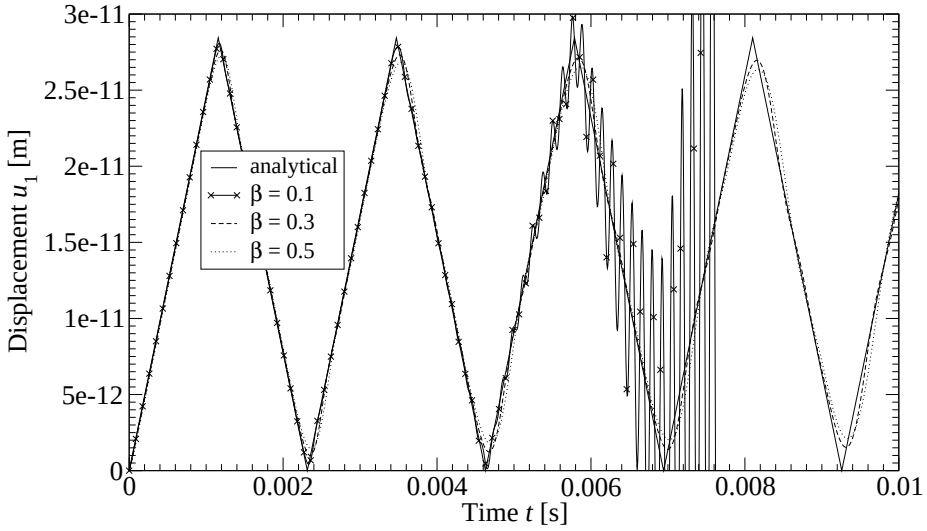

(c) 700 Elements

Figure 6.18: Displacement solutions at the free end for three different meshes

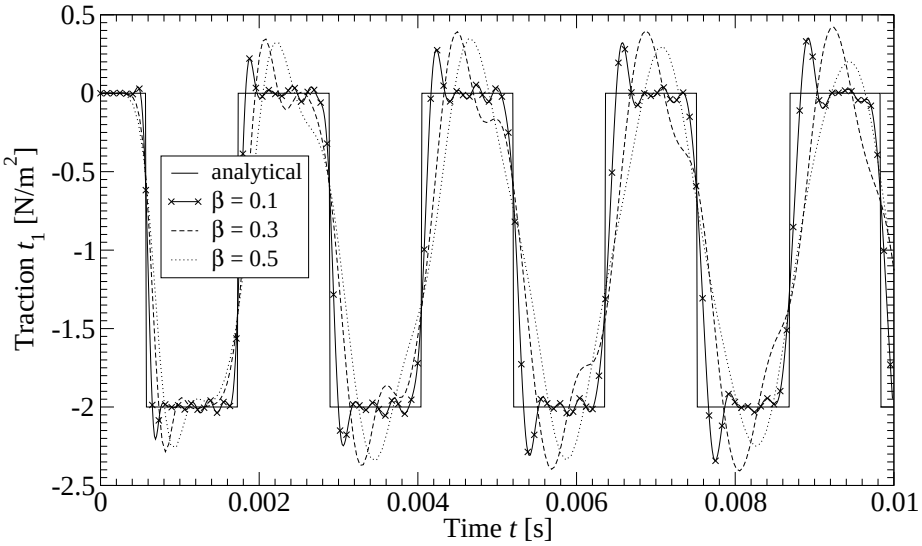

(a) 112 Elements

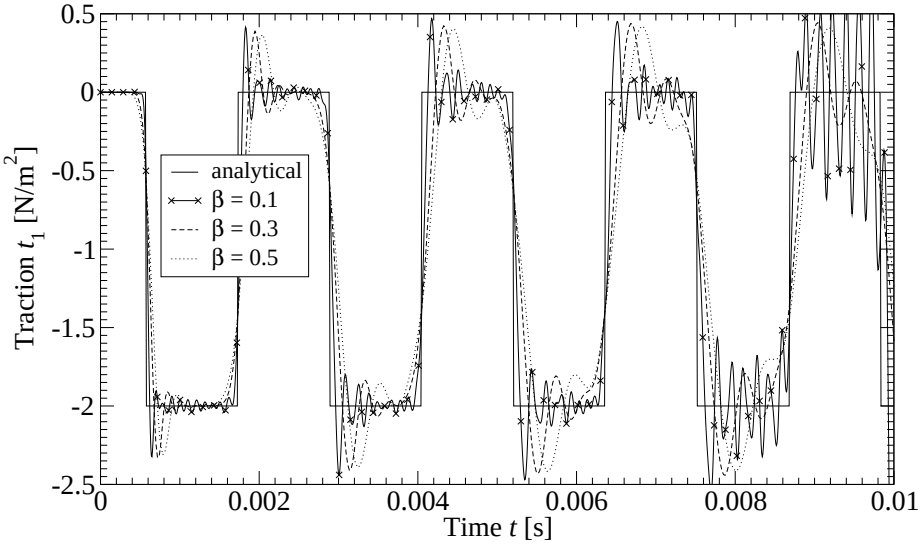

(b) 448 Elements

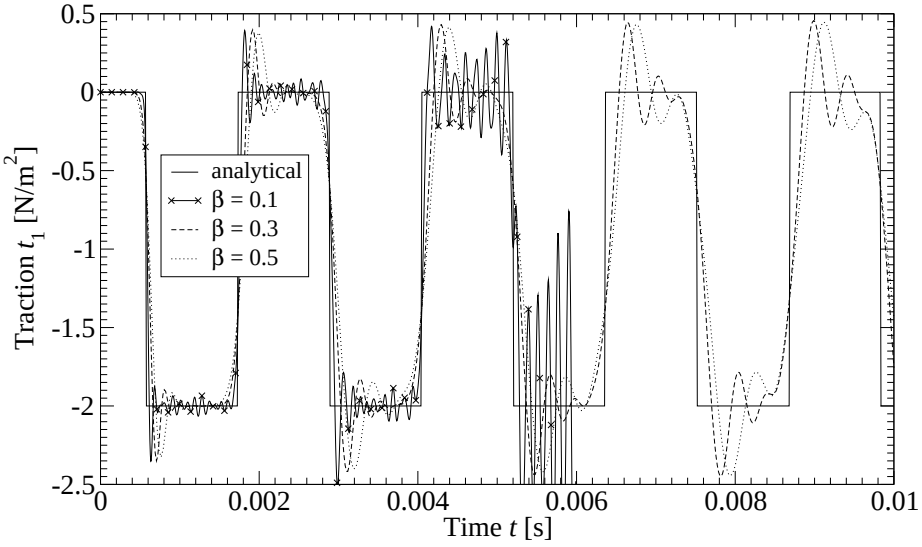

(c) 700 Elements

Figure 6.19: Traction solutions at the fixed end for three different meshes

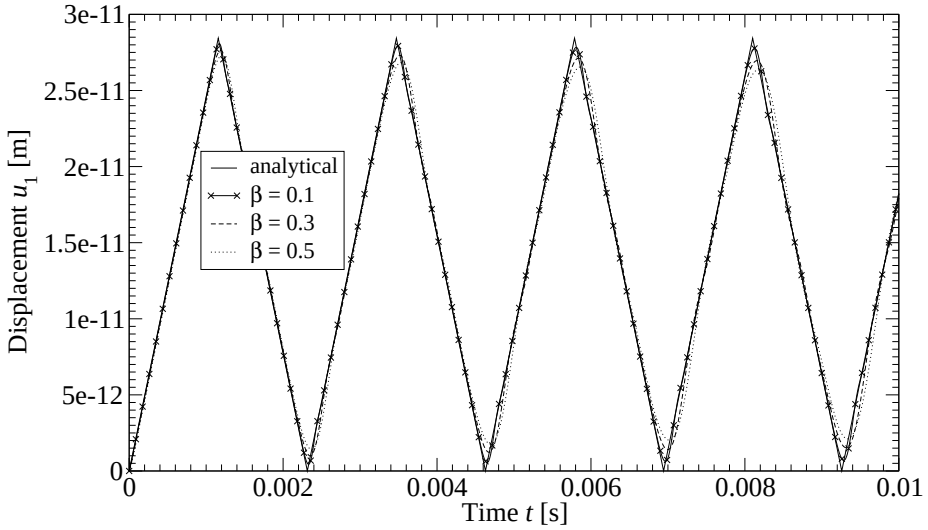

Figure 6.20: Influence of the numerical Quadrature: Improved displacement solution for the 700-element mesh

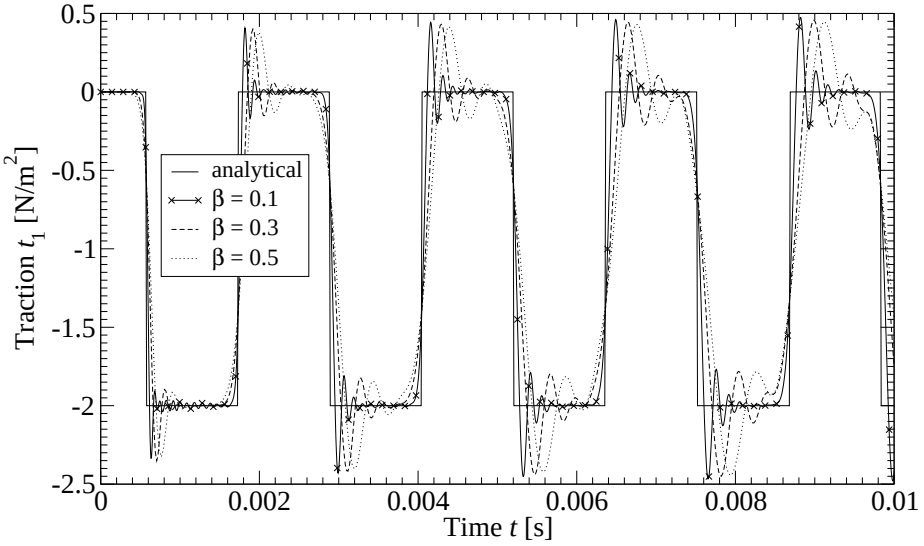

Figure 6.21: Influence of the numerical Quadrature: Improved traction solution for the 700-element mesh

numerical integrations have been performed with six Gauss points per element. Comparing those results with the respective solutions in Fig. 6.18c and 6.19c the better stability properties become obvious. Finally, the spatial quadrature's influence on the Convolution Quadrature Method's stability confirms a proof of Lubich [78] who states that the CQM is unconditionally stable if the underlying spatial integrations are performed exact. This last statement illustrates the enormous importance of reliable quadrature schemes within Boundary Element Methods. Unfortunately, at the moment such schemes are either too slow or they are simply not available for the considered integral kernels. Thus, for a reliable numerical scheme more research on this topic is needed in the future.

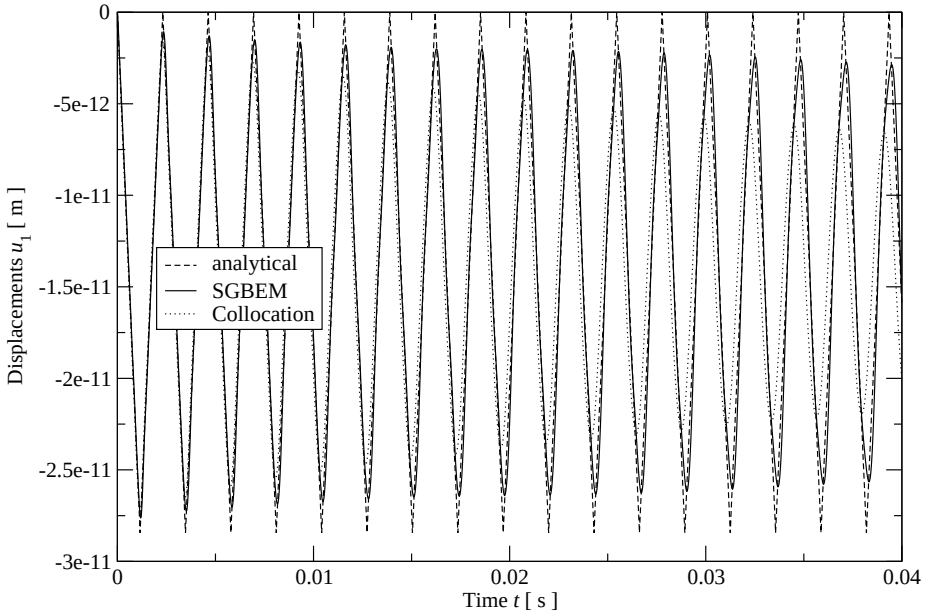

Figure 6.22: SGBEM versus collocation: Long time displacement solution for the 112-element mesh

Finally, this section is closed with a comparison of a collocation based Boundary Element Method as it is stated in [111] and the present symmetric method. The Figures 6.22 and 6.23 depict the displacement and traction solutions for the coarsest mesh within a longer time interval of 0.04s. The CFL number has been chosen to $\beta = 0.14$. To exclude the aforementioned quadrature errors as far as possible the solution corresponding to the present numerical scheme has been obtained by using entirely six Gauss points per element. On the other hand the collocation solution has been calculated with 48 Gauss points per triangular element. More details on that formulation are given in the monograph of Schanz [111]. Clearly, the displacement solution in Fig. 6.22 exhibits much more numerical damping effects in the collocation case than it does for the symmetric Galerkin method. The collocation result has also a phase shift for large times which is not visible for the Galerkin formulation. Besides the increasing damping for the displacement solution the collocation method reveals numerical instabilities with regard to the traction solution (see Fig. 6.23). This traction solution becomes completely instable and is therefore only

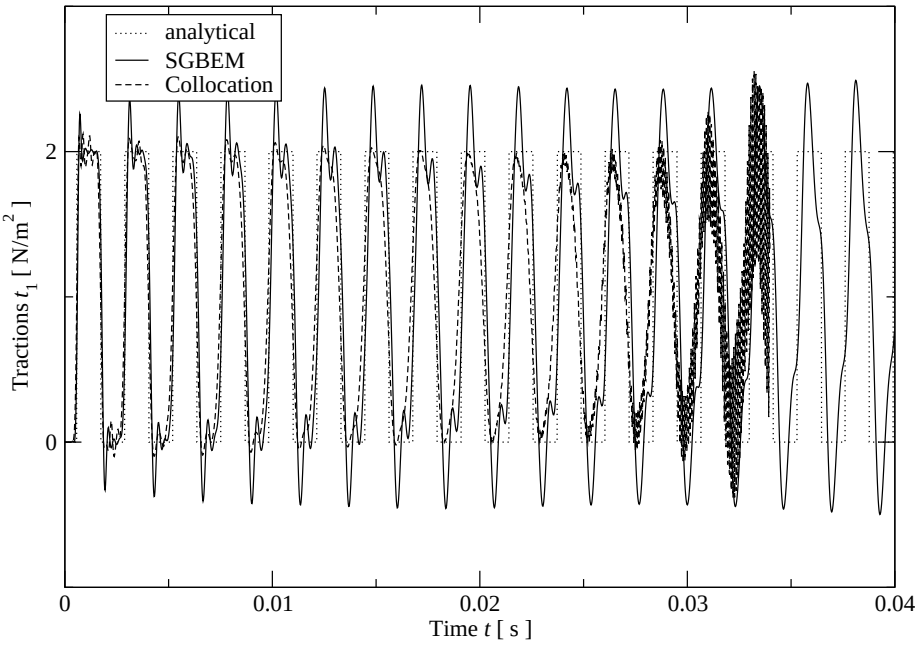

Figure 6.23: SGBEM versus collocation: Long time traction solution for the 112-element mesh

depicted up to the time $t = 0.034$s. In contrast to this instability the Galerkin method is still stable during the whole observation time, although the numerical solution's quality decreases with increasing time.

With the last result, one can state that the Symmetric Galerkin Boundary Element Method is not only more robust in case of static problems but also for dynamic problems.

6.5 Elastodynamic cavity

The following example serves more or less as benchmark for the regularized elastodynamic hypersingular bilinear form (4.100). This example consists in a spherical cavity centered at the origin with radius $r = 0.5$m (see Fig. 6.24a). Then, the geometry specifications for the region of interest are

$$\Omega := \{\tilde{\mathbf{x}} \in \mathbb{R}^3 : |\tilde{\mathbf{x}}| > r\}$$
$$\Gamma = \{\mathbf{y} \in \mathbb{R}^3 : |\mathbf{y}| = r\} .$$

For this spherical cavity the following initial boundary value problem is stated for the outer domain Ω

$$\begin{aligned}
\left[\left(\mathcal{L}+\varrho_0\frac{\partial^2}{\partial t^2}\right)\mathbf{u}\right](\tilde{\mathbf{x}},t) &= \mathbf{0} && \forall\,(\tilde{\mathbf{x}},t)\in\Omega\times(0,\infty)\\
\mathbf{t}(\mathbf{y},t) &= -p_0 H(t)\mathbf{n}(\mathbf{y}) && \forall\,(\mathbf{y},t)\in\Gamma\times(0,\infty)\\
\mathbf{u}(\tilde{\mathbf{x}},0^+) &= \mathbf{0} && \forall\,\tilde{\mathbf{x}}\in\Omega\\
\dot{\mathbf{u}}(\tilde{\mathbf{x}},0^+) &= \mathbf{0} && \forall\,\tilde{\mathbf{x}}\in\Omega\,.
\end{aligned} \tag{6.20}$$

Above, $\mathcal{L}$ is the Lamé-Navier operator from (2.34), $H(t)$ denotes the Unit step function from (6.19), $\mathbf{n}(\mathbf{y})$ is the outward unit normal vector at the point $\mathbf{y}$, and p_0 is the prescribed traction being given as $p_0 = 1\mathrm{N}/\mathrm{m}^2$. The problem (6.20) is perfectly symmetric by what it possesses an analytical solution. Here, the solution is taken from the book of Achenbach [2] and it is given in the appendix A.5.

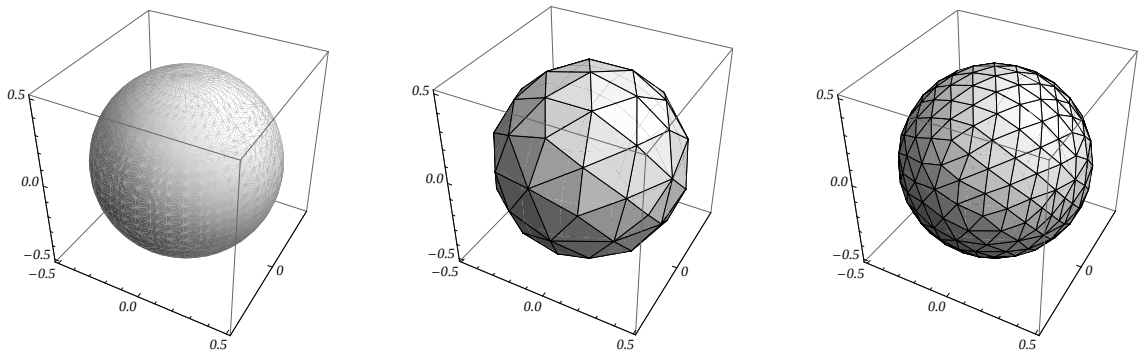

(a) Spherical cavity (b) 122 elements (c) 488 elements

Figure 6.24: Geometry and spatial discretizations of the elastodynamic cavity

Beside the cavity's geometry Fig. 6.24 shows two of its discretizations. The first mesh in Fig. 6.24b is made of 122 TLC-elements while the second discretization in Fig. 6.24c consists of 488 TLC-elements. Moreover, a CFL number of $\beta = 0.3$ has been used for both discretizations.

No. of elems. [−]	h_G [m]	q_G [m]	$\overline{h}_G$ [m]
122	0.298	1.398	0.262
488	0.154	1.433	0.134

Table 6.4: Discretization information of the spherical cavity

In Tab. 6.4, some more information concerning the spherical cavity's discretizations are summarized. There, the global Mesh size h_G, the quasi-uniformity q_G, and the mean mesh

size $\overline{h}_G = \text{mean}_{\tau_i \in G}\{h_i\}$ are listed. The computation of the CFL numbers are based on the mean mesh size $\overline{h}_G$.

In terms of boundary integral equations the initial boundary value problem (6.20) is equivalent to the variational form

$$\langle \mathcal{D} * \mathbf{u}, \mathbf{v} \rangle_\Gamma = \langle (\tfrac{1}{2}\mathcal{I} - \mathcal{K}') * \mathbf{t}, \mathbf{v} \rangle_\Gamma \,. \tag{6.21}$$

Since the boundary Γ is closed and since no rigid body motions take place due to the dynamic problem the bilinear form (6.21) is supposed to be solvable.

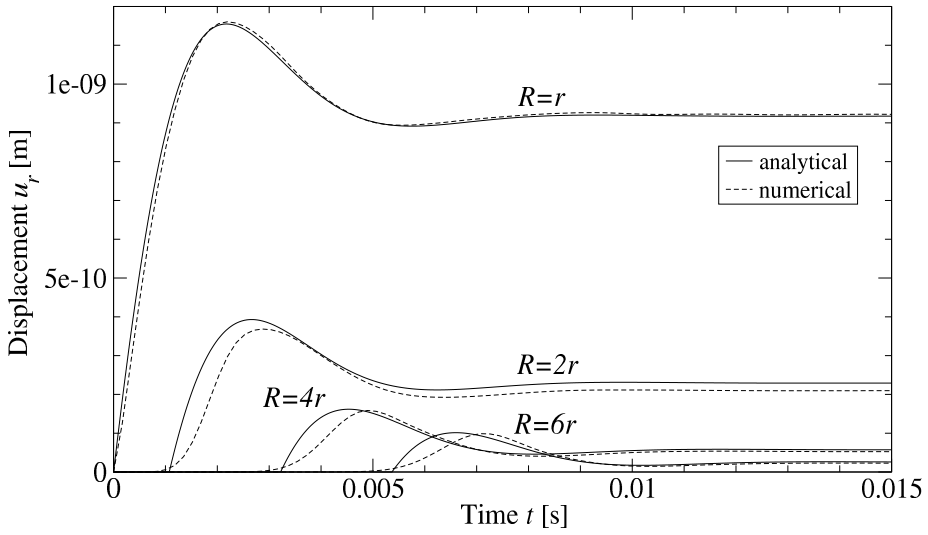

(a) 122 elements

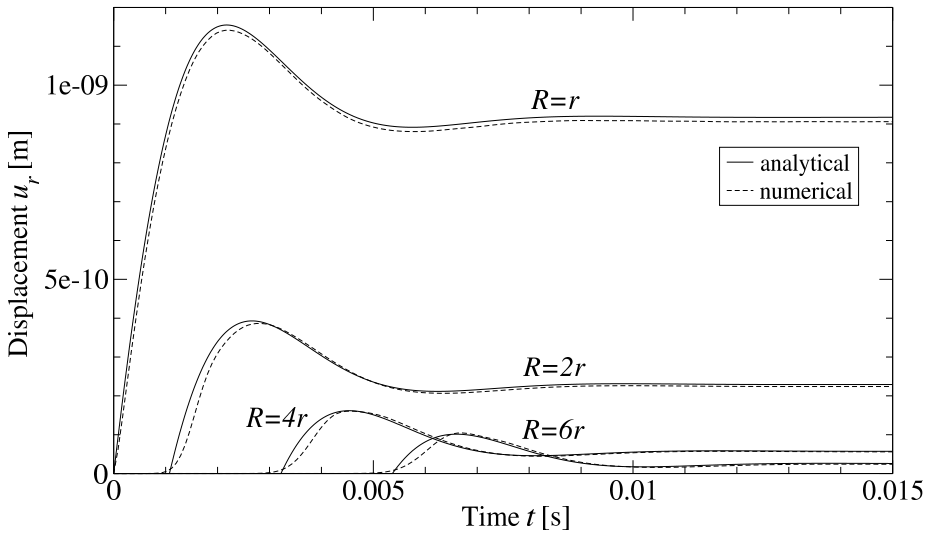

(b) 488 elements

Figure 6.25: Radial displacements of an elastodynamic cavity

The Figure 6.25 shows the radial displacements $u_r = \sqrt{\langle \mathbf{u}, \mathbf{u} \rangle}$ versus the time interval $0 \leq t \leq 0.015$s for several distances R away from the origin. Thus, the results for $R = r$

represent the Cauchy data on the cavity's surface while the remaining distances are the results within the domain Ω. Clearly, for those solutions the representation formula (3.14) has been exploited with the complete Cauchy data $\mathbf{u}_\Gamma$ and $\mathbf{t}_\Gamma$.

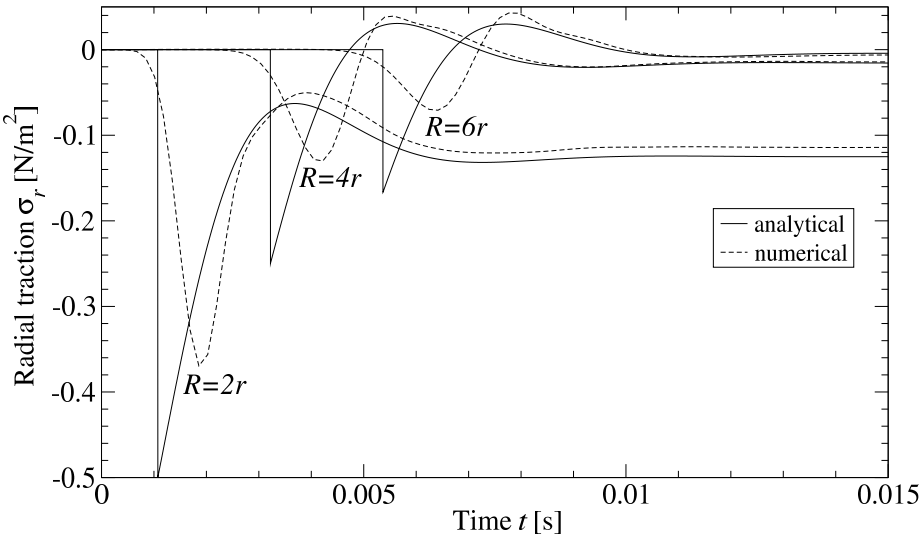

(a) 122 elements

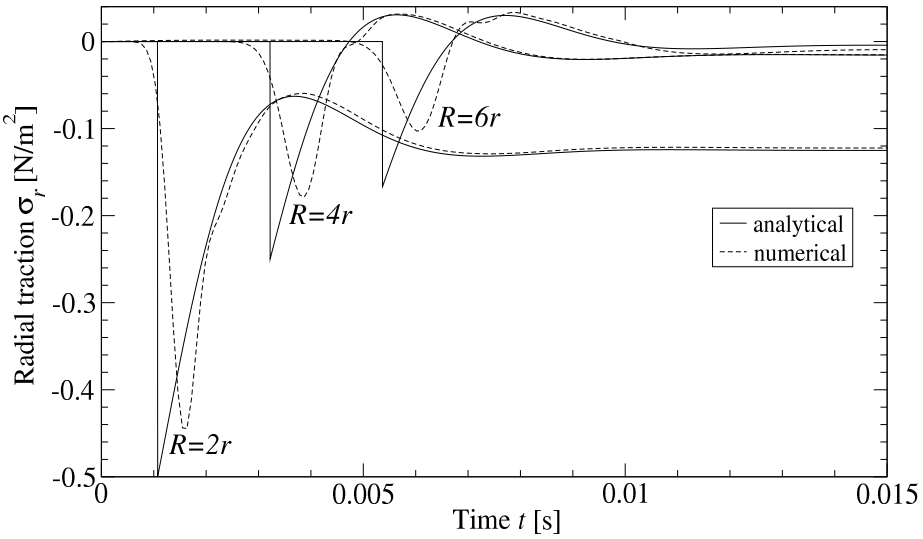

(b) 488 elements

Figure 6.26: Radial tractions of an elastodynamic cavity

The Figures 6.25a and 6.25b illustrate the good convergence of the displacements with the analytical solution. While the displacements at the cavity's surface are almost congruent for the coarse mesh the numerical solution for the finer mesh slightly diverges compared to the analytical solution. Nevertheless, the solutions for the displacement field within the domain are more accurate for the finer mesh. There, the wave fronts are sharper resolved than it is the case for the coarser mesh. Of course, this reflects the influence of the time discretization since, again, the CFL number has been kept constant so that the time step

size scales down with a decreasing mesh size.

In Figure 6.26, the radial tractions σ_r are depicted for the distances $R = 2r$, $R = 4r$, and $R = 6r$, respectively. Thereby, the tractions are obtained by a posterior calculation using the representation formula (3.41). The traction solutions confirm the previously made observations. The finer time resolution in the 488 element mesh ensures the sharper wave fronts within the tractions (see Fig. 6.26b) while for the coarser mesh the solution considerably differs with respect to the analytical reference (see Fig. 6.26b).

Finally, both discretizations are capable of the sufficient approximation with respect to the initial boundary value problem (6.20). Hence, the present Boundary Element formulation being based on the variational form (6.21) is obviously appropriate to handle also such class of problems.

6.6 Viscoelastic examples

In this section, the proposed Boundary Element Method is applied to a viscous solid. Analogous to section 6.4, the 3m rod with its geometry specifications from (6.1) is considered in the two subsections 6.6.1 and 6.6.2, respectively. The Dirichlet- and Neumann-boundaries are chosen in accordance to (6.2). Thus again, this rod is fixed on one side and is attracted by a longitudinal unit step load on the opposite end. The material data are those of the PMMA strip from Table 6.2c.

In fact, the numerical solution technique concerning the viscoelastic media is somehow similar to the deduction of the corresponding 1-dimensional analytical and semi-analytical solutions which are stated in appendix A.4. There, the system is transformed to the Laplace domain and then the correspondence principle is inserted. Afterwards the viscoelastic solution is transferred back into the time-domain. Within the proposed Boundary Element Method the time convolution integrals are performed by using the Convolution Quadrature method which itself needs the Laplace transformed fundamental solutions. Hence, inserting the correspondence principle into the respective fundamental solutions and applying the CQM onto the resulting kernel functions yields the viscoelastic solution in the time domain.

6.6.1 Quasi-static rod with a longitudinal step load

Firstly, the quasi-static case is considered where the balance equations are formulated without taking the inertia terms into account. With the generalized Lamé-Navier operator from (2.61) the boundary value problem reads as

$$\begin{aligned} (\mathcal{L} * \mathrm{d}\mathbf{u})(\tilde{\mathbf{x}},t) &= \mathbf{0} && \forall\,(\tilde{\mathbf{x}},t) \in \Omega^{(3)} \times (0,\infty) \\ \mathbf{u}(\mathbf{y},t) &= \mathbf{0} && \forall\,(\mathbf{y},t) \in \Gamma_D \times (0,\infty) \\ \mathbf{t}(\mathbf{y},t) &= \tilde{\mathbf{g}}(\mathbf{y},t) && \forall\,(\mathbf{y},t) \in \Gamma_N^{(3)} \times (0,\infty)\,. \end{aligned} \tag{6.22}$$

Note that the Laplace transform of the generalized Lamé-Navier operator is nothing but $\hat{\mathcal{L}} = -(\hat{\lambda} + \hat{\mu})\nabla\nabla\cdot - \hat{\mu}\Delta$ with the complex moduli $\hat{\lambda}(s)$ and $\hat{\mu}(s)$, respectively. The according fundamental solution of this operator is formally the elastostatic fundamental solution from (4.46) but evaluated for the complex moduli according to the correspondence principle from (2.59).

The following numerical examples have been performed with the rod's spatial discretization from Fig. 6.17a and with a CFL number of $\beta = 0.3$. Note that the CFL-number has almost no influence in case of the quasi-static analysis and even a higher CFL number does not corrupt the result. This is due to the fact that in quasi-statics there exist no waves which have to be resolved by the time marching scheme.

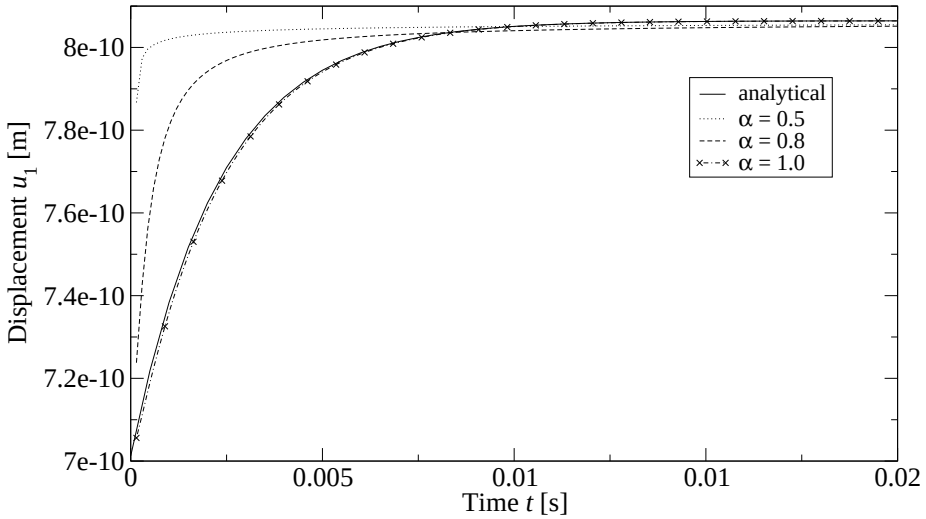

Figure 6.27: Displacements u_1 at the free end for the quasi-static 1-dimensional rod with varying fractional derivative α

Analogous to the elastodynamic results from section 6.4, in Fig. 6.27 the displacements at the rod's free end are depicted. There, the continuous line denotes the 1-dimensional solution stated in (A.17). Comparing this solution with the numerical solution for $\alpha = 1$ shows, clearly, a good agreement between both solutions.

The two remaining solutions are obtained by decreasing the derivative order α within the material model (2.59). The results are as expected. Within the material model (2.59) the Laplace parameter s tends to one as the fractional derivative α tends to zero. Hence, the time influence in the material decreases such that the creeping phase becomes less distinctive. This is what the Fig. 6.27 illustrates. As α decreases the displacements tend earlier to the static solution as it is the case for $\alpha = 1$.

Due to the good agreement with the analytical solution and due to the plausible results for varying the derivative orders α, the proposed Boundary Element Method obviously works very sufficient in conjunction with time-dependent linear material models.

6.6.2 Viscoelastodynamic rod with a longitudinal step load

Now, the mixed boundary value problem (6.22) is transferred to the viscoelastodynamic case where, in addition, the inertia terms are taking into account. Hence, the corresponding initial boundary value problem reads as

$$\begin{aligned}
\left(\mathcal{L} * \mathrm{d}\mathbf{u} + \varrho_0 \frac{\partial^2 \mathbf{u}}{\partial t^2}\right)(\tilde{\mathbf{x}},t) &= \mathbf{0} && \forall\,(\tilde{\mathbf{x}},t) \in \Omega^{(3)} \times (0,\infty) \\
\mathbf{u}(\mathbf{y},t) &= \mathbf{0} && \forall\,(\mathbf{y},t) \in \Gamma_D \times (0,\infty) \\
\mathbf{t}(\mathbf{y},t) &= \tilde{\mathbf{g}}(\mathbf{y},t) && \forall\,(\mathbf{y},t) \in \Gamma_N^{(3)} \times (0,\infty) \\
\mathbf{u}(\tilde{\mathbf{x}},0^+) &= \mathbf{0} && \forall\,\tilde{\mathbf{x}} \in \Omega \\
\dot{\mathbf{u}}(\tilde{\mathbf{x}},0^+) &= \mathbf{0} && \forall\,\tilde{\mathbf{x}} \in \Omega\,.
\end{aligned}$$

As before, $\mathcal{L}$ denotes the generalized Lamé-Navier operator from (2.61) and both the geometry definition as well as the Dirichlet- and Neumann-boundary specifications are that of (6.1) and (6.2), respectively. Equivalent to the quasi-static case, now the Laplace transformed system is equivalent to the Laplace transformed elastodynamic system except that it features the complex moduli $\hat{\lambda}(s)$ and $\hat{\mu}(s)$. Hence, the fundamental solution of the underlying operator $\hat{\mathcal{L}}(s) + \varrho_0 s^2$ is that of the elastodynamic system but evaluated with the complex moduli according to the viscoelastic material model from (2.59).

The following numerical tests are done by using the rod's discretization of 448 TLC-elements from Fig. 6.17b. Moreover, as this problem deals with wave propagation, again, the influence of the time-discretization is represented by the three CFL numbers $\beta = 0.15$, $\beta = 0.3$, and $\beta = 0.6$, respectively.

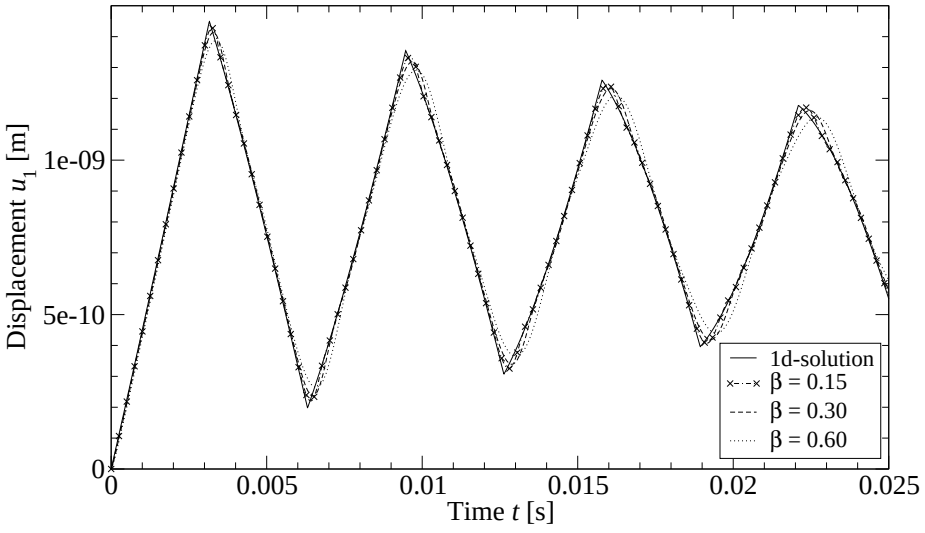

Figure 6.28: Displacements u_1 for the viscoelastodynamic 1-dimensional rod with varying CFL numbers

The displacement and traction solutions in the Figs. 6.28 and 6.29, respectively, obey the same characteristics as the elastodynamic solutions from section 6.4 do. Again, a finer time grid results in a better resolution of the wave fronts.

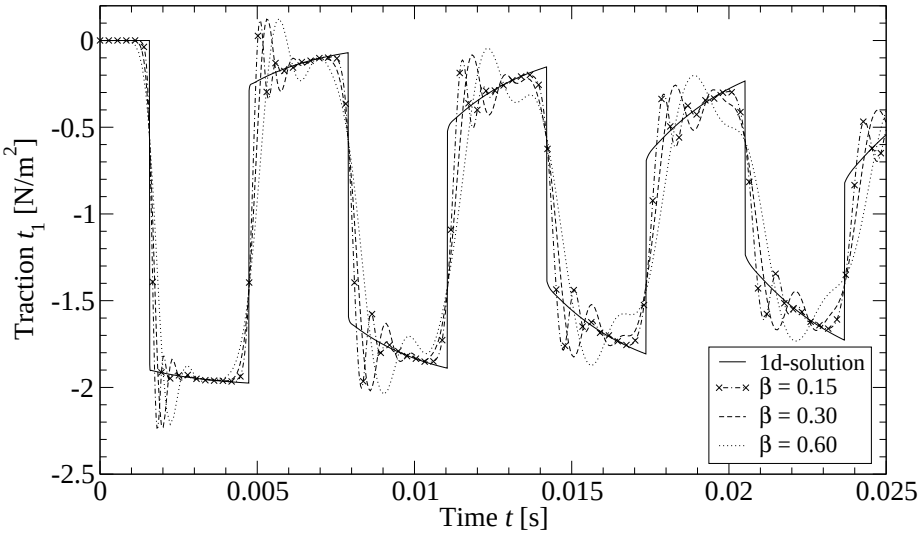

Figure 6.29: Tractions t_1 for the viscoelastodynamic 1-dimensional rod with varying CFL numbers

Concerning the material model the differences between the viscous material and the non-dissipative elastic solid from section 6.4 are eye-catching. Both the displacement as well as the traction solution suffer internal energy losses which are embodied by the decreasing amplitudes in the Figs. 6.28 and 6.29.

Many more studies according the choice of the viscoelastic material parameters can be found in the monograph of Schanz [111]. Here, it is sufficient to state that the present formulation is sufficiently capable to deal also with viscous material models. Finally, with view on the present viscoelastic Boundary Element Method's implementation it has to be mentioned that actually just the underlying fundamental solutions are evaluated with the respective viscous material model. In contrast, in classical collocation methods the implementation effort is considerably higher since the viscous material model also affects the computation of the so-called C-matrix. And possibly, this matrix is difficult to compute in case of a viscous material. More details on this topic can be found in [110, 111].

6.7 Half-space examples

This section is devoted to some examples concerning the half-space problem. This problem has been addressed several times within this thesis. The more theoretical aspects have been mentioned in section 3.4 and in section 5.5 the concept of infinite elements has been introduced to overcome the discretization problem of a semi-infinite domain. Now, it is

time to present some numerical results according to this classical problem. In section 6.7.1, some static results are given and afterwards in section 6.7.2 an attempt is undertaken to cover also the dynamic problem. In both cases the geometry of the semi-infinite half-space is simply

$$\Omega \coloneqq \{\tilde{\mathbf{x}} \in \mathbb{R}^3 \colon \tilde{x}_3 < 0\}$$
$$\Gamma_\infty = \{\mathbf{y} \in \mathbb{R}^3 \colon y_3 = 0\} \, .$$

Additionally, for the static as well as for the dynamic problem the material data corresponds to soil from Tab. 6.2b and the half-space's surface suffers the prescribed boundary traction

$$\tilde{\mathbf{g}}(\mathbf{y}) \coloneqq \begin{cases} \mathbf{t}_0 & \mathbf{y} \in \Gamma \wedge \|\mathbf{y}\|_1 \leq 1 \\ \mathbf{0} & \mathbf{y} \in \Gamma \wedge \|\mathbf{y}\|_1 > 1 \end{cases} \tag{6.23}$$

being zero almost everywhere except within a rectangle given by $\|\mathbf{y}\|_1 \leq 1$. There, the half-space is stressed by the loading $\mathbf{t}_0 \coloneqq [0, 0, -1]^\top \mathrm{N/m^2}$ acting normal to the surface.

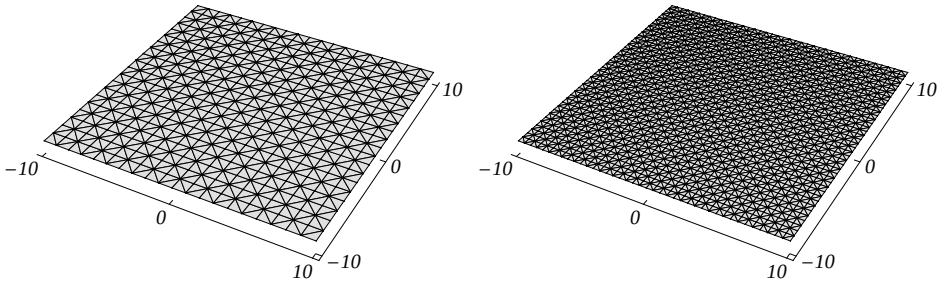

(a) Mesh 1A: 800 elements (b) Mesh 1B: 3200 elements

(c) Mesh 2A: 200 elements (d) Mesh 2B: 800 elements

Figure 6.30: Discretizations of the elastic half-space

In Figure 6.30, four different meshes for the half-space are depicted. Naturally, in those illustrations only the finite boundary elements are drawn and the infinite ones are spared out. The meshes 1A and 1B show an half-space's surface area of 20m × 20m while the two remaining meshes 2A and 2B feature only an area of 10m × 10m being approximated by finite boundary elements. The respective discretization characteristics are summarized in Tab. 6.5. It is somehow difficult to measure the discretizations' mesh sizes since h_{τ_∞} tends

to infinity for the infinite boundary elements τ_∞. Therefore, the global mesh size h_G also becomes infinitely large. To overcome this drawback, the triangulation G^* is introduced which consists of all finite boundary elements τ. Then, the global mesh size h_G^* is just defined as before, i.e., $h_G^* := \max_{\tau_i \in G^*}\{h_i\}$.

	#finite elements	#infinite elements	mesh size h_G^*
mesh 1A	800	80	1.41
mesh 1B	3200	160	0.71
mesh 2A	200	40	1.41
mesh 2B	800	80	0.71

Table 6.5: Number of finite/infinite elements and mesh sizes for several half-space discretizations

Finally, all numerical examples have been performed by using the TLC-elements from Tab. 6.1 for the finite discretization of the boundary.

6.7.1 Static solution

The boundary value problem in case of the elastostatic half-space has been already stated in (5.50) and is recalled here

$$\begin{aligned} (\mathcal{L}\mathbf{u})(\tilde{\mathbf{x}}) &= \mathbf{0} && \forall \tilde{\mathbf{x}} \in \Omega \\ \mathbf{t}(\mathbf{y}) &= \tilde{\mathbf{g}}(\mathbf{y}) && \forall \mathbf{y} \in \Gamma_\infty \\ \lim_{|\mathbf{x}|\to\infty} |\mathbf{x}|\mathbf{u}(\mathbf{x}) &= \mathbf{0} && \forall \mathbf{x} \in \Omega \cup \Gamma_\infty \,. \end{aligned} \tag{6.24}$$

Note that, contrary to the outer problems, the decay condition above is not restricted to the domain Ω but also includes the boundary Γ_∞. Hence, there exists something like a *Dirichlet boundary condition at infinity* and the problem cannot be denoted as a typical Neumann problem. Nevertheless, the underlying bilinear form

$$\langle \widehat{\mathcal{D}}\mathbf{u}, \mathbf{v}\rangle_{\Gamma_\infty} = \langle (\tfrac{1}{2}\widehat{\mathcal{I}} - \widehat{\mathcal{K}}')\tilde{\mathbf{g}}, \mathbf{v}\rangle_{\Gamma_\infty}$$

demands the discretization of the hypersingular operator $\widehat{\mathcal{D}}$ on the complete boundary Γ_∞. For this discretization the infinite elements from section 5.5 are used in order to incorporate the complete boundary surface into the discrete hypersingular operator. Thereby, the numerical examples are performed with the mapping functions from (5.55) and with a scale factor of $\alpha = 1$. Moreover, the directions to infinity $\mathbf{z}_i$ are computed using the expressions (5.56) and (5.57), respectively. Finally, the test- and trial-functions according to the infinite elements match the definition (5.64) with an exponent of $n = 3$. Note that this exponent is primarily chosen for consistency reasons. In fact, an exponent of 2 would be sufficient with view on the demanded kernels' regularity (5.62). But since the kernels

in the time-dependent case claim an exponent of 3 and since there exist no physical reasons for choosing different orders of test- and trial-function the exponent is set to $n = 3$ throughout this section.

If the prescribed traction is just a point load at the origin the boundary value problem (6.24) exhibits an analytical solution which is commonly denoted as the Boussinesq-solution. This solution is a singular solution since the displacements become infinitely large at the origin due to the point load. The Boussinesq solution may be found, e.g., in the book of Love [75]. A more general solution can also be found in the paper of Mindlin [83] where the point load is not restricted to act on the surface but also may be placed within the solid.

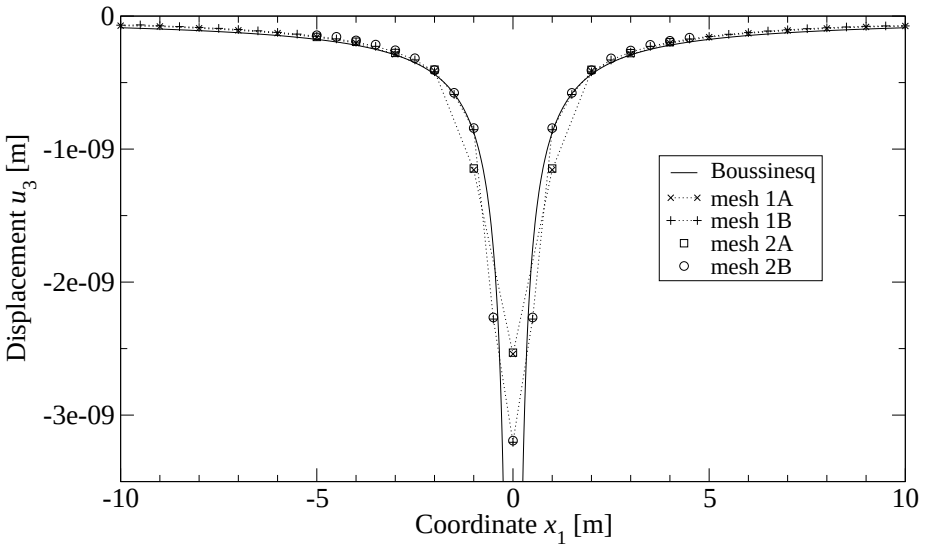

Figure 6.31: Vertical displacements of an elastostatic half-space

The Figure 6.31 presents the vertical displacements $u_3(\mathbf{x})$ for the sample points $\mathbf{x} \in L$ lying on the line $L := \{\mathbf{x} \in \Gamma_\infty : x_2 = 0\}$. The numerical results show a very good convergence in comparison with the Boussinesq solution except around the region where the inhomogeneous tractions are applied. Of course, this deviation is due to the different loading in the numerical examples compared to the single point load in the Boussinesq solution.

The observation continues also for the radial displacements $u_1(\mathbf{x})$ with the same sample points $\mathbf{x} \in L$ as before. Those results are depicted in Fig. 6.32 and the radial displacements are coincident with the Boussinesq solution beyond the region of loading.

Moreover, it can be observed that the results for the vertical as well as for the radial displacements coincide for the respective larger and smaller discretizations, i.e., the results for mesh 1A and the mesh 2A are almost identical. And the same holds for the discretizations 1B and 2B. Even the variations between the mesh 1A and the mesh 1B are rather small. Hence, two main conclusions could be made. Firstly, the results for the finest mesh vary just slightly from the results which are obtained for the coarsest mesh. Secondly, and

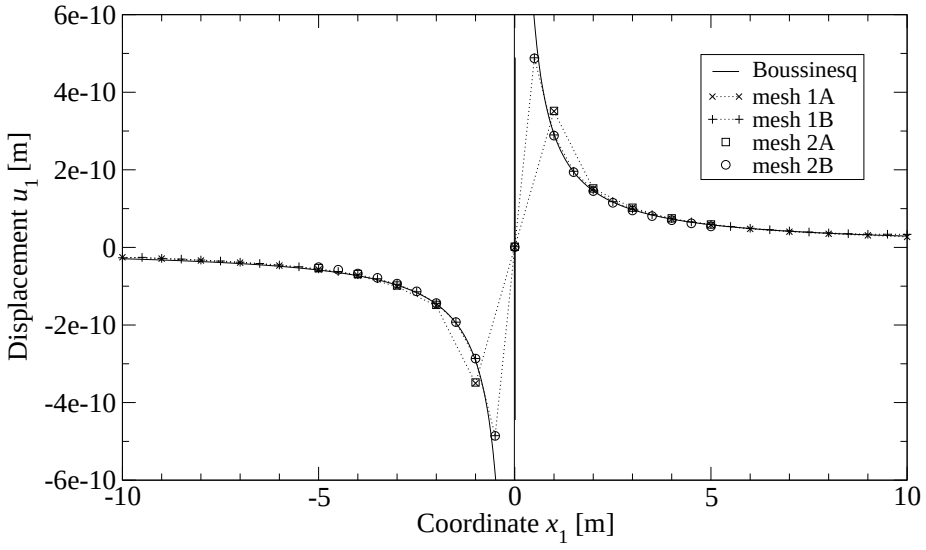

Figure 6.32: Horizontal displacements of an elastostatic half-space

even more important, the infinite element-approach yields meaningful results which are in good agreement with the analytical reference solution. Actually, this means that the far field Dirichlet condition is included in the hypersingular bilinear form $\langle \widehat{\mathcal{D}}\mathbf{u}, \mathbf{v} \rangle_{\Gamma_\infty}$.

6.7.2 Dynamic solution

The initial boundary value problem according to the elastodynamic half-space problem reads as

$$\begin{aligned} \left[\left(\mathcal{L} + \varrho_0 \frac{\partial^2}{\partial t^2} \right) \mathbf{u} \right] (\tilde{\mathbf{x}}, t) &= \mathbf{0} && \forall (\tilde{\mathbf{x}}, t) \in \Omega \times (0, \infty) \\ \mathbf{t}(\mathbf{y}, t) &= \tilde{\mathbf{g}}(\mathbf{y}) H(t) && \forall (\mathbf{y}, t) \in \Gamma_\infty \times (0, \infty) \\ \mathbf{u}(\tilde{\mathbf{x}}, 0^+) &= \mathbf{0} && \forall \tilde{\mathbf{x}} \in \Omega \\ \dot{\mathbf{u}}(\tilde{\mathbf{x}}, 0^+) &= \mathbf{0} && \forall \tilde{\mathbf{x}} \in \Omega \end{aligned} \tag{6.25}$$

with its corresponding boundary integral representation

$$\langle \mathcal{D} * \mathbf{u}, \mathbf{v} \rangle_{\Gamma_\infty} = \langle (\tfrac{1}{2}\mathcal{I} - \mathcal{K}') * \tilde{\mathbf{g}}, \mathbf{v} \rangle_{\Gamma_\infty} \, .$$

In (6.25), the prescribed tractions $\tilde{\mathbf{g}}$ are that of (6.23) and the differential operator $\mathcal{L}$ is the Lamé-Navier operator (2.34). Analogous to the elastostatic half-space, for the equivalent elastodynamic problem there exists an analytical solution which has been deduced by Pekeris [95]. As the Boussinesq solution the dynamic half-space solution supposes that the semi-infinite domain is stressed by a single point load applied at the origin.

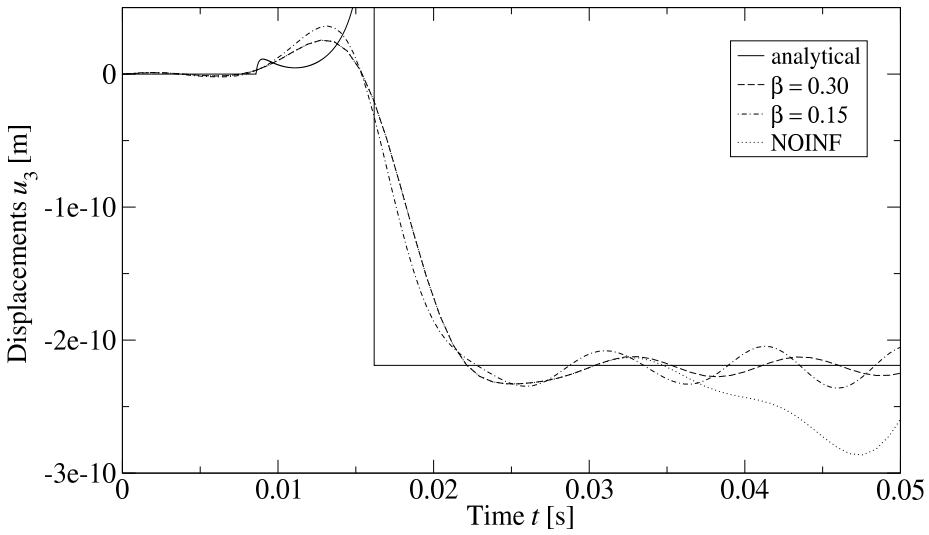

Figure 6.33: Vertical displacements of an elastodynamic half-space at the observation point $\mathbf{x}^*$

In the previous subsection, the presented examples show that the results' quality is almost independent of the discretization. Therefore, in the following the numerical tests are performed using the discretization 1A (see Fig. 6.30a) only. Moreover, the infinite elements are the same as before but with the test- and trial-functions corresponding to (5.63).

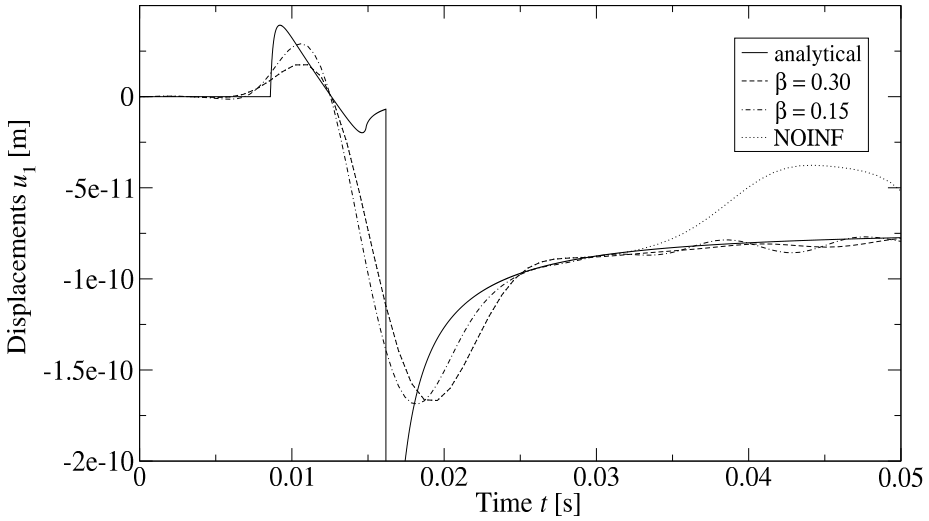

Figure 6.34: Radial displacements of an elastodynamic half-space at the observation point x^*

The Figs. 6.33 and 6.34 depict the vertical and radial solutions $u_3(\mathbf{x}^*,t)$ and $u_1(\mathbf{x}^*,t)$ at the observation point $\mathbf{x}^* = [4, 0, 0]^\top$. Thereby, at least three different calculations have been performed. The first two numerical solutions are done by using infinite elements but with varying time step sizes. The last numerical solution has been obtained without invoking

the infinite elements.

The first and the second numerical solution reveal in general the same behavior. Compared to the analytical solution [95] both displacement solutions exhibit oscillations for larger times which are presumably due to artificial reflections at the crossing of finite and infinite boundary elements. But beside these effects, both numerical solutions show approximately the characteristics of the analytical solution. Contrary, a computation without infinite elements but with the same time step size as the first depicted numerical solution yields a defective result for times larger than 0.034s. This is exactly the time the compression wave with the velocity $c_1 = \sqrt{\lambda+2\mu/\varrho} = 465.8\,\mathrm{m/s}$ has to travel from the center of loading to the truncated boundary and back to the observation point $\mathbf{x}^*$. Therefore, the infinite element approach for the treatment of semi-infinite domains is also worth to be applied to the time-domain. Nevertheless, it must be mentioned that the results obtained here, reach not the quality of those which are gained by the more classical collocation methods using the first boundary integral equation only [105, 111].

7 CONCLUSION

In this work, a unified Symmetric Galerkin Boundary Element Method (SGBEM) has been presented which covers some classical mechanical problems. Since a meaningful Boundary Element Method can be formulated within a linear setting only, all underlying constitutive equations have been derived under the assumptions of linear kinematics as well as a linear, homogeneous, and isotropic material behavior. Explicitly, the derived constitutive equations correspond to the acoustic fluid and to the system of elastodynamics. Additionally, both material models have been reduced to their static counterparts which are the Laplace equation and the elastostatic system. Further, as an enhancement to a perfectly elastic solid the concept of linear viscoelasticity has been introduced in order to model also physical problems with energy losses.

Based on the previously mentioned governing equations the equivalent elliptic and hyperbolic boundary integral equations have been deduced. Therefore, the so-called reciprocity theorems were employed in order to derive the representation formulae. Then, after an application of proper limiting processes a system of boundary integral equations has been obtained by means of the first and the second boundary integral equation. This system of equations depicts the prerequisite for the symmetric Galerkin formulation which embeds the system of integral equations into a variational form. In fact, this variational form serves as the starting point for the later proposed discretization scheme.

As a preliminary work with view to a numerical scheme, the necessary regularizations concerning the integral kernels' singularities have been performed extensively in chapter 4. Those regularizations are based on variations of the Stokes theorem and in some sense they form the backbone of this work. Especially, the regularization of the Laplace transformed hypersingular bilinear form of elastodynamics marks original research. The reason why those regularizations are essential is the fact that independent of the actual physical problem and independent of the particular integral kernel the final occurring singularities are always at least of weakly singular type. Fortunately, there exist some rather general and easy to implement quadrature rules by what the resulting singular kernels are computable without any further modifications. This advantage not only simplifies the implementation of the SGBEM considerably but gives also great freedom concerning the choice of test- and trial-spaces as well as concerning the approximation of the geometry. Another advantage of the regularization consists in the fact that the hypersingular bilinear forms are originally defined as a finite part integrals which hardly allow a purely numerical treatment — at least not in the 3-dimensional space. Hence, the reduction to weakly singular integral kernels guarantees their robust numerical evaluation.

With the knowledge of dealing with weakly singular integrals only the final step, namely the deduction of the SGBEM, has been straightforward. Standard techniques known from

the Finite Element Method have been used for the spatial discretization while the temporal discretization has been performed by means of the Convolution Quadrature Method. Since this temporal discretization scheme uses the Laplace transformed fundamental solutions the aforementioned consideration of dissipative material models poses no problems. It is simply done by making use of the elastic-viscoelastic correspondence principle.

Within the discretization just one additional problem has arisen which, somehow, goes back to the regularization of the method's integral kernels. The half-space problem is typically a kind of Neumann problem by what it demands the discretization of the hypersingular bilinear form on the complete surface. But actually, this surface is of infinite extent and, therefore, it cannot be approximated by finite boundary elements only. On the other hand, approximating just a finite surface patch of the infinite boundary is impossible as well since the regularization demands either a closed surface or assumes vanishing kernel functions at infinity. To overcome this problem the concept of infinite boundary elements has been picked up in order to avoid both the discretization error as well as the regularization error. And although infinite elements are widely known the use of them within the symmetric Galerkin Boundary Element Method is done herein probably for the first time.

Finally, the present Boundary Element Method has underwent a set of different numerical tests in order to validate the method and to illustrate it's capabilities. Except one numerical test, the method succeeded in every other numerical experiment. Beside the numerical confirmation of the theoretical prediction concerning the systems' conditioning, the method has delivered very good results in case of the static examples as well as in the dynamic examples. Additionally, also the interior stress evaluation has shown extraordinary convergence against the respective reference solutions. Further, a comparison of the present method with the more common Collocation Boundary Element Method has shown the robustness of the SGBEM in the time domain. At least, also the elastostatic half-space has been performed very well by the SGBEM.

The method's only problem has been the elastodynamic half-space. This is disappointing since this problem is the classical case where Boundary Element Methods are supposed to be superior compared to other numerical schemes. But in contrast to the classical collocation schemes where the Boundary Element Methods seem to work well in an almost magical but somehow causeless way also on a truncated mesh, the reasons for the present failure are mostly explainable. Beside a possible implementation fault the major problem consist in the fact that, contrary to the elastostatic half-space, the integration on the infinite elements is done over oscillating kernel functions. Therefore, in conjunction with the infinite mapping the integrations are finally performed over a semi-infinite domain with oscillating kernel functions and, additional, weak singularities. With the proposed rather naive quadrature implementation the integrals' approximation quality is uncontrollable.

Of course, the quadrature with respect to the infinite elements marks in a sense the worst case but it reflects another major weakness of the present formulation. Until now, the involved quadratures are performed by using heuristic rules only. Although there exist some error estimates which have been deduced for the standard finite boundary elements

there exist no such estimates in case of infinite boundary elements. Hence, it would be preferable to use some adaptive integration schemes in the future. In the very personal author's opinion the development of reliable numerical integration schemes should be one of the major topics in future research.

At the end, it must be mentioned that one of the method's characteristics are the resulting fully populated system matrices. Moreover, the complexity of the computation for each matrix entry is considerably high due to the Galerkin scheme with its double integrations. A reduction of this complexity is strongly required in order to apply this method also to much larger problems. Fortunately, there exists a broad range of so-called Fast Boundary Element Methods which have been developed in the recent years. Those methods are the Fast Multipole Method, the Adaptive Cross Approximation, $\mathcal{H}$-matrices, and Panel Clustering techniques just to note a few of them. In fact, all of these techniques are based on some low-rank approximations of the systems matrices and they apply some iterative solver schemes to the final system of equations. At this point in time, those methods are mostly applied to symmetric Galerkin Boundary Element Methods dealing with elliptic problems but there exist ambitions to transfer those techniques also to hyperbolic problems. Obviously, the present Galerkin method results in very good conditioned, and positive definite systems also in the time-domain by what the incorporation of fast methods should be possible. Hence, the present work marks one step towards a fast symmetric Galerkin Boundary Element Method in time-domain.

A APPENDIX

A.1 Integral kernels for inner stress evaluations

The numerical examples in sections 6.2.3 and 6.5 are done by employing the representation formulae for the interior stresses. These formulae are derived in section 3.5. But contrary to the rather abstract notation given there, here, the detailed expressions of the involved integral kernels are presented. Naturally, those kernels are intended to be used within some Boundary element implementation. For this purpose, the kernel functions are given in indical notation in the following. Although this notation is not consistent with the notation being used for the rest of this work it is considerably more advantageous from an implementation point of view. First, some useful abbreviations concerning the spatial and normal derivative

$$r_{,i} \coloneqq \frac{\partial r}{\partial y_i} = \frac{y_i - x_i}{r}$$
$$r_{,n} \coloneqq \frac{\partial r}{\partial \mathbf{n}(\mathbf{y})} = \langle \nabla_{\mathbf{y}} r, \mathbf{n}(\mathbf{y}) \rangle$$

of the distance function $r \coloneqq |\mathbf{y} - \mathbf{x}|$ from (4.51) are introduced. Above, x_i, y_i, and n_i denote the i-th component of the respective expression.

Elastostatic kernels. In the elastostatic case the underlying stress representation formula is

$$\boldsymbol{\sigma}(\tilde{\mathbf{x}}) = (\mathcal{S}_1 \mathbf{t}_\Gamma)(\tilde{\mathbf{x}}) - (\mathcal{S}_2 \mathbf{u}_\Gamma)(\tilde{\mathbf{x}}) \qquad \forall \tilde{\mathbf{x}} \in \Omega$$

with the operators

$$\begin{aligned} (\mathcal{S}_1 \mathbf{t}_\Gamma)(\tilde{\mathbf{x}}) &\coloneqq \int_\Gamma \left(\overset{(4)}{\mathbf{C}} \colon \widetilde{\nabla}_{\tilde{\mathbf{x}}} \mathbf{U}^{ES} \right) (\mathbf{y} - \tilde{\mathbf{x}}) \mathbf{t}_\Gamma(\mathbf{y}) \, \mathrm{d}s_{\mathbf{y}} \\ (\mathcal{S}_2 \mathbf{u}_\Gamma)(\tilde{\mathbf{x}}) &\coloneqq \int_\Gamma \left[\mathcal{T}_{\mathbf{y}} \left(\overset{(4)}{\mathbf{C}} \colon \widetilde{\nabla}_{\tilde{\mathbf{x}}} \mathbf{U}^{ES} \right) \right] (\mathbf{y} - \tilde{\mathbf{x}}) \mathbf{u}_\Gamma(\mathbf{y}) \, \mathrm{d}s_{\mathbf{y}} \qquad \forall \mathbf{y} \in \Gamma \, . \end{aligned} \tag{A.1}$$

In Eqn. (A.1), $\mathbf{U}^{ES}$ denotes the elastostatic fundamental solution (4.46) and $\widetilde{\nabla}_{\tilde{\mathbf{x}}}$ is the symmetric gradient. With the definitions of the third order tensors

$$\begin{aligned} \overset{(3)}{\mathbf{S}}_1 &\coloneqq \overset{(4)}{\mathbf{C}} \colon \widetilde{\nabla}_{\tilde{\mathbf{x}}} \mathbf{U}^{ES} \\ \overset{(3)}{\mathbf{S}}_2 &\coloneqq \mathcal{T}_{\mathbf{y}} \left(\overset{(4)}{\mathbf{C}} \colon \widetilde{\nabla}_{\tilde{\mathbf{x}}} \mathbf{U}^{ES} \right) \end{aligned}$$

the tensors' components are

$$
\begin{aligned}
S_1[k,i,j](\mathbf{y},\mathbf{x}) &= \frac{1}{8\pi(1-\nu)r^2}\left[(1-2\nu)(\delta_{kj}r_{,i}+\delta_{ki}r_{,j}-r_{,k}\delta_{ij})+3r_{,i}r_{,j}r_{,k}\right]\\
S_2[k,i,j](\mathbf{y},\mathbf{x}) &= \frac{E}{8\pi(1-\nu)(1+\nu)r^3}\left[3r_{,n}\left((1-2\nu)\delta_{ij}r_{,k}+\nu r_{,i}\delta_{jk}+\nu\delta_{ik}r_{,j}-5r_{,i}r_{,j}r_{,k}\right)\right.\\
&\qquad +3n_k(1-2\nu)r_{,i}r_{,j}+n_i\left((1-2\nu)\delta_{jk}+3\nu r_{,j}r_{,k}\right)\\
&\qquad \left.+n_j\left((1-2\nu)\delta_{ik}+3\nu r_{,i}r_{,k}\right)-n_k\delta_{ij}(1-4\nu)\right]\,.
\end{aligned}
\tag{A.2}
$$

In (A.2), δ_{ij} denotes the Kronecker delta from (4.41). Moreover, for brevity, the stress kernels are given in terms of the Young's modulus E and the Poisson's ratio ν.

Elastodynamic kernels. Since all time-domain computations are done by utilizing the Convolution Quadrature Method it is sufficient to formulate the elastodynamic representation formula (3.41) in the Laplace domain. This gives

$$
\hat{\boldsymbol{\sigma}}(\tilde{\mathbf{x}},s) = (\hat{\mathcal{S}}_1\hat{\mathbf{t}}_\Gamma)(\tilde{\mathbf{x}},s)-(\hat{\mathcal{S}}_2\hat{\mathbf{u}}_\Gamma)(\tilde{\mathbf{x}},s)\qquad \forall\,\tilde{\mathbf{x}}\in\Omega,\, s\in\mathbb{C}
$$

with the operators

$$
\begin{aligned}
(\hat{\mathcal{S}}_1\hat{\mathbf{t}}_\Gamma)(\tilde{\mathbf{x}},s) &\coloneqq \int_\Gamma \left(\overset{(4)}{\mathbf{C}}\colon \widetilde{\nabla}_{\tilde{\mathbf{x}}}\hat{\mathbf{U}}^{ED}\right)(\mathbf{y}-\tilde{\mathbf{x}},s)\hat{\mathbf{t}}_\Gamma(\mathbf{y},s)\,\mathrm{d}s_{\mathbf{y}}\\
(\hat{\mathcal{S}}_2\hat{\mathbf{u}}_\Gamma)(\tilde{\mathbf{x}},s) &\coloneqq \int_\Gamma \left[\mathcal{T}_{\mathbf{y}}\left(\overset{(4)}{\mathbf{C}}\colon \widetilde{\nabla}_{\tilde{\mathbf{x}}}\hat{\mathbf{U}}^{ED}\right)\right](\mathbf{y}-\tilde{\mathbf{x}},s)\hat{\mathbf{u}}_\Gamma(\mathbf{y},s)\,\mathrm{d}s_{\mathbf{y}}\qquad \forall\,\mathbf{y}\in\Gamma\,.
\end{aligned}
$$

As before, two third order tensors

$$
\begin{aligned}
\overset{(3)}{\hat{\mathbf{S}}}_1 &\coloneqq \overset{(4)}{\mathbf{C}}\colon \widetilde{\nabla}_{\tilde{\mathbf{x}}}\hat{\mathbf{U}}^{ED}\\
\overset{(3)}{\hat{\mathbf{S}}}_2 &\coloneqq \mathcal{T}_{\mathbf{y}}\left(\overset{(4)}{\mathbf{C}}\colon \widetilde{\nabla}_{\tilde{\mathbf{x}}}\hat{\mathbf{U}}^{ED}\right)
\end{aligned}
$$

are defined whose components are

$$
\begin{aligned}
\hat{S}_1[i,j,k](\mathbf{y},\mathbf{x},s) &= \frac{1}{4\pi r}\left[\eta_1 r_{,i}\delta_{jk}+\eta_1 r_{,j}\delta_{ik}-2r_{,k}(\eta_2 r_{,i}r_{,j}-\eta_3\delta_{ij})\right]\\
\hat{S}_2[i,j,k](\mathbf{y},\mathbf{x},s) &= \frac{E}{8\pi r^2(1+\nu)}\left[r_{,n}\left(\eta_4 r_{,i}\delta_{jk}+\eta_4 r_{,j}\delta_{ik}+4r_{,k}(\eta_5 r_{,i}r_{,j}-\eta_6\delta_{ij})\right)\right.\\
&\qquad -4n_{,k}\left(\eta_6 r_{,i}r_{,j}-\eta_7\delta_{ij}\right)\\
&\qquad \left.+n_{,i}\left(\eta_4 r_{,j}r_{,k}+2\eta_1\delta_{jk}\right)+n_{,j}\left(\eta_4 r_{,i}r_{,k}+2\eta_1\delta_{ik}\right)\right]\,.
\end{aligned}
$$

Analogous to the elastostatic kernels (A.2) the kernels above are given in terms of the Young modulus E and Poisson's ratio ν. The abbreviations $\eta_1, \ldots, \eta_7$ are given as

$$\eta_1 := 2\chi + \left(1+\tilde{k}_2\right)\frac{\exp(-\tilde{k}_2)}{r}$$

$$\eta_2 := 6\chi - 3\psi + \left(3+\tilde{k}_2\right)\frac{\exp(-\tilde{k}_2)}{r} - \tilde{k}_1\frac{c_2^2}{c_1^2}\frac{\exp(-\tilde{k}_1)}{r}$$

$$\eta_3 := \frac{1}{1-2\nu}\left[\chi - \nu\left(2\chi - \left(1+\tilde{k}_1\right)\frac{c_2^2}{c_1^2}\frac{\exp(-\tilde{k}_1)}{r}\right)\right]$$

$$\eta_4 := -24\chi + 12\psi - \left(15+7\tilde{k}_2+\tilde{k}_2^2\right)\frac{\exp(-\tilde{k}_2)}{r} + 4\tilde{k}_1\frac{c_2^2}{c_1^2}\frac{\exp(-\tilde{k}_1)}{r}$$

$$\eta_5 := 30\chi + 15\psi + \tilde{k}_2\left(10+\tilde{k}_2\right)\frac{\exp(-\tilde{k}_2)}{r} - \frac{c_2^2}{c_1^2}\left(15+10\tilde{k}_1+\tilde{k}_1^2\right)\frac{\exp(-\tilde{k}_1)}{r}$$

$$\eta_6 := \frac{1}{1-2\nu}\left[5(1-2\nu)\chi + (1+\tilde{k}_2)(1-2\nu)\frac{\exp(-\tilde{k}_2)}{r} - \frac{c_2^2}{c_1^2}((1-5\nu)(1+\tilde{k}_1) - \nu\tilde{k}_1^2)\frac{\exp(-\tilde{k}_1)}{r}\right]$$

$$\eta_7 := \frac{1}{(1-2\nu)^2}\left[(1-4\nu+4\nu^2)\chi + \frac{c_2^2}{c_1^2}\nu\left(2(1-2\nu)(1+\tilde{k}_1) - \nu\tilde{k}_1^2\right)\frac{\exp(-\tilde{k}_1)}{r}\right]$$

with the auxiliary functions

$$\psi(r,s) := -\frac{c_2^2}{c_1^2}\left(\frac{1}{\tilde{k}_1^2}+\frac{1}{\tilde{k}_1}\right)\frac{\exp(-\tilde{k}_1)}{r} + \left(\frac{1}{\tilde{k}_2^2}+\frac{1}{\tilde{k}_2}+1\right)\frac{\exp(-\tilde{k}_2)}{r}$$

$$\chi(r,s) := -\frac{c_2^2}{c_1^2}\left(3\frac{1}{\tilde{k}_1^2}+3\frac{1}{\tilde{k}_1}+1\right)\frac{\exp(-\tilde{k}_1)}{r} + \left(3\frac{1}{\tilde{k}_2^2}+3\frac{1}{\tilde{k}_2}+1\right)\frac{\exp(-\tilde{k}_2)}{r},$$

and with

$$\tilde{k}_i := k_i r = \frac{s}{c_i}r, \qquad i = 1,2\,.$$

A.2 Mapping functions

All of the following functions confer to the configurations of the boundary elements which are stated in section 5.1. All mapping functions are based on the reference elements depicted in Fig. 5.1 on page 87.

- **3-node triangle**

  Monoms:

$$\boldsymbol{\psi}(\hat{\mathbf{x}}) = \begin{bmatrix} 1 & \hat{x}_1 & \hat{x}_2 \end{bmatrix}$$

Shape-, trial-, and test-functions:

$$\boldsymbol{\varphi}_3^1(\hat{\mathbf{x}}) = \begin{bmatrix} \varphi_1^1(\hat{\mathbf{x}}) \\ \varphi_2^1(\hat{\mathbf{x}}) \\ \varphi_3^1(\hat{\mathbf{x}}) \end{bmatrix} = \begin{bmatrix} 1-\hat{x}_1 \\ \hat{x}_1-\hat{x}_2 \\ \hat{x}_2 \end{bmatrix}$$

- **6-node triangle**

  Monoms:

$$\boldsymbol{\psi}(\hat{\mathbf{x}}) = \begin{bmatrix} 1 & \hat{x}_1 & \hat{x}_2 & \hat{x}_1^2 & \hat{x}_1\hat{x}_2 & \hat{x}_2^2 \end{bmatrix}$$

  Shape-, trial-, and test-functions:

$$\boldsymbol{\varphi}_6^2(\hat{\mathbf{x}}) = \begin{bmatrix} \varphi_1^2(\hat{\mathbf{x}}) \\ \varphi_2^2(\hat{\mathbf{x}}) \\ \varphi_3^2(\hat{\mathbf{x}}) \\ \varphi_4^2(\hat{\mathbf{x}}) \\ \varphi_5^2(\hat{\mathbf{x}}) \\ \varphi_6^2(\hat{\mathbf{x}}) \end{bmatrix} = \begin{bmatrix} 1-3\hat{x}_1+2\hat{x}_1^2 \\ (1-2\hat{x}_1+2\hat{x}_2)(\hat{x}_2-\hat{x}_1) \\ \hat{x}_2(2\hat{x}_2-1) \\ 4(1-\hat{x}_1)(\hat{x}_1-\hat{x}_2) \\ 4(\hat{x}_1-\hat{x}_2)\hat{x}_2 \\ 4(1-\hat{x}_1)\hat{x}_2 \end{bmatrix}$$

- **4-node quadrilateral**

  Monoms:

$$\boldsymbol{\psi}(\hat{\mathbf{x}}) = \begin{bmatrix} 1 & \hat{x}_1 & \hat{x}_2 & \hat{x}_1\hat{x}_2 \end{bmatrix}$$

  Auxiliary functions:

$$\phi_1(\hat{x}) = 1-\hat{x}, \quad \phi_2(\hat{x}) = \hat{x}, \quad \hat{x} \in [0,1]$$

  Shape-, test-, and trial-functions:

$$\boldsymbol{\varphi}_4^1(\hat{\mathbf{x}}) = \begin{bmatrix} \varphi_1^1(\hat{\mathbf{x}}) \\ \varphi_2^1(\hat{\mathbf{x}}) \\ \varphi_3^1(\hat{\mathbf{x}}) \\ \varphi_4^1(\hat{\mathbf{x}}) \end{bmatrix} = \begin{bmatrix} \phi_1(\hat{x}_1)\,\phi_1(\hat{x}_2) \\ \phi_2(\hat{x}_1)\,\phi_1(\hat{x}_2) \\ \phi_2(\hat{x}_1)\,\phi_2(\hat{x}_2) \\ \phi_1(\hat{x}_1)\,\phi_2(\hat{x}_2) \end{bmatrix}$$

- **9-node quadrilateral**

  Monoms:

$$\boldsymbol{\psi}(\hat{\mathbf{x}}) = \begin{bmatrix} 1 & \hat{x}_1 & \hat{x}_2 & \hat{x}_1^2 & \hat{x}_1\hat{x}_2 & \hat{x}_2^2 & \hat{x}_1^2\hat{x}_2 & \hat{x}_1\hat{x}_2^2 & \hat{x}_1^2\hat{x}_2^2 \end{bmatrix}$$

  Auxiliary functions:

$$\phi_1(\hat{x}) = 1-3\hat{x}+2\hat{x}^2, \quad \phi_2(\hat{x}) = \hat{x}(2\hat{x}-1), \quad \phi_3(\hat{x}) = 4\hat{x}(1-\hat{x}), \quad \hat{x} \in [0,1]$$

Shape-, test-, and trial-functions:

$$\boldsymbol{\varphi}_9^2(\hat{\mathbf{x}}) = \begin{bmatrix} \varphi_1^2(\hat{\mathbf{x}}) \\ \varphi_2^2(\hat{\mathbf{x}}) \\ \varphi_3^2(\hat{\mathbf{x}}) \\ \varphi_4^2(\hat{\mathbf{x}}) \\ \varphi_5^2(\hat{\mathbf{x}}) \\ \varphi_6^2(\hat{\mathbf{x}}) \\ \varphi_7^2(\hat{\mathbf{x}}) \\ \varphi_8^2(\hat{\mathbf{x}}) \\ \varphi_9^2(\hat{\mathbf{x}}) \end{bmatrix} = \begin{bmatrix} \phi_1(\hat{x}_1)\,\phi_1(\hat{x}_2) \\ \phi_2(\hat{x}_1)\,\phi_1(\hat{x}_2) \\ \phi_2(\hat{x}_1)\,\phi_2(\hat{x}_2) \\ \phi_1(\hat{x}_1)\,\phi_2(\hat{x}_2) \\ \phi_3(\hat{x}_1)\,\phi_1(\hat{x}_2) \\ \phi_2(\hat{x}_1)\,\phi_3(\hat{x}_2) \\ \phi_3(\hat{x}_1)\,\phi_2(\hat{x}_2) \\ \phi_1(\hat{x}_1)\,\phi_3(\hat{x}_2) \\ \phi_3(\hat{x}_1)\,\phi_3(\hat{x}_2) \end{bmatrix}$$

A.3 Computation of relevant time steps

The integration weights ω_n can be estimated by

$$\omega_n \approx \frac{\eta^n}{n!}\exp(-\frac{3}{2}\eta) \qquad \eta = \frac{r_{\max}}{c_2\,\Delta t}\,, \tag{A.3}$$

where $r_{\max}$ is the maximum distance in the discretized body, c_2 is the velocity of the shear wave, and Δt is the time step size. Figure A.1 depicts the integration weights (A.3) schematically.

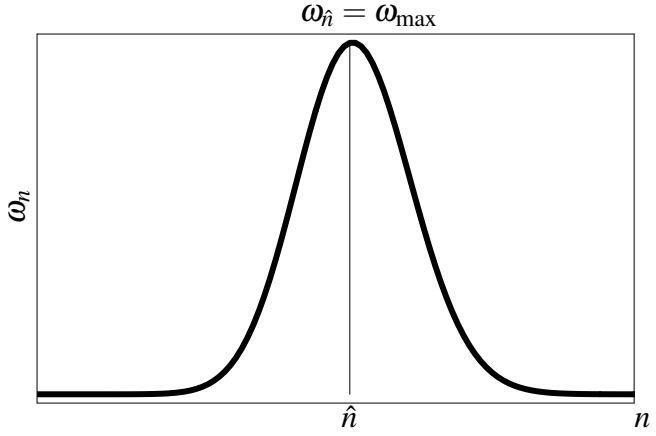

Figure A.1: Integration weights ω_n

The influence of those integration weights is assumed to vanish if there exist a $\bar{n}$ such that

$$\left|\frac{\omega_{\bar{n}} - \omega_{\bar{n}-1}}{\omega_{\max}}\right| \overset{!}{\leq} \varepsilon \tag{A.4}$$

is fulfilled for some pre-defined tolerance ε.

To compute the time step $\hat{n}$ for the maximal integration weight $\omega_{\max}$ the condition

$$\omega_{\hat{n}+1} \overset{!}{<} \omega_{\hat{n}} \tag{A.5}$$

holds. Inserting (A.3) into (A.5) and using $(n+1)! = n! \cdot (n+1)$ yields

$$\frac{\eta^{\hat{n}}}{\hat{n}!}\frac{\eta}{\hat{n}+1}\exp(-\frac{3}{2}\eta) < \frac{\eta^{\hat{n}}}{\hat{n}!}\exp(-\frac{3}{2}\eta) \quad \Longrightarrow \quad \hat{n} > \eta - 1 \quad \Longrightarrow \quad \hat{n} = \lceil \eta \rceil - 1\,. \tag{A.6}$$

Above, $\lceil \eta \rceil$ is the smallest integer greater or equal η. Moreover, the difference $\omega_{\bar{n}} - \omega_{\bar{n}-1}$ can be expressed by

$$\omega_{\bar{n}} - \omega_{\bar{n}-1} = \left(\frac{\eta^{\bar{n}}}{\bar{n}!} - \frac{\eta^{\bar{n}-1}}{(\bar{n}-1)!}\right)\exp(-\frac{3}{2}\eta) = \frac{\eta^{\bar{n}}}{\bar{n}!}\left(1 - \frac{\bar{n}}{\eta}\right)\exp(-\frac{3}{2}\eta)\,. \tag{A.7}$$

Inserting the results from (A.6) and (A.7) into the left hand side of (A.4) gives

$$\left|\frac{\omega_{\bar{n}} - \omega_{\bar{n}-1}}{\omega_{\max}}\right| = \left|\frac{\eta^{\bar{n}}}{\eta^{\hat{n}}}\frac{\hat{n}!}{\bar{n}!}\left(1 - \frac{\bar{n}}{\eta}\right)\right|\,. \tag{A.8}$$

Obviously the condition $\bar{n} > \hat{n}$ holds. Therefore, $\bar{n} = \hat{n} + i$ holds for some positive integer $i \geq 1$. Inserting this expression into (A.8) yields an error ε_i

$$\varepsilon_i = \eta^i \frac{\hat{n}!}{(\hat{n}+i)!}\left(1 - \frac{\hat{n}+i}{\eta}\right)\,. \tag{A.9}$$

The identity

$$(\hat{n}+i)! = \hat{n}! \cdot (\hat{n}+1) \cdot \ldots \cdot (\hat{n}+i) = \hat{n}! \cdot \prod_{k=1}^{i}(\hat{n}+k)$$

simplifies (A.9) to

$$\varepsilon_i = \underbrace{\eta^i \prod_{k=1}^{i}(\hat{n}+k)^{-1}}_{\alpha_i} \cdot \underbrace{\left(1 - \frac{\hat{n}+i}{\eta}\right)}_{\beta_i} = \alpha_i \beta_i\,.$$

It is easy to proof that α_i and β_i can be recursively defined

$$\alpha_i = \alpha_{i-1}\frac{\eta}{\hat{n}+i}$$
$$\beta_i = \beta_{i-1} - \frac{1}{\eta}\,.$$

Therefore, also the error ε_i can be formulated recursively

$$\begin{aligned}\varepsilon_i &= \alpha_i \beta_i \\ &= \frac{\eta}{\hat{n}+i}\alpha_{i-1}\left(\beta_{i-1} - \frac{1}{\eta}\right) \\ &= \frac{1}{\hat{n}+i}\left(\eta\,\varepsilon_{i-1} - \alpha_{i-1}\right)\,.\end{aligned}$$

Note that for an application of the FFTW it is necessary to demand that $\bar{n}$ is equal. This is ensured by the final statement of the following algorithm:

Algorithm 1 Compute the number of relevant time steps

1: define a tolerance ε_T, (e.g., $\varepsilon_T = 10^{-4}$)
2: compute $\eta = r_{\max}/(c_2 \Delta t)$
3: compute $\hat{n} = \lceil \eta \rceil - 1$
4: compute $\alpha = \eta/(\hat{n}+1)$ // α_1
5: compute $\varepsilon = \alpha - 1$ // ε_1
6: initialize iterator $i = 2$
7: **repeat**
8: compute $\varepsilon = \frac{1}{\hat{n}+i}(\eta\varepsilon - \alpha)$
9: compute $\alpha = \frac{\eta}{\hat{n}+i}\alpha$
10: increment i by 1
11: **until** $|\varepsilon| < \varepsilon_T$
12: compute $\bar{n} = \hat{n} + i - 1$
13: **if** $\bar{n}\%2 \neq 0$ **then**
14: $\bar{n} = \bar{n} + 1$
15: **end if**

A.4 Analytical solutions for the 1-dimensional column

Here, the analytical and semi-analytical solutions for the 1-dimensional rod are recalled. All solutions are obtained via the Laplace transform of the original initial boundary value problem and they are restricted to a unit step load as impact force. A more general time-domain solution is given in the textbook of Graff [47], and more details concerning the viscoelastodynamic solution can be found in the thesis of Schanz [109].

The Figure A.2 depicts a 1-dimensional rod of ℓm length. It is fixed at $x = 0$ and is loaded at the free end $x = \ell$ by the impact force $F(t) = F_0 H(t)$.

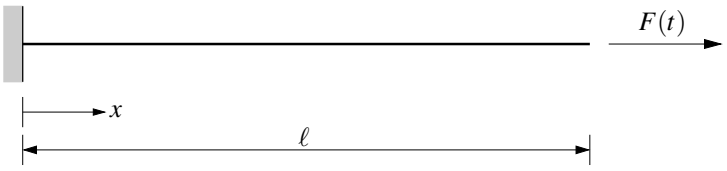

Figure A.2: 1-dimensional rod with longitudinal step load

Governing equations. For this system the homogeneous initial boundary value problem for the longitudinal displacement $u(x,t)$ is

$$\begin{aligned} -\frac{\partial^2 u}{\partial x^2} + \frac{1}{c^2}\frac{\partial^2 u}{\partial t^2} &= 0 && \forall (x,t) \in (0,\ell)\times(0,\infty) \\ u(0,t) &= 0 && \forall t \in (0,\infty) \\ N(\ell,t) &= F_0 H(t) && \forall t \in (0,\infty) \\ u(x,0^+) &= 0 && \forall x \in (0,\ell) \\ \dot{u}(x,0^+) &= 0 && \forall x \in (0,\ell)\,. \end{aligned} \tag{A.10}$$

Above, the force $N(x,t) \coloneqq \sigma(x,t)A$ is nothing but the stress σ times the constant cross-sectional area A.

With the Laplace transform $\hat{w}(s) = \mathscr{L}\{w\}(s) \coloneqq \int_0^\infty w(t)\exp(-st)\,\mathrm{d}t$ and under consideration of the initial conditions $u(x,0^+) = 0$ and $\dot{u}(x,0^+) = 0$ the system (A.10) transforms as

$$\begin{aligned} -\frac{\partial^2 \hat{u}}{\partial x^2} + k_c^2 \hat{u} &= 0 && \forall x \in (0,\ell) \\ \hat{u}(0,s) &= 0 \\ \hat{N}(\ell,s) &= F_0 \frac{1}{s} \end{aligned} \tag{A.11}$$

with the complex wave number $k_c \coloneqq s/c$. Using the definition of $N(x,t)$ in addition with the one-dimensional Hooke's law $\hat{\sigma}(x,s) = 2\mu\frac{\partial \hat{u}}{\partial x}$ the last boundary condition becomes $\frac{\partial \hat{u}}{\partial x} = \frac{F_0}{2\mu s A}$. Defining the prescribed traction as $\sigma_0 \coloneqq F_0/A$ and substituting the Lamé parameter such that $2\mu = c^2\varrho_0$ is expressed via the wave velocity and the mass density the solution of (A.11) in accordance to the boundary conditions is

$$\hat{u}(x,s) = \frac{\sigma_0}{\varrho_0 c}\frac{1}{s^2}\exp((\ell - x)k_c)\frac{\exp(2k_c x) - 1}{\exp(2k_c\ell) + 1}\,. \tag{A.12}$$

Time-domain solution. Next, the time domain solution $u(x,t)$ is obtained by the inverse Laplace transform of (A.12). Since $\mathrm{Re}(s) > 0$ holds the absolute value of $\exp(-2k_c\ell)$ is always lower than 1. This property enables the use of the identity

$$\frac{1}{1+\exp(-2k_c\ell)} = \sum_{n=0}^{\infty}(-1)^n \exp(-2k_c n\ell)$$

which is nothing more than the infinite geometric series. Thus, the expression (A.12) can, finally, be transformed into

$$\hat{u}(x,s) = \frac{\sigma_0}{\varrho_0 c}\sum_{n=0}^{\infty}(-1)^n\left[\frac{\exp(-k_c((2n+1)\ell - x))}{s^2} - \frac{\exp(-k_c((2n+1)\ell + x))}{s^2}\right].$$

Now, the expression above is appropriate for the application of the inverse Laplace transform. With the auxiliary function

$$\chi_n(x,t) := t - \frac{(2n+1)\ell + x}{c} .$$

this gives the displacement and traction solution

$$\begin{aligned} u(x,t) &= \frac{\sigma_0}{\varrho_0 c} \sum_{n=0}^{\infty} (-1)^n \left[\chi_n(-x,t)\, H\left(\chi_n(-x,t)\right) - \chi_n(x,t)\, H\left(\chi_n(x,t)\right) \right] \\ \sigma(x,t) &= 2\mu \frac{\partial u(x,t)}{\partial x} = \sigma_0 \sum_{n=0}^{\infty} (-1)^n \left[H\left(\chi_n(-x,t)\right) + H\left(\chi_n(x,t)\right) \right] . \end{aligned} \tag{A.13}$$

Viscoelastodynamic solution. From section 2.3, it is known that the Laplace transformed time-domain solution can be used to obtain the Laplace transformed viscoelastic solution. Therefore, the correspondence principle (2.51) has to be applied. For the 1-dimensional rod this correspondence principle is

$$\mu \Longleftrightarrow \underbrace{\mu \frac{1+qs^\alpha}{1+ps^\alpha}}_{=:\hat{\mu}(s)} ,$$

which is the 1-dimensional analogue to the 5-parameter model from (2.59). With the complex modul $\hat{\mu}(s)$ and the complex valued wave velocity $\hat{c}(s) = \sqrt{2\hat{\mu}(s)/\varrho_0}$ the viscoelastodynamic displacement solution is obtained

$$\hat{u}(x,s) = \frac{\sigma_0}{\varrho_0 \hat{c}} \frac{1}{s^2} \exp((\ell - x)k_{\hat{c}}) \frac{\exp(2k_{\hat{c}}x) - 1}{\exp(2k_{\hat{c}}\ell) + 1} . \tag{A.14}$$

Consequently, the tractions $\hat{\sigma}(x,s)$ are

$$\hat{\sigma}(x,s) = 2\hat{\mu} \frac{\partial \hat{u}}{\partial x} = \frac{\sigma_0}{s} \exp((\ell - x)k_{\hat{c}}) \frac{\exp(2k_{\hat{c}}x) + 1}{\exp(2k_{\hat{c}}\ell) + 1} . \tag{A.15}$$

In general, it is impossible to transform the viscoelastic solutions (A.14) and (A.15) analytically into the time-domain. Therefore, one has to be content with a numerical inversion of those solutions. Within this work this numerical inversion is done by using an algorithm based on Talbot's method [86].

Quasistatic solution. Neglecting the effects due to the inertia terms in (A.10) or (A.11), respectively, yields the so-called quasi-static solution. Performing the limit $\lim_{|k_{\hat{c}}| \to 0} \hat{u}$ for the viscoelastodynamic displacement solution (A.14) yields

$$\hat{u}(x,s) = \frac{\sigma_0}{2} \frac{1}{\hat{\mu} s} x = \frac{\sigma_0}{2\mu} \frac{1+ps^\alpha}{(1+qs^\alpha)s} x . \tag{A.16}$$

Again, a general inversion of the expression above is hardly possible but it is easy to obtain a solution if the derivative order is set to one, i.e., if $\alpha = 1$ holds. In this case the inverse of (A.16) is simply

$$u(x,t) = \frac{\sigma_0}{2\mu}\left[1 + \left(\frac{p}{q} - 1\right)\exp(-t/q)\right]x\,. \tag{A.17}$$

Note that this solution corresponds to the Poynting model from section 2.3.

A.5 Analytical solution for the pressurized spherical cavity

The initial boundary value problem for a spherical cavity of radius $R > 0$ is considered (Fig. A.3). Let $\Omega = \{\mathbf{x} \in \mathbb{R}^3 \colon |\mathbf{x}| > R\}$ denote the domain, and let $\Gamma = \partial\Omega = \{\mathbf{x} \in \mathbb{R}^3 \colon |\mathbf{x}| = R\}$ be its boundary. Using spherical coordinates the initial boundary value problem (6.20) reads as

$$\begin{aligned} \frac{\partial^2 u}{\partial r^2} + \frac{2}{r}\frac{\partial u}{\partial r} - \frac{2u}{r^2} &= \frac{1}{c_1^2}\frac{\partial^2 u}{\partial t^2} && \forall\, r > R,\ t \in (0,\infty) \\ \sigma_r(r,t) &= -p_0 H(t) && \forall\, r = R,\ t \in (0,\infty) \\ u(r,0) = \dot{u}(r,0) &= 0 && \forall\, r > R,\ t = 0\,. \end{aligned} \tag{A.18}$$

In (A.18), $r = \sqrt{\langle \mathbf{x}, \mathbf{x} \rangle}$ denotes the the Euclidean norm of a vector $\mathbf{x}$. Analogously, the absolute value of the displacement field is given by $u = \sqrt{\langle \mathbf{u}, \mathbf{u} \rangle}$. Finally, c_1 is the velocity of the compressional wave and σ_r is the stress field in radial direction.

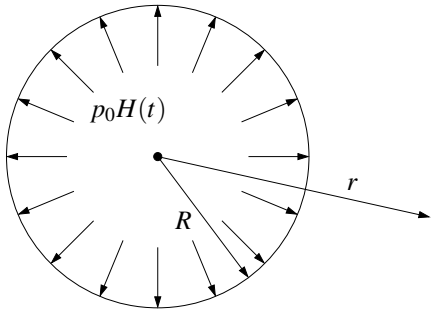

Figure A.3: Pressurized spherical cavity

The solution of (A.18) is taken from [2] and is given given by

$$u(r,t) = \frac{\partial \varphi}{\partial r} \tag{A.19}$$

where the function $\phi(r,t)$ can be expressed as

$$\varphi(r,t) = -\frac{R^3 p_0}{4\mu}\frac{1}{r}\left[1 - \sqrt{2(1-\nu)}\exp(-\alpha s)\sin(\beta s + \gamma)\right]H(s)$$

with the parameters

$$\alpha = \frac{1-2\nu}{1-\nu}\frac{c_1}{R}$$
$$\beta = \frac{\sqrt{1-2\nu}}{1-\nu}\frac{c_1}{R}$$
$$\gamma = \arctan\frac{1}{\sqrt{1-2\nu}}\,.$$

The argument $s = s(r,t)$ represents the retarded time

$$s(r,t) = t - \frac{r-R}{c_1}\,.$$

Finally, the normal stress σ_r in the radial direction and the normal stress σ_θ perpendicular to r are determined by

$$\begin{aligned}\sigma_r(r,t) &= \frac{\varrho_0 c_1^2}{1-\nu}\left[\frac{1-\nu}{c_1^2 r}\frac{\partial^2 f}{\partial s^2} - 2(1-2\nu)\frac{u(r,t)}{r}\right]\\ \sigma_\theta(r,t) &= \frac{\varrho_0 c_1^2}{1-\nu}\left[\frac{\nu}{c_1^2 r}\frac{\partial^2 f}{\partial s^2} + (1-2\nu)\frac{u(r,t)}{r}\right]\end{aligned} \tag{A.20}$$

using the mass density ϱ_0 and a function $f(s) = r\varphi(r,t)$.

Implementation details. By defining some auxiliary functions

$$\begin{aligned}u_{st}(r) &= \frac{R^3 p_0}{4\mu}\frac{1}{r^2}\\ \psi_0(s) &= \sqrt{2(1-\nu)}\exp(-\alpha s)\\ \psi_1(s) &= \sin(\beta s+\gamma)\\ \tilde{\varphi}(s) &= [1-\psi_0(s)\psi_1(s)]H(s)\end{aligned}$$

the displacement solution (A.19) reads as

$$u(r,t) = u_{st}\left(\tilde{\varphi} + \frac{r}{c_1}\frac{\mathrm{d}\tilde{\varphi}}{\mathrm{d}s}\right)H(s)$$

with

$$\frac{\mathrm{d}\tilde{\varphi}}{\mathrm{d}s} = \psi_0\left(\alpha\psi_1 - \frac{\mathrm{d}\psi_1}{\mathrm{d}s}\right), \quad \frac{\mathrm{d}\psi_1}{\mathrm{d}s} = \beta\cos(\beta s+\gamma)\,.$$

The stress solutions (A.20) are computed straightforward using the identity

$$\frac{\partial^2 f}{\partial s^2} = -u_{st} r^2\left[(\beta^2-\alpha^2)\psi_1 + 2\alpha\frac{\mathrm{d}\psi_1}{\mathrm{d}s}\right]\psi_0 H(s)\,.$$

REFERENCES

[1] Abramowitz, M.; Stegun, I.A. (eds.): *Pocketbook of Mathematical Functions*. Verlag Harri Deutsch, Thun, Frankfurt/Main, 1984. Abridged edition of Handbook of Mathematical Functions.

[2] Achenbach, J.D.: *Wave propagation in elastic solids*. North-Holland, 2005.

[3] Alvermann, S.: *Effective Viscoelastic Behavior of Cellular Auxetic Materials*, vol. 1 of *Monographic Series TU Graz: Computation in Engineering and Science*. Verlag der Technischen Universität Graz, 2008.

[4] Anderson, E.; Bai, Z.; Bischof, C.; Blackford, S.; Demmel, J.; Dongarra, J.; Du Croz, J.; Greenbaum, A.; Hammarling, S.; McKenney, A.; Sorensen, D.: *LAPACK Users' Guide*. Society for Industrial and Applied Mathematics, Philadelphia, PA, third edn., 1999. ISBN 0-89871-447-8 (paperback).

[5] Antes, H.: *Anwendungen der Methode der Randelemente in der Elastodynamik und der Fluiddynamik*, vol. 9 of *Mathematische Methoden in der Technik*. B. G. Teubner, Stuttgart, 1988.

[6] Bagley, R.L.; Torvik, P.J.: A Theoretical Basis for the Application of Fractional Calculus to Viscoelasticity. *Journal of Rheology*, **27**(3):201–210, 1983.

[7] Bagley, R.L.; Torvik, P.J.: On the Fractional Calculus Model of Viscoelastic Behavior. *Journal of Rheology*, **30**(1):133–155, 1986.

[8] Bathe, K.J.: *Finite-Element-Methoden*. Springer, Berlin Heidelberg, 2nd edn., 2002.

[9] Bebendorf, M.: *Hierarchical matrices*, vol. 63 of *Lecture Notes in Computational Science and Engineering*. Springer, Berlin, 2008.

[10] Bebendorf, M.; Rjasanow, S.: Adaptive Low-Rank Approximation of Collocation Matrices. *Computing*, **70**:1–24, 2003.

[11] Becache, E.; Nedelec, J.C.; Nishimura, N.: Regularization in 3D for anisotropic elastodynamic crack and obstacle problems. *Journal of Elasticity*, **31**(1):25–46, 1993.

[12] Beer, G.; Meek, J.L.: 'Infinite domain' elements. *International Journal for Numerical Methods in Engineering*, **17**:43–52, 1981.

[13] Beer, G.; Watson, J.O.: Infinite boundary elements. *International Journal for Numerical Methods in Engineering*, **28**:1233–1247, 1989.

[14] Benthien, G.W.; Schenk, H.A.: Nonexistence and nonuniqueness problems associated with integral equation methods in acoustics. *Computers and Structures*, **65**(3):295–305, 1997.

[15] Beskos, D.E.: Boundary element methods in dynamic analysis. *Applied Mechanics Review*, **40**(1):1–23, 1987.

[16] Beskos, D.E.: Boundary element methods in dynamic analysis: Part II (1986-1996). *Applied Mechanics Review*, **50**(3):149–197, 1997.

[17] Bettes, P.: *Infinite Elements*. Penshaw Press, 1992.

[18] Bonnet, M.: *Boundary integral equation methods for solids and fluids*. Wiley, New York, 1995.

[19] Bonnet, M.; Bui, H.D.: Regularization of the Displacement and Traction BIE for 3D Elastodynamics Using Indirect Methods. *In* J.H. Kane; G. Maier; N. Tosaka; S.N. Atluri (eds.), *Advances in Boundary Element Techniques*, Springer series in computational mechanics, pp. 1–29. Springer Verlag Berlin Heidelberg New York, 1993.

[20] Bonnet, M.; Maier, G.; Polizzotto, C.: Symmetric Galerkin boundary element methods. *Applied Mechanics Review*, **51**(11):669–703, 1998.

[21] Braess, D.: *Finite Elemente*. Springer-Verlag, Berlin, Heidelberg, 4th edn., 2007.

[22] Brebbia, C.A.; Telles, J.C.F.; Wrobel, L.C.: *Boundary Element Techniques – Theory and Applications in Engineering*. Springer-Verlag, Berlin, Heidelberg, 1984.

[23] Burton, A.J.; Miller, G.F.: The Application of Integral Equation Methods to the Numerical Solution of Some Exterior Boundary-Value Problems. *Proceedings of the Royal Society of London, Series A*, **323**(1553):201–210, 1971. doi: http://dx.doi.org/10.1098/rspa.1971.0097.

[24] Chapko, R.; Kress, R.: Rothe's method for the heat equation and boundary integral equations. *Journal of Integral Equations and Applications*, **9**(1):47–69, 1997.

[25] Christensen, R.M.: *Theory of viscoelasticity*. Academic Press, New York, 1971.

[26] Chudinovich, I.: Boundary Equations in Dynamic Problems of the Theory of Elasticity. *Acta Applicandae Mathematicae*, **65**:169–183, 2001.

[27] Chudinovich, I.Y.: The Boundary Equation Method in the Third Initial Boundary Value Problem of the Theory of Elasticity Part 1: Existence Theorems. *Mathematical Methods in the Applied Sciences*, **16**:203–215, 1993.

[28] Chudinovich, I.Y.: The Boundary Equation Method in the Third Initial Boundary Value Problem of the Theory of Elasticity Part 2: Methods for Approximate Solutions. *Mathematical Methods in the Applied Sciences*, **16**:217–227, 1993.

[29] Costabel, M.: *Time-dependent problems with the boundary integral equation method*, vol. 1 of *Encyclopedia of Computational Mechanics*, chap. 25. John Wiley & Sons, New York, Chister, Weinheim, 2005.

[30] Costabel, M.; Dauge, M.: On Representation Formulas and Radiation Conditions. *Mathematical Methods in the Applied Sciences*, **20**:133–150, 1997.

[31] Courant, R.; Friedrichs, K.; Lewy, H.: Über die partiellen Differenzengleichungen der mathematischen Physik. *Mathematische Annalen*, **100**:32–74, 1928.

[32] Cruse, T.A.; Rizzo, F.J.: A Direct Formulation and Numerical Solution of the General Transient Elastodynamic Problem. I. *Journal of Mathematical Analysis and Applications*, **22**:244–259, 1968.

[33] Doetsch, G.: *Anleitung zum praktischen Gebrauch der Laplace-Transformation und der Z-Transformation*. Oldenbourg Verlag, München, Wien, 6th edn., 1989.

[34] Domínguez, J.: *Boundary Elements in Dynamics*. Computational Mechanics Publications, Southampton, Boston, 1993.

[35] Duffy, M.G.: Quadrature over a pyramid or cube of integrands with a singularity at a vertex. *SIAM Journal on Numerical Analysis*, **19**(6):1260–1262, 1982.

[36] Dunavant, D.A.: High degree efficient symmetrical Gaussian quadrature rules for the triangle. *International Journal for Numerical Methods in Engineering*, **21**:1129–1148, 1985.

[37] Erichsen, S.; Sauter, S.A.: Efficient automatic quadrature in 3-d Galerkin BEM. *Computer Methods in Applied Mechanics and Engineering*, **157**:215–224, 1998.

[38] Feynman, R.P.; Leighton, R.B.; Sands, M.: *The Feynman lectures on physics*. Addison-Wesley, 1973.

[39] Flügge, W.: *Viscoelasticity*. Springer-Verlag, Berlin, Heidelberg, New York, 2nd edn., 1975.

[40] Frigo, M.; Johnson, S.G.: The design and implementation of FFTW3. *Proceedings of the IEEE*, **93**(2):216–231, 2005. Special issue on "Program Generation, Optimization, and Platform Adaptation".

[41] Gaul, L.; Kögl, M.; Wagner, M.: *Boundary Element Methods for Engineers and Scientists*. Springer-Verlag Berlin Heidelberg, 2003.

[42] Gerdes, K.: A summary of Infinite Element formulations for exterior Helmholtz problems. *Computer Methods in Applied Mechanics and Engineering*, **164**:95–105, 1998.

[43] Gerdes, K.; Demkowicz, L.: Solution of 3D-Laplace and Helmholtz equation in exterior domains using *hp*-infinite elements. *Computer Methods in Applied Mechanics and Engineering*, **137**:239–273, 1996.

[44] Givoli, D.: *Numerical Methods for Problems in Infinite Domains*, vol. 33 of *Studies in applied mechanics*. Elsevier, 1992.

[45] Goldstein, H.: *Klassische Mechanik*. Akademische Verlagsgesellschaft, Wiesbaden, 1981.

[46] Golub, G.H.; van Loan, C.F.: *Matrix Computations*. The John Hopkins University Press, 1996.

[47] Graff, K.F.: *Wave motions in elastic solids*. Dover Publications, 1991.

[48] Graffi, D.: Über den Reziprozitätssatz in der Dynamik elastischer Körper. *Ingenieur Archiv*, **22**:45–46, 1954.

[49] Greengard, L.: *The rapid evaluation of potential fields in particle systems*. Ph.D. thesis, Massachusetts Institute of Technology, 1987.

[50] Guiggiani, M.: Formulation and numerical treatment of boundary integral equations with hypersingular kernels. *In* V. Sladek; J. Sladek (eds.), *Singular Integrals in Boundary Element Methods*, pp. 85–124. Computational Mechanics Publications, 1998.

[51] Günter, N.M.: *Potential theory, and its applications to basic problems of mathematical physics*. Frederick Ungar Publishing, New York, 1967.

[52] Gurtin, M.E.; Sternberg, E.: On the linear theory of viscoelasticity. *Archive for Rational Mechanics and Analysis*, **11**(1):291–356, 1962.

[53] Ha-Duong, T.: On Retarded Potential Boundary Integral Equations and their Discretisation. *In* M. Ainsworth; P. Davies; D. Duncan; P. Martin; B. Rynne (eds.), *Topics in Computational Wave Propagation: Direct and Inverse Problems*, pp. 301–336. Springer-Verlag Berlin, 2003.

[54] Hackbusch, W.: *Integralgleichungen – Theorie und Numerik*, vol. 68 of *Leitfäden der angewandten Mathematik und Mechanik LAMM*. B.G. Teubner, 1989.

[55] Hackbusch, W.; Schwarz, H.R.; Zeidler, E.: *Teubner-Taschenbuch der Mathematik*. B. G. Teubner Verlag / GWV Fachverlage GmbH, Wiesbaden, 2nd edn., 2003.

[56] Hackbush, W.: A Sparse Matrix Arithmetic Based on $\mathcal{H}$-Matrices. Part I: Introduction to $\mathcal{H}$-Matrices. *Computing*, **62**:89–108, 1999.

[57] Hadamard, J.: *Lectures on Cauchy's problem in linear partial differential equations*. Dover Publications, Inc. *(reprint)*, 1952.

[58] Han, H.: The boundary integro-differential equations of three-dimensional Neumann problem in linear elasticity. *Numerische Mathematik*, **68**:269–281, 1994.

[59] Hartmann, F.: *Methode der Randelemente*. Springer-Verlag, Berlin, Heidelberg, 1987.

[60] Helmholtz, H.: Über Integrale der hydrodynamischen Gleichungen welche den Wirbelbewegungen entsprechen. *Journal für die reine und angewandte Mathematik*, **55**, 1858.

[61] Higham, N.J.: Fortran codes for estimating the one-norm of a real or complex matrix, with applications to condition estimation. *ACM Transactions on Mathematical Software*, **14**(4):381–396, 1988. ISSN 0098-3500. doi: http://doi.acm.org/10.1145/50063.214386.

[62] de Hoop, A.T.: An elastodynamic reciprocity theorem for linear, viscoelastic media. *Applied Scientific Research*, **16**(1):39–45, 1966.

[63] Hsiao, G.C.; Wendland, W.L.: *Boundary Integral Equations*, vol. 164 of *Applied Mathematical Sciences*. Springer-Verlag GmbH, 2008.

[64] Kielhorn, L.; Schanz, M.: Convolution Quadrature Method based symmetric Galerkin Boundary Element Method for 3-d elastodynamics. *International Journal for Numerical Methods in Engineering*, **76**(11):1724–1746, 2008.

[65] Knops, R.J.; Payne, L.E.: *Uniqueness theorems in Linear Elasticity*, vol. 19 of *Springer Tracts in Natural Philosophy*. Springer-Verlag, Berlin, Heidelberg, New York, 1971.

[66] Krawietz, A.: *Materialtheorie - Mathematische Beschreibung des phänomenologischen thermomechanischen Verhaltens*. Springer-Verlag, Berlin, Heidelberg, Tokyo, New York, Toronto, 1986.

[67] Krishnasamy, G.; Schmerr, L.W.; Rudolphi, T.J.; Rizzo, F.J.: Hypersingular Boundary Integral Equations: Some Applications in Acoustic and Elastic Wave Scattering. *Journal of Applied Mechanics*, **57**:404–414, 1990.

[68] Krommer, A.R.; Ueberhuber, C.W.: *Computational Integration*. SIAM, Philadelphia, Pa., 1998.

[69] Kupradze, V.D.: *Dynamical problems in elasticity*, vol. 3 of *Progress in Solid Mechanics*. North-Holland Publishing Company, 1963.

[70] Kupradze, V.D. (ed.): *Three-dimensional problems of the mathematical theory of elasticity and thermoelasticity*, vol. 25 of *Applied mathematics and mechanics*. North Holland, Amsterdam, 1979.

[71] Lachat, J.C.; Watson, J.O.: Effective numerical treatment of boundary integral equations: A formulation for three-dimensional elastostatics. *International Journal for Numerical Methods in Engineering*, **10**(5):991–1005, 1976.

[72] Lakes, R.S.: *Viscoelastic solids*, vol. 6 of *Mechanical engineering*. CRC Press LLC, Boca Raton, London, New York, Washington, D. C., 1998.

[73] Lambert, J.D.: *Numerical Methods for Ordinary Differential Systems*. John Wiley & Sons, Inc., New York, 1991.

[74] Lipschutz, S.: *Lineare Algebra*. McGraw-Hill, Maidenhead, Berkshire, 2nd edn., 1999. Original Edition: Schaum's Outline of Theory and Problems of Linear Algebra.

[75] Love, A.E.H.: *A treatise on the mathematical theory of elasticity*, vol. 1. Cambridge University Press, 1892.

[76] Lubich, C.: Convolution quadrature and discretized operational calculus I. *Numerische Mathematik*, **52**:129–145, 1988.

[77] Lubich, C.: Convolution quadrature and discretized operational calculus II. *Numerische Mathematik*, **52**:413–425, 1988.

[78] Lubich, C.: On the multistep time discretization of linear initial-boundary value problems and their boundary integral equations. *Numerische Mathematik*, **67**:365–389, 1994.

[79] Lubich, C.; Schneider, R.: Time discretization of parabolic boundary integral equations. *Numerische Mathematik*, **63**:455–481, 1992.

[80] Mansur, W.J.: *A Time-Stepping Technique to Solve Wave Propagation Problems Using the Boundary Element Method*. Ph.D. thesis, University of Southampton, 1983.

[81] Mantič, V.: A new formula for the C-matrix in the Somigliana identity. *Journal of Elasticity*, **33**(3):191–201, 1993.

[82] Maue, A.W.: Zur Formulierung eines allgemeinen Beugungsproblems durch eine Integralgleichung. *Zeitschrift für Physik*, **126**(7–9):601–618, 1949.

[83] Mindlin, R.D.: Force at a Point in the Interior of a Semi-Infinite Solid. *Physics*, **7**(5):195–202, 1936.

[84] Morse, P.M.; Ingard, K.U.: *Theoretical Acoustics*. Princeton University Press, 1986.

[85] Moser, W.; Duenser, C.; Beer, G.: Mapped infinite elements for three-dimensional multi-region boundary element analysis. *International Journal for Numerical Methods in Engineering*, **61**:317–328, 2004.

[86] Murli, A.; Rizzardi, M.: Algorithm 682: Talbot's method of the Laplace inversion problems. *ACM Transactions on Mathematical Software*, **16**(2):158–168, 1990. ISSN 0098-3500. doi:http://doi.acm.org/10.1145/78928.78932.

[87] Nedelec, J.: Integral equations with non integrable kernels. *Integral Equations and Operator Theory*, **5**:563–672, 1982.

[88] Nishimura, N.; Kobayashi, S.: A regularized boundary integral equation method for elastodynamic crack problems. *Computational Mechanics*, **4**:319–328, 1989.

[89] Of, G.: *BETI-Gebietszerlegungsmethoden mit schnellen Randelementverfahren und Anwendungen*. Ph.D. thesis, Institut für Angewandte Analysis und Numerische Simulation, Universität Stuttgart, 2006.

[90] Ogden, R.W.: *Non-Linear Elastic Deformations*. Dover Publications, inc., Mineola, New York, 1997.

[91] Ohayon, R.; Soize, C.: *Structural Acoustics and Vibration*. Academic Press, 1998.

[92] Oldham, K.B.; Spanier, J.: *The Fractional Calculus*, vol. 111 of *Mathematics in science and engineering*. Academic Press, New York, 1974.

[93] Ortner, N.: Regularisierte Faltung von Distributionen. Teil 1: Zur Berechnung von Fundamentallösungen. *Zeitschrift für angewandte Mathematik und Physik (ZAMP)*, **31**, 1980.

[94] Ortner, N.: Regularisierte Faltung von Distributionen. Teil 2: Eine Tabelle von Fundamentallösungen. *Zeitschrift für angewandte Mathematik und Physik (ZAMP)*, **31**:153–173, 1980.

[95] Pekeris, C.L.: The seismic surface pulse. *Proceedings of the National Academy of Sciences of the United States of America*, **41**:469–480, 1955.

[96] Podlubny, I.: *Fractional Differential Equations*, vol. 198 of *Mathematics in Science and Engineering*. Academic Press, San Diego, Boston, New York, London, Sydney, Tokyo, Toronto, 1999.

[97] Poljanin, A.D.; Manžirov, A.V.: *Handbook of integral equations*. CRC Press, Boca Raton, 1998.

[98] Reddy, B.D.: *Introductory Functional Analysis*, vol. 27 of *Texts in Applied Mathematics*. Springer, New York, 1998.

[99] Rizzo, F.J.: An integral equation approach to boundary value problems of classical elastostatics. *The Quarterly of Applied Mathematics*, **25**(1):83–95, 1967.

[100] Rjasanow, S.; Steinbach, O.: *The Fast Solution of Boundary Integral Equations*, vol. 7 of *Mathematical and Analytical Techniques with Applications to Engineering*. Springer Science+Business Media, LLC, New York, 2007.

[101] Roach, G.F.: *Green's functions*. Cambridge University Press, 2nd edn., 1982.

[102] Ross, B.: A Brief History and Exposition of the Fundamental Theory of Fractional Calculus. *In* B. Ross (ed.), *Fractional Calculus and Its Applications*, vol. 457 of *Lecture Notes in Mathematics*, pp. 1–36. Springer-Verlag, Berlin, Heidelberg, New York, 1975.

[103] Ross, B.: Fractional Calculus. *Mathematics Magazine*, **50**(3):115–122, 1977.

[104] Rossikhin, Y.A.; Shitikova, M.V.: Applications of fractional calculus to dynamic problems of linear and nonlinear hereditary mechanics of solids. *Applied Mechanics Review*, **50**(1):15–67, 1997.

[105] Rüberg, T.: *Non-conforming Coupling of Finite and Boundary Element Methods in Time Domain*, vol. 3 of *Monographic Series TU Graz: Computation in Engineering and Science*. Verlag der Technischen Universität Graz, 2008.

[106] Sauter, S.: *Über die effiziente Verwendung des Galerkinverfahrens zur Lösung Fredholmscher Integralgleichungen*. Ph.D. thesis, Christian-Albrechts-Universität zu Kiel, 1992.

[107] Sauter, S.; Schwab, C.: *Randelementmethoden*. B.G. Teubner Verlag, Stuttgart Leipzig Wiesbaden, 2004.

[108] Sauter, S.A.; Lage, C.: Transformation of hypersingular integrals and black-box cubature. *Mathematics of Computation*, **70**:223–250, 2001.

[109] Schanz, M.: *Eine Randelementformulierung im Zeitbereich mit verallgemeinerten viskoelastischen Stoffgesetzen*, vol. 1 of *Bericht aus dem Institut A für Mechanik*. Universität Stuttgart, 1994.

[110] Schanz, M.: A boundary element formulation in time domain for viscoelastic solids. *Communications in Numerical Methods in Engineering*, **15**(11):799–809, 1999.

[111] Schanz, M.: *Wave Propagation in Viscoelastic and Poroelastic Continua: A Boundary Element Approach*, vol. 2 of *Lecture Notes in Applied Mechanics*. Springer-Verlag Berlin Heidelberg, 2001.

[112] Schanz, M.; Antes, H.: A new visco- and elastodynamic time domain Boundary Element formulation. *Computational Mechanics*, **20**:452–459, 1997.

[113] Schenk, H.A.: Improved Integral Formulation for Acoustic Radiation Problems. *Journal of the Acoustical Society of America*, **44**(1):41–58, 1968.

[114] Shilov, G.E.: *Elementary Real and Complex Analysis*. Dover Publications, Inc., New York, 1996. *(reprint)*.

[115] Sirtori, S.: General stress analysis method by means of integral equations and boundary elements. *Meccanica*, **14**:210–218, 1979.

[116] Sommerfeld, A.: Die Greensche Funktion der Schwingungsgleichung. *Jahresbericht der Deutschen Mathematiker-Vereinigung*, **21**:309–353, 1912.

[117] Sommerfeld, A.: *Partial Differential Equations in Physics*. Academic Press, New York, 1949.

[118] Sommerfeld, A.: *Mechanik der deformierbaren Medien*, vol. 2 of *Vorlesungen über theoretische Physik*. Akademische Verlagsgesellschaft Geest & Portig K.-G., Leipzig, 1957.

[119] Stakgold, I.: *Green's functions and Boundary Value Problems*. Pure and applied Mathematics. John Wiley & Sons, Inc., New York, 1998.

[120] Steinbach, O.: *Numerical Approximation Methods for Elliptic Boundary Value Problems*. Springer Science+Business Media, LLC, New York, 2008.

[121] Strang, G.; Fix, G.J.: *An Analysis of the Finite Element Method*. Wellesley-Cambridge Press, 3rd edn., 1997.

[122] Strehmel, K.; Weiner, R.: *Numerik gewöhnlicher Differentialgleichungen*. B.G. Teubner, Stuttgart, 1995.

[123] Szabó, I.: *Höhere Technische Mechanik*. Springer-Verlag, New York, Heidelberg, Berlin, 5th edn., 1977.

[124] Timoshenko, S.; Goodier, J.N.: *Theory of Elasticity*. Engineering Societies Monographs. McGrgaw-Hill Book Company, Inc., New York, Toronto, London, 1951.

[125] Watson, J.O.: Boundary Elements from 1960 to the Present Day. *Electronic Journal of Boundary Elements*, **1**(1):34–46, 2003.

[126] Wheeler, L.T.; Sternberg, E.: Some theorems in classical elastodynamics. *Archive for Rational Mechanics and Analysis*, **31**:51–90, 1968.

[127] Zienkiewicz, O.C.; Taylor, R.L.; Zhu, J.Z.: *The Finite Element Method*. Elsevier, Oxford, 6th edn., 2005.

Monographic Series TU Graz

Computation in Engineering and Science

Vol. 1 Steffen Alvermann
Effective Viscoelastic Behaviour of Cellular Auxetic Materials
2008
ISBN 978-3-902465-92-4

Vol. 2 Sendy Fransiscus Tantono
The Mechanical Behaviour of a Soilbag under Vertical Compression
2008
ISBN 978-3-902465-97-9

Vol. 3 Thomas Rüberg
Non-conforming FEM/BEM Coupling in Time Domain
2008
ISBN 978-3-902465-98-6

Vol. 4 Dimitrios E. Kiousis
Biomechanical and Computational Modeling of Atherosclerotic Arteries
2008
ISBN 978-3-85125-023-7

Vol. 5 Lars Kielhorn
A Time-Domain Symmetric Galerkin BEM for Viscoelastodynamics
2009
ISBN 978-3-85125-042-8